

# **Development, Characterization of Mechanical Properties, Wear behaviour and Machining Analysis of Ceramic Composites for Bio-Medical Applications**

**Amit Kumar Mehar**



Department of Mechanical Engineering  
**National Institute of Technology Rourkela**

**Development, Characterization of Mechanical Properties, Wear Behaviour and Machining Analysis of Ceramic Composites for Bio-Medical Applications**

*Dissertation submitted in partial fulfilment  
of the requirements of the degree of*

***Doctor of Philosophy***

*In*

***Mechanical Engineering***

*by*

***Amit Kumar Mehar***

*(Roll Number: 512ME1043)*

*based on research work carried out*

*under the supervision of*

***Prof. S. S. Mahapatra***

*and*

***Prof. S. K. Patel***



October, 2017

Department of Mechanical Engineering  
**National Institute of Technology Rourkela**



Department of Mechanical Engineering  
**National Institute of Technology Rourkela**

October 23, 2017

## Certificate of Examination

Roll Number: 512ME1043

Name: *Amit Kumar Mehar*

Title of Dissertation: *Development, Characterization of Mechanical Properties, Wear Behaviour and Machining Analysis of Ceramic Composites for Bio-Medical Applications*

We the below signed, after checking the dissertation mentioned above and the official record book (s) of the student, hereby state our approval of the dissertation submitted in partial fulfillment of the requirement of the degree of *Doctor of Philosophy in Mechanical Engineering at National Institute of Technology, Rourkela*. We are satisfied with the volume, quality, correctness, and originality of the work.

\_\_\_\_\_  
Saroj Kumar Patel  
Co-Supervisor

\_\_\_\_\_  
Raj Kishore Patel  
Member, DSC

\_\_\_\_\_  
Kunal Pal  
Member, DSC

\_\_\_\_\_  
Dayal Ramkrushna Parhi  
Chairperson, DSC

\_\_\_\_\_  
Siba Sankar Mahapatra  
Principle Supervisor

\_\_\_\_\_  
Subrata Kumar Panda  
Member, DSC

\_\_\_\_\_  
Prof. S. K. Sharma, IIT, BHU  
External Examiner

\_\_\_\_\_  
Dayal Ramkrushna Parhi  
Head of the Department



Department of Mechanical Engineering  
**National Institute of Technology Rourkela**

---

**Prof. Siba Sankar Mahapatra**  
Professor

**Prof. Saroj Kumar Patel**  
Associate Professor

October 23, 2017

## **Supervisor's Certificate**

This is to certify that the work presented in this dissertation entitled "*Development, Characterization of Mechanical Properties, Wear Behaviour and Machining Analysis of Ceramic Composites for Bio-Medical Applications*" by "*Amit Kumar Mehar*", Roll Number: 512ME1043, is a record of original research carried out by him under my supervision and guidance in partial fulfillment of the requirements of the degree of *Doctor of philosophy* in *Mechanical Engineering*. Neither this dissertation nor any part of it has been submitted for any degree or diploma to any institute or university in India or abroad.

---

Saroj Kumar Patel

Associate Professor

---

Siba Sankar Mahapatra

Professor



*Dedicated*  
*To*  
*My Wife Vidyanani*  
*&*  
*My Daughter Ananta*

Signature

# Declaration of Originality

I, *Amit Kumar Mehar*, Roll Number: *512ME1043* hereby declare that this dissertation entitled “*Development, Characterization of Mechanical Properties, Wear Behaviour and Machining Analysis of Ceramic Composites for Bio-Medical Applications*” represents my original work carried out as a doctoral student of NIT Rourkela and, to the best of my knowledge, it contains no material previously published or written by another person, nor any material presented for the award of any degree or diploma of NIT Rourkela or any other institution. Any contribution made to this research by others, with whom I have worked at NIT Rourkela or elsewhere, is explicitly acknowledged in the dissertation. Works of other authors cited in this dissertation have been duly acknowledged under the section “Bibliography”. I have also submitted my original research records to the scrutiny committee for evaluation of my dissertation.

I am fully aware that in case of my non-compliance detected in the future, the Senate of NIT Rourkela may withdraw the degree awarded to me on the basis of the present dissertation.

October 23, 2017  
NIT Rourkela

*Amit Kumar Mehar*

# Acknowledgement

My special thanks goes to my helpful and honorable research supervisors Dr. S. S. Mahapatra, Professor, and Dr. S. K. Patel, Associate Professor, Department of Mechanical Engineering, National Institute of Technology, Rourkela for their able and continual guidance.

I owe a great many thanks to a great many people who helped and supported me during the entire project work. Apart from the efforts of me, the success of any project depends largely on the encouragement and guidelines of many others. I take this opportunity to express my gratitude to the people who have been instrumental in the successful completion of this project.

I express my heartfelt thanks to Prof. A. Biswas, Director, N.I.T., Rourkela for providing me the facilities to carry out this project.

I express my thanks to Dr. S. Datta, Dr. B. K. Nanda, Dr. S. K. Sahoo, Dr. M. Masanta and Dr. S. Sen for their advice and constructive suggestion for the improvement of my work.

I take this opportunity to thank Dr. N. Panda and Dr. R. K. Patel, Department of Chemistry, who have helped me to a very great extent, even in off-days and off-hours to conduct various related experiments for completion of this thesis. My special thanks are also due to Mr. Ramesh Sahoo and Mr. Satish Samantaray, Research scholars, Department of Chemistry, N.I.T., Rourkela who have helped to very great extent for completion of this thesis.

I thank to Dr. S. K. Pratihari, Associate professor, Department of Ceramic Engg., for his kind support and technical advice for completion of this project work. I would also express my sincere thanks to Mr. Yugojoyti Nayak, and Mr. Sanjay Kr. Swain, Research scholars, Department of Ceramic Engg., N.I.T., Rourkela for their constant practical assistance and help whenever required.

Submitting this thesis would have been an extremely difficult job, without the constant help, encouragement, support, and suggestions from my friends, especially Mr. Shailesh Kumar Dewangan, Mr. Swayam Bikash Mishra, Mr. Raviteja Buddala, Mr. Ankit Kumar Pandey, Mr. Suman Chatterjee, Mr. Dilip Sen, Miss Sanjita Jaipuria and Mrs. Bijaya Bijeta Nayak for their time to help. I also extend my heartfelt thanks to my family and well-wishers.

October 23, 2017

NIT, Rourkela (Odisha)

Amit Kumar Mehar

Roll No. 512ME1043

# Abstract

Ceramic composites incorporating synthetic hydroxyapatite (HAp) particulate and thermoplastic polymer matrices are finding wide spread applications in bio-medical field. The fractured or damaged bone can be repaired or replaced by artificial bone materials. HAp has been tested many times as an artificial bone, especially as augmentation material in surgery work or as a coating material on bio-inert implants materials. It has shown excellent biocompatibility and bonding characteristics. Many implant materials used for last three decades are basically metals, alloys, ceramics and polymers etc. Most metals and ceramics are much stiffer than bone tissue resulting in mechanical mismatch (i.e. "stress shielding") between the implant and the adjacent bone tissue. Metals are too stiff and pose other biocompatibility problems whereas ceramics are too brittle but polymers are too flexible and weak to meet the mechanical strength. However, polymers are popular due to their low density, good mechanical strength and easy formability. Therefore, polymeric bone implants are widely used. HAp particulates are mixed with polymer matrix through a series of processing stages involving melt compounding, granulating and micro-injection moulding. HAp is a suitable ceramic material for hard tissue replacement. In the present work, HAp is synthesized by wet chemical precipitation route. The mechanical properties such as tensile, compressive, flexural, impact and hardness are assessed for the composites varying HAp volume percentage in polycarbonate (PC) and polysulfone (PSU) polymers. The wear resistance of composites in abrasion, erosion, sliding and fretting mode is assessed in dry environment. Adaptive neuro-fuzzy inference system (ANFIS) model is proposed for prediction of wear behaviour of composites. The effect of drilling parameters on surface integrity of internal holes made on composite is assessed to provide insight into machinability (i.e. drilling) aspects of composites. The aim of this study is to develop material that has similar mechanical properties to that of human bone in order to achieve mechanical compatibility in the body, examine the various mechanical properties of ceramic composites, assess the performance of the ceramic composites under different wear modes and evaluate the performance of the composites in drilling operation. The samples were characterized by x-ray diffraction (XRD), fourier transform infrared test (FTIR), and scanning electron microscopy (SEM). Two-body abrasion wear behaviour of the composite is evaluated using pin-on-disc friction and wear test rig (ASTM G99). The experiment is conducted using three different water proof silicon carbide (SiC) abrasive papers of 400, 600 and 1000 grit size. Taguchi's  $L_{27}$  orthogonal array is used to evaluate the tribological property with four control variables such as HAp volume percentage, load applied, sliding speed and track radius, each at three levels. The highest abrasive wear loss is noticed in the specimens worn with 400 grit size SiC paper. Erosion wear of ceramic composites is performed on air jet erosion test rig (ASTM G76). In this study, dry silica sand (spherical) of different particle size of 300 $\mu$ m, 400 $\mu$ m and 500 $\mu$ m are used as erodent. Taguchi's  $L_{27}$  design is used to evaluate the tribological property with three control variables such as pressure, HAp volume, and impingement angle, each at three levels. The higher erosive wear loss is noticed in the specimens worn with 500 $\mu$ m erodent particle size as compared to both 300 $\mu$ m and 400 $\mu$ m erodent particle size. The sliding wear test of ceramic composites is performed on ball on plate wear tester (ASTM G194). Taguchi's  $L_{27}$  design is designed to evaluate the tribological properties with three control variables such as HAp volume percentage, load applied and sliding speed, each at three levels. The fretting wear test of ceramic composites is performed on high frequency reciprocating rig (HFRR) testing machine (ASTM D6079). Taguchi's  $L_{27}$  orthogonal array is used to evaluate the tribological properties with three control variables such as HAp volume, load applied and frequency, each at three levels. Since drilling is used to join the composite material with adjacent bone tissue in orthopaedic surgery, it is important to study drilling performance of the composite. Experiments have been conducted on a CNC milling machine using Taguchi's  $L_{27}$  design with four control variables such as HAp volume percentage, drilling

speed, feed rate and drill bit diameter, each at three levels. The responses considered are circularity at entry and exit, torque and thrust force. The circularity at both entry and exit is measured using the ratio of minimum diameter ( $D_{\min}$ ) to maximum diameter ( $D_{\max}$ ) of the drilled hole. The torque and thrust force are measured using drill dynamometer. Best parametric setting for simultaneous optimization of multiple performance measures such as circularity at entry, circularity at exit, torque and thrust in drilling operation is suggested using principal component analysis.

**Keywords:** *Hydroxyapatite; Polycarbonate; Polysulfone; Injection molding; Biocompatibility; Adaptive neuro fuzzy inference system; Drilling; X-ray diffraction; Scanning electron microscopy; Abrasion; Erosion; Sliding; Fretting; Circularity.*

# Contents

<b>Certificate of Examination</b>	<b>ii</b>
<b>Supervisor's Certificate</b>	<b>lii</b>
<b>Dedication</b>	<b>lv</b>
<b>Declaration of Originality</b>	<b>v</b>
<b>Acknowledgement</b>	<b>vi</b>
<b>Abstract</b>	<b>vii</b>
<b>Table of Contents</b>	<b>ix</b>
<b>List of Figures</b>	<b>xii</b>
<b>List of Tables</b>	<b>xvii</b>
<b>List of Abbreviations</b>	<b>xx</b>
<b>List of Symbols</b>	<b>xxi</b>
<b>Chapter 1 General Introduction</b>	<b>1</b>
1.1 Introduction	1
1.2 Bone	2
1.2.1 Structure and composition of bone	3
1.2.2 Mechanical properties of bone	5
1.2.3 Types of bone	5
1.2.4 Types of bone cells	6
1.2.5 Bone healing	6
1.2.6 Bone grafting	6
1.3 Biomaterials	7
1.3.1 Metals	7
1.3.2 Polymers	8
1.3.3 Ceramics	8
1.3.4 Requirement of biomaterial	9
1.3.5 Hydroxyapatite (HAp)	9
1.4 Concept of biocompatibility	9
1.5 Background and Motivation	10
1.6 Objectives of the research work	11
1.7 Novelty of the proposed research work	11
1.8 Organisation of the thesis	12
1.9 Conclusion	13
<b>Chapter 2 Literature Review</b>	<b>15</b>
2.1 Introduction	15
2.2 Classification of Literature	17
2.2.1 Development of hydroxyapatite (HAp) through wet chemical precipitation route	17
2.2.2 Processing and fabrication of ceramic composites	19
2.2.3 Characterization of mechanical properties of ceramic composites	21
2.2.4 Wear behaviour of ceramic composites	23
2.2.5 Machining analysis of ceramic composites	24
2.3 Critical review	24
2.4 Conclusion	26
<b>Chapter 3 Materials and Methods</b>	<b>27</b>
3.1 Introduction	27
3.2 Specifications of the materials used	27
3.3 Methods of HAp preparation	28
3.4 HAp preparation through wet chemical precipitation	31
3.5 Processing and fabrication of ceramic composites	32

3.5.1 Preparation of HAp/PC composite	32
3.5.2 Preparation of HAp/PSU composite	33
3.6 Results and discussion	34
3.6.1 Particle size analysis	34
3.6.2 XRD analysis	35
3.6.3 FTIR analysis	36
3.6.4 SEM analysis of ceramic composites	38
3.6.4.1 SEM analysis of HAp/PC composite	39
3.6.4.2 SEM analysis of HAp/PSU composite	39
3.7 Conclusion	39
<b>Chapter 4 A Study on Characterization of Mechanical Properties of Ceramic Composites</b>	<b>42</b>
4.1 Introduction	42
4.2 Density and void fraction	42
4.3 Results and discussion	43
4.3.1 Tensile load-displacement curves, tensile modulus, tensile strength, compressive strength, flexural strength, impact strength, hardness and inter-laminar shear stress	43
4.4 Conclusion	50
<b>Chapter 5 A Study on performance of Ceramic Composites under various wear modes</b>	<b>51</b>
5.1 Introduction to wear	51
5.1.1 Abrasive wear	51
5.1.2 Adhesive wear	52
5.1.3 Erosive wear	52
5.1.4 Sliding wear	52
5.1.5 Fretting wear	52
5.1.6 Tribo-chemical or corrosion wear	52
5.1.7 Surface fatigue wear	52
5.2 Results and discussion	53
5.2.1 Experimental details of two-body abrasive wear behaviour of ceramic composites	53
5.2.1.1 Prediction of abrasive wear behaviour of composites	86
5.2.1.1.1 ANFIS methodology used for HAp/PC composite (at 400 grit size)	86
5.2.1.1.2 ANFIS methodology used for HAp/PSU composite (at 400 grit size)	95
5.2.1.1.3 ANFIS methodology used for HAp/PC composite (at 600 grit size)	99
5.2.1.1.4 ANFIS methodology used for HAp/PSU composite (at 600 grit size)	102
5.2.1.1.5 ANFIS methodology used for HAp/PC composite (at 1000 grit size)	106
5.2.1.1.6 ANFIS methodology used for HAp/PSU composite (at 1000 grit size)	109
5.2.1.2 Worn surface morphology	113
5.2.2 Experimental details of erosion wear behaviour of ceramic composites	115
5.2.2.1 Prediction of erosive wear behaviour of composites	128
5.2.2.1.1 ANFIS methodology used for HAp/PC composite (at 300 micron size)	128
5.2.2.1.2 ANFIS methodology used for HAp/PSU composite (at 300 micron size)	134
5.2.2.1.3 ANFIS methodology used for HAp/PC composite (at 400 micron size)	137
5.2.2.1.4 ANFIS methodology used for HAp/PSU composite (at	141

400 micron size)	
5.2.2.1.5 ANFIS methodology used for HAp/PC composite (at 500 micron size)	144
5.2.2.1.6 ANFIS methodology used for HAp/PSU composite (at 500 micron size)	148
5.2.2.2 Worn surface morphology	151
5.2.3 Experimental details of sliding wear behaviour of ceramic composites	153
5.2.3.1 Prediction of sliding wear behaviour of composites	157
5.2.3.1.1 ANFIS methodology used for HAp/PC composite	157
5.2.3.1.2 ANFIS methodology used for HAp/PSU composite	163
5.2.3.2 Worn surface morphology	166
5.2.4 Experimental details of fretting wear behaviour of ceramic composites	168
5.2.4.1 Prediction of fretting wear behaviour of composites	175
5.2.4.1.1 ANFIS methodology used for HAp/PC composite	175
5.2.4.1.2 ANFIS methodology used for HAp/PSU composite	181
5.2.4.2 Worn surface morphology	184
5.3 Conclusion	185
<b>Chapter 6 A Study on Machining Analysis of Ceramic Composites</b>	<b>187</b>
6.1 Introduction	187
6.2 Machining parameters and their levels	187
6.3 Specifications of CNC milling machine	187
6.4 Experimental details	189
6.5 Results and discussion	190
6.5.1 Experimental data collection for HAp/PC composite	190
6.5.1.1 Prediction of optimal responses	191
6.5.1.1.1 Optimization of multiple responses	193
6.5.1.1.2 Analysis of multi-objective responses	196
6.5.2 Experimental data collection for HAp/PSU composite	197
6.5.2.1 Prediction of optimal responses	197
6.5.2.1.1 Optimization of multiple responses	199
6.5.2.1.2 Analysis of multi-objective responses	202
6.5.3 SEM of drilled holes in composites	203
6.6 Conclusion	204
<b>Chapter 7 Executive Summary and Conclusions</b>	<b>205</b>
<b>Scope for Future Research Work</b>	<b>211</b>
<b>References</b>	<b>212</b>
<b>Dissemination</b>	<b>221</b>
<b>Index</b>	<b>223</b>
<b>Curriculum vitae</b>	<b>224</b>



# List of Figures

1.1	Classification of Composites	2
1.2	Hierarchical structure of human compact bone	4
2.1	Percentage of paper reviewed	17
3.1	Flow chart of wet chemical precipitation route for HAp preparation	31
3.2	Batch Mixer	32
3.3	Micro-injection molding machine	32
3.4	An Electric Oven	33
3.5	Micro-compounder	33
3.6	Particle size analyser	34
3.7	Particle Size Distribution by Intensity of Dry Hydroxyapatite (DHAp)	34
3.8	Particle Size Distribution by Intensity of Sintered Hydroxyapatite (SHAp)	35
3.9	X-ray diffractometer	35
3.10	XRD analysis of Dry HAp	36
3.11	XRD analysis of sintered HAp	36
3.12	FTIR spectrometer	37
3.13	FTIR of dry HAp	37
3.14	FTIR of HAp (calcined at 850°C) powder pellet	38
3.15	Scanning electron microscope	38
3.16	Auto fine coater	38
3.17	SEM image of 10 vol. % HAp/PC	39
3.18	SEM image of 20 vol. % HAp/PC	39
3.19	SEM image of 10 vol. % HAp/PSU	39
3.20	SEM image of 20 vol. % HAp/PSU	39
4.1	Tensile load-displacement curve of 10 vol. % HAp/PC	44
4.2	Tensile load-displacement curve of 20 vol. % HAp/PC	44
4.3	Tensile load-displacement curve of 10 vol. % HAp/PSU	44
4.4	Tensile load-displacement curve of 20 vol. % HAp/PSU	44
4.5	Graph between Young's Modulus and HAp Volume of HAp/PC Composite	45
4.6	Graph between Young's Modulus and HAp Volume of HAp/PSU Composite	45
4.7	Graph between Tensile Strength and HAp Volume of HAp/PC Composite	45
4.8	Graph between Tensile Strength and HAp Volume of HAp/PSU Composite	45
4.9	Graph between Compressive Strength and HAp Volume of HAp/PC Composite	45
4.10	Graph between Compressive Strength and HAp Volume of HAp/PSU Composite	45
4.11	Graph between Izod Impact Strength and HAp Volume of HAp/PC Composite	46
4.12	Graph between Izod Impact Strength and HAp Volume of HAp/PSU Composite	46
4.13	Graph between Tensile Modulus of HAp/PC and HAp/PSU Composite	46
4.14	Graph between Tensile Strength of HAp/PC and HAp/PSU Composite	46
4.15	Graph between Compressive Strength of HAp/PC and HAp/PSU Composite	47
4.16	Graph between Izod Impact Strength of HAp/PC and HAp/PSU Composite	47
4.17	Graph between Micro-indentation hardness and HAp Volume of HAp/PC Composite	47
4.18	Graph between Micro-indentation hardness and HAp Volume of HAp/PSU Composite	47
4.19	Graph between Micro-indentation hardness of HAp/PC and HAp/PSU Composites	47
4.20	Graph between Flexural Strength and HAp Volume of HAp/PC Composite	47
4.21	Graph between Flexural Strength and HAp Volume of HAp/PSU Composite	48
4.22	Graph between Flexural Strength of HAp/PC and HAp/PSU Composites	48
4.23	Graph between Inter laminar shear strength and HAp Volume of HAp/PC Composite	48
4.24	Graph between Inter laminar shear strength and HAp Volume of HAp/PSU Composite	48
4.25	Graph between Inter laminar shear strength of HAp/PC and HAp/PSU Composites	48
5.1	Pin-on-disc friction and wear test rig	53
5.2	Main effects plot for means of S/N ratio	56
5.3	Normal probability plot for S/N ratio	56
5.4	Interaction plot for S/N ratio	56
5.5	Main effects plot for means of S/N ratio	59
5.6	Normal probability plot for S/N ratio	59

5.7	Interaction plot for S/N ratio	59
5.8	Load vs Wear loss (at 300 rpm on 400 grit size paper)	61
5.9	Load vs Wear loss (at 400 rpm on 400 grit size paper)	61
5.10	Load vs Wear loss (at 500 rpm on 400 grit size paper)	62
5.11	Sliding distance vs Specific wear rate (at 400 grit size paper)	62
5.12	Sliding distance vs Wear loss (at 400 grit size paper)	63
5.13	Sliding speed vs Specific wear rate (at 0 vol. % and 400 grit size paper)	63
5.14	Sliding speed vs Specific wear rate (at 10 vol. % and 400 grit size paper)	64
5.15	Sliding speed vs Specific wear rate (at 20 vol. % and 400 grit size paper)	64
5.16	Sliding speed vs Wear loss (at 0 vol. % and 400 grit size paper)	65
5.17	Sliding speed vs Wear loss (at 10 vol. % and 400 grit size paper)	65
5.18	Sliding speed vs Wear loss (at 20 vol. % and 400 grit size paper)	66
5.19	Specific wear rate vs. Load (at 0 vol. % at 400 grit size paper)	66
5.20	Specific wear rate vs. Load (at 10 vol. % at 400 grit size paper)	67
5.21	Specific wear rate vs. Load (at 20 vol. % at 400 grit size paper)	67
5.22	Sliding Distance vs. COF (at 400 grit size paper)	68
5.23	Main effects plot for means of S/N ratio	69
5.24	Normal probability plot for S/N ratio	69
5.25	Interaction plot for S/N ratio	70
5.26	Main effects plot for means of S/N ratio	72
5.27	Normal probability plot for S/N ratio	72
5.28	Interaction plot for S/N ratio	72
5.29	Load vs Wear loss (at 300 rpm on 600 grit size paper)	74
5.30	Load vs Wear loss (at 400 rpm on 600 grit size paper)	74
5.31	Load vs Wear loss (at 500 rpm on 600 grit size paper)	75
5.32	Sliding distance vs Wear loss (at 600 grit size paper)	75
5.33	Sliding distance vs Specific wear rate (at 600 grit size paper)	76
5.34	Sliding Distance vs. COF (at 600 grit size paper)	76
5.35	Main effects plot for means of S/N ratio	78
5.36	Normal probability plot for S/N ratio	78
5.37	Interaction plot for S/N ratio	78
5.38	Main effects plot for means of S/N ratio	81
5.39	Normal probability plot for S/N ratio	81
5.40	Interaction plot for S/N ratio	81
5.41	Load vs Wear loss (at 300 rpm on 1000 grit size paper)	83
5.42	Load vs Wear loss (at 400 rpm on 1000 grit size paper)	83
5.43	Load vs Wear loss (at 500 rpm on 1000 grit size paper)	84
5.44	Sliding distance vs Wear loss (at 1000 grit size paper)	84
5.45	Sliding distance vs Specific wear rate (at 1000 grit size paper)	85
5.46	Sliding Distance vs. COF (at 1000 grit size paper)	85
5.47	A typical architecture of ANFIS system	86
5.48	Flow chart of ANFIS model	88
5.49	FIS editor	89
5.50	Membership function editor of Input 1	89
5.51	Membership function editor of Input 2	90
5.52	Membership function editor of Input 3	90
5.53	Membership function editor of Input 4	91
5.54	Membership function editor for output of HAp/PC composite	91
5.55	ANFIS model structure	92
5.56	Distribution of predicted and actual data (Training)	92
5.57	Distribution of predicted and actual data (Testing)	93
5.58	Rule editor	93
5.59	Rule viewer	94
5.60	Membership function editor for output of HAp/PSU composite	95
5.61	Distribution of predicted and actual data (Training)	96
5.62	Distribution of predicted and actual data (Testing)	96
5.63	Rule editor	97
5.64	Rule viewer	97
5.65	Membership function editor for output of HAp/PC composite	99
5.66	Distribution of predicted and actual data (Training)	99

5.67	Distribution of predicted and actual data (Testing)	100
5.68	Rule editor	100
5.69	Rule viewer	101
5.70	Membership function editor for output of HAp/PSU composite	102
5.71	Distribution of predicted and actual data (Training)	103
5.72	Distribution of predicted and actual data (Testing)	103
5.73	Rule editor	104
5.74	Rule viewer	104
5.75	Membership function editor for output of HAp/PC composite	106
5.76	Distribution of predicted and actual data (Training)	106
5.77	Distribution of predicted and actual data (Testing)	107
5.78	Rule editor	107
5.79	Rule viewer	108
5.80	Membership function editor for output of HAp/PSU composite	109
5.81	Distribution of predicted and actual data (Training)	110
5.82	Distribution of predicted and actual data (Testing)	110
5.83	Rule editor	111
5.84	Rule viewer	111
5.85	Abrasive wear of 0 vol. % HAp/PC composite at the magnification of $\times 100$	113
5.86	Abrasive wear of 10 vol. % HAp/PC composite at the magnification of $\times 100$	113
5.87	Abrasive wear of 20 vol. % HAp/PC composite at the magnification of $\times 100$	113
5.88	Abrasive wear of 0 vol. % HAp/PSU composite at the magnification of $\times 100$	113
5.89	Abrasive wear of 10 vol. % HAp/PSU composite at the magnification of $\times 100$	113
5.90	Abrasive wear of 20 vol. % HAp/PSU composite at the magnification of $\times 100$	113
5.91	Air jet erosion test rig	115
5.92	Air compressor	115
5.93	Accelerating chamber	115
5.94	Main effects plot for means of S/N ratio	117
5.95	Normal probability plot for S/N ratio	117
5.96	Interaction plot for S/N ratio	117
5.97	Main effects plot for means of S/N ratio	119
5.98	Normal probability plot for S/N ratio	119
5.99	Interaction plot for S/N ratio	119
5.100	Main effects plot for means of S/N ratio	121
5.101	Normal probability plot for S/N ratio	121
5.102	Interaction plot for S/N ratio	121
5.103	Main effects plot for means of S/N ratio	123
5.104	Normal probability plot for S/N ratio	123
5.105	Interaction plot for S/N ratio	123
5.106	Main effects plot for means of S/N ratio	125
5.107	Normal probability plot for S/N ratio	125
5.108	Interaction plot for S/N ratio	125
5.109	Main effects plot for means of S/N ratio	125
5.110	Normal probability plot for S/N ratio	127
5.111	Interaction plot for S/N ratio	127
5.112	FIS editor	128
5.113	Membership function editor of Input 1	128
5.114	Membership function editor of Input 2	129
5.115	Membership function editor of Input 3	129
5.116	Membership function editor for output of HAp/PC composite	130
5.117	ANFIS model structure	130
5.118	Distribution of predicted and actual data (Training)	131
5.119	Distribution of predicted and actual data (Testing)	131
5.120	Rule editor	132
5.121	Rule viewer	132
5.122	Membership function editor for output of HAp/PSU composite	134
5.123	Distribution of predicted and actual data (Training)	134
5.124	Distribution of predicted and actual data (Testing)	135
5.125	Rule editor	135
5.126	Rule viewer	136

5.127	Membership function editor for output of HAp/PC composite	137
5.128	Distribution of predicted and actual data (Training)	138
5.129	Distribution of predicted and actual data (Testing)	138
5.130	Rule editor	139
5.131	Rule viewer	139
5.132	Membership function editor for output of HAp/PSU composite	141
5.133	Distribution of predicted and actual data (Training)	141
5.134	Distribution of predicted and actual data (Testing)	142
5.135	Rule editor	142
5.136	Rule viewer	143
5.137	Membership function editor for output of HAp/PC composite	144
5.138	Distribution of predicted and actual data (Training)	145
5.139	Distribution of predicted and actual data (Testing)	145
5.140	Rule editor	146
5.141	Rule viewer	146
5.142	Membership function editor for output of HAp/PSU composite	148
5.143	Distribution of predicted and actual data (Training)	148
5.144	Distribution of predicted and actual data (Testing)	149
5.145	Rule editor	149
5.146	Rule viewer	150
5.147	Erosive wear of 0 vol. % HAp/PC composite at the magnification of x50	151
5.148	Erosive wear of 10 vol. % HAp/PC composite at the magnification of x50	151
5.149	Erosive wear of 20 vol. % HAp/PC composite at the magnification of x50	151
5.150	Erosive wear of 0 vol. % HAp/PSU composite at the magnification of x50	152
5.151	Erosive wear of 10 vol. % HAp/PSU composite at the magnification of x50	152
5.152	Erosive wear of 20 vol. % HAp/PSU composite at the magnification of x50	152
5.153	Ball on plate wear tester	153
5.154	Main effects plot for means of S/N ratio	154
5.155	Normal probability plot for S/N ratio	154
5.156	Interaction plot for S/N ratio	154
5.157	Main effects plot for means of S/N ratio	156
5.158	Normal probability plot for S/N ratio	156
5.159	Interaction plot for S/N ratio	156
5.160	FIS editor	157
5.161	Membership function editor of Input 1	157
5.162	Membership function editor of Input 2	158
5.163	Membership function editor of Input 3	158
5.164	Membership function editor for output of HAp/PC composite	159
5.165	ANFIS model structure	159
5.166	Distribution of predicted and actual data (Training)	160
5.167	Distribution of predicted and actual data (Testing)	160
5.168	Rule editor	161
5.169	Rule viewer	161
5.170	Membership function editor for output of HAp/PSU composite	163
5.171	Distribution of predicted and actual data (Training)	163
5.172	Distribution of predicted and actual data (Testing)	164
5.173	Rule editor	164
5.174	Rule viewer	165
5.175	Sliding wear of 0 vol. % HAp/PC composite at the magnification of x50	166
5.176	Sliding wear of 10 vol. % HAp/PC composite at the magnification of x50	166
5.177	Sliding wear of 20 vol. % HAp/PC composite at the magnification of x50	166
5.178	Sliding wear of 0 vol. % HAp/PSU composite at the magnification of x50	167
5.179	Sliding wear of 10 vol. % HAp/PSU composite at the magnification of x50	167
5.180	Sliding wear of 20 vol. % HAp/PSU composite at the magnification of x50	167
5.181	High frequency reciprocating rig (HFRR) and their parts	168
5.182	Main effects plot for means of S/N ratio	170
5.183	Normal probability plot for S/N ratio	170
5.184	Interaction plot for S/N ratio	170
5.185	Main effects plot for means of S/N ratio	172
5.186	Normal probability plot for S/N ratio	172

5.187	Interaction plot for S/N ratio	172
5.188	COF of 0 vol. % HAp/PC composite loaded at 2N and 60 Hz frequency	173
5.189	COF of 10 vol. % HAp/PC composite loaded at 4N and 50 Hz frequency	173
5.190	COF of 20 vol. % HAp/PC composite loaded at 5N and 40 Hz frequency	173
5.191	COF of 0 vol. % HAp/PSU composite loaded at 2N and 60 Hz frequency	174
5.192	COF of 10 vol. % HAp/PSU composite loaded at 4N and 50 Hz frequency	174
5.193	COF of 20 vol. % HAp/PSU composite loaded at 5N and 40 Hz frequency	174
5.194	FIS editor	175
5.195	Membership function editor of Input 1	175
5.196	Membership function editor of Input 2	176
5.197	Membership function editor of Input 3	176
5.198	Membership function editor for output of HAp/PC composite	177
5.199	ANFIS model structure	177
5.200	Distribution of predicted and actual data (Training)	178
5.201	Distribution of predicted and actual data (Testing)	178
5.202	Rule editor	179
5.203	Rule viewer	179
5.204	Membership function editor for output of HAp/PSU composite	181
5.205	Distribution of predicted and actual data (Training)	181
5.206	Distribution of predicted and actual data (Testing)	182
5.207	Rule editor	182
5.208	Rule viewer	183
5.209	Fretting wear of 0 vol. % HAp/PC at the magnification of $\times 50$	184
5.210	Fretting wear of 10 vol. % HAp/PC at the magnification of $\times 50$	184
5.211	Fretting wear of 20 vol. % HAp/PC at the magnification of $\times 50$	184
5.212	Fretting wear of 0 vol. % HAp/PSU at the magnification of $\times 50$	185
5.213	Fretting wear of 10 vol. % HAp/PSU at the magnification of $\times 50$	185
5.214	Fretting wear of 20 vol. % HAp/PSU at the magnification of $\times 50$	185
6.1	CNC Maxmill Machine	189
6.2	Drilling of composites	189
6.3	Main effects plot for means of torque	191
6.4	Main effects plot for means of load	191
6.5	Main effects plot for means of circularity at entry	192
6.6	Main effects plot for means of circularity at entry	192
6.7	Main effects plot for MPI	196
6.8	Main effects plot for means of torque	198
6.9	Main effects plot for means of load	198
6.10	Main effects plot for means of circularity at entry	199
6.11	Main effects plot for means of circularity at entry	199
6.12	Main effects plot for MPI	202
6.13	SEM of 0 vol. % HAp/PC (15 $\times$ ) at drilling speed of 500 rpm, feed rate of 50 mm/min, and 4 mm drill bit diameter	203
6.14	SEM of 10 vol. % HAp/PC (15 $\times$ ) at drilling speed of 1000 rpm, feed rate of 60 mm/min, and 6 mm drill bit diameter	203
6.15	SEM of 20 vol. % HAp/PC (15 $\times$ ) at drilling speed of 1500 rpm, feed rate of 70 mm/min, and 8 mm drill bit diameter	203
6.16	SEM of 0 vol. % HAp/PSU (15 $\times$ ) at drilling speed of 500 rpm, feed rate of 50 mm/min, and 4 mm drill bit diameter	203
6.17	SEM of 10 vol. % HAp/PSU (15 $\times$ ) at drilling speed of 1000 rpm, feed rate of 60 mm/min, and 6 mm drill bit diameter	203
6.18	SEM of 20 vol. % HAp/PSU (15 $\times$ ) at drilling speed of 1500 rpm, feed rate of 70 mm/min, and 8 mm drill bit diameter	204

# List of Tables

1.1	Composition of bone	5
1.2	Metals used for implants	7
1.3	Polymers used in biomedical applications	8
1.4	Ceramics used in biomedical applications	9
1.5	Classification of interactions of implants with hard tissue	10
2.1	Summary of publications referred	15-16
4.1	Theoretical density, actual density and volume fraction of voids	43
4.2	Specification of Machines used for Testing	49
5.1	Control parameters and their levels	54
5.2	Experimental data for HAp/PC composite conducted at 400 grit size paper	55
5.3	ANOVA Table for S/N ratio of HAp/PC composite	55
5.4	Calculation data for HAp/PC composite conducted at 400 grit size paper	57
5.5	Experimental data for HAp/PSU composite conducted at 400 grit size paper	58
5.6	ANOVA table for S/N ratio of HAp/PC composite	58
5.7	Calculation data for HAp/PSU composite conducted at 400 grit size paper	60
5.8	Experimental data for HAp/PC composite conducted at 600 grit size paper	68
5.9	ANOVA table for S/N ratio of HAp/PC composite	69
5.10	Calculation data for HAp/PC composite conducted at 600 grit size paper	70
5.11	Experimental data for HAp/PSU composite conducted at 600 grit size paper	71
5.12	ANOVA table for S/N ratio of HAp/PSU composite	71
5.13	Calculation data for HAp/PSU composite conducted at 600 grit size paper	73
5.14	Experimental data for HAp/PC composite conducted at 1000 grit size paper	77
5.15	ANOVA table for S/N ratio of HAp/PC composite	77
5.16	Calculation data for HAp/PC composite conducted at 1000 grit size paper	79
5.17	Experimental data for HAp/PSU composite conducted at 1000 grit size paper	80
5.18	ANOVA table for S/N ratio of HAp/PSU composite	80
5.19	Calculation data for HAp/PSU composite conducted at 1000 grit size paper	82
5.20	Input and output data with ANFIS predicted value of HAp/PC composite at 400 grit size (Training)	94
5.21	Input and output data with ANFIS predicted value of HAp/PC composite at 400 grit size (Testing))	95
5.22	Input and output data with ANFIS predicted value of HAp/PSU composite at 400 grit size (Training)	98
5.23	Input and output data with ANFIS predicted value of HAp/PSU composite at 400 grit size (Testing)	98
5.24	Input and output data with ANFIS predicted value of HAp/PC composite at 600 grit size (Training)	101
5.25	Input and output data with ANFIS predicted value of HAp/PC composite at 600 grit size (Testing)	102
5.26	Input and output data with ANFIS predicted value of HAp/PSU composite at 600 grit size (Training)	105
5.27	Input and output data with ANFIS predicted value of HAp/PSU composite at 600 grit size (Testing)	105
5.28	Input and output data with ANFIS predicted value of HAp/PC composite at 1000 grit size (Training)	108
5.29	Input and output data with ANFIS predicted value of HAp/PC composite at 1000 grit size (Testing)	109
5.30	Input and output data with ANFIS predicted value of HAp/PSU composite at 1000 grit size (Training)	112
5.31	Input and output data with ANFIS predicted value of HAp/PSU composite at 1000 grit size (Testing)	112
5.32	Control parameters and their levels	115
5.33	Experimental data for HAp/PC composite conducted at 300µm erodent particle size	116
5.34	ANOVA Table for S/N ratio of HAp/PC composite	116
5.35	Experimental data for HAp/PSU composite conducted at 300µm erodent particle size	118

5.36	ANOVA Table for S/N ratio of HAp/PSU composite	118
5.37	Experimental data for HAp/PC composite conducted at 400µm erodent particle size	120
5.38	ANOVA Table for S/N ratio of HAp/PC composite	120
5.39	Experimental data for HAp/PSU composite conducted at 400µm erodent particle size	122
5.40	ANOVA Table for S/N ratio of HAp/PSU composite	122
5.41	Experimental data for HAp/PC composite conducted at 500µm erodent particle size	124
5.42	ANOVA Table for S/N ratio of HAp/PC composite	124
5.43	Experimental data for HAp/PSU composite conducted at 500µm erodent particle size	126
5.44	ANOVA Table for S/N ratio of HAp/PSU composite	126
5.45	Input and output data with ANFIS predicted value of HAp/PC composite at 300 micron size (Training)	133
5.46	Input and output data with ANFIS predicted value of HAp/PC composite at 300 micron size (Testing)	133
5.47	Input and output data with ANFIS predicted value of HAp/PSU composite at 300 micron size (Training)	136
5.48	Input and output data with ANFIS predicted value of HAp/PSU composite at 300 micron size (Testing)	137
5.49	Input and output data with ANFIS predicted value of HAp/PC composite at 400 micron size (Training)	140
5.50	Input and output data with ANFIS predicted value of HAp/PC composite at 400 micron size (Testing)	140
5.51	Input and output data with ANFIS predicted value of HAp/PSU composite at 400 micron size (Training)	143
5.52	Input and output data with ANFIS predicted value of HAp/PSU composite at 400 micron size (Testing)	144
5.53	Input and output data with ANFIS predicted value of HAp/PC composite at 500 micron size (Training)	147
5.54	Input and output data with ANFIS predicted value of HAp/PC composite at 500 micron size (Testing)	147
5.55	Input and output data with ANFIS predicted value of HAp/PSU composite at 500 micron size (Training)	150
5.56	Input and output data with ANFIS predicted value of HAp/PSU composite at 500 micron size (Testing)	151
5.57	Control parameters and their levels	153
5.58	Experimental data for HAp/PC composite	153
5.59	ANOVA Table for S/N ratio of HAp/PC composite	154
5.60	Experimental data for HAp/PSU composite	155
5.61	ANOVA Table for S/N ratio of HAp/PSU composite	155
5.62	Input and output data with ANFIS predicted value of HAp/PC composite (Training)	162
5.63	Input and output data with ANFIS predicted value of HAp/PC composite (Testing)	162
5.64	Input and output data with ANFIS predicted value of HAp/PSU composite (Training)	165
5.65	Input and output data with ANFIS predicted value of HAp/PSU composite (Testing)	166
5.66	Control parameters and their levels	168
5.67	Experimental data for HAp/PC composite	169
5.68	ANOVA Table for S/N ratio of HAp/PC composite	169
5.69	Experimental data for HAp/PSU composite	171
5.70	ANOVA Table for S/N ratio of HAp/PSU composite	171
5.71	Input and output data with ANFIS predicted value of HAp/PC composite (Training)	180
5.72	Input and output data with ANFIS predicted value of HAp/PC composite (Testing)	180
5.73	Input and output data with ANFIS predicted value of HAp/PSU composite (Training)	183
5.74	Input and output data with ANFIS predicted value of HAp/PSU composite (Testing)	184
6.1	Control parameters and their levels	187

6.2	Machine specifications	188
6.3	X-Axis drive data	188
6.4	Y-Axis drive data	188
6.5	Z-Axis drive data	188
6.6	Electrical Specification	189
6.7	Specification of Spindle Motor	189
6.8	Specification of X, Y & Z Axis Drive	189
6.9	Drill bit Specification	189
6.10	Collection of data for both circularity at entry and exit, torque and load of HAp/PC composite	190
6.11	ANOVA Table for Torque	191
6.12	ANOVA Table for Load	191
6.13	ANOVA Table for circularity at entry	192
6.14	ANOVA Table for circularity at exit	192
6.15	Eigen value, proportion, cumulative and eigen vector for all components	194
6.16	Normalized values of responses, principal components and MPI values	195
6.17	ANOVA Table for MPI	196
6.18	Collection of data for both circularity at entry and exit, torque and load of HAp/PC composite	197
6.19	ANOVA Table for Torque	197
6.20	ANOVA Table for Load	198
6.21	ANOVA Table for circularity at entry	198
6.22	ANOVA Table for circularity at exit	199
6.23	Eigen value, proportion, cumulative and eigen vector for all components	200
6.24	Normalized values of responses, principal components and MPI values	201
6.25	ANOVA Table for MPI	202



# List of Abbreviations

HAp	Hydroxyapatite
PC	Polycarbonate
PSU	Polysulfone
ANFIS	Adaptive neuro fuzzy inference system
XRD	X-ray diffraction
FTIR	Fourier transform infrared
SEM	Scanning electron microscope
CMC	Ceramic matrix composites
PMC	Polymer matrix composites
MMC	Metal matrix composites
PP	Polypropylene
HDPE	High density polyethylene
UHMWPE	Ultra high molecular weight polyethylene
EVA	Ethylene vinyl acetate
PLA	Polylactic acid
PEEK	Polyetheretherketone
PA	Polyhexamethyleneapdamide
PMMA	Polymethylmethacrylate
CNC	Computer numeric control
ANOVA	Analysis of variance
PCA	Principal component analysis
TCP	Tri calcium phosphate
TEM	Transmission electron microscopy
PHB	Polyhydroxybutyrate
PHV	Polyhydroxyvalerate
PLGA	Polylactic-co-Glycolic acid
nHAp	Nano-hydroxyapatite
COF	Coefficient of friction
PI	Polyimide
MRR	Material removal rate
ASTM	American society for testing and materials
DHAp	Dry hydroxyapatite
SHAp	Sintered hydroxyapatite
ILSS	Inter laminar shear stress
MPI	Multi performance index

Note: The abbreviations other than above have been explained in the text.

# List of Symbols

SiC	Silicon carbide
CaP	Calcium phosphate
Ca(OH) <sub>2</sub>	Calcium hydroxide
H <sub>3</sub> PO <sub>4</sub>	Ortho phosphoric acid
CaO	Calcium oxide
pH	Power of hydrogen
Ca	Calcium
P	Phosphorous
KBr	Potassium bromide
L <sub>27</sub>	Orthogonal array
Ca <sub>10</sub> (PO <sub>4</sub> ) <sub>6</sub> (OH) <sub>2</sub>	Hydroxyapatite
ρ <sub>ct</sub>	Theoretical density of composites materials
V	Volume fraction
ρ	Density
ρ <sub>ca</sub>	Actual density of composite materials
V <sub>v</sub>	Volume fraction of voids
p	Pressure
b	Width of the specimen
t	Thickness of the specimen
L	Load
d	Sliding distance
S/N	Signal to noise ratio
LTB	Lower the Better
r	Track radius
t	Time

Note: The symbols other than above have been explained in the text.

## Chapter 1

# General Introduction

## 1.1 Introduction

A composite can be defined as a material having two or more chemically distinct phases, which at the microscopic scale are separated by a distinct interface. A composite exhibits a combination of properties of two or more components held together by the same type of matrix. In essence, a composite possesses superior properties than the individual constituents. (According to Kannan et al. [1]) A composite has light weight, high strength to weight ratio and stiffness properties and replaces the conventional materials such as metals and wood. The classification of composites is presented in Figure 1.1. (According to Ramakrishna et al. [2]) Composites can be mainly categorized on the basis of matrix and type of reinforcement. The classifications according to matrix type are ceramic matrix composites (CMC), polymer matrix composites (PMC) and metal matrix composites (MMC). The classifications according to type of reinforcement are particulate composites (composed of particles), fibrous composites (composed of fibres) and laminate composites (composed of laminates). Fibrous composites can be further divided on the basis of natural / biofibre or synthetic fibre. Biofibre encompassing composites are referred to as biocomposites. Biocomposites can be again divided on the basis of matrix i.e. non-biodegradable matrix and biodegradable matrix. Biocomposites made from natural/biofibre and biodegradable polymers are referred to as green composites. These can be further divided as hybrid composites and textile composites. Hybrid composites comprise of a combination of two or more types of fibres.

In fibrous composites, fibres are the load carrying members while the surrounding matrix keeps them in desired location and orientation. (According to Meredith [3]) The matrix acts as a load transfer medium, provides shape to the composite structure and protects the fibres from environmental damage. The matrix also gives toughness and compressional strength to the composite. The selection of suitable fibres is determined by the required value of stiffness and tensile strength of the composite. Other deciding factors are thermal stability, adhesion of fibres and matrix, dynamic and long term behaviour, price and processing costs.

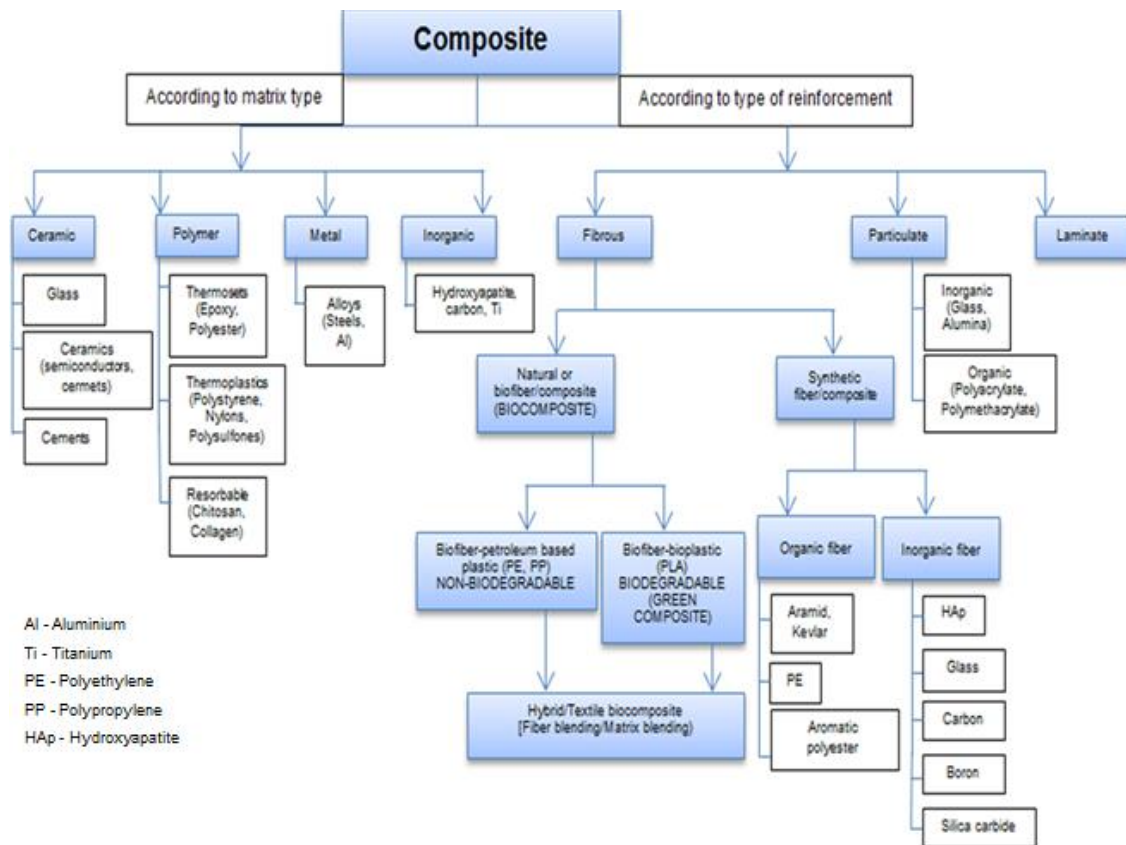


Figure 1.1 Classification of Composites

## 1.2 Bone

(According to Amini et al. [4]) Bone is the primary mineralized tissue in mammalian bodies whose main function is “load-carrying”. (According to Bauer et al. [5]) The major constituents of bone tissues are minerals, organic material and water; the organic material is mainly collagen and the mineral is mainly hydroxyapatite ( $\text{Ca}_{10}(\text{PO}_4)_6(\text{OH})_2$ ) which accounts for 69% of the weight of the bone. Collagen makes bones flexible (elastic), mineral makes bones rigid, and water in the interstitial space stores nutrients. It is very much similar to a composite material being made up of a collagen fiber matrix stiffened by HAp crystals. (According to Sarkar et al. [6]) The strength of bone is higher than both of its constituents. The softer component in the bone prevents the stiff one from brittle cracking while the stiff component prevents the soft one from yielding.

(According to Dorozhkin [7]) HAp reinforced polymer composites have been developed in recent years as analogue materials for bone replacement, adhesive bone cements and degradable internal fixation devices. (According to Hribar et al. [8]) In recent years, HAp/PP (Polypropylene), HAp/HDPE (High density poly ethylene), HAp/Ultra high molecular weight polyethylene (UHMWPE), HAp/Ethylene vinyl acetate (EVA), HAp/Poly lactic acid (PLA), HAp/PEEK (Polyetheretherketone) and nano-HAp/Poly hexamethyleneapideamide (PA) composite materials have been developed as bone

substitute materials. Among several candidate polymers, synthetic biocompatible polymers including Ultra High Molecular Weight Poly Ethylene (UHMWPE), Polyetheretherketone (PEEK) and High Density Poly Ethylene (HDPE) have been successfully reinforced with bioactive HAp for replacement or healing of bone.

(According to Ramesh et al. [9]) The motivation behind making such composites is to strengthen the polymer and enhance the bone holding properties of the material since it has been found that including HAp into a polymer grid may transform an at first non-bioactive polymer into a bone holding composite and may at the same time enhance the mechanical properties. The interfacial holding amongst inorganic and natural stage assumes a critical part in deciding definitive mechanical properties of the composites. A solid interfacial holding between the two stages typically is important for the composites to accomplish better mechanical properties.

To carry out the experimental work in this research study, HAp is mixed with Polycarbonate (PC) and Polysulfone (PSU) polymers with different volume percentage. The resulting composite material is injection molded to prepare standard tensile, compressive, impact and flexural test specimens. Thereafter, mechanical properties of the prepared specimens are examined. (According to Kalita et al. [10]) Traditionally, metallic materials such as stainless steel, titanium alloys and cobalt-chromium alloys have been widely used as bone implants in orthopedic applications. (According to Sarkar et al. [6]) Ceramic reinforced HAp polymer composites for different load-bearing orthopedic applications have been developed recently.

### **1.2.1 Structure and composition of bone**

Outlining a manufactured material which is devoted to effectively supplant tissue in a living being, the length sizes of the key auxiliary order must be considered into record. (According to Zhou and Lee [11]) The progressive structure of tissue in the living creature traverses roughly eight requests i.e. beginning at the sub-atomic scale to plainly visible level. This implies for designing fitting manufactured materials for the utilization as a biomedical material framework, the entire length scale from the nanoscale upto macroscale should be considered.

(According to Bauer et al. [5]) Human bone is a characteristic composite which can be depicted as takes after. Beginning from the naturally visible shape, it displays a rich progressive structure as appeared in Figure 1.2. On the microstructural level, one can watch osteons, which are extensive (200  $\mu\text{m}$  distance across) empty strands made out of concentric lamellae and of pores. (According to Garnette and Dieppe [12]) The lamellae are made of filaments, and these strands contain fibrils. At the ultra-basic level of the nanoscale, the filaments are a composite of the mineral hydroxyapatite (HAp) and the protein collagen. These nanoscale building pieces created through self-get together yield

a settled structure. These settled structures themselves might be shaped without anyone else get together, regularly with the assistance of cells. In the field of implantology, comprehension the various leveled structures of bone is a fundamental matter to at long last acquire embed materials that fit to given basic requests.

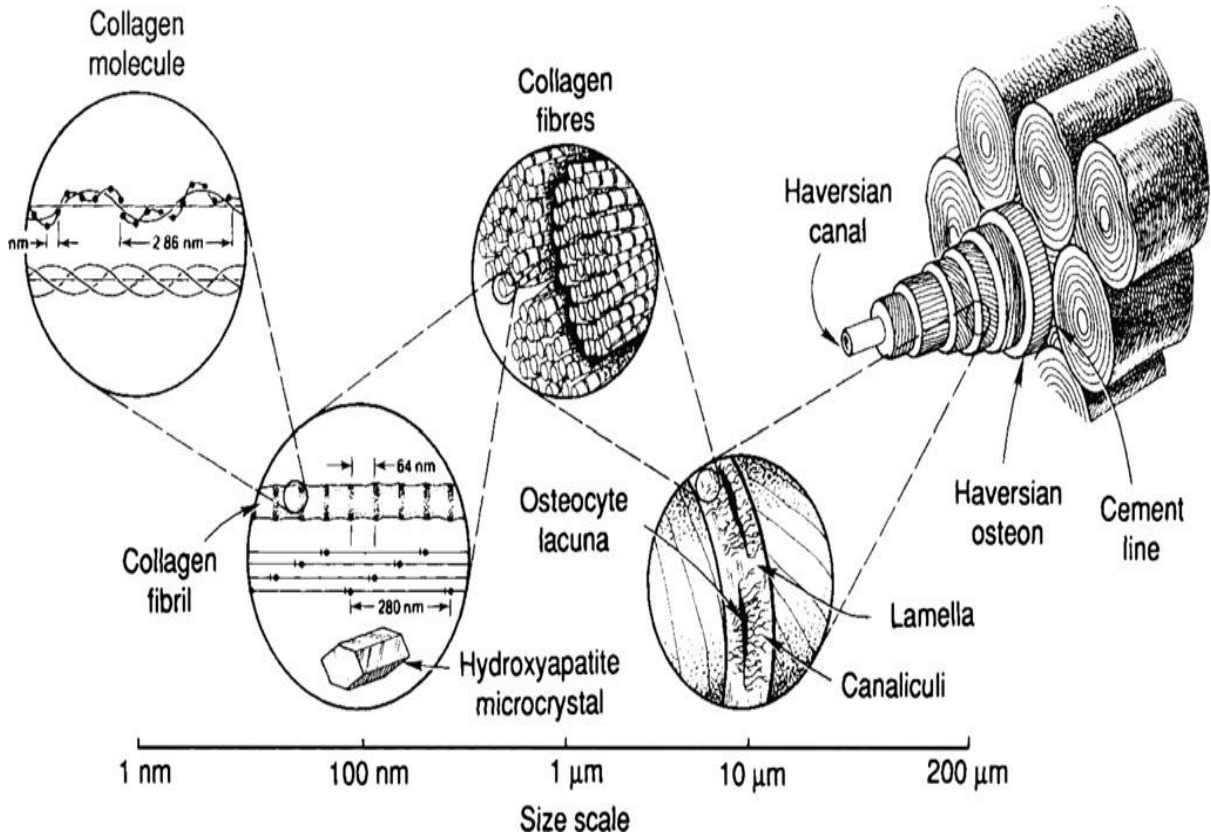


Figure 1.2 Hierarchical structure of human compact bone [5]

The length scales in multiscale living life form can be coordinated with manufactured materials. The essential synthetic structure of materials at the length size of bonds can emphatically be affected by the decision of the material. The similarity of an embed material is firmly controlled by the essential compound structure.

The higher request in the mass structure (1-100 nm) of materials can be used to tailor tissue particular properties of inserts, as the precious stone structure for controlled degeneration of polymers, the short range request of free system structures as found in bioactive glasses, or the self-get together of amphiphilic atoms as utilized as a part of the liposomal sedate conveyance frameworks. The structure at the micrometer level ( $>1 \mu\text{m}$ ) of materials bears another variable in the connection between's the impacts of length scale on the properties of the material and the impact on the tissue. Grain measure impacts or second stage encourages can influence quality, flexibility or wear resistance and metallurgical strategies can be utilized to change these properties. Another component that assumes an imperative part at the micron-size of embed materials is the nearness of porosity, cavities or channels that may permit a controlled ingrowth of tissue

into the artificially shaped material. Subsequently not just an all-around interlinked association between the artificially framed material and the tissue from the living creature can be shaped additionally implies for the ingrowth of veins (vascularization) can be given. The creation of bone is given in Table 1.1.

Table 1.1 Composition of bone

S.No.	Component	Weight Percentage
1	<i>Hydroxyapatite (HAp)</i>	69%
2	<i>Organic matrix (such as collagen, other organic matter)</i>	22%
3	<i>Water</i>	9%

### 1.2.2 Mechanical properties of bone

(According to Garnette and Dieppe [12]) The essential tissue of bone, rigid tissue, is a generally hard and lightweight composite material. It is for the most part comprised of a composite material fusing the mineral (calcium phosphate) in the compound plan named calcium hydroxyapatite (this is the bony tissue that gives bones their unbending nature) and collagen (a versatile protein which enhances break resistance).

It has as of now moderately high compressive quality of around 170 MPa however poor rigidity of 104-121 MPa and low shear quality 51.6 MPa, which means it opposes pushing powers well, yet not pulling or torsional powers.

While bone is basically fragile, it has a critical level of versatility, contributed primarily by collagen. All bones comprise of living or dead cells installed in the mineralized natural framework that makes up the bony tissue. Bone is not a consistently strong material, but instead has a few spaces between its hard components.

### 1.2.3 Types of bone

Bones are classified into two categories namely cortical (compact or dense) bone and cancellous (trabecular or spongy). The hard outer layer of bones is composed of compact bone tissue, so called due to its minimal gaps and spaces. Its porosity is 5 to 30%. This tissue gives bones their smooth, white, and solid appearance, and accounts for 80% of the total bone mass of an adult skeleton. (According to Garnette and Dieppe [12]) Filling the interior of the bone is the trabecular bone, which is composed of a network of rod and plate like elements that make the overall organ lighter and allow room for blood vessels. Its porosity is 30 to 90% and accounts for 20% of total bone mass but has nearly ten times the surface area of compact bone. The microscopic difference between compact and cancellous bone is that compact bone consists of haversian sites and osteons, while cancellous bones do not. Also, bone surrounds blood in the compact bone, while blood surrounds bone in the cancellous bone.

### **1.2.4 Types of bone cells**

Cells in our bones are responsible for bone production, maintenance and modelling. Mainly there are three types of bone cells, which can be classified according to their functions.

Osteoblasts are gotten from mesenchymal undifferentiated cells and are in charge of bone lattice combination and its ensuing mineralization. In the grown-up skeleton, the larger part of bone surfaces that are not experiencing development or resorption are lined by bone covering cells. Osteocytes are osteoblasts that get to be distinctly consolidated inside the recently framed osteoid, which in the long run gets to be calcified bone. Osteocytes arranged somewhere down in bone framework keep up contact with recently fused osteocytes in osteoid, and with osteoblasts and bone coating cells on the bone surfaces. They are thought to be in a perfect world arranged to react to changes in physical strengths upon bone and to transduce messages to cells on the bone surface, guiding them to start resorption or development reactions. Osteoclasts are extensive multinucleated cells, similar to macrophages, got from the hematopoietic ancestry. Osteoclasts work in the resorption of mineralized tissue and are discovered connected deep down surface at locales of dynamic bone resorption.

### **1.2.5 Bone healing**

All broken bones go through the same healing process. The bone healing process has three overlapping stages i.e. inflammation, bone production, and bone remodelling.

Inflammation starts immediately after the bone is fractured. When the bone is fractured there is bleeding into the area, leading to inflammation and clotting of blood at the fracture site. This provides the initial structural stability and framework for producing new bone. Bone production begins when the clotted blood formed by inflammation is replaced with fibrous tissue and cartilage. As the healing progresses, the cartilage is replaced with hard bone. In remodelling, bone continues to form and becomes compact, returning to its original shape. In addition to this, the blood circulation in the area improves.

### **1.2.6 Bone grafting**

Bone joining is a surgical procedure that replaces missing bone all together bone cracks that are to a great degree complex, represent a critical wellbeing danger to the patient, or neglect to mend legitimately. Bone for the most part can recover totally yet requires a little break space or some kind of framework to do as such. Bone unions might be autologous (bone gathered from the patient's own body), allograft (bone more often than not acquired from bone bank), or engineered (frequently made of hydroxyapatite or other actually happening and biocompatible substances) with comparative mechanical properties to bone. Most bone unions are required to be reabsorbed and supplanted as



the characteristic bone mends over a couple of months' chance. Autologous or autogenous bone uniting includes using bone got from a similar individual accepting the join. At the point when a piece join will be performed, autogenous bone is the most favored in light of the fact that there is a less danger of the unite dismissal on the grounds that the join began from the patient's own particular body. Allograft is reaped from an individual other than the one getting the unite. Allograft bone is taken from dead bodies that have given their bone with the goal that it can be utilized for living individuals who need it. Manufactured bone can be made from ceramics, for example, calcium phosphates (i.e. hydroxyapatite, tricalcium phosphate), bioglass and calcium sulphate, all of which bioactive to various degrees are relying upon solvency in the physiological environment. These materials can be treated with development components, particles, for example, strontium or blended with bone marrow to increment biological activity. This technique is less compared to autogenous bone joining however disease and dismissal of the graft is substantially less of a hazard.

### 1.3 Biomaterials

Biomaterials are ordinarily portrayed as materials used to develop manufactured organs, recovery gadgets, or inserts to supplant characteristic body tissues. More particular, biomaterials are materials that are utilized as a part of close or direct contact with the body to enlarge or supplant defective materials.

It is one of the essential parts of the biomaterials pro to pick fitting materials for a particular application. By and large, materials fall into three classifications metals, polymers and ceramics.

#### 1.3.1 Metals

Metals are inorganic materials possessing non-directional metallic bonds with highly mobile electrons. In addition to their ability to conduct electricity, metals are strong and relatively easily formed into complex shapes. Implants based on metals are mainly used in two fields of application either for the total joint replacement as hip, knee or shoulder, or for the fixation of fractures or vessels in the form of nails, screws, or stents. A list of commonly used biomedical applications of metals is given in Table 1.2.

Table 1.2 Metals used for implants

<b>Metal</b>	<b>Application</b>
Cobalt-chromium alloys	Artificial heart valves, orthopaedic fixation plates, artificial joint components
Stainless steel	orthopaedic fixation plates, Dental prosthesis
Titanium alloys	Artificial heart valves, dental implants, artificial joint components, orthopaedic screws
Gold or platinum	Dental fillings
Silver-tin-copper alloys	Dental fillings

### 1.3.2 Polymers

(According to Orlovskii et al. [13]) Polymers are organic materials possessing long chains with a large number of small repeating units (monomers) that are held together by directional covalent bonds. Polymers are widely used in biomedical applications due to the range of physical and chemical properties possible with these materials. (According to Abdurrahim and Sopyan [14]) Polymers can be easily fabricated to various complex shapes and structures and additionally surface properties can be easily tuned. (According to Math and Basu [15]) Polymers that are used as implant materials can be either derived from natural sources such as proteins or from synthetic sources. Examples for synthetic and natural polymers are listed in Table 1.3.

Table 1.3 Polymers used in biomedical applications

<b>Polymer</b>	<b>Application</b>
<b>Synthetically derived</b>	
Polyethylene	Orthopaedic joint implants, syringes
Polypropylene	Heart valves, sutures, syringes
Polymethylmethacrylate	Bone cements, dental implants, intraocular contact lenses
Polyethyleneglycol	Pharmaceutical fillers, wound dressings
Polytetrafluoroethylene	Vascular grafts, sutures
Polyvinylchloride	Blood bags, blood tubes
<b>Naturally derived</b>	
Collagen	Orthopaedic repair matrices, nerve repair matrices, tissue engineering matrices
Hyaluronic acid	Orthopaedic repair matrices
Elastin	Skin repair matrices
Chitosan	Wound dressing
Alginate	Wound dressing

### 1.3.3 Ceramics

(According to Zhang and Sirivisoot [16]) Ceramics are inorganic materials composed of non-directional ionic or covalent bonds and which are generally formed at elevated temperatures. (According to Chakraborty and Basu [17]) The class of biocompatible ceramics consists of the crystalline materials such as alumina, zirconia, calcium phosphates and bioactive glasses and glass ceramics. Ceramics are very hard and more resistant to degradation in many environments than metals. However, they are quite brittle due to nature of ionic bonds. The similarity in the chemistry of ceramics and that of native bone, makes ceramics often used as a part of orthopaedic implants or as dental materials. (According to Cavanaugh [18]) Mostly biocompatible ceramics are used in coherence with the human skeleton, bones, joints and teeth. Due to the high abrasive strength, ceramics are used as bearing balls in artificial joints or as bone conductive coatings on metal based implants. Most frequently used ceramic biomaterials are listed in Table 1.4.

Table 1.4 Ceramics used in biomedical applications

<b>Ceramic</b>	<b>Application</b>
Aluminium oxides	Orthopaedic joint replacement, orthopaedic load-bearing implants, implant coatings, dental implants
Zirconium oxides	Orthopaedic joint replacement, dental implants
Calcium phosphates	Orthopaedic and dental implant coatings, dental implant materials, bone graft substitute materials
Bioactive glasses	Orthopaedic and dental implant coatings, dental implants, bone graft substitute materials, bone cements

### 1.3.4 Requirement of biomaterial

(According to Liu and Webster [19]) Bio-medical prosthetic devices are artificial replacements that are used in the human body to function as original parts. (According to Parchi et al. [20]) Materials used for such prosthetic aids must be non-toxic, biologically and chemically stable, and have sufficient mechanical integrity and strength to withstand physiological loads.

### 1.3.5 Hydroxyapatite (HAp)

Hydroxyapatite ( $\text{Ca}_{10}(\text{PO}_4)_6(\text{OH})_2$ ; HAp) is the major inorganic segment of regular bone and has been utilized as an orthopedic and dental material. HAp has been generally utilized as a part of therapeutic field as a bone repair material on account of its amazing bioactive and biocompatibility properties. (According to Jagur [21]) HAp is known for its biocompatible, bioactive, osteoconductive, non-lethal, non-provocative, and non-immunogenic properties. Therefore, HAp is one of the perfect materials for bone substitutions because of the way of its biocompatibility and mechanical quality. Other calcium phosphates apatites including sintered HAp have been broadly utilized for repair and substitution of harmed or damaged bone tissues.

## 1.4 Concept of bio-compatibility

To effectively apply embeds in the human body, a satisfactory level of resistance of the material utilized with the living being is required, (at the end of the day, a high review of biocompatibility). Biocompatibility has been characterized as "the capacity of a material to perform with a suitable host reaction in a particular application". This implies the material or any leachable items from it don't bring about cell demise, perpetual aggravation or other impedance of cell or tissue capacities. Inserts not just must be bio-safe and bio-stable as far as cytotoxicity and corruption, they likewise need to coordinate with the organic prerequisites of any basic biocompatibility. As it were, shape, internal structure and outline of an embed should be adjusted to the attributes of the tissue to be

supplanted. Conceivable collaborations of inserts with hard tissue are recorded in Table 1.5.

Table 1.5 Classification of interactions of implants with hard tissue

<b>Term</b>	<b>Definition</b>
Incompatible	Release of substances in toxic concentrations that lead to inharmonious effects with the living organism that may result in a rejection of the implant
Bio-tolerant	Release of substances but not in toxic concentrations that may lead to an encapsulation within connective tissue
Bio-inert	No release of any toxic substances
Bio-active	Positive interaction with differentiation of tissue that leads to a close adhesion and interconnection along the interface of implant and tissue

## 1.5 Background and Motivation

The present work rests in the scope of polymeric additions for bone repair and substitution, and particular is a HAp-polymer composite. Fruitful outline of an embed to supplant skeletal tissue requires learning of the structure and mechanical properties of bone and a comprehension of the methods by which joins get to be distinctly fused into the body. This data can then be utilized to characterize attractive attributes of the embed to guarantee that the join capacities in a way tantamount to natural tissue. The mechanical properties of bone are identified with the inward association of the material. Cortical bone is delegated a material of under 30% porosity while cancellous/trabecular bone has a porosity of 50 to 90%. The material properties of bone depend on judgments of the versatile modulus, rigidity and compressive quality. Systems by which bone may come up short incorporate fragile crack from effect stacking and weariness from steady or cyclic anxiety. Stresses may act in strain, pressure or shear along at least one of the hub of the bone. An engineered bone substitute must oppose disappointment by any of these anxieties. A join might be important when bone falls flat and does not repair itself in the ordinary measure of time or when bone misfortune happens through crack or tumor. Osteoinduction and osteoconduction are two instruments by which a join may animate the development of new bone. The bone redesigning cycle is a nonstop occasion including the resorption of prior bone by osteoclasts and the arrangement of new bone by the work of osteoblasts. Regularly, these two stages are synchronous and bone mass stays steady. Osteoclasts resorb the unite, a procedure which may take months. After join has been resorbed, bone arrangement starts. Bone mass and mechanical quality come back to close ordinary. Exhibit strategies for the repair of hard deformities

incorporate unions of natural and manufactured development. Utilization of calcium phosphates in bone joining has been explored on account of the synthetic similitudes between the pottery and the mineral grid found in the teeth and bones of vertebrates. This normal for the material makes it a decent hopeful as a wellspring of osteogenesis.

To address the requirement for mediation in bone related harm because of cracks and uniting systems, numerous materials are right now being used to repair or supplant bone that has been harmed because of injury or infection, for example, bone tumors, imperfections and breaks. These incorporate an assortment of biomaterials in light of metals, earthenware production and polymers. Metals experience the ill effects of mechanical properties far surpassing those of bone bringing about anxiety protecting and the resulting debilitating of the host bone tissue creating it defenceless to re-break. Earthenware productions, especially calcium phosphate based, for example, HAp, are fragile and hard to work into wanted shapes. To address the confinements of individual materials, materials in view of composites of earthenware production and polymers have been proposed.

## **1.6 Objectives of the research work**

Based on above discussions, it is decided to assess the behaviour of HAp and polymer composites in terms of mechanical properties, wear resistance, and machining characteristics (drilling) before recommending for medical applications. Specifically, the study aims to develop material that has similar mechanical properties to that of human bone in order to achieve mechanical compatibility in the body, examine the various mechanical properties of composites, assess the performance of the composites under different wear modes and assess the performance of the composites in drilling operation.

## **1.7 Novelty of the proposed research work**

In literature review, it is found that vast majority of the researchers have used the various prediction methods such as artificial neural network (ANN), fuzzy inference system (FIS) etc. for prediction of wear behaviour of composites. The novelty of this thesis is mostly in light of utilizing neuro-fuzzy modelling (ANFIS) for prediction of wear behaviour of ceramic composites under various wear modes such as abrasive, erosive, sliding and fretting wear.

In this research work, the impact of machining parameters in drilling of HAp/PC and HAp/PSU composites has been studied and such a study is hardly found in the the literature.

## 1.8 Organisation of the Thesis

This thesis is organised into seven chapters including this chapter. A brief outline of each chapter is given as follows:

### ❖ **Chapter 2: Literature Review**

This chapter reviews literature to provide background information on the issues to be considered in the thesis and emphasize the relevance of the present study. The chapter deals with important research papers available related to the theory of ceramic reinforced polymer composites and their applications. The study is categorized into five categories i.e. development of hydroxyapatite through wet-chemical precipitation route, processing and fabrication of ceramic composites, characterization of mechanical properties of ceramic composites, different wear modes and their behaviour of ceramic composites, and machining analysis of ceramic composites.

### ❖ **Chapter 3: Materials Used and Experimental Details**

This chapter describes the detailed experimental procedure for Hydroxyapatite (HAp) powder preparation at laboratory level. The materials used for HAp preparation are calcium hydroxide ( $\text{Ca}(\text{OH})_2$ ) white powder, ortho phosphoric ( $\text{H}_3\text{PO}_4$ ) acid and ammonia ( $\text{NH}_3$ ) (if required). Two amorphous thermoplastic polymers i.e. Polycarbonate (PC) and Polysulfone (PSU) granules were used for mixing purpose with HAp. The detailed specifications of these materials provided by the suppliers are discussed in this chapter. Different methods of HAp preparation, preparation methods of both composites i.e. HAp/PC and HAp/PSU are briefly discussed under this chapter. Some analysis like particle size analysis, XRD analysis, FTIR analysis, and SEM analysis are also discussed in this chapter.

### ❖ **Chapter 4: A Study on Characterization of Mechanical Properties of Ceramic Composites**

This chapter describes the characterization of mechanical properties i.e. tensile, compressive, flexural, impact and hardness of both ceramic composites i.e. HAp/PC and HAp/PSU composites. The density and void fraction of each composition for both composites are shown in this chapter. Some comparison graphs between both composites of each variation of HAp volume percentage, and specifications of machines used for mechanical testing of specimens in tabular form are shown in this chapter.

### ❖ **Chapter 5: A Study on performance of Ceramic Composites under various wear modes**

This chapter describes the introduction of wear, definition of wear and classifications of wear i.e. abrasive wear, adhesive wear, erosive wear, sliding wear, fretting wear, corrosive wear and surface fatigue wear. However, in this study, we focussed mainly on

abrasive wear, erosive wear, sliding wear, and fretting wear along with their experimental procedure in different machines are discussed briefly. ANFIS (Adaptive neuro-fuzzy inference system) model is proposed for prediction of wear behaviour of composites. Some SEM images of worn surfaces under various wear modes are also shown and discussed in this chapter.

#### ❖ **Chapter 6: A Study on Machining Analysis of Ceramic Composites**

This chapter describes the drilling of ceramic composites. Selection of machining parameter combinations for obtaining optimum circularity at both entry and exit, and optimum torque and thrust force is a challenging task owing to the presence of a large number of process variables. There is no perfect combination of parameters that can simultaneously result in higher circularity at both entry and exit with lower torque and thrust force. The aim is to develop a strategy for predicting machining parameter settings for the generation of the maximum circularity at both entry and exit with minimum torque and thrust force. Experiments have been conducted on a CNC milling machine using Taguchi's  $L_{27}$  design with four control variables such as HAp volume (%), drilling speed (rpm), feed rate (mm/min) and drill bit diameter (mm) each at three levels. The responses considered are circularity at entry and exit, torque and thrust force. The circularity at both entry and exit is measured using the ratio of minimum diameter ( $D_{min}$ ) to maximum diameter ( $D_{max}$ ) of the hole. The torque and thrust force are measured using dynamometer. Best parametric setting for simultaneous optimization of multiple performance measures in drilling operation is suggested using principal component analysis.

#### ❖ **Chapter 7: Executive Summary and Conclusions**

This chapter describes the summary and conclusions of each chapter and discussed briefly.

#### **Scope for Future Research Work**

This section describes the various issues which should be considered for future research and development.

## **1.9 Conclusion**

This chapter highlights the necessity of ceramic composites in the field of bio-medical applications. It suggests use of combination of ceramic/polymer composites to overcome the limitations of other conventional composites. The classification of composites has been discussed. This chapter also focuses on literature gap in this field of study and sets the objectives for the present investigation. Finally layout of the thesis has been discussed briefly. The motivation behind making such composites is to fortify the polymer and enhance the bone holding properties of the material. The interfacial holding amongst

inorganic and natural stage assumes an essential part in deciding definitive mechanical properties of the composites. Bone has generally high compressive quality of around 170 MPa however poor elasticity of 104-121 MPa and low shear quality 51.6 MPa, which means it opposes pushing strengths well, yet not pulling or torsional powers. Distinctive materials have been portrayed with their applications out of which polymers are generally utilized as a part of biomedical applications because of the scope of physical and substance properties conceivable with these materials. Polymers can be effectively created to different complex shapes and structures and furthermore surface properties can be effortlessly tuned. Polymers that are utilized as embed materials can be either gotten from common sources, for example, proteins or from engineered sources. Then again, the similitude in the science of earthenware production and that of local bone, makes pottery regularly utilized as a piece of orthopedic inserts or as dental materials. For the most part biocompatible earthenware production is utilized as a part of rationality with the human skeleton, bones, joints and teeth. HAp is one of the perfect materials for bone substitutions because of the way of its biocompatibility and mechanical quality. Generally, metallic materials, for example, stainless steel, titanium combinations and cobalt-chromium composites have been broadly utilized as bone embeds in orthopedic applications. Clay strengthened HAp polymer composites for various load-bearing orthopedic applications have been created as of late.



## Chapter 2

# Literature Review

### 2.1 Introduction

The present chapter deals with critical analysis of articles available related to the theory of ceramic reinforced polymer composites and their applications. Many implant materials made of metals, alloys, ceramics and polymers have been tried earlier with reports of both successes and failures. Then, the search for an alternative was emphasized in the form of ceramic-polymer composite. The possibilities of combining the advantages of different materials have attracted material scientists to pay much attention in ceramic-polymer composite. Literature suggests that systematic research work by physicians and biomaterial scientists is essential for successful development of novel materials with improved biocompatibility. Although the concept of ceramic composite appeared in the literature in the mid-1990s, review of the literature begins with research papers published with maximum attention after 1995. Table 2.1 provides the source and number of citations from each source. The majority of citations are found in peer reviewed journals namely Journal of Biomaterials and Journal of Composites Science and Technology.

Table 2.1 Summary of publications referred

Source	No. of Citations
Journal of Biomaterials	10
Journal of Materials Science and Engineering C	5
Journal of Materials Science: Materials in Medicine	4
Journal of Materials Synthesis and Processing	2
Journal of Materials Letters	2
Journal of Materials Processing Technology	3
Journal of Ceramics International	5
Journal of the European Ceramic Society	5
Journal of Materials and Design	2
Journal of American Ceramic Society	2
Journal of Materials Research	3
Journal of Applied Biomaterials and Biomechanics	5
Journal of Acta Biomaterialia	9
Journal of Materials Science and Engineering A	3
Journal of Materials Research Bulletin	2
Journal of Materials Science	5
Journal of Nanoparticle Research	1
Journal of the Korean Ceramic Society	2
Journal of Composites Science and Technology	10
Journal of Processing and Application of Ceramics	5

Journal of Chemistry of Materials	3
Journal of Materials Characterization	5
Journal of Biomechanical Engineering	3
Journal of Materials Engineering and Performance	2
Journal of Biomaterials and Nanobiotechnology	3
Journal of Progress in Materials Science	3
International Journal of Advanced Manufacturing Technology	5
International Journal of Biological Macromolecules	2
Journal of Progress in Biomaterials	3
Journal of Materials	2
Journal of Composite Structures	1
Journal of Applied Polymer Science	3
Journal of Materials: Design and Applications	1
Journal of Composites	3
Journal of Biomedical Materials Research	2
Journal of Biomedical Science and Engineering	3
Journal of Biomaterials Applications	5
Journal of Mechanical Behavior of Biomedical Materials	4
Journal of Inorganic Materials: Applied Research	1
Journal of Applied Sciences	2
International Journal of Polymer Science	3
International Journal of the Physical Sciences	1
Journal of Progress in Polymer Science	2
Journal of Ceramic Processing Research	3
Journal of Advanced Ceramics	3
Journal of Materials Science Technology	3
Journal of ActaMaterialia	3
Journal of Advances in Materials Science and Applications	2
Journal of Materials Science and Engineering B	3
Journal of Wear	3
Journal of Materials Education	1
Journal of Bone and Joint Surgery	2
Journal of Materials Science and Engineering	3
Journal of Computational Materials Science	2
Journal of Minerals and Materials Characterization and Engineering	2
Journal of Tribology International	5
Journal of Tribology Transactions	2
Journal of Biomechanics	2
Journal of Biosurface and Biotribology	1
Journal of Materials Today	2
Journal of Materials Research and Technology	3
Journal of Measurement	3
Journal of Mechanics of Advanced Materials and Structures	1
Journal of Thermoplastic Composite Materials	3
Journal of Polymer Composites	3
Thesis	2
Books	2
Conference Papers	3
<b>Total</b>	<b>209</b>

## 2.2 Classification of Literature

The literature is classified into five categories i.e. development of hydroxyapatite, processing and fabrication of ceramic composites, characterization of mechanical properties of ceramic composites, wear study and behaviour of ceramic composites, and machining analysis of ceramic composites as illustrated in Figure 2.1. Next sections provide brief discussions on these issues. Finally, the chapter is concluded by summarizing the advancement taken place in ceramic-polymer composite and possible research gap so that the relevance of the present study can be emphasized.

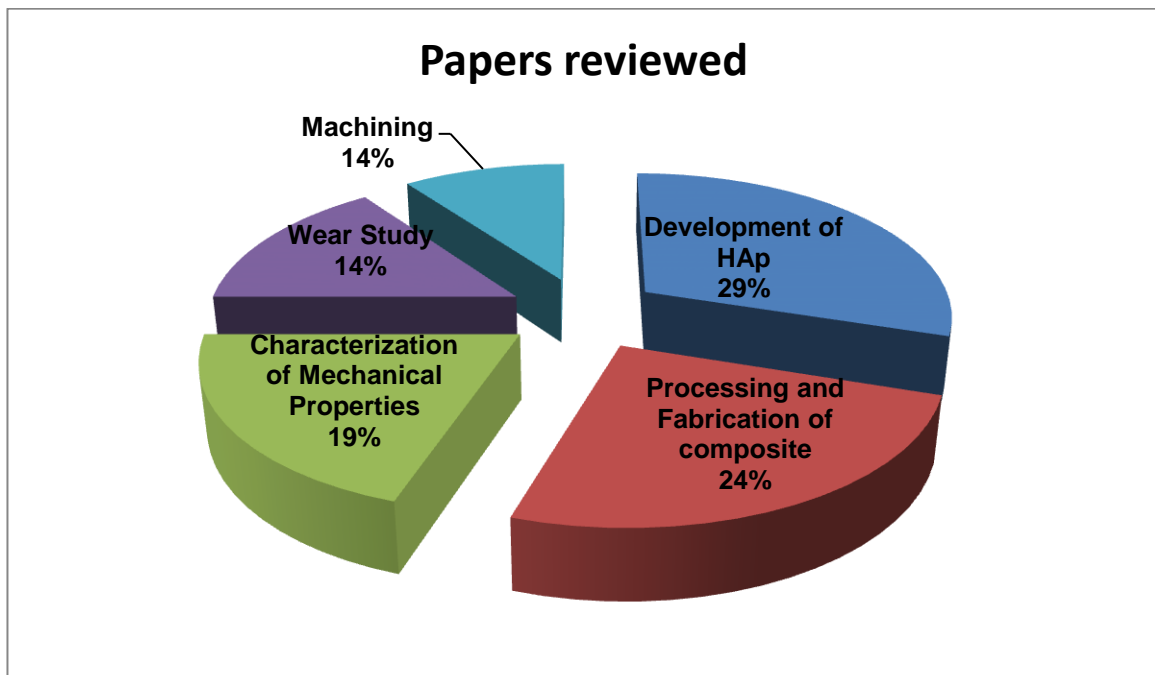


Figure 2.1 Percentage of paper reviewed

### 2.2.1 Development of Hydroxyapatite through Wet Chemical Precipitation Route

Ruys et al. [41] have studied on effect of sintering temperature on the tensile strength of HAp and found that higher tensile strength can be achieved at sintering temperature above 800°C due to less porosity. Yeong et al. [45] have tried to improve fine HAp powder compaction and found that good compaction is possible when sintered at 1000°C. Kweh et al. [28] have studied on preparation and characterization of HAp powder through spray drying method and concluded that development of undesirable phases can be restricted at high calcination temperature (1000°C). Tas [36] has studied the preparation of nano-size HAp through a novel chemical precipitation method and concluded that nano-size HAp powders have been synthesized effectively from a novel synthetic body solution containing dissolved calcium nitrate and di-ammonium hydrogen

phosphate salts in appropriate amounts. Muralithran and Ramesh [31] have studied the impact of sintering temperature on the physical properties of HAp and concluded that the optimum sintering temperature for HAp should be 1250°C. Orlovskii et al. [13] have studied the preparation of HAp and HAp/Polymer composite and found that HAp powder can be prepared by wet chemical, solid state reactions, and hydrothermal treatment route. The preparation technique significantly influences the powder crystallinity of the HAp powder. Saeri et al. [33] have studied on synthesis of hydroxyapatite (HAp) powder by wet precipitation method using ortho-phosphoric acid and calcium hydroxide as raw materials and concluded that heating HAp for 850°C to 1200°C causes increase in crystallinity. However, heating more than 1200°C causes lower crystallinity. Anee et al. [25] have studied on synthesis of HAp by a novel method using agarose gel in a high alkaline medium at a relatively low temperature at 85°C. Afshar et al. [24] have studied on the important parameters in the wet precipitation procedure of HAp and conclude that pH value, extra acid solution, stirring speed, and post chemical treatment largely influence on quality of powder. Pang and Bao [38] have studied on effect of temperature, ripening time and calcination on the morphology and crystallinity of HAp nanoparticles and concluded that crystallinity and crystallite size increases with the increase in synthetic temperature and ripening time. Pramanik et al. [39] have studied on the development of high strength HAp for hard tissue replacement through solid state reactions in temperature near 1250°C and conclude that large pored HAp material with high strength and density close to that of real femoral bone can be produced. Ramesh et al. [9] have studied on effect of rapid sintering by microwave heating on the properties of nanocrystalline Hap bioceramic powder and concluded that fine grain size of 0.12  $\mu\text{m}$  can be achieved when sintered at 1000°C. Zhang and Lu [47] have studied on development of highly crystalline nano-HAp at low temperature and concluded that ultra-fine complete spherical HAp particles with diameter range of 20–50 nm can be obtained through fast mixing mode at 40°C. Monmaturapoj [30] has studied on preparation of nano-HAp powders by wet chemical precipitation method and concluded that the density of 4.05  $\text{g}/\text{cm}^3$  and specific surface area of 89.58  $\text{m}^2/\text{g}$  as well as uniform grain size morphology can be achieved. Yoruc and Kocahave [46] studied on precipitation of nano-HAp powder through a novel method and concluded that the HAp powders can be synthesized from aqueous suspensions containing  $\text{H}_3\text{PO}_4$  and  $\text{Ca}(\text{OH})_2$  with magnetic, ultrasonic and double step stirring (magnetic + ultrasonic stirrings) methods under atmospheric pressure and room temperature. It is concluded that hydroxyapatite powder prepared with double step stirring procedure (DSS-HAp) has highest HAp content and nano-sized. Eslami et al. [27] have studied on synthesis of HAp by wet precipitation technique and concluded that bulk Ca/P molar proportion of 1.71 which is higher than the standard stoichiometric proportion

of 1.667 can produce a pure HAp phase. Salma et al. [34] have studied the preparation of calcium phosphate bio-ceramics by modifying the wet chemical precipitation method and concluded that pure, crystalline and highly thermally stable HAp bio-ceramics with homogenous microstructure and grain size up to 200-250 nm can be obtained. Nayak [22] has studied on various synthesis methodologies of HAp and concluded that the wet chemical precipitation technique is chosen widely to synthesize HAp compared to other procedures because relatively large amount of HAp can be produced in absence of organic solvents at a reasonable cost. Ramesh et al. [40] have studied on the sintering behaviour of HAp preparation through three different types of hydroxyapatite (HAp) i.e. a commercial powder (HAp(C)), a synthesized powder by wet chemical precipitation technique (HAp(W)) and a synthesized powder by mechanochemical technique (HAp (M)) at temperature range of 1000-1350°C. It has been concluded that the sinterability and mechanical properties of the synthesized HAp (W) is essentially higher than that of the HAp (C) and HAp (M). Pramanik and Kar [32] have studied the synthesis of nano-HAp by continuous rapid precipitation from calcium oxide and concluded that the best result is obtained using a pH value of 9. Santhosh and Prabu [35] have studied on the synthesis of nano (HAp) by a wet chemical reaction route using powdered sea shells (CaO) as starting material and concluded that microwave heated HAp has low crystallite size than furnace heated samples. The presence of hydroxyl group in HAp-structure has added to microwave heating and results in good crystallinity than furnace heated HAp done at higher temperature.

### **2.2.2. Processing and Fabrication of Ceramic Composites**

Juang and Hon [65] have studied on fabrication and mechanical properties of HAp/Alumina composites and concluded that addition of  $Al_2O_3$  increases the mechanical strength of the composites. Sim et al. [75] have studied on the injection molding of HAp/HDPE composites and found that a reasonably homogenous injection mouldable mix can be achieved up to 20 vol. % loading of HAp without the use of additives. Greater volume loading, however, requires the use of lubricant because of increased viscosity. Wang et al. [79] have studied on fabrication of HAp/Polysulfone (PSU) and concluded that the HAp particles are well dispersed in the PSU matrix. Increasing the HAp content in the composite leads to increase in viscosity and shear stress. However, viscosity and shear stress can decrease with an increase in temperature. Chen and Wang [94] have studied the biodegradable composites and concluded that the Young's modulus and micro-hardness of the composites increase with an increase in the volume percentage of HAp particles. Joseph et al. [64] have studied on effect of surface morphology of HAp on the rheology and processability of HAp/HDPE composite. It has been concluded that low

surface area of HAp in composites can reduce the shear stress. The specific surface area of HAp can easily be modified by a controlled sintering process. Wang et al. [80] have studied on development of biomimetic nHAp/poly(hexamethyleneadipamide) composites and concluded that these synthesized n-HAp crystals are like bone apatite in size, phase composition and crystal structure. The biomimetic nHAp crystals are consistently distributed in the polymer matrix. Ramay and Jhang [101] have studied on preparation of porous hydroxyapatite scaffolds by mixing of the gel-casting and polymer sponge techniques and found that the scaffolds have an open, uniform and interconnected porous structure with a pore size of 200-400  $\mu\text{m}$ . Bakar et al. [119] have studied on polyetheretherketone (PEEK)/hydroxyapatite composites for load-bearing orthopaedic implants and found that the bioactive PEEK composite approaches the regime of that of cortical bone. Szaraniec et al. [77] have studied on mechanical and biological properties of carbon/carbon (CC) composites and polysulfone modified by hydroxyapatite (HAp), both natural (nano-particles) and manufactured (micro-particles), and concluded that increase of hydroxyapatite to CC composites does not influence on mechanical properties. Addition of hydroxyapatite to polysulfone causes an increment of Young's modulus of the composite, a decrease in strength and reduces the creep. The best mechanical parameters is observed for the composite with nanoHAp that is obtained by the pre-preg technique. Degirmenbasi et al. [96] have studied on bio-composites of HAp mixing with different binders including poly(vinyl-alcohol) (PVA), and collagen and concluded that nanoparticles of hydroxyapatite can be synthesized with collagen or collagen in addition to PVA to produce n-HAp/PVA, n-HAp/collagen and n-HAp/PVA/collagen bio-composites. Wahl and Czernuszka [78] have studied on composites of a natural polymer (collagen) and a natural ceramic (HAp) for use in bone tissue repair and concluded that the addition of a (calcium/phosphate) compound to collagen sheets gives higher stability, resistance to 3D swelling and enhanced mechanical properties. Liu and Wang [70] have studied on fabrication and characteristics of HAp/PP as a bone biomaterial and concluded that HAp/polypropylene (PP) composite containing up to 25 vol. % of HAp can be effectively manufactured. A satisfactory dispersion and distribution of HAp particles in the composite is achieved. The thermal and mechanical properties of HAp/PP composite are influenced by the amount of HAp in the composite. The addition of HAp particles causes a decrease in crystallinity of the PP matrix polymer. Fang et al. [62] have studied on nano-sized hydroxyapatite (HAp) particles reinforced with ultra high molecular weight polyethylene (UHMWPE) for biomedical applications and concluded that the bio-composite with HAp volume of 50 vol. % can be effectively processed by twin-screw extruder, compression molding, and hot drawing. Liu and Wang [69] have studied on development of HAp/polyhydroxybutyrate

(PHB) composite and concluded that injection molding can effectively build HAp/PHB composite plate containing HAp up to 40 vol. %. Sarkar et al. [6] have studied on ceramic reinforced (HAp) polymer composites for orthopedic application and concluded that osteogenesis and osteoconductivity could be controlled through the addition of nano-HAphase. Beherei et al. [93] have studied on preparation of HAp/CA (Calcium Aluminate) composites and concluded that increase of CA substance prevents the transformation of HAp to  $\beta$ -tri calcium phosphate (TCP) compound. Li et al. [114] have studied on the development of nHAp/Polycarbonate (PC) composite and concluded that the composite possesses good biocompatibility with no risk to surrounding tissue. This composite can stimulate the development of new bone showing it as an osteoconductive material. The n-HAp/PC composite shows a great potential of becoming an excellent biomaterial for clinical applications. Liao et al. [67] have studied on multi-walled carbon nanotubes (MWNTs) of 0.1 and 0.3 wt. % and hydroxyapatite nanorods (nHAs) of 8-20 wt. % incorporated into polypropylene (PP) to form bio-composites using melt-compounding and injection molding techniques. It is concluded that hybridizing MWNTs of low loadings with nHAp in the PP matrix results inconsiderable improvement in mechanical strength, impact toughness, thermal and dimensional stability. The PP/0.3%MWNT-20%nHAp composite is biocompatible with a superior cell proliferation rate compared with the PP/20%nHAp composite. Zhou et al. [131] have studied on preparation of HAp/Collagen composite as potential scaffold for the repair of load-bearing bones and found that the reinforcement effect can be controlled by calcium phosphate (CaP) porous structure, collagen content and cross-linking technique. Robinson et al. [73] have studied on HAp/polysulphone (PSU) composite and found that the toughness and modulus value of HAp/ polysulphone (PSU) composite are within the range of cortical bone.

### **2.2.3 Characterization of Mechanical Properties of Ceramic Composites**

Bakar et al. [119] have studied on mechanical properties of HAp/PEEK composites and concluded that Young's modulus, compressive strength and micro-indentation hardness increase with increase in amount of HAp particulate while tensile strength decreases. Wan et al. [147] have studied on effect of bone mineral fraction on mechanical properties of bone and concluded that the percentage of solid materials content in cortical bone has significant effect on mechanical properties of bone like Young's modulus, ultimate stress and toughness than mineral substance. Converse et al. [120] have studied on mechanical properties of HAp/Polyetherketoneketone (PEKK)

composite and concluded that increase of HAp reinforcement results in increase in elastic modulus for 0 to 20 vol. % HAp and a consequent decrease for 20 to 40 vol. %. Asuke et al. [118] have studied on effect of uncarbonized and carbonized bone particle on the microstructure and properties of polypropylene (PP) /bone ash particulate composites and concluded that addition of carbonized bone particles reinforcement causes increase in compressive strength, hardness, tensile strength and flexural strength and decrease in strain rate and impact energy as compared to addition of uncarbonized bone particles in the composite. Jaggi et al. [124] have studied on performance of structural and mechanical response of HAp/high density poly-ethylene (HDPE) bio-composites and concluded that elastic and flexural properties increase while impact strength decrease linearly with HAp content. Ahmad et al. [117] have studied on mechanical properties of HAp-polyethylene glycol PEG/UHMWPE bioactive composite and concluded that polyethylene glycol (PEG) decreases the melt viscosity of UHMWPE/HDPE. The mechanical and bioactive properties are improved with the addition of HAp particles. Nainar et al. [126] have studied on mechanical properties of HAp/PLA bio-composites and found that 10wt% HAp/PLA has better tensile strength compared with 20wt% HAp/PLA and 30wt% HAp/PLA composites. Subsequently, Young's modulus of the HAp/PLA composites increases with the addition of HAp content. The strain rate at break is decreased with the increase in the HAp contents. Li et al. [154] have studied on the characterization of mechanical properties of a novel composite comprising of porous titanium (Ti) part loaded with chitosan/HAp sponge for load-bearing applications and found that the mechanical properties of porous Ti with porosities of ~60 to 75% are analyzed by means of a compressive test. Hossan et al. [121] have studied on mechanical properties of HAp/Gelatin composite for bone tissue engineering and concluded that the mechanical properties of composites have been analysed by thermo-mechanical analyzer (TMA), Vickers micro hardness analyser, and universal testing machine. It is observed that the composite has maximum tensile strength of 37.13 MPa. These results exhibit that the prepared composite scaffold is a potential candidate for bone tissue engineering. Kang et al. [125] have studied on mechanical properties of micro and nano-hydroxyapatite reinforced with ultrahigh molecular weight polyethylene composites and concluded that the compression strength, micro-indentation hardness, creep resistance, crystallinity, and melting temperature of micro and nano-HAp/UHMWPE composites are improved with the increase of micro and nano-HAp particles. The properties of nano-HAp/UHMWPE composites are higher than micro-HAp/UHMWPE composites with a similar substance of HAp.



## 2.2.4 Wear Behaviour of Ceramic Composites

Harsha and Tewari [171] have studied on mechanical and tribological properties of different injection molded polyaryletherketones (PAEKs). It is observed that factors like sliding distance, load and abrasive grit size have significant influence on abrasive wear performance. Hu et al. [163] have studied on effect of microstructure of the composite on abrasive wear and concluded that wear of a composite increases with increase in the size ratio. Chowdhury et al. [162] have studied on wear behaviour and biocompatibility of HAp/collagen composites and concluded that HAp/collagen composite with 10% hyaluronic acid offer suitable mechanical strength, good friction and wear characteristics. Karanjai et al. [172] have studied on fretting wear on Ti-Ca-P composite in dry and simulated body fluid (SBF) conditions and concluded that coefficient of friction is in the range 0.7-0.8 in dry conditions. Under SBF medium, the co-efficient of friction (COF) is around 0.35 and do not vary much with load. Younesi et al. [166] have studied on prediction of wear behaviours of nickel free stainless steels-HAp composites using artificial neural network and concluded that back propagation neural network has the ability to predict the wear volume loss of composites during wear test for various wear loads, wear distances, and HAp volume fractions. Mohan et al. [164] have studied on effect of silicon carbide (SiC) particulate fillers incorporation on two-body abrasive wear behaviour of Glass Fibre-Epoxy (GE) composites and concluded that the two-body abrasive wear performance of GE and GE-SiC composites significantly depend on abrading distance and grit size of the abrasive paper. The wear loss is found to increase in composites with the increase in abrading distances. The performance of SiC-filled GE composite is found superior to unfilled GE composite. Tan et al. [174] have studied on characteristics of fretting wear resistance for thermoplastics and concluded that polyimide (PI), HDPE and UHMWPE exhibit better wear resistance over other thermoplastics. Yoon et al. [175] have studied on effect of surface roughness on fretting wear. Silva et al. [165] have studied on role of abrasive material in micro-abrasion wear tests. Liu et al. [173] have studied on fretting wear behaviour of hot pressed HAp/poly-lactic acid (PLA) fibrous composites as potential orthopaedic implants and concluded that the addition of HAp nano particles into fibrous composites decrease the coefficients of friction (COFs) and wear rates. Chauhan and Thakur [161] have studied on effect of particle size, particle loading and sliding distance on the friction and wear behaviour of vinylester composites sliding against hardened ground steel on a pin on disc wear testing machine and concluded that the submicron particles and microparticles can improve both the mechanical and wear resistance of the cenosphere filled vinylester composites. The submicron sized particles are more effective in improving the wear resistance compared with the micro-sized particles. It is seen that the hardness, flexural strength and

compressive strength can be increased with reduction in cenosphere filled vinylester composite which is because of strong bond amongst particles and the matrix. Singh et al. [179] have studied on prediction of surface roughness during machining of glass fiber reinforced epoxy composites using artificial neuro fuzzy inference system (ANFIS) and concluded that ANFIS can reduce the simulation time. Sahu et al. [180] have studied on prediction of entrance length for low Reynolds' number flow in pipe by using ANFIS and concluded that the model generates prediction of entrance length accurately.

### **2.2.5 Machining Analysis of Ceramic Composites**

Chandramohan and Marimuthu [183, 184] have studied on drilling of natural fiber reinforced composite materials for application as bone implants. It is concluded that the thrust and torque mainly depend on feed, cutting speed, tool geometry, machine tool, and cutting tool rigidity. It is observed that thrust force increases with the increase in fiber volume fraction. Moshat et al. [189] have studied on optimization of machining process for multiple quality characteristics like surface finish and material removal rate (MRR) using principal component analysis (PCA) based hybrid Taguchi technique. Krishnaraj et al. [188] have studied on optimization of machining parameters of carbon fiber reinforced plastic (CFRP) laminates and concluded that feed rate has a greater influence on thrust force, push-out delamination and drilled diameter of the hole. Spindle speed is one of the significant determinants for the circularity of the drilled hole. Rajmohan et al. [192] have studied on surface integrity analysis in drilling of metal matrix composites and hybrid composites and concluded that drilled surface shows the presence of cracks, pulling-out and shearing of particles. Pandey and Panda [190, 191] have worked on optimization of bone drilling process with multiple performance characteristics to minimize the drilling induced bone tissue damage. Singh et al. [193] have studied on drilling parameters like rotational speed, feed rate and the type of tool for optimizing surface roughness and material removal rate.

## **2.3 Critical review**

It has been observed that higher tensile strength can be achieved at sintering temperature above 800°C due to less porosity. It has been found that development of undesirable phases can be restricted at high calcination temperature (1000°C). It has been observed that optimum sintering temperature for HAp should be 1250°C. It has been observed that heating HAp for 850°C to 1200°C causes increase in crystallinity. However, heating more than 1200°C causes lower crystallinity. It has been found that crystallinity and crystallite size increases with the increase in synthetic temperature and

ripening time. It has been observed that the wet chemical precipitation technique is chosen widely to synthesize HAp compared to other procedures because relatively large amount of HAp can be produced in absence of organic solvents at a reasonable cost.

It has been observed that addition of  $Al_2O_3$  increases the mechanical strength of the composites. It has been found that the HAp particles are well dispersed in the PSU matrix. Increasing the HAp content in the composite leads to increase in viscosity and shear stress. However, viscosity and shear stress can decrease with an increase in temperature. It has been observed that the Young's modulus and micro-hardness of the composites increase with an increase in the volume percentage of HAp particles. It has been found that addition of hydroxyapatite to polysulfone causes an increment of Young's modulus of the composite, a decrease in strength and reduces the creep. It has been found that the thermal and mechanical properties of HAp/PP composite are influenced by the amount of HAp in the composite. The addition of HAp particles causes a decrease in crystallinity of the PP matrix polymer. It has been found the toughness and modulus value of HAp/polysulphone (PSU) composite are within the range of cortical bone.

It has been found that Young's modulus, compressive strength and micro-indentation hardness increase with increase in amount of HAp particulate while tensile strength decreases. It has been observed that addition of carbonized bone particles reinforcement causes increase in compressive strength, hardness, tensile strength and flexural strength and decrease in strain rate and impact energy as compared to addition of uncarbonized bone particles in the composite. It has been found that the compression strength, micro-indentation hardness, creep resistance, crystallinity, and melting temperature of micro and nano-HAp/UHMWPE composites are improved with the increase of micro and nano-HAp particles. The properties of nano-HAp/UHMWPE composites are higher than micro-HAp/UHMWPE composites with a similar substance of HAp.

It has been observed that factors like sliding distance, load and abrasive grit size have significant influence on abrasive wear performance. It has been found that back propagation neural network has the ability to predict the wear volume loss of composites during wear test for various wear loads, wear distances, and HAp volume fractions. It has been observed that the addition of HAp nano particles into fibrous composites decrease the coefficients of friction (COFs) and wear rates.

It has been observed that the thrust and torque mainly depend on feed, cutting speed, tool geometry, machine tool, and cutting tool rigidity. It has been found that thrust force increases with the increase in fiber volume fraction.

## **2.4 Conclusion**

This chapter reviews the literature to provide background information of ceramic composites in bio-medical applications and emphasize the relevance of the present study. The study is categorized into five categories i.e. development of hydroxyapatite through wet-chemical precipitation route, processing and fabrication of ceramic composites, characterization of mechanical properties of ceramic composites, different wear modes and their behaviour of ceramic composites, and machining analysis of ceramic composites.

## Chapter 3

# Materials and Methods

### 3.1 Introduction

This chapter describes the detailed experimental procedure for Hydroxyapatite (HAp) powder preparation at laboratory level. The materials used for HAp preparation are Calcium hydroxide ( $\text{Ca}(\text{OH})_2$ ) white powder, Ortho phosphoric ( $\text{H}_3\text{PO}_4$ ) acid and Ammonia ( $\text{NH}_3$ ) (if required). Two amorphous thermoplastic polymers i.e. Polycarbonate (PC) and Polysulfone (PSU) granules were used for mixing purpose with HAp. The detailed specifications of these materials provided by the suppliers are discussed in this chapter.

### 3.2 Specification of the materials used

The specification of the various materials given by the suppliers is outlined below:

#### 3.2.1 Calcium hydroxide ( $\text{Ca}(\text{OH})_2$ ) GR (Merck Specialities Private Limited) Mumbai,

[www.merckspecialities.com](http://www.merckspecialities.com)

( $\text{Ca}(\text{OH})_2$ ) molecular weight (M) = 74.10 g/mol

Assay (acidimetric): min. 96.0%

Substances insoluble in hydrochloric acid: max. 0.1%

Carbonate (as  $\text{CaCO}_3$ ): max. 3.0%

Chloride (Cl): max. 0.005%

Sulfate ( $\text{SO}_4$ ): max. 0.2%

Heavy metals (as Pb): max. 0.005%

Iron (Fe): max. 0.05%

Substances not precipitated by ammonium oxalate (as sulphate): max. 2.5%

#### 3.2.2 Ortho phosphoric acid ( $\text{H}_3\text{PO}_4$ ) (Merck Specialities Private Limited) Mumbai,

[www.merck-chemicals.com](http://www.merck-chemicals.com)

$\text{H}_3\text{PO}_4$  molecular weight (M) = 98.00 g/mol (1 ltr. = 1.73 Kg)

Assay ( $\text{H}_3\text{PO}_4$ )  $\geq$  85%

Heavy metals (as Pb)  $\leq$  0.002%

Insoluble matter  $\leq$  0.01%

3.2.3 Ammonia (NH<sub>3</sub>) (Merck Specialities Private Limited) Mumbai, [www.merck-chemicals.com](http://www.merck-chemicals.com)

NH<sub>3</sub> molecular weight (M) = 17.03 g/mol (1 ltr. = 0.91 Kg)

Assay (NH<sub>3</sub>) ≥ 25%

Test solution – Conforms

Non-volatile substances ≤ 0.002%

3.2.4 Polycarbonate (PC) thermoplastic polymer (Raza Traders, Mumbai)

Density (ρ) = 1.20 g/cm<sup>3</sup>

Glass transition temperature (T<sub>g</sub>) = 147°C

Working Temperature (T<sub>w</sub>) = 230°C to 250°C

3.2.5 Polysulfone (PSU) thermoplastic polymer (Raza Traders, Mumbai)

Density (ρ) = 1.24 g/cm<sup>3</sup>

Glass transition temperature (T<sub>g</sub>) = 185°C

Working Temperature (T<sub>w</sub>) = 310°C to 360°C

### 3.3 Methods of HAp preparation

(According to Nayak [22]) During the past decade, many diverse methods have claimed to prepare HAp nanoparticles with precise control over its microstructure. These methods involve various types of known chemical synthesis routes. In each method, processing conditions can be varied across a wide range resulting in several sub-methods. (According to Sadat et al. [23]) HAp preparation methods are classified into two groups: dry methods (with two sub-groups i.e. solid state method and mechano-chemical method) and wet methods (with six-subgroups i.e. chemical precipitation method, hydrolysis method, sol-gel method, hydrothermal method, emulsion method, and sonochemical method).

(According to Sadat et al. [23]) Dry techniques do not use a solvent unlike wet methods. The characteristics of powder synthesized by a dry method are not strongly influenced by the processing parameters; hence most dry methods do not require controlled conditions making them suitable for mass production of powders. A number of scientists have therefore adapted well-known dry methods including solid-state synthesis and the mechano-chemical process for the preparation of HAp powder. Solid state method is a relatively simple technique in the mass production of HAp powder. In this method, precursors are first milled and then calcined at a very high temperature (e.g. 1000°C). The precursors can be calcium and phosphate containing chemicals of various

types or simply a previously prepared CaP salt. The high temperature of calcination leads to the formation of a well-crystallized structure.

(According to Sadat et al. [23]) The mechano-chemical technique is a simple dry method for fabrication of various advanced materials such as nano-crystalline alloys and ceramics. Contrary to the solid state method in which heterogeneous particles with irregular shape are usually produced, powder synthesized using a mechano-chemical route usually possesses a well-defined structure. So, the mechano-chemical process has the advantage of simplicity to perform mass production and the basic characteristics to generate a powder with an acceptable microstructure.

(According to Sadat et al. [23]) HAp powder generated from a typical dry technique is usually large in size and irregular in shape. Hence, wet methods have conventionally been applied to the preparation of HAp particles having a nano-sized structure with a regular morphology. Wet chemical reactions have advantages in their ability to control the morphology and the mean size of the powder and based on many experimental data, they are found to be the most promising procedures for the fabrication of nano-HAp powder. Wet procedures are usually easy to conduct and development conditions can be directly controlled by adjusting the reaction parameters. Among the various wet preparing methods, conventional wet precipitation is the easiest route for the synthesis of nano-HAp powder. The chemical precipitation is based on the fact that, at room temperature and at pH value 4.2, HAp is the least soluble and usually the most stable CaP phase in an aqueous solution. The precipitation reaction is, however, usually conducted at pH values higher than 4.2 and temperatures extending from room temperature to temperature near the boiling point of the water. To produce HAp nanoparticles, chemical precipitation can be accomplished utilizing different calcium and phosphate containing reagents like calcium hydroxide or calcium nitrate as the  $\text{Ca}^{2+}$  source and orthophosphoric acid or diammonium hydrogen phosphate as the  $\text{PO}_4^{3-}$  source. A typical procedure includes the drop-wise addition of one reagent to another under nonstop and gentle mixing while the molar proportion of components (Ca/P) is kept at stoichiometry as per its proportion in HAp (1.67). The resultant suspension may be aged under atmospheric pressure or promptly washed, filtered, dried and crushed into a powder. The morphology, crystallinity and size dispersion of the subsequent nanoparticles are strongly dependent on the synthesis method and ripening time. (According to Sadat et al. [23]) HAp nano-particles can be prepared by the hydrolysis of other CaP phases including dicalcium phosphate dihydrate (DCPD), dicalcium phosphate anhydrous (DCPA) and tricalcium phosphate (TCP). The hydrolysis technique is, however, considered as a distinct method when one intends to change a prepared or a commercially available CaP into HAp powder. At pH values under 6 to 7, DCPA and DCPD phases are transforming into HAp. These phase

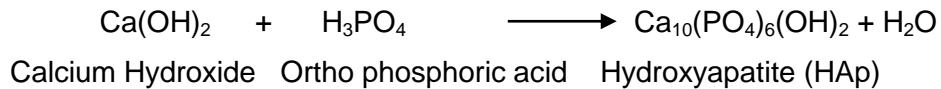
transformations depend to a great extent on the pH value, temperature and presence of other ions besides excess calcium and phosphate. (According to Sadat et al. [23]) The sol-gel strategy was one of the primary methods proposed for the wet synthesis of HAp. Sol-gel offers advantage of atomic level blending of reactants enhancing the chemical homogeneity of the resulting powder. Low-temperature formation and combination of the prepared crystals are other outstanding advantages of the sol-gel process. Moreover, a powder obtained by a typical sol-gel method generally shows a stoichiometric structure with a large surface area and a small cluster size (ranging from 50 nm to around 1  $\mu\text{m}$  depending upon the preparing parameters). Hydrothermal method is one of the most common methods for preparation of HAp powder. It is generally distinguished by the reaction of chemicals in an aqueous solution at elevated temperature and pressure. Hydrothermal synthesis can also be considered as chemical precipitation in which the aging step is conducted at a high temperature regularly over the boiling point of water inside an autoclave or pressure vessel. It has been shown that HAp nano-particles obtained from the hydrothermal conditions is generally stoichiometric and very crystalline. Also, phase purity and Ca/P proportion of HAp fundamentally enhance with increasing the hydrothermal temperature. Emulsion technique is proposed to be more productive to decrease the molecule size, control the morphology, and constrain the agglomeration of HAp particles. Sonochemical techniques, which always yield nano-sized items, depend on the chemical reactions initiated by capable ultrasound radiation. The physical mechanism behind the sonochemical synthesis is acoustic cavitation in an aqueous phase where the formation, growth and collapse of micro-bubbles occur. It has recently been shown that sonication increases the rate of HAp crystal development up to 5.5 times. It has also been reported that HAp nanoparticles combined by a sonochemical procedure have more uniform, smaller, and purer crystals with minimal agglomeration.

However, wet chemical precipitation method is chosen widely to synthesize HAp in comparison to the other techniques because of relatively large amount of HAp can be produced by precipitation technique in absence of organic solvents at a reasonable cost. The size, shape and surface area of the HAp particles obtained by this reaction are very sensitive to the orthophosphoric acid addition rate and the reaction temperature. The orthophosphoric acid addition rate is strongly linked to the pH obtained at the end of the synthesis and also to the suspension stabilization.



### 3.4 HAp preparation through wet chemical precipitation technique

(According to Afshar et al. [24] to Yeong et al. [45]) Analytical grade calcium Hydroxide ( $\text{Ca}(\text{OH})_2$ ) powder (Merck, 96%) and orthophosphoric ( $\text{H}_3\text{PO}_4$ ) acid (Merck, 85%) were weighted at molar ratio of  $\text{Ca}/\text{P}=1.67$  to prepare HAp powder as homogenous solution. The chemical reaction for wet chemical process may be expressed as follows:



This type of method is known as wet chemical precipitation route. The flow chart of wet chemical precipitation route for HAp preparation is shown in Figure 3.1. In this method, ten grams of calcium hydroxide is initially weighted in a weighing machine (Mettler Toledo, 0.01 g accuracy). It is mixed with water about 40 times. The solution is stirred by a magnetic stirrer (Remi Equipments Pvt. Ltd.) at  $50^\circ\text{C}$  to  $60^\circ\text{C}$  for 3 to 4 hours. Then, orthophosphoric acid is mixed with the solution at the rate of 30 drops/minute through a burette and continuously stirred but heat input to the solution is stopped. Care is taken to reach at pH value of the solution at 8 to 10. If pH value of the solution drops below the threshold values, ammonia solution (Merck, 25%) may be added to increase the pH value. After 5 to 6 hours, magnetic stirrer is stopped and the mixer is keep for 12 hours at room temperature. Then, precipitations are collected using a filter paper. (According to Yoruc and Koca [46] to Wang et al. [60]) The HAp precipitations are dried at  $80^\circ\text{C}$  in an oven and calcined at  $850^\circ\text{C}$  for 2 to 3 hours in muffle furnace.

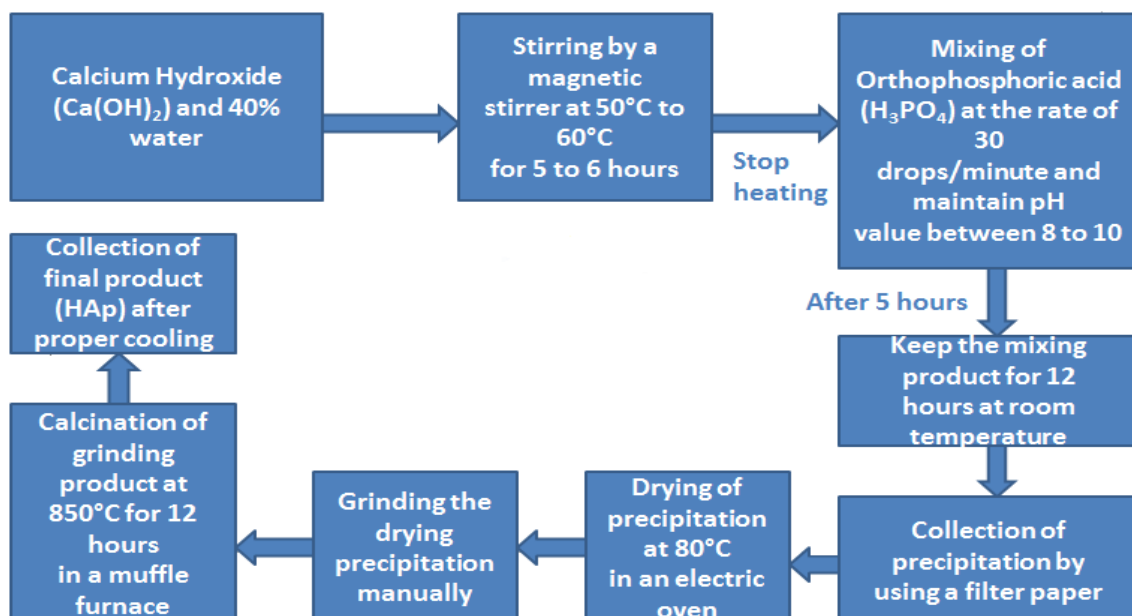


Figure 3.1 Flow chart of wet chemical precipitation route for HAp preparation

## 3.5 Processing and fabrication of ceramic composites

### 3.5.1 Preparation of HAp/PC composite

Composites with various amounts of HAp (0, 10, 20 vol. %) were fabricated by mixing through Batch Mixer (Rheomix 600, Germany) (Figure 3.2), granulating, melting and micro-injection molding (Figure 3.3). (According to Bakar et al. [61] to Liu and Ma [68]) Initially, the raw materials (i.e. HAp powder and Polymers) were pre-dried in an oven (Figure 3.4) at 120°C for 4 hours. Dried HAp powder is mixed with PC polymer with a density of 3.15 g/cm<sup>3</sup> and mean particle size of 2.248 µm through Batch Mixer. The mixtures were then granulated into small granules manually through cutter. The granules were then again pre-dried in an oven at 120°C for 4 hours and melted through Micro-Compounder (XPLORE, 15 ml, DSM, Netherlands) (Figure 3.5) and molded through Micro-injection molding machine to produce standard dog bone shaped tensile specimen (ASTM D638), Compressive specimen (ASTM D695), Flexural specimen (ASTM D790) and impact specimens (ASTM D256).

(According to Liu and Wang [69] to Sousa et al. [76]) The micro-injection molding machine parameters were injection pressure of 6 to 7 bar, mould temperature of 85°C, melt temperature of 230°C to 240°C, heating in three front zones as well as in three rear zones were maintained at a temperature of 210°C, 220°C and 230°C, rotor speed of 100 rpm, time required for loading, holding, and cooling is of 5 seconds, 30 seconds and 30 seconds respectively, mixing time is of 1 to 2 minutes and nozzle temperature is of 240°C.



Figure 3.2 Batch Mixer



Figure 3.3 Micro-injection molding machine

### 3.5.2 Preparation of HAp/PSU composite

(According to Szaraniec et al. [77] to Wang [85]) As viscosity is too high of this composite, it is not possible to mix HAp in large amount with PSU polymer in Batch mixer as well as in twin screw extruder. (According to Wang [86] to Ignjatovic and Uskokovic [105]) Therefore, composites with various small amounts of HAp (0, 10, 20 vol. %) were fabricated by mixing and melting through Micro-Compounder (XPLORE, 15 ml, DSM, Netherlands) and molded through Micro-injection molding machine directly to produce standard dog bone shaped tensile specimen (ASTM D638), Compressive specimen (ASTM D695), Flexural specimen (ASTM D790) and impact specimens (ASTM D256). Initially, the raw materials (i.e. HAp powder and Polymers) were pre-dried at 120°C for 4 hours. (According to Kim et al. [106] to Tayton et al. [116]) Dried HAp powder is mixed and melted with PSU polymer with a density of 3.15 g/cm<sup>3</sup> and mean particle size of 2.248 μm through micro-compounder and molded through Micro-injection molding machine. The micro injection molding machine parameters were injection pressure of 7 to 8 bar, mould temperature of 80°C, melt temperature of 345°C to 360°C, heating in three front zones as well as in three rear zones were maintained at a temperature of 330°C, 340°C and 350°C, rotor speed of 100 rpm, time required for loading, holding, and cooling is of 5 seconds, 30 seconds and 30 seconds respectively, mixing time is of 3 to 4 minutes and nozzle temperature is of 360°C.



Figure 3.4 An Electric Oven



Figure 3.5 Micro-compounder

## 3.6 Results and discussion

### 3.6.1 Particle size analysis

Particle size analysis for dry HAp and sintered HAp was done through particle size analyser (Malvern zetasizer, Nano-ZS90, England, UK) (Figure 3.6) is shown in Figure 3.7 and Figure 3.8 respectively.



Figure 3.6 Particle size analyser

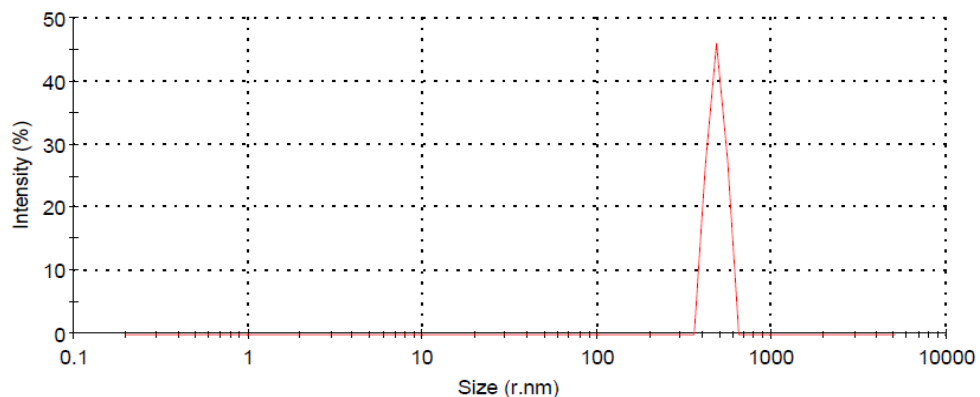


Figure 3.7 Particle Size Distribution by Intensity of Dry Hydroxyapatite (DHAp)

Figure 3.7 shows the particle size distribution by intensity of Dry Hydroxyapatite (DHAp) which has taken randomly a single peak of radius size of 481 nm and radius width of 51.8 nm with 100% intensity while the average radius size of DHAp is 1418 nm. The calculated average diameter of dry HAp is 2.836  $\mu\text{m}$ .

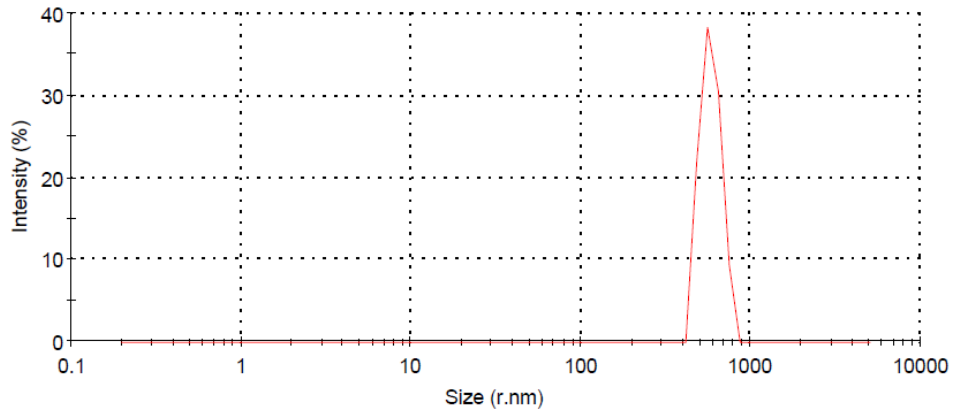


Figure 3.8 Particle Size Distribution by Intensity of Sintered Hydroxyapatite (SHAp)

Figure 3.8 shows the particle size distribution by intensity of Sintered Hydroxyapatite (SHAp) which has taken randomly a single peak of radius size of 581.1 nm and radius width of 78.39 nm with 100% intensity while the average radius size of SHAp is 1124 nm. The calculated average diameter of sintered HAp is 2.248  $\mu\text{m}$ .

### 3.6.2 X-Ray Diffraction (XRD) analysis

XRD analysis of dry HAp and sintered HAp was done through X-ray diffractometer (Ultima IV, Japan) (Figure 3.9) is shown in Figure 3.10 and Figure 3.11 respectively.



Figure 3.9 X-ray diffractometer



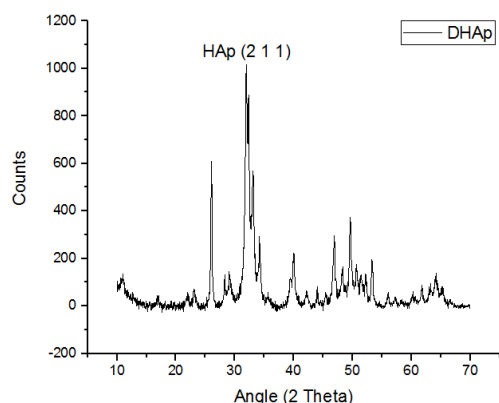


Figure 3.10 XRD analysis of Dry HAp

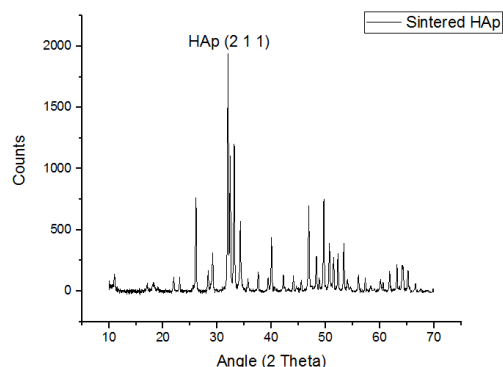


Figure 3.11 XRD analysis of sintered HAp

XRD analysis of dry HAp is shown in Figure 3.10 which reveals that there is a very broad peak means it shows non-crystalline in nature of HAp while XRD analysis of sintered HAp which is shown in Figure 3.11 results that there is a very narrow peak as compared to dry HAp means it shows crystalline in nature of HAp.

### **Name and formula**

Reference code:	74-0566
Mineral name:	Hydroxyapatite
ICSD name:	Calcium Hydroxide Phosphate
Empirical formula:	$\text{Ca}_{10}\text{H}_2\text{O}_{26}\text{P}_6$
Chemical formula:	$\text{Ca}_{10}(\text{PO}_4)_6(\text{OH})_2$

### **Crystallographic parameters**

Crystal system:	Hexagonal
a (Å):	9.4240
b (Å):	9.4240
c (Å):	6.8790
Alpha (°):	90.0000
Beta (°):	90.0000
Gamma (°):	120.0000
Calculated density:	3.15
Volume of cell:	529.09

### **3.6.3 Fourier transform infrared (FTIR) analysis**

FTIR analysis of dry HAp and sintered HAp was done through FTIR spectrometer (Perkin Elmer, Model no. Spectrum Two, Serial no. 99302, USA) (Figure 3.12) with KBr powder in pellet form is shown in Figure 3.13 and Figure 3.14 respectively. For this very small amount of HAp powder is first mixed with KBr powder and then fills it in pellet

maker machine with pressure maintained at 10 tons through hydraulic press to make required pellets for FTIR test.



Figure 3.12 FTIR spectrometer

An FTIR spectrum of dry HAp is shown in Figure 3.13. FTIR spectra were recorded in the transmission mode in the range 4000 to 400  $\text{cm}^{-1}$ . The lower wavelength limit was chosen to encompass the highest known vibration frequency due to a fundamental molecular vibration. Broad peak between 3500 and 3000  $\text{cm}^{-1}$  were noticed on IR spectra indicated that the vibration of absorbed water ( $\text{OH}^-$ ) in the apatite lattice in accords with the HAp chemical formula ( $\text{Ca}_{10}(\text{PO}_4)_6(\text{OH})_2$ ).

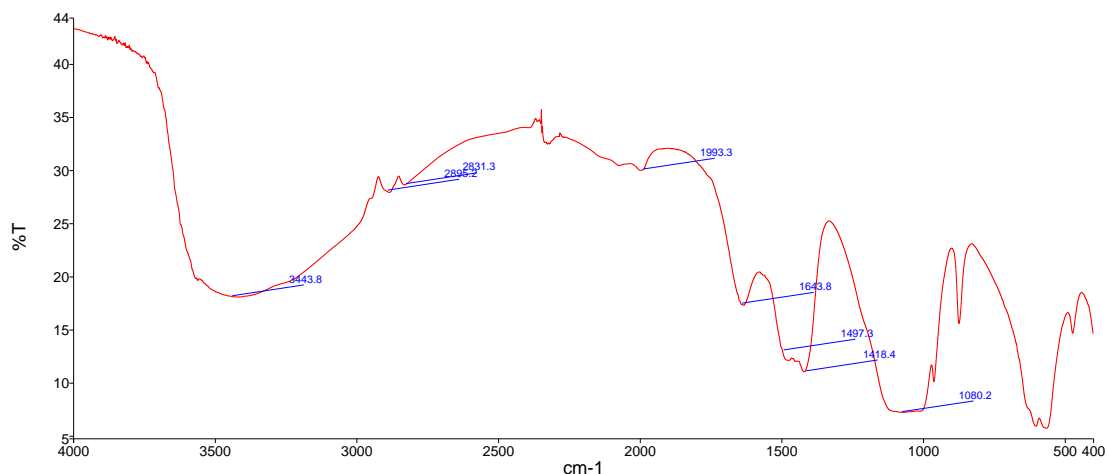


Figure 3.13 FTIR of dry HAp

There are various vibration modes representing the phosphate functional group. Those vibration modes were found on the FTIR spectra, thus confirming that the dry HAp powders were composed of phosphate group. The peaks of phosphate group were represented between 700 and 900  $\text{cm}^{-1}$  and 1200 and 1400  $\text{cm}^{-1}$ .

An FTIR spectrum of sintered HAp is shown in Figure 3.14. FTIR spectra were recorded in the transmission mode in the range 4000 to 400  $\text{cm}^{-1}$ . The lower wavelength

limit was chosen to encompass the highest known vibration frequency due to a fundamental molecular vibration. Broad peak between 3500 and 3300  $\text{cm}^{-1}$  were noticed on IR spectra indicated that the vibration of absorbed water ( $\text{OH}^-$ ) in the apatite lattice in accords with the HAP chemical formula ( $\text{Ca}_{10}(\text{PO}_4)_6(\text{OH})_2$ ).

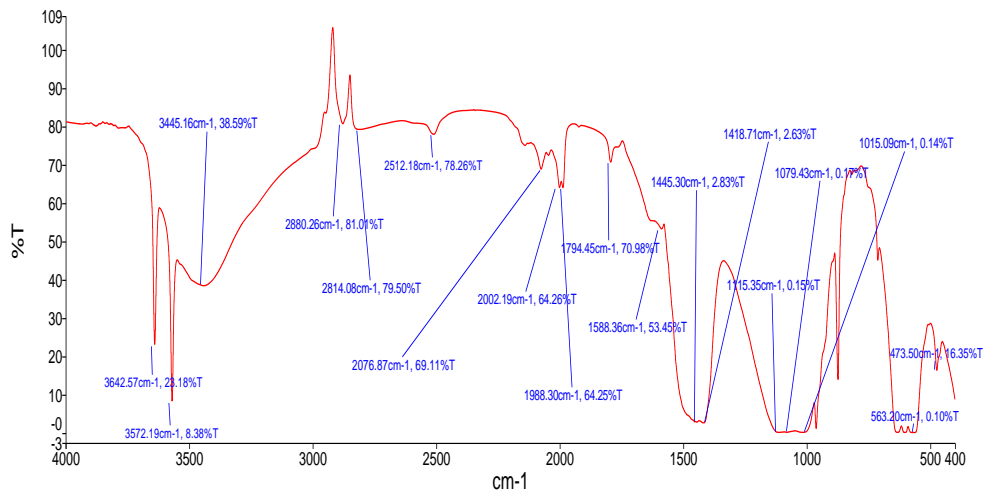


Figure 3.14 FTIR of HAP (calcined at 850°C) powder pellet

There are various vibration modes representing the phosphate functional group. Those vibration modes were found on the FTIR spectra, thus confirming that the calcined HAP powders were composed of phosphate group also. The peaks of phosphate group were represented between 600 and 800  $\text{cm}^{-1}$  and 1100 and 1400  $\text{cm}^{-1}$ .

### 3.6.4 Scanning electron microscope (SEM) analysis of ceramic composites

Scanning electron microscope (SEM) analysis of HAp/PC and HAp/PSU composites was done through scanning electron microscope machine (JEOL JSM-6480 LV) (Figure 3.15). For this initially the composite samples were fine coated through auto fine coater (JEOL JFC-1600) (Figure 3.16).



Figure 3.15 Scanning electron microscope



Figure 3.16 Auto fine coater



#### 3.6.4.1 SEM analysis of HAp/PC composite

SEM images of HAp/PC composite for 10 vol. % HAp and 20 vol. % HAp is shown in Figure 3.17 and Figure 3.18 respectively.

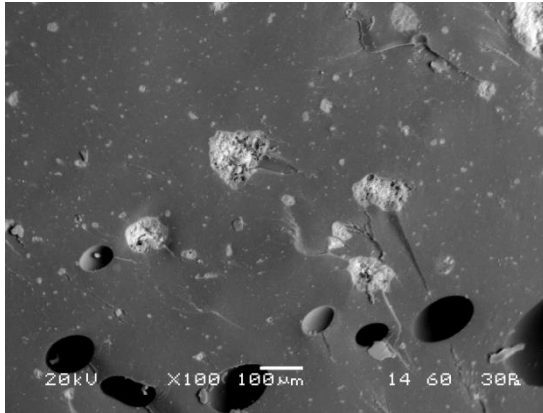


Figure 3.17 SEM image of 10 vol. % HAp/PC

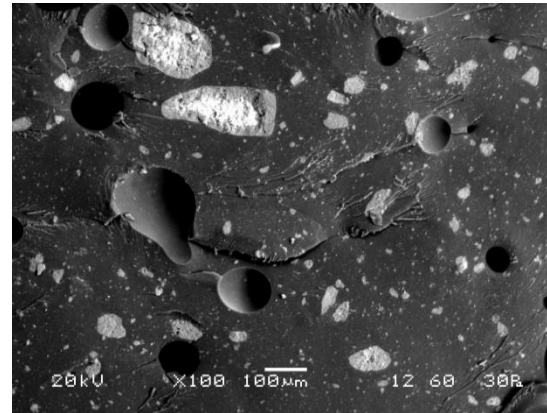


Figure 3.18 SEM image of 20 vol. % HAp/PC

SEM micrograph of HAp/PC from Figure 3.17 and Figure 3.18 shows that voids in the composite increases as HAp content increases from 10 vol. % to 20 vol. %. However, there is a uniform distribution of HAp particles into PC polymer matrix increasing bonding characteristics of HAp/PC composite.

#### 3.6.4.2 SEM analysis of HAp/PSU composite

SEM images of HAp/PSU composite for 10 vol. % HAp and 20 vol. % HAp is shown in Figure 3.19 and Figure 3.20 respectively.

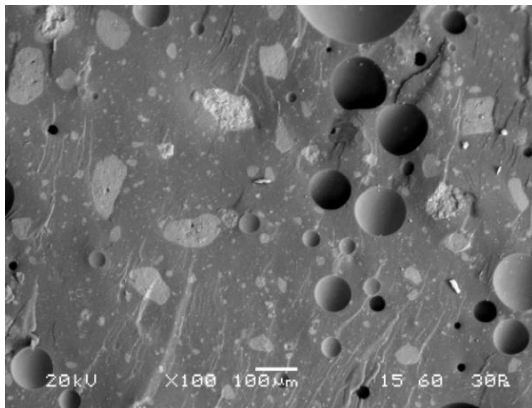


Figure 3.19 SEM image of 10 vol. % HAp/PSU

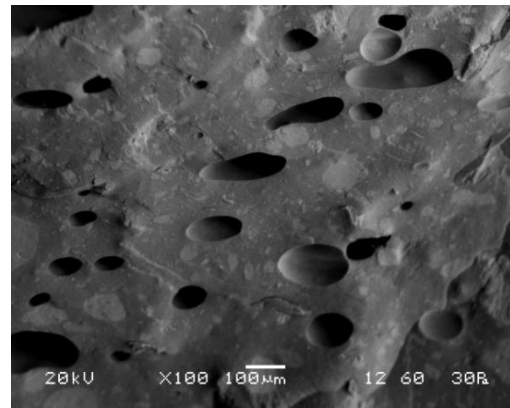


Figure 3.20 SEM image of 20 vol. % HAp/PSU

SEM micrographs of HAp/PSU from Figure 3.19 and Figure 3.20 show that there is very less chance of increasing voids as compared to HAp/PC composite when HAp content increases from 10 vol. % to 20 vol. %.

### 3.7 Conclusion

This chapter describes the detailed experimental procedure for Hydroxyapatite (HAp) powder preparation at laboratory level. The detailed specifications of the required

materials provided by the suppliers are discussed in this chapter. Different methods of HAp preparation, preparation methods of both composites i.e. HAp/PC and HAp/PSU are briefly discussed in this chapter. Dry methods do not use a solvent unlike wet methods. The characteristics of a powder synthesized by a dry method are not strongly influenced by the processing parameters; hence, most dry methods do not require precisely controlled conditions making them suitable for mass production of powders.

HAp powder generated from a typically dry method is usually large in size and irregular in shape. Therefore, wet methods have conventionally been applied to the preparation of HAp particles having a nano-sized structure with a regular morphology. Wet chemical reactions have advantages in their ability to control the morphology and the mean size of the powder, and, based on many experimental data, they are the most promising techniques for the fabrication of nano-HAp powder. Wet processes are usually easy to conduct and growth conditions can be directly controlled by adjusting the reaction parameters. Among the various wet processing methods, conventional chemical precipitation is the simplest route for the synthesis of nano-HAp powder. Wet chemical precipitation method is chosen widely to synthesize HAp in comparison to the other techniques because of relatively large amount of HAp can be produced by precipitation technique in absence of organic solvents at a reasonable cost. The size, shape and surface area of the HAp particles obtained by this reaction are very sensitive to the orthophosphoric acid addition rate and the reaction temperature. The orthophosphoric acid addition rate is strongly linked to the pH obtained at the end of the synthesis and also to the suspension stabilization.

The calculated average diameter of dry HAp is 2.836  $\mu\text{m}$  while the calculated average diameter of sintered HAp is 2.248  $\mu\text{m}$ .

XRD analysis of dry HAp reveals that there is a very broad peak means it shows non-crystalline in nature of HAp, while, in other hand, XRD analysis of sintered HAp results that there is a very narrow peak as compared to dry HAp means it shows crystalline in nature of HAp with pure phase.

An FTIR spectrum of dry HAp were recorded in the transmission mode in the range 4000 to 400  $\text{cm}^{-1}$ . The lower wavelength limit was chosen to encompass the highest known vibration frequency due to a fundamental molecular vibration. Broad peak between 3500 and 3000  $\text{cm}^{-1}$  were noticed on IR spectra indicated that the vibration of absorbed water ( $\text{OH}^-$ ) in the apatite lattice in accords with the HAp chemical formula ( $\text{Ca}_{10}(\text{PO}_4)_6(\text{OH})_2$ ), there are various vibration modes representing the phosphate functional group. Those vibration modes were found on the FTIR spectra, thus confirming that the dry HAp powders were composed of phosphate group. The peaks of phosphate group were represented between 700 and 900  $\text{cm}^{-1}$  and 1200 and 1400  $\text{cm}^{-1}$ , while, the

peaks of phosphate group were represented between 600 and 800  $\text{cm}^{-1}$  and 1100 and 1400  $\text{cm}^{-1}$  in the spectrum of sintered HAp.

SEM micrograph of HAp/PC shows that as HAp content increases from 10 vol. % to 20 vol. % there is a more chances of increasing voids however there is a very good distribution of HAp particles into PC polymer matrix which increases bonding characteristics of HAp/PC composite, while, SEM micrograph of HAp/PSU shows that as HAp content increases from 10 vol. % to 20 vol. % there is a very less chances of increasing voids as compared to HAp/PC composite.

## Chapter 4

# A Study on Characterization of Mechanical Properties of Ceramic Composites

### 4.1 Introduction

This chapter describes the characterization of mechanical properties of both ceramic composites i.e. HAp/PC and HAp/PSU composites. The density and void fraction of each composition for both composites are obtained in this chapter. Some comparison graphs between both composites of each variation of HAp volume percentage, tensile load displacement curves, and specifications of machines used for mechanical testing of specimens in tabular form are shown and also discussed in this chapter.

### 4.2 Density and void fraction

The theoretical density ( $\rho_{ct}$ ) of composite materials in terms of volume fraction can easily be obtained as per the following Equation 2 given by Agarwal and Broutman

$$\rho_{ct} = \rho_c V_c + \rho_p V_p \quad (4.1)$$

where  $V$  and  $\rho$  represent the volume fraction and density respectively. The suffix  $c$ ,  $p$  and  $ct$  stand for the ceramic, polymer and composite respectively. (According to Ahmad et al. [117]) The actual density ( $\rho_{ca}$ ) of the composite was evaluated by determining the test piece mass using weighing machine with the accuracy of  $\pm 10^{-2}$  gm and its volume basing on the apparent mass loss by immersing in water. The volume fraction of the voids (porosity) expressed as  $V_v$  in the composite is calculated as follows

$$V_v = (\rho_{ct} - \rho_{ca}) / \rho_{ct} \times 100 \quad (4.2)$$

The theoretical and actual densities along with the corresponding volume fraction of voids are presented in Table 4.1.

Table 4.1 Theoretical density, actual density and volume fraction of voids

Composite name	Composite designation	Theoretical density ( $\rho_{ct}$ ) (in g/cm <sup>3</sup> )	Actual density ( $\rho_{ca}$ ) (in g/cm <sup>3</sup> )	Volume fraction of voids ( $V_v$ ) (in %)
0 vol.% HAp/PC	A0	1.220	1.220	0.000
10 vol.% HAp/PC	A1	1.395	1.346	3.512
20 vol.% HAp/PC	A2	1.590	1.343	15.534
0 vol.% HAp/PSU	B0	1.240	1.240	0.000
10 vol.% HAp/PSU	B1	1.431	1.264	11.670
20 vol.% HAp/PSU	B2	1.622	1.352	16.646

It may be noted that the composite density values calculated theoretically from volume fractions using eq. 4.1 are not exactly same as the measured or actual values. This difference is a measure of voids present in the composites. It is clear from Table 4.1 that in A0 and B0 the volume fraction of voids is negligible and this is due to the absence of ceramic particles. With the addition of ceramic particles, more voids are found in the composite. As the ceramic content increases, the volume fraction of voids is also found to be increasing. This is due to the presence of empty spaces near sharp edges of the ceramic particles. This trend is observed in both the ceramic polymer composites from A1 to A2 and B1 to B2 irrespective of the ceramic particles. Density of a composite depends on the relative proportion of the matrix and reinforcing material and this is one of the most important factor determining the properties of the composites. The voids significantly affect some of the mechanical properties and even the performance of the composites. The knowledge of void content is desirable for estimation of the quality of the composites. It is understandable that an excellent composite should have fewer voids.

## 4.3 Results and discussion

### 4.3.1 Tensile load-displacement curves, tensile modulus, tensile strength, compressive strength, flexural strength, impact strength, hardness and inter-laminar shear stress

Tensile load-displacement curves of HAp/PC and HAp/PSU with each variation of HAp volume percentage is shown in Figure 4.1 to Figure 4.4.

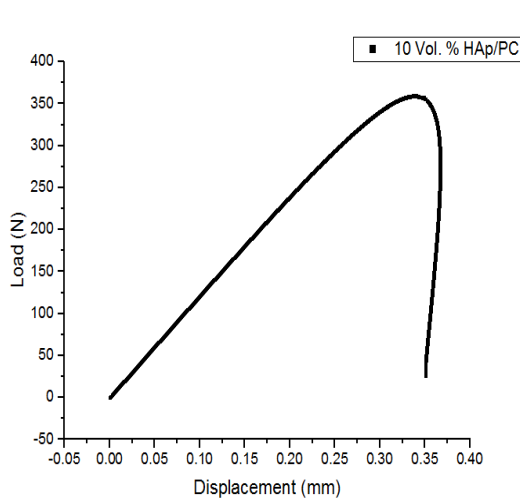


Fig. 4.1 Tensile load-displacement curve of 10 vol. % HAp/PC

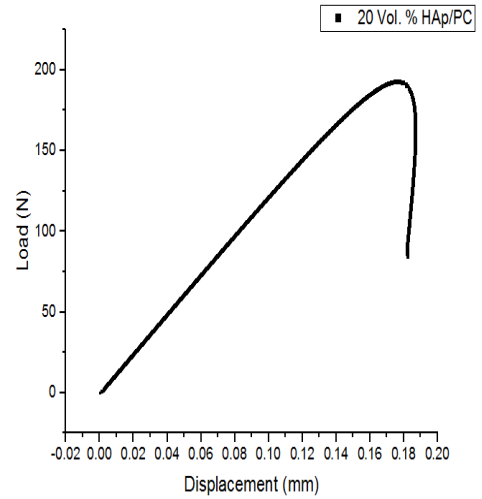


Fig. 4.2 Tensile load-displacement curve of 20 vol. % HAp/PC

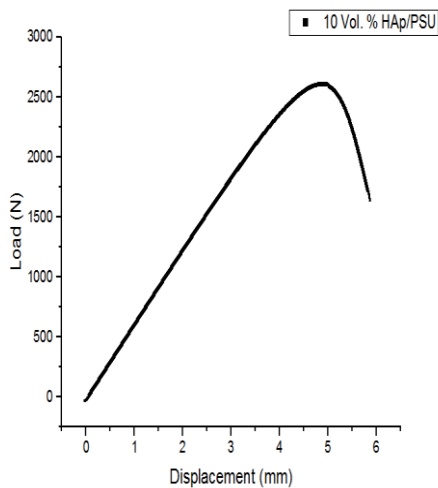


Fig. 4.3 Tensile load-displacement curve of 10 vol. % HAp/PSU

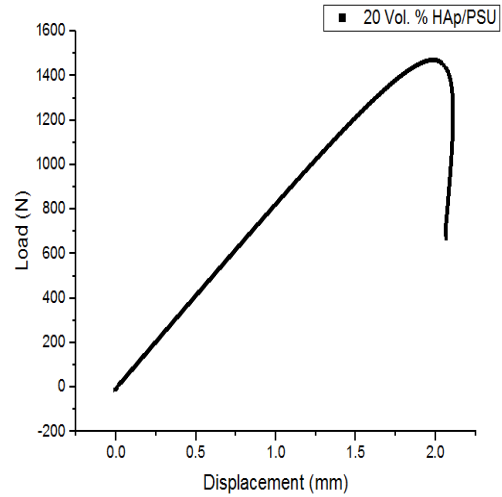


Fig. 4.4 Tensile load-displacement curve of 20 vol. % HAp/PSU

(According to Asuke et al. [118] to Kang et al. [125]) The specification of all machines used for testing is shown in Table 4.2. It can be seen from Figure 4.5 that Young's modulus continuously increasing from 0 vol. % up to 30 vol. % and then it is decreased in 40 vol. %. Hence, 30 vol. % gives maximum Young's modulus. Figure 4.6 shows that 15 vol. % gives maximum Young's modulus. Figure 4.7 and Figure 4.8 shows decrease in tensile strength as HAp volume percentage in composite increases.

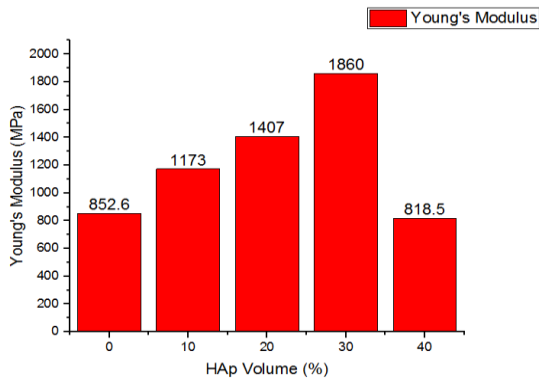


Figure 4.5 Graph between Young's Modulus and HAp Volume of HAp/PC Composite

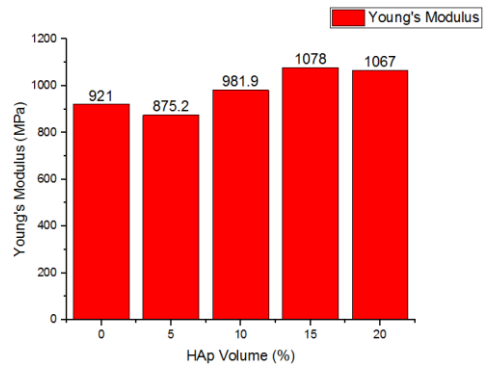


Figure 4.6 Graph between Young's Modulus and HAp Volume of HAp/PSU Composite

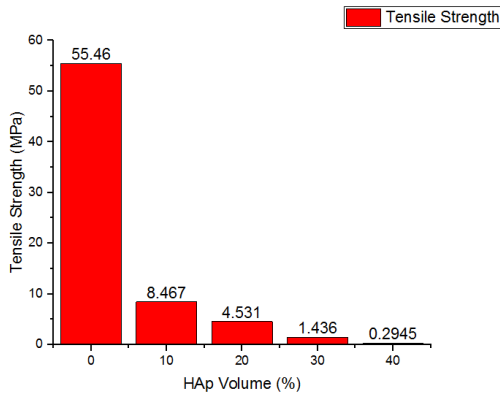


Figure 4.7 Graph between Tensile Strength and HAp Volume of HAp/PC Composite

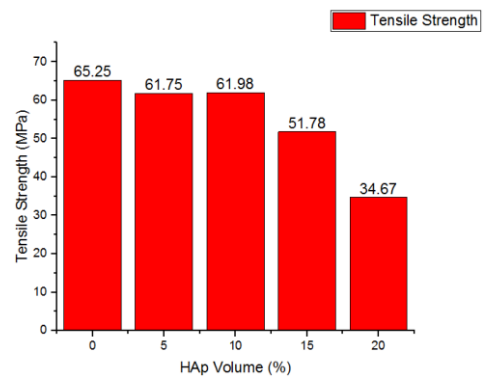


Figure 4.8 Graph between Tensile Strength and HAp Volume of HAp/PSU Composite

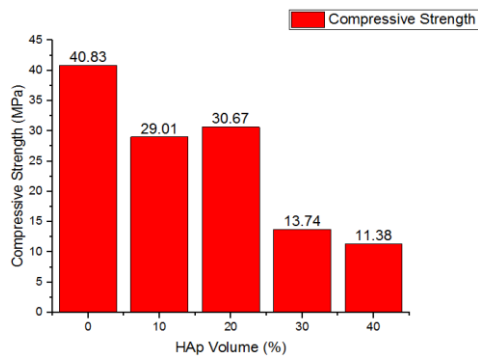


Figure 4.9 Graph between Compressive Strength and HAp Volume of HAp/PC Composite

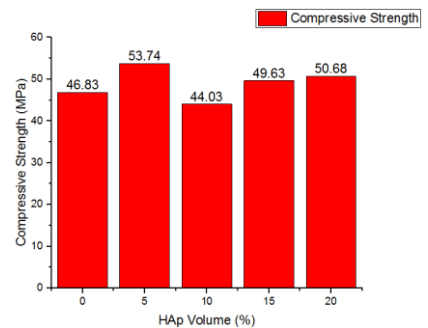


Figure 4.10 Graph between Compressive strength and HAp Volume of HAp/PSU Composite

(According to Nainar et al. [126] to Estevez et al. [135]) It can be seen from Figure 4.9 that compressive strength is initially increasing and then it is gradually decreasing as HAp vol. % increasing while Figure 4.10 shows that it is initially decreasing and then increasing as HAp vol. % increases. Figure 4.11 shows that 40 vol. % gives maximum impact strength while it can be seen from Figure 4.12 that impact strength initially increases and then decreases as HAp vol. % increases. Figure 4.13 to Figure 4.16 shows comparison graph between both composites on the basis of Young's modulus, tensile strength, compressive strength and impact strength. From Figure 4.17 and Figure 4.18, it can be seen that micro-indentation hardness increases as HAp vol. % increases. Figure 4.19 shows clearly the comparison graph between both composites on the basis of micro-indentation hardness.

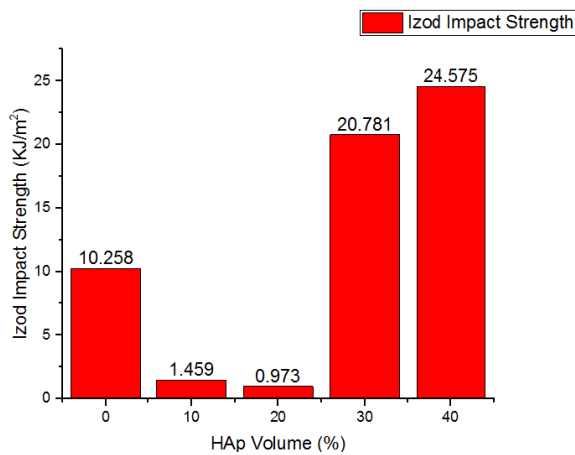


Figure 4.11 Graph between Izod Impact Strength and HAp Volume of HAp/PC Composite

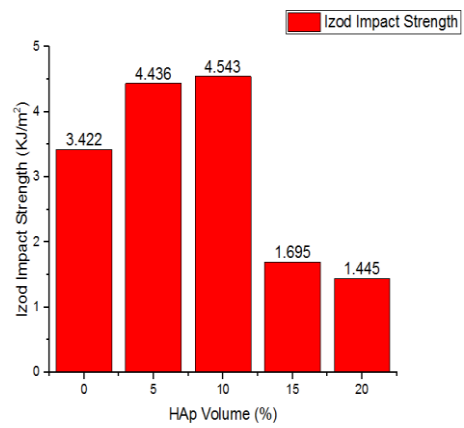


Figure 4.12 Graph between Izod Impact Strength and HAp Volume of HAp/PSU Composite

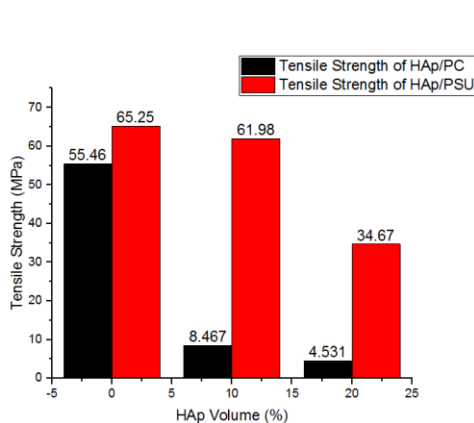


Figure 4.13 Graph between Tensile Strength of HAp/PC and HAp/PSU Composite

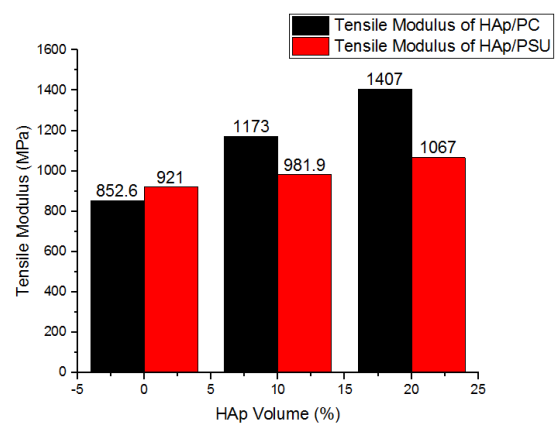


Figure 4.14 Graph between Young's Modulus of HAp/PC and HAp/PSU Composite



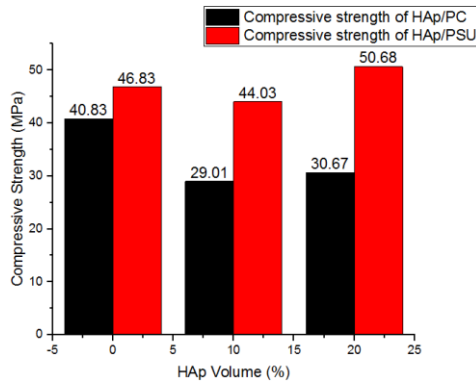


Figure 4.15 Graph between Compressive Strength of HAp/PC and HAp/PSU Composite

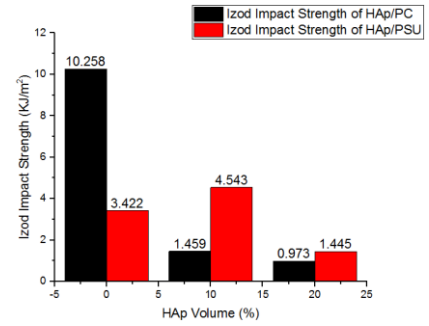


Figure 4.16 Graph between Izod Impact Strength of HAp/PC and HAp/PSU Composite

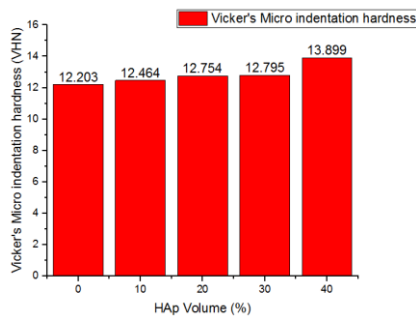


Figure 4.17 Graph between Micro-indentation hardness and HAp Volume of HAp/PC

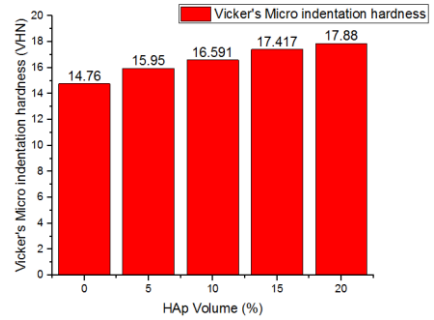


Figure 4.18 Graph between Micro-indentation hardness and HAp Volume of HAp/PSU

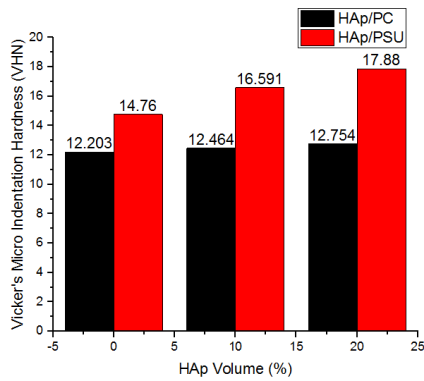


Figure 4.19 Graph between Micro-indentation hardness of HAp/PC and HAp/PSU

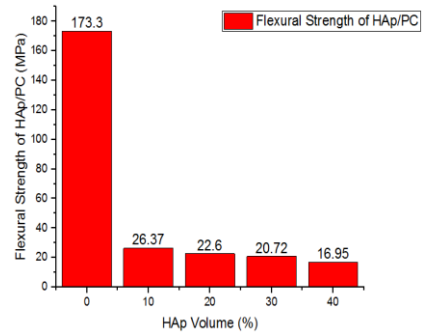


Figure 4.20 Graph between Flexural Strength and HAp Volume of HAp/PC

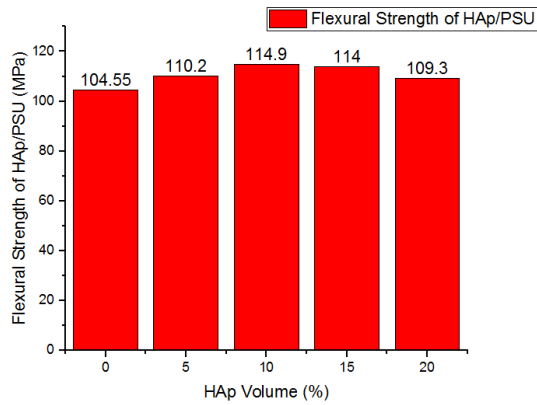


Figure 4.21 Graph between Flexural Strength and HAp Volume of HAp/PSU

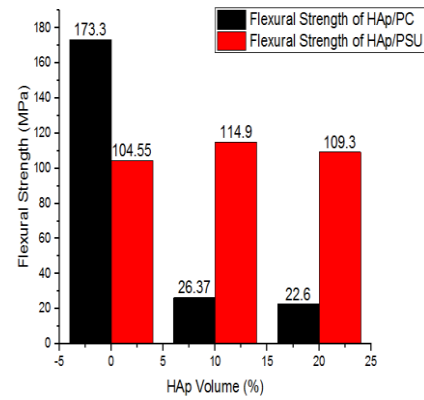


Figure 4.22 Graph between Flexural Strength of HAp/PC and HAp/PSU

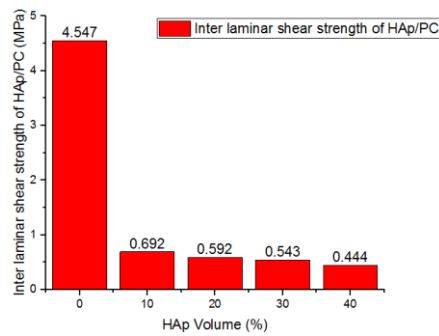


Figure 4.23 Graph between Inter laminar shear strength and HAp Volume of HAp/PC

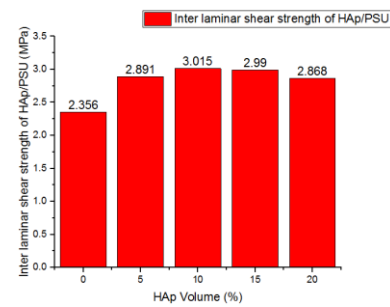


Figure 4.24 Graph between Inter laminar shear strength and HAp Volume of HAp/PSU

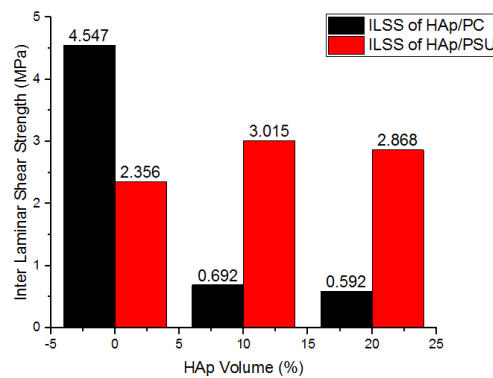


Figure 4.25 Graph between Inter laminar shear strength of HAp/PC and HAp/PSU Composites

(According to Griesh and Brown [136] to Ribeiro et al. [145]) Figure 4.20 shows that flexural strength gradually decreases as HAp vol. % increases while Figure 4.21 shows that initially flexural strength increases and then it decreases as HAp vol. % increases. Figure 4.22 shows the comparison graph between both composites on the basis of flexural strength. The data recorded in the flexural test is also used to determine the inter-laminar shear stress (ILSS) value which is calculated as:

$$ILSS = \frac{3P}{4bt} \quad (4.3)$$

where P is the maximum load, b is the width and t is the thickness of the specimen.

By calculating with the help of above equation, Figure 4.23 shows that inter laminar shear strength gradually decreases as HAp vol. % increases while Figure 4.24 shows that inter laminar shear strength initially increases and then it decreases as HAp vol. % increases. (According to Uskokovic et al. [146] to Zhang et al. [159]) Figure 4.25 shows the comparison graph between both composites on the basis of inter laminar shear strength.

Table 4.2 Specification of Machines used for Testing

Sl. No.	Testing Name	Machine Used	Variables	No. of Specimen Tested	ASTM Standard Used
1.	Tensile Testing	INSTRON 1195	Load cell: 100 KN Full scale load range: 20 KN Crosshead speed range : 1 mm/min to 5 mm/min	10×2	ASTM D638
2.	Compression Testing	INSTRON 1195	Load cell: 100 KN Full scale load range: 20 KN to 50 KN Crosshead speed range : 1 mm/min	10×2	ASTM D695
3.	Flexural Testing (3 point bend test)	INSTRON 1195	Load cell: 100 KN Full scale load range: 20 KN Crosshead speed range : 2 mm/min	10×2	ASTM D790
4.	Impact Testing	Pendulum type Izod Impact tester machine (Model: VEEKAYTLVS4)	Maximum hammer capacity: 21.4 J Striking angle: 150°	10×2	ASTM D256
5.	Hardness Testing	Vicker's Micro-hardness tester machine (Model: Vaiseshika, 7005, AP-32)	Load: 50 gram force	10×2	

## 4.4 Conclusion

This chapter describes the characterization of mechanical properties i.e. tensile, compressive, flexural, impact and hardness of both ceramic composites i.e. HAp/PC and HAp/PSU composites. The density and void fraction of each composition for both composites are obtained in this chapter. Some comparison graphs between both composites of each variation of HAp volume percentage, tensile load displacement curves, and specifications of machines used for mechanical testing of specimens in tabular form are shown and also discussed in this chapter.

It is clear that the volume fraction of voids in A0 and B0 is negligible due to the absence of ceramic particles. With the addition of ceramic particles, more voids are found in the composite. As the ceramic content increases, the volume fraction of voids is also found to be increasing. This is due to the presence of empty spaces near sharp edges of the ceramic particles. This trend is observed in both the ceramic polymer composites from A1 to A2 and B1 to B2 irrespective of the ceramic particles. Density of a composite depends on the relative proportion of the matrix and reinforcing material and this is one of the most important factor determining the properties of the composites. The voids significantly affect some of the mechanical properties and even the performance of the composites. The knowledge of void content is desirable for estimation of the quality of the composites. It is understandable that an excellent composite should have fewer voids.

It can be seen that in HAp/PC composite, Young's modulus continuously increasing from 0 vol. % up to 30 vol. % and then it is decreased in 40 vol. %. Hence, 30 vol. % gives maximum Young's modulus while in case of HAp/PSU composite, 15 vol. % gives maximum Young's modulus. It is revealed that tensile strength decreases as HAp volume percentage increases for the both composites. It can be seen that compressive strength is initially increasing and then it is gradually decreasing as HAp vol. % increasing in HAp/PC composite while it is initially decreasing and then increasing as HAp vol. % increases for HAp/PSU composite. It clearly observed that HAp/PC composite of 40 vol. % gives maximum impact strength while it can be seen that impact strength initially increases and then decreases as HAp vol. % increases in HAp/PSU composite. It can also be seen that in both composites, micro-indentation hardness increases as HAp vol. % increases. It is clear that flexural strength gradually decreases as HAp vol. % increases in HAp/PC composite while flexural strength initially increases and then decreases as HAp vol. % increases in HAp/PSU composite.

## Chapter 5

# A Study on Performance of Ceramic Composites under various Wear Modes

### 5.1 Introduction to wear

(According to Bodhak et al. [160]) Wear can be defined as a progressive loss of material from the surface of a body. As soon as the base body and counter-body come into contact, wear occurs. Signs of wear are small detached wear particles, material removal from a body due to friction, and material and shape changes of the tribologically loaded material zone of one or both friction parts.

(According to Hu et al. [163]) Wear is a process of removal of material from one or both of two solid surfaces in solid state contact, occurring when these two solid surfaces are in sliding or rolling motion together.

(According to Mohan et al. [164]) Wear is the progressive damage involving material loss which occurs on the surface of a component as result of its motion relative to the adjacent working parts.

Wear processes can be classified into different types i.e. abrasive wear, adhesive wear, erosive wear, sliding wear, fretting wear, corrosive wear and surface fatigue wear. However, in this study, we focussed mainly on abrasive wear, erosive wear, sliding wear, and fretting wear.

#### 5.1.1 Abrasive wear

Abrasive wear occurs whenever a solid object is loaded against particles of a material that have equal or greater hardness. Abrasive wear is caused due to hard particles that are forced against to move along a solid surface. Abrasive wear is usually divided into two modes: two-body and three-body abrasion. The situation where exactly two bodies are involved in the interaction is known as two-body abrasion. (According to Chauhan and Thakur [161]) Two-body abrasive wear is caused by the displacement of material from a solid surface due to hard particles sliding along the surface or when rigidly held grits pass over the surface like a cutting tool. In three body abrasive wear, the grits are free to roll as well as slide over the surface.

### **5.1.2 Adhesive wear**

(According to Chowdhury et al. [162]) Adhesive wear is a phenomenon which occurs when two metals rub together with sufficient force to cause the removal of material from the less-wear resistant surface. This wear is dependent on physical and chemical factors such as material properties, presence of corrosive atmosphere or chemicals and dynamics like velocity and applied load.

### **5.1.3 Erosive wear**

(According to Hu et al. [163]) Erosive wear can be defined as the process of material removal due to impingement of solid particles on a surface. Erosion is caused by a gas or a liquid, which may or may not carry entrained solid particles, impinging on a surface

### **5.1.4 Sliding wear**

(According to Mohan et al. [164]) Sliding wear can be defined as it is a process of removal of material from one surface due to sliding of another surface over the other without any abrasives used in the base body. Sliding wear occurs when two same or different materials are contacted to each other.

### **5.1.5 Fretting wear**

Fretting wear can be defined as it is a surface damage phenomenon that occurs between two contacting surfaces experiencing cyclic motion (oscillatory tangential displacement) of small amplitude.

### **5.1.6 Tribo-chemical or corrosive wear**

Corrosive wear is defined as the damage caused by synergistic attack of wear and corrosion when wear occurs in a corrosive environment (atmosphere, moisture accumulation, bacteria, acids, electrolytes, process chemicals or lubricant by-products).

### **5.1.7 Surface fatigue wear**

Surface fatigue wear is caused due to fatigue-related cracks and flaking triggered by repeated alternating tribological stress cycles (e.g. rolling fatigue). This wear usually occurs in systems involving rolling (such as rail and wheel systems) or repeated sliding which results in surface or sub-surface cracks due to tensile and/or shear stresses. Surface fatigue wear does not occur in a system in which other forms of wear are occurring.

## 5.2 Results and discussion

### 5.2.1 Experimental details of Two-body abrasive wear behavior of ceramic composites

The two-body abrasion wear test of hydroxyapatite (HAp)/polycarbonate (PC) and HAp/polysulfone (PSU) composites were performed on pin-on-disc friction and wear test rig (Model: MAGNUM Engineers, An ISO 9001:2000 Company) (ASTM G99) is shown in Figure 5.1.



Figure 5.1 Pin-on-disc friction and wear test rig

(According to Silva et al. [165]) The experiment was conducted using three different water proof silicon carbide (SiC) abrasive papers of 400, 600 and 1000 grit size. To proceed further, Taguchi's  $L_{27}$  orthogonal array was used to evaluate the tribological properties with four control variables such as HAp volume, load applied, sliding speed and track radius each at three levels. The highest wear loss was noticed at the specimens worn on 400 grit size SiC paper than 600 grit size and 1000 grit size SiC paper. This is due to the larger size of the abrasive grains in 400 grit size SiC paper causing greater damage to the specimen surface. The experimental data of wear test of the composites showed that the wear behavior of the composites strongly depends on the grit size of the abrasive papers.

Two-body abrasion wear test was conducted on pin-on-disc friction and wear test rig. It consists of loaded lever arm, load cell, steel disc plate of 164 mm diameter, and square pin holder of  $8 \times 8 \text{ mm}^2$  with the screw. The length, width and thickness of the composite pin are kept as 25mm, 6mm and 3.32 mm respectively. The surface of the specimens is cleaned with acetone before conducting the test on it. Initially and finally for each experimental run, the pin is weighed in weighing machine (Mettler Toledo, 0.001 g

accuracy) and fixed in pin holder with the help of the screw. Then, it is fixed with the lever arm in such a way that the pin is just touch on abrasive paper which is glued on a steel disc. After that through load cell, load is applied on the pin with the help of the lever arm. The difference between initial and final weight of the sample gives wear loss of the composite. The weight loss was converted into volume loss by using the density of the composite. The specific wear rate (Ks) was calculated using following mathematical relation:

$$\text{Specific wear rate (Ks)} = \frac{\Delta V}{L \times d} \quad \text{m}^3/\text{Nm} \quad (5.1)$$

where,  $\Delta V$  is the volume loss in  $\text{m}^3$ , L is the load in Newton and d is the sliding distance in meters.

The selected input parameters and their levels of abrasive wear for both composites are shown in Table 5.1.

Table 5.1 Control parameters and their levels

Control Parameters	Symbol	Level			Unit
		1	2	3	
HAp Volume	A	0	10	20	%
Load Applied	B	10	20	30	N
Sliding Speed	C	300	400	500	RPM
Track Radius	D	20	30	40	mm

There are four factors; each factor is varied at three levels. A full factorial design would have required 81 experiments. However, Taguchi design was applied to reduce the number of experiments. The total number of experimental runs is 27 ( $L_{27}$ ). The output value is abrasion wear loss (in gram) which is the difference between initial and final weight of the pin. Each experiment was run for 5 minutes. The experimental observations for abrasion wear loss are transformed into Signal to Noise (S/N) ratio. S/N ratio is used to determine the performance characteristics. Generally, S/N ratio used are lower-the-better, higher-the-better, and nominal-the-best. Since wear loss is undesirable characteristic, lower-the better characteristic is used. Irrespective of the type of the performance characteristics, the larger signal to noise ratio corresponds to the better performance characteristic. The objective of the experimental layout is to minimize the abrasion wear loss. The signal to noise ratio of lower-the-better performance characteristic can be expressed as

$$(S/N)_{\text{LTB}} = -10 \log \sum y_i^2$$

where,  $y_i$  is the output value.



The experimental data for HAp/PC composite conducted at 400 grit size paper is shown in Table 5.2.

Table 5.2 Experimental data for HAp/PC composite conducted at 400 grit size paper

Exp. No.	Factor A (HAp Volume) %	Factor B (Load Applied) N	Factor C (Sliding Speed) RPM	Factor D (Track Radius) mm	Wear Loss (gm)	S/N ratio (Lower The Better)
1	0	10	300	20	0.017	35.391
2	0	10	300	20	0.015	36.478
3	0	10	300	20	0.016	35.917
4	0	20	400	30	0.059	24.582
5	0	20	400	30	0.060	24.436
6	0	20	400	30	0.061	24.293
7	0	30	500	40	0.084	21.514
8	0	30	500	40	0.083	21.618
9	0	30	500	40	0.085	21.411
10	10	10	400	40	0.297	10.544
11	10	10	400	40	0.296	10.574
12	10	10	400	40	0.296	10.574
13	10	20	500	20	0.251	12.006
14	10	20	500	20	0.253	11.937
15	10	20	500	20	0.252	11.971
16	10	30	300	30	0.119	18.489
17	10	30	300	30	0.117	18.636
18	10	30	300	30	0.118	18.562
19	20	10	500	30	0.106	19.493
20	20	10	500	30	0.107	19.412
21	20	10	500	30	0.108	19.331
22	20	20	300	40	0.059	24.582
23	20	20	300	40	0.061	24.293
24	20	20	300	40	0.060	24.436
25	20	30	400	20	0.100	20.000
26	20	30	400	20	0.102	19.827
27	20	30	400	20	0.101	19.913

The analysis of variance (ANOVA) table for S/N ratio of HAp/PC composite is shown in Table 5.3.

Table 5.3 ANOVA Table for S/N ratio of HAp/PC composite

Source	DF value	Seq SS	Adj SS	Adj MS	F value	P value	Percentage Contribution
A	2	835.05	835.05	417.52	10186.11	0.000	62.339
B	2	20.44	20.44	10.22	249.30	0.000	1.525
C	2	419.43	419.43	209.72	5116.37	0.000	31.311
D	2	63.86	63.86	31.93	779.02	0.000	4.767
Error	18	0.74	0.74	0.04			
Total	26	1339.52					

S = 0.202458, R-Sq = 99.94%, and R-Sq(adj) = 99.92%

From percentage contribution, it can be concluded here that significance of factors is in the order of Factor A, C, D and B.

Main effects plot for S/N ratio, normal probability plot and interaction plot are shown in Figure 5.2, 5.3 and 5.4 respectively.

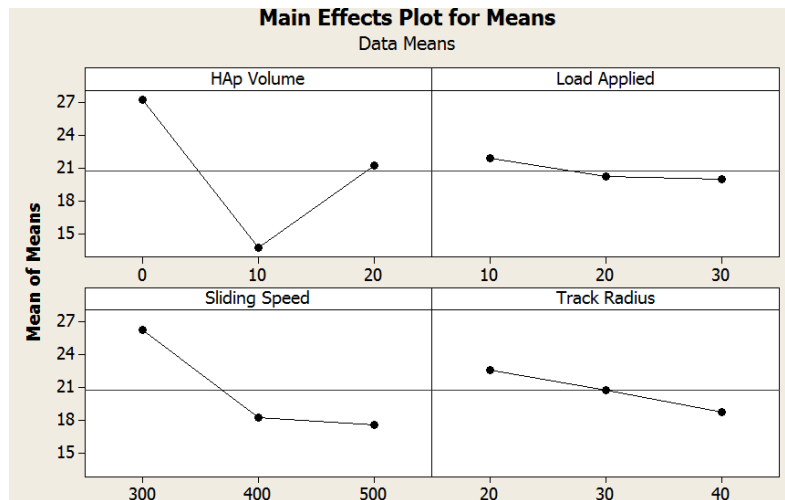


Figure 5.2 Main effects plot for means of S/N ratio

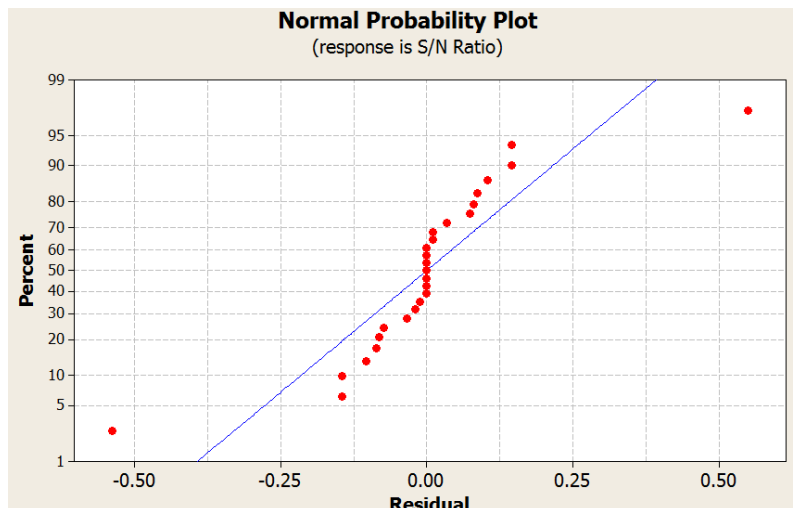


Figure 5.3 Normal probability plot for S/N ratio

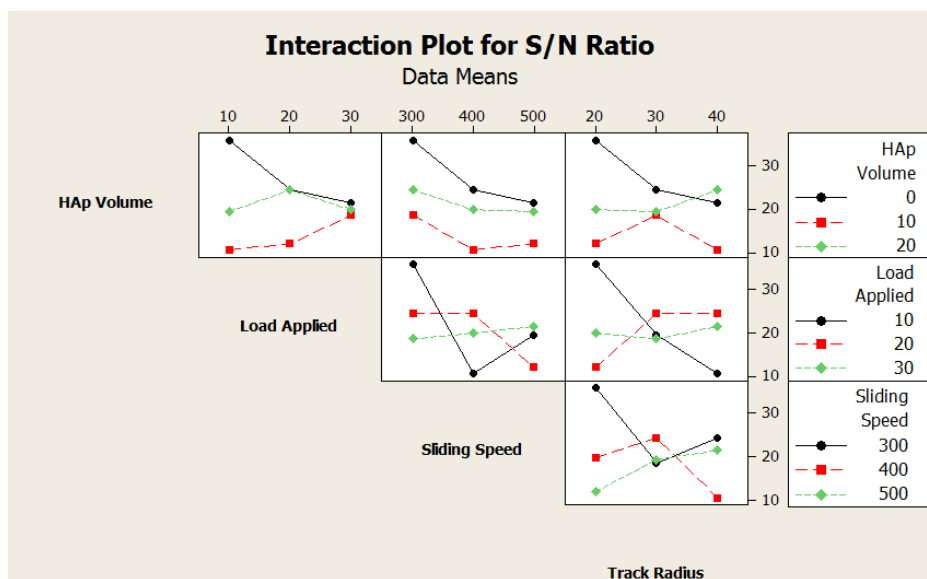


Figure 5.4 Interaction plot for S/N ratio

According to Figure 5.2, it is concluded that the optimal parametric combination is A<sub>1</sub>B<sub>1</sub>C<sub>1</sub>D<sub>1</sub>. When HAp volume is 0 vol. %, Load is 10 N, Sliding speed is 300 RPM and Track radius is 20 mm then minimum abrasive wear can be obtained. Referring to Figure 5.3, it can be concluded that the ANOVA proceeds in a satisfactory manner as the residuals follow a normal distribution. Figure 5.4 shows that two factor interaction of controllable factors seems to exist. However, the interaction of factors has not been considered for the sake of simplicity.

The calculation for volume loss, sliding distance, wear rate, and specific wear rate are shown in Eq. 5.2, Eq. 5.3, Eq. 5.4, and Eq. 5.5 respectively.

$$Volume\ loss = \frac{Weight\ loss}{Density} \quad (5.2)$$

where weight loss is in gm and density is in gm/cm<sup>3</sup>

$$Sliding\ Distance = \pi \times 2r \times N \times t \quad (5.3)$$

where r is the track radius in mm, N is the rpm, and t is the time in minutes

$$Wear\ rate = \frac{Volume\ loss}{Sliding\ distance} \quad (5.4)$$

where volume loss is in cm<sup>3</sup> and sliding distance is in m

$$Specific\ wear\ rate = \frac{Volume\ loss}{Sliding\ distance \times load} \quad (5.5)$$

where volume loss is in cm<sup>3</sup>, sliding distance is in m, and load is in N

Table 5.4 shows the calculation data for HAp/PC composite conducted at 400 grit size paper in terms of volume loss, sliding distance, wear rate and specific wear rate

Table 5.4 Calculation data for HAp/PC composite conducted at 400 grit size paper

Experiment No.	Weight Loss (gm)	Volume Loss (cm <sup>3</sup> )	Sliding Distance (m)	Wear Rate 10 <sup>-6</sup> (cm <sup>3</sup> /m)	Specific Wear Rate 10 <sup>-6</sup> (cm <sup>3</sup> /Nm)
1	0.017	0.014	188.495	74.272	7.427
2	0.015	0.012	188.495	63.662	6.366
3	0.016	0.013	188.495	68.967	6.896
4	0.059	0.049	376.991	129.976	6.498
5	0.060	0.050	376.991	132.629	6.631
6	0.061	0.051	376.991	135.281	6.764
7	0.084	0.070	628.318	111.408	3.713
8	0.083	0.069	628.318	109.817	3.660
9	0.085	0.071	628.318	113.000	3.766
10	0.297	0.247	502.654	491.391	4.913
11	0.296	0.246	502.654	489.402	4.894
12	0.296	0.246	502.654	489.402	4.894
13	0.251	0.209	314.159	665.268	33.263
14	0.253	0.211	314.159	671.634	33.581
15	0.252	0.210	314.159	668.451	33.422
16	0.119	0.099	282.743	350.141	11.671
17	0.117	0.097	282.743	343.067	11.435
18	0.118	0.098	282.743	346.604	11.553
19	0.106	0.088	471.238	186.742	1.867
20	0.107	0.089	471.238	188.864	1.888
21	0.108	0.090	471.238	190.986	1.909
22	0.059	0.049	376.991	129.976	6.498
23	0.061	0.050	376.991	132.629	6.631
24	0.060	0.050	376.991	132.629	6.631
25	0.100	0.084	251.327	334.225	11.140
26	0.102	0.085	251.327	338.204	11.273
27	0.101	0.084	251.327	334.225	11.140

Similarly, the experimental data for HAp/PSU composite conducted at 400 grit size paper is shown in Table 5.5.

Table 5.5 Experimental data for HAp/PSU composite conducted at 400 grit size paper

Experiment No.	Factor A (HAp Volume) %	Factor B (Load Applied) N	Factor C (Sliding Speed) RPM	Factor D (Track Radius) mm	Wear Loss (gm)	S/N ratio (Lower The Better)
1	0	10	300	20	0.022	33.151
2	0	10	300	20	0.021	33.555
3	0	10	300	20	0.023	32.765
4	0	20	400	30	0.041	27.744
5	0	20	400	30	0.040	27.958
6	0	20	400	30	0.039	28.178
7	0	30	500	40	0.085	21.411
8	0	30	500	40	0.084	21.514
9	0	30	500	40	0.086	21.310
10	10	10	400	40	0.110	19.172
11	10	10	400	40	0.111	19.093
12	10	10	400	40	0.110	19.172
13	10	20	500	20	0.077	22.270
14	10	20	500	20	0.079	22.047
15	10	20	500	20	0.078	22.158
16	10	30	300	30	0.091	20.819
17	10	30	300	30	0.090	20.915
18	10	30	300	30	0.092	20.724
19	20	10	500	30	0.095	20.445
20	20	10	500	30	0.094	20.537
21	20	10	500	30	0.097	20.264
22	20	20	300	40	0.112	19.015
23	20	20	300	40	0.110	19.172
24	20	20	300	40	0.113	18.938
25	20	30	400	20	0.045	26.935
26	20	30	400	20	0.046	26.744
27	20	30	400	20	0.044	27.130

The ANOVA table for S/N ratio of HAp/PSU composite is shown in Table 5.6.

Table 5.6 ANOVA table for S/N ratio of HAp/PSU composite

Source	DF value	Seq SS	Adj SS	Adj MS	F value	P value	Percentage Contribution
A	2	231.653	231.653	115.827	3385.13	0.000	41.328
B	2	8.422	8.422	4.211	123.07	0.000	1.502
C	2	61.258	61.258	30.629	895.16	0.000	10.928
D	2	258.568	258.568	129.284	3778.44	0.000	46.130
Error	18	0.616	0.616	0.034			
Total	26	560.518					

S = 0.184976, R-Sq = 99.89%, and R-Sq(adj) = 99.84%

From percentage contribution, it can be concluded here that significance of factors is in the order of Factor D, A, C and B.

Main effects plot for means of S/N ratio, normal probability plot and interaction plot are shown in Figure 5.5, 5.6 and 5.7 respectively.

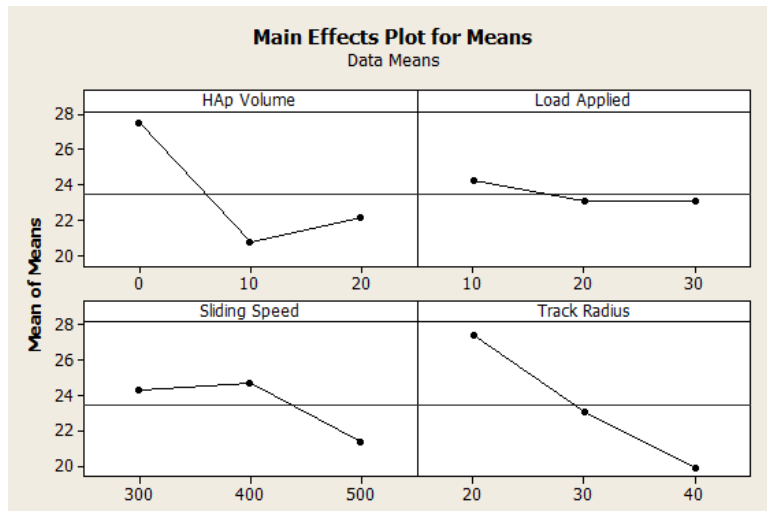


Figure 5.5 Main effects plot for means of S/N ratio

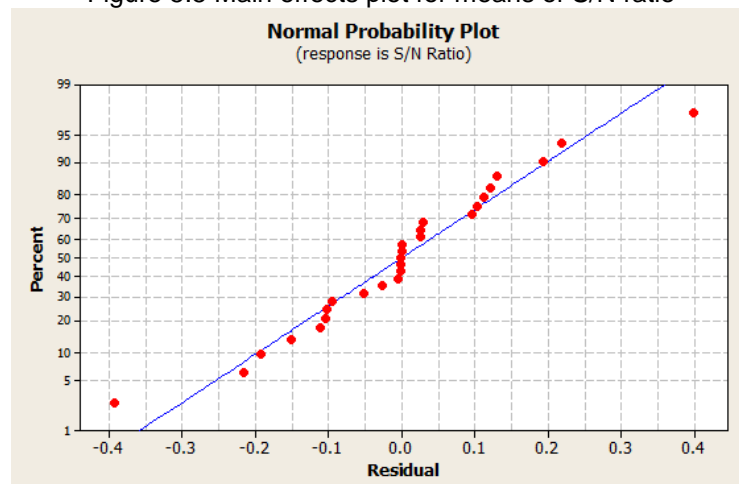


Figure 5.6 Normal probability plot for S/N ratio

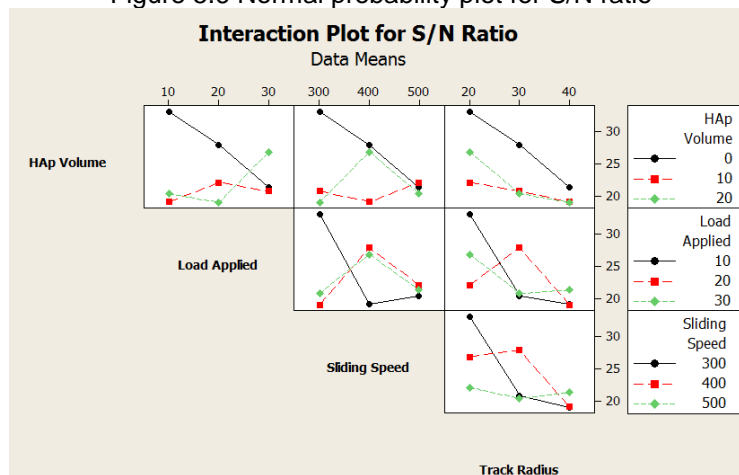


Figure 5.7 Interaction plot for S/N ratio

According to Figure 5.5, it is concluded that the optimal parametric combination is  $A_1B_1C_2D_1$ . When HAp volume is 0 vol. %, Load is 10 N, Sliding speed is 400 RPM and Track radius is 20 mm then minimum abrasive wear can be obtained. Referring to Figure 5.6, it can be concluded that the ANOVA proceeds in a satisfactory manner as the residuals follow a normal distribution. Figure 5.7 shows that two factor interaction of

controllable factors seems to exist. However, the interaction of factors has not been considered for the sake of simplicity.

Table 5.7 shows the calculation data for HAp/PSU composite conducted at 400 grit size paper in terms of volume loss, sliding distance, wear rate and specific wear rate.

Table 5.7 Calculation data for HAp/PSU composite conducted at 400 grit size paper

<b>Experiment No.</b>	<b>Weight Loss (gm)</b>	<b>Volume Loss (cm<sup>3</sup>)</b>	<b>Sliding Distance (m)</b>	<b>Wear Rate 10<sup>-6</sup>(cm<sup>3</sup>/m)</b>	<b>Specific Wear Rate 10<sup>-6</sup>(cm<sup>3</sup>/Nm)</b>
1	0.022	0.017	188.495	90.188	9.018
2	0.021	0.016	188.495	84.882	8.488
3	0.023	0.018	188.495	95.493	9.549
4	0.041	0.033	376.991	87.535	4.376
5	0.040	0.032	376.991	84.882	4.244
6	0.039	0.031	376.991	82.230	4.111
7	0.085	0.068	628.318	108.225	3.607
8	0.084	0.067	628.318	106.633	3.554
9	0.086	0.069	628.318	109.817	3.660
10	0.110	0.088	502.654	175.070	17.507
11	0.111	0.089	502.654	177.060	17.706
12	0.110	0.088	502.654	175.070	17.507
13	0.077	0.062	314.159	197.352	9.867
14	0.079	0.064	314.159	203.718	10.185
15	0.078	0.063	314.159	200.535	10.026
16	0.091	0.073	282.743	258.184	8.606
17	0.090	0.072	282.743	254.648	8.488
18	0.092	0.074	282.743	261.721	8.724
19	0.095	0.076	471.238	161.277	1.612
20	0.094	0.075	471.238	159.155	1.591
21	0.097	0.078	471.238	165.521	1.655
22	0.112	0.090	376.991	238.732	11.936
23	0.110	0.088	376.991	233.427	11.671
24	0.113	0.091	376.991	241.385	12.069
25	0.045	0.036	251.327	143.239	4.774
26	0.046	0.037	251.327	147.218	4.907
27	0.044	0.035	251.327	139.260	4.642

It can be observed from Figure 5.8 that wear loss increases for HAp/PC composite when load increases from 10 N to 30 N whereas wear loss increases for load from 10 N to 20 N and then decreases at 30 N for HAp/PSU composite at 300 rpm and 400 grit size paper. It can be observed from Figure 5.9 that wear loss decreases when load increases from 10 N to 20 N and then increases at 30 N for both HAp/PC and HAp/PSU composites at 400 rpm and 400 grit size paper.

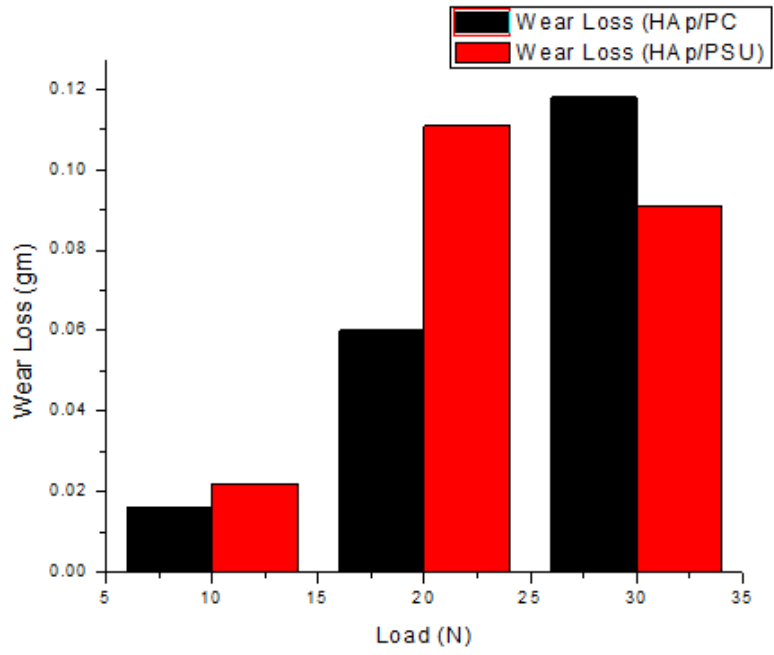


Figure 5.8 Load vs Wear loss (at 300 rpm on 400 grit size paper)

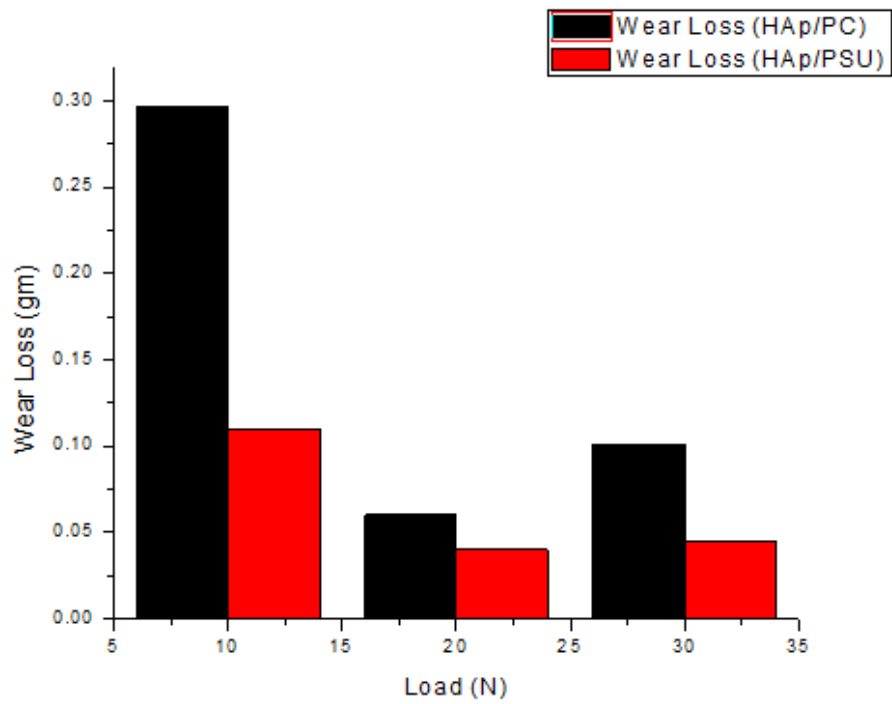


Figure 5.9 Load vs Wear loss (at 400 rpm on 400 grit size paper)

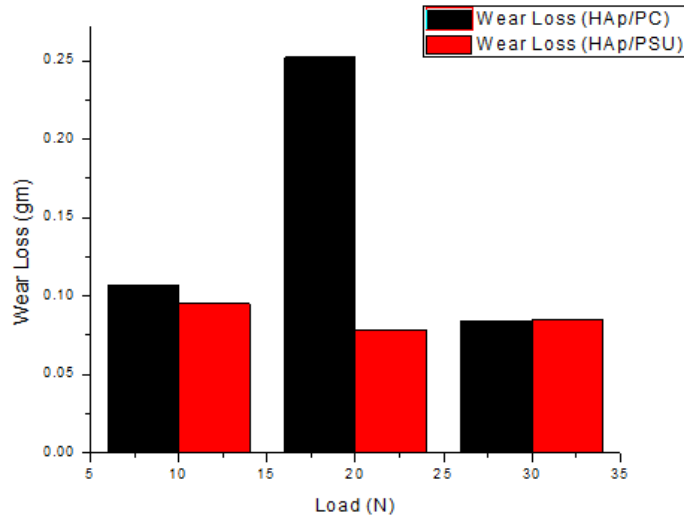


Figure 5.10 Load vs Wear loss (at 500 rpm on 400 grit size paper)

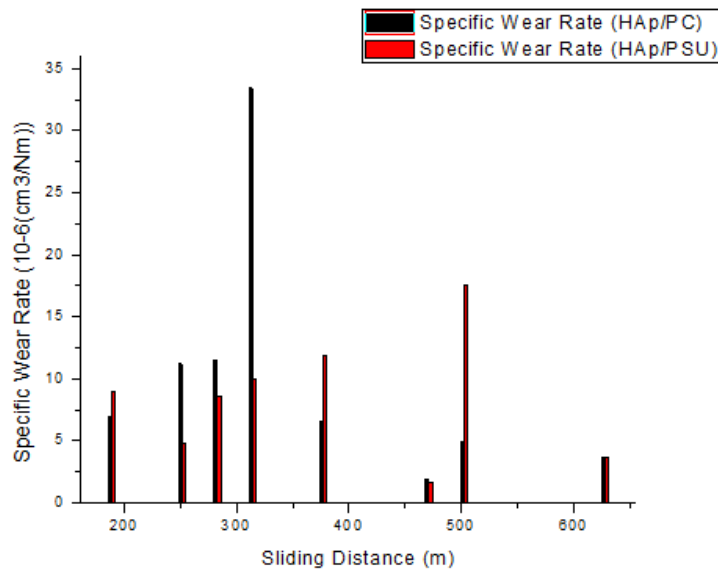


Figure 5.11 Sliding distance vs Specific wear rate (at 400 grit size paper)

It can be observed from Figure 5.10 that wear loss increases for load 10 N to 20 N and then decreases at 30 N for HAp/PC composite whereas wear loss decreases for load 10 N to 20 N and then increases at 30 N for HAp/PSU composite at 500 rpm and 400 grit size paper. It can be observed from Figure 5.11 that specific wear rate increases for sliding distance 188.495 m to 314.159 m and then decreases at 471.238 m, and then again it is increases at 502.654 m and decreases at 628.318 m for HAp/PC composite. For HAp/PSU composite, specific wear rate decreases for sliding distance 188.495 m to 251.327 m and then increases at 376.991 m and then again decreases at 471.238 m and increases at 502.654 m, and then decreases at 628.318 m at 400 grit size paper.



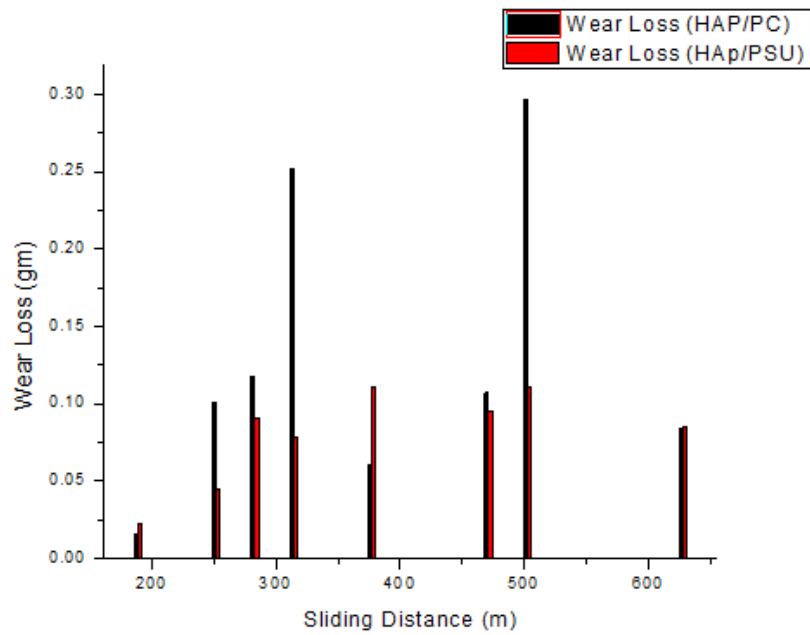


Figure 5.12 Sliding distance vs Wear loss (at 400 grit size paper)

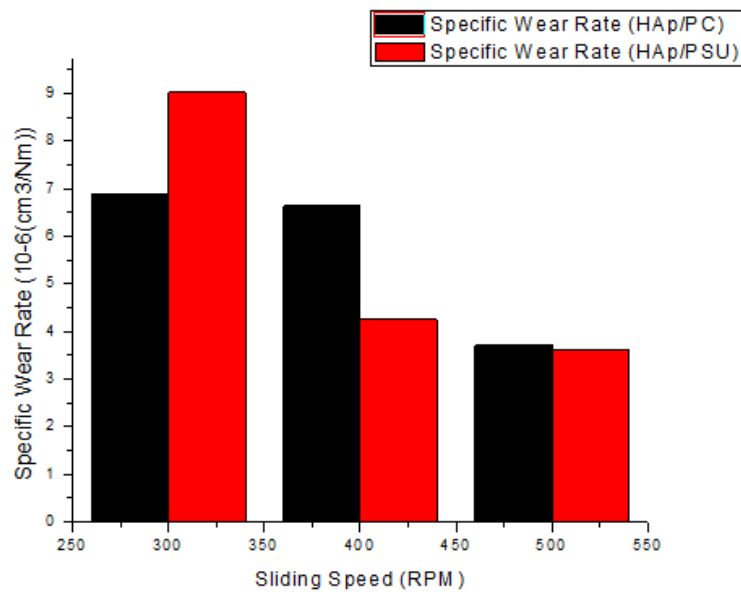


Figure 5.13 Sliding speed vs Specific wear rate (at 0 vol. % and 400 grit size paper)

It can be observed from Figure 5.12 that wear loss increases for sliding distance 188.495 m to 314.159 m and then decreases at 376.991 m and then again increases at 502.654 m and decreases at 628.318 m for HAp/PC composite whereas for HAp/PSU composite, wear loss increases for sliding distance 188.495 m to 282.743 m and then decreases at 314.159 m and then again it is increasing and decreasing manner up to 628.318 m at 400 grit size paper. It can be observed from Figure 5.13 that specific wear rate decreases when sliding speed increases from 300 rpm to 500 rpm for both HAp/PC and HAp/PSU composites at HAp volume of 0 vol. % and 400 grit size paper.

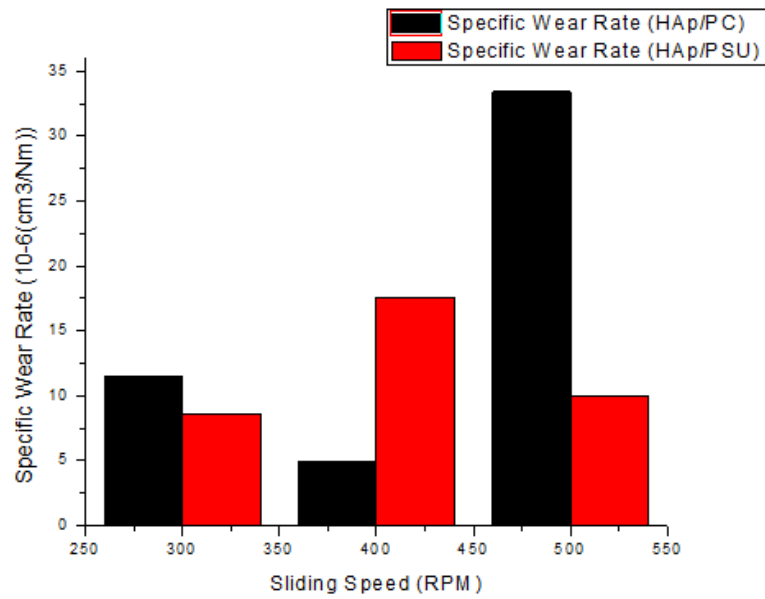


Figure 5.14 Sliding speed vs Specific wear rate (at 10 vol. % and 400 grit size paper)

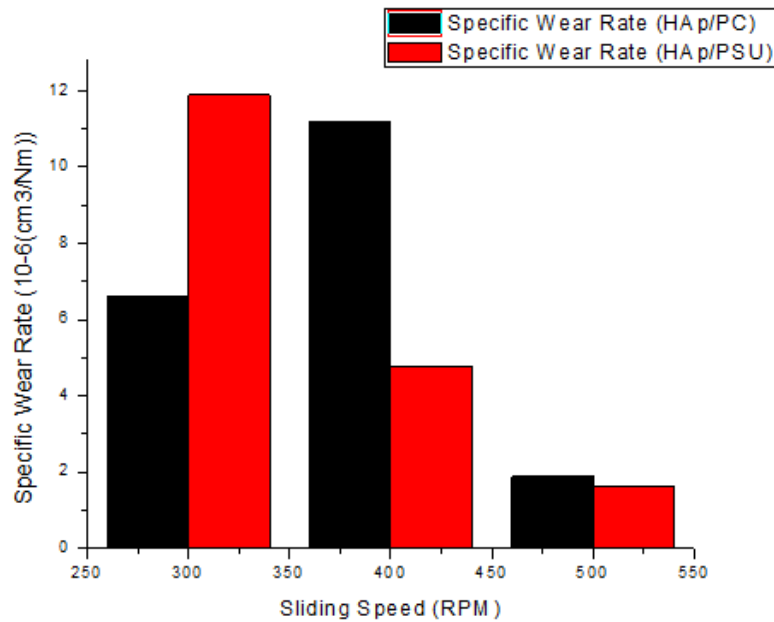


Figure 5.15 Sliding speed vs Specific wear rate (at 20 vol. % and 400 grit size paper)

It can be observed from Figure 5.14 that specific wear rate decreases for sliding speed 300 rpm to 400 rpm and then increases at 500 rpm for HAp/PC composite whereas, for HAp/PSU composite, initially specific wear rate increases for sliding speed 300 rpm to 400 rpm and then decreases at 500 rpm at 10 vol. % and 400 grit size paper. It can be observed from Figure 5.15 that specific wear rate increases, when sliding speed increases for 300 rpm to 400 rpm and then decreases at 500 rpm for HAp/PC composite whereas for HAp/PSU composite, specific wear rate decreases for sliding speed 300 rpm to 500 rpm at 20 vol. % and 400 grit size paper.

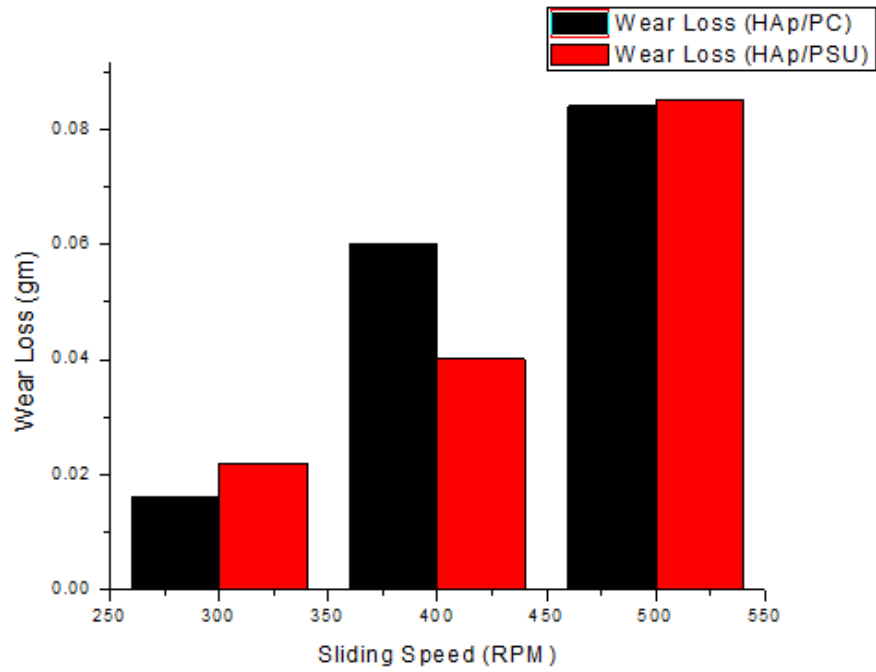


Figure 5.16 Sliding speed vs Wear loss (at 0 vol. % and 400 grit size paper)

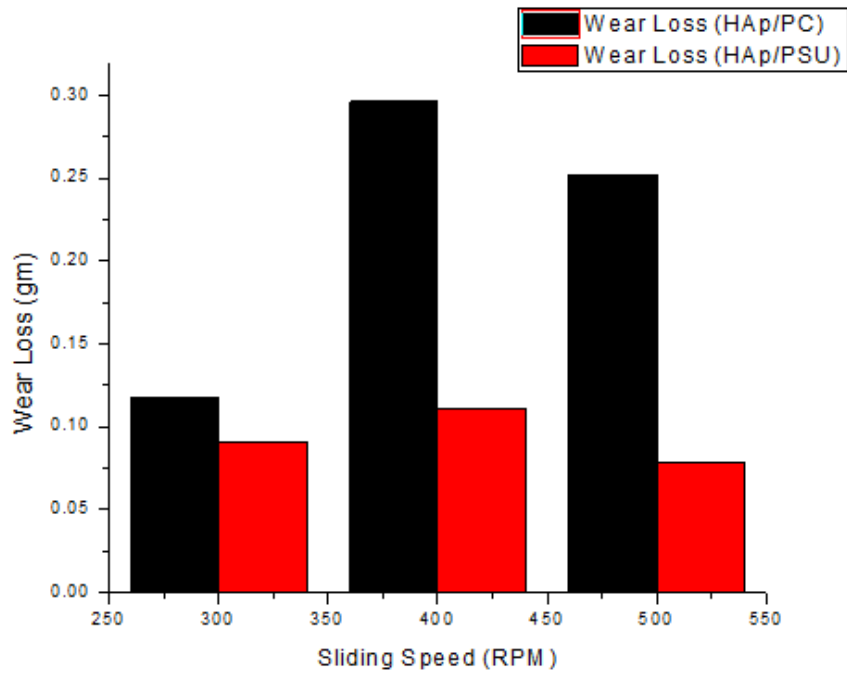


Figure 5.17 Sliding speed vs Wear loss (at 10 vol. % and 400 grit size paper)

It can be observed from Figure 5.16 that wear loss increases when sliding speed increases for 300 rpm to 500 rpm for both HAp/PC and HAp/PSU composites at 0 vol. % and 400 grit size paper. It can be observed from Figure 5.17 that wear loss increases when sliding speed increases for 300 rpm to 400 rpm and then decreases at 500 rpm for both HAp/PC and HAp/PSU composites at 10 vol. % and 400 grit size paper.

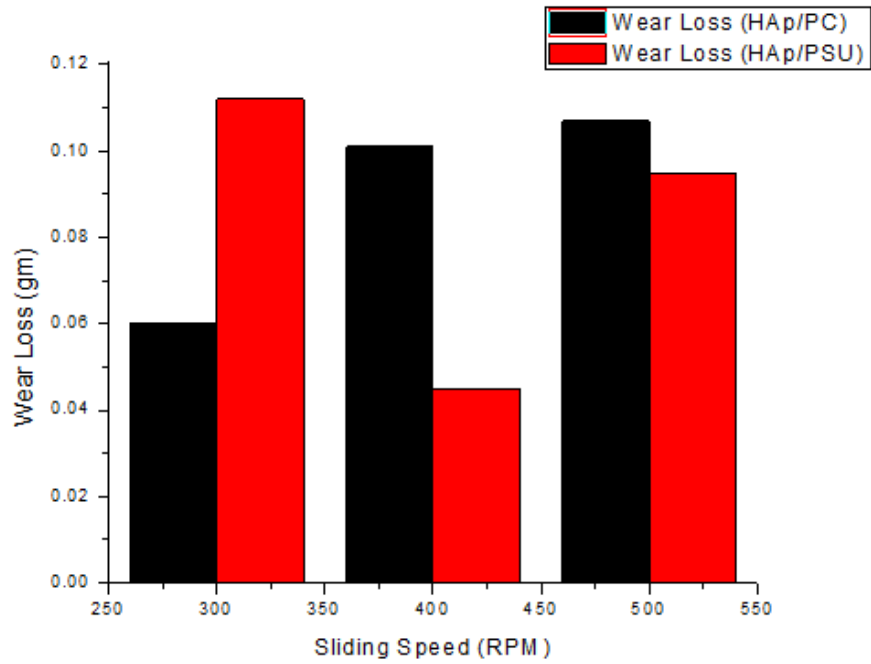


Figure 5.18 Sliding speed vs Wear loss (at 20 vol. % and 400 grit size paper)

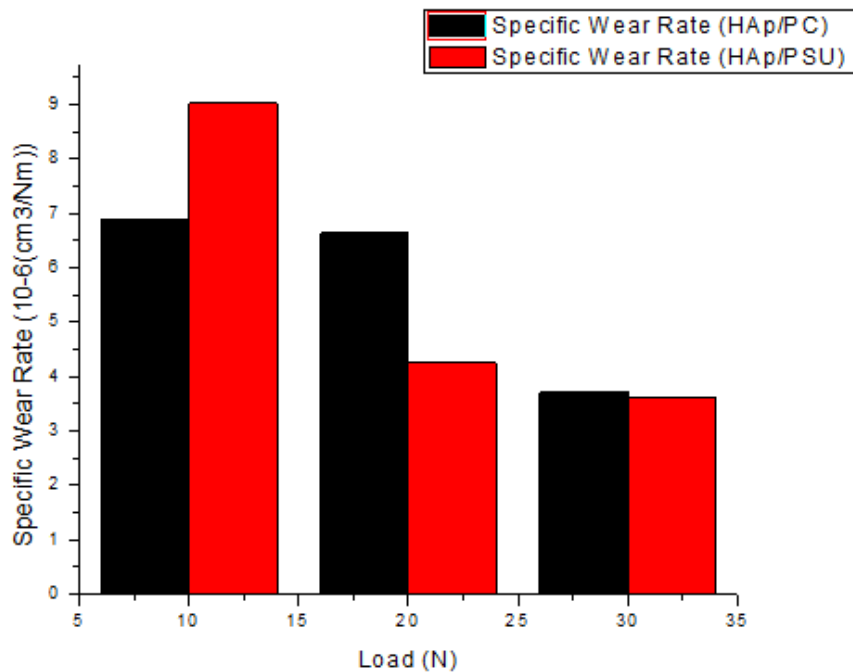


Figure 5.19 Specific wear rate vs. Load (at 0 vol. % at 400 grit size paper)

It can be observed from Figure 5.18 that wear loss increases when sliding speed increases for 300 rpm to 500 rpm for HAp/PC composite at whereas wear loss decreases for sliding speed 300 rpm to 400 rpm and then increases at 500 rpm for HAp/PSU composite at 10 vol. % and 400 grit size paper. It can be observed from Figure 5.19 that specific wear rate decreases when load increases for 10 N to 30 N for both HAp/PC and HAp/PSU composites at 0 vol. % and 400 grit size paper.

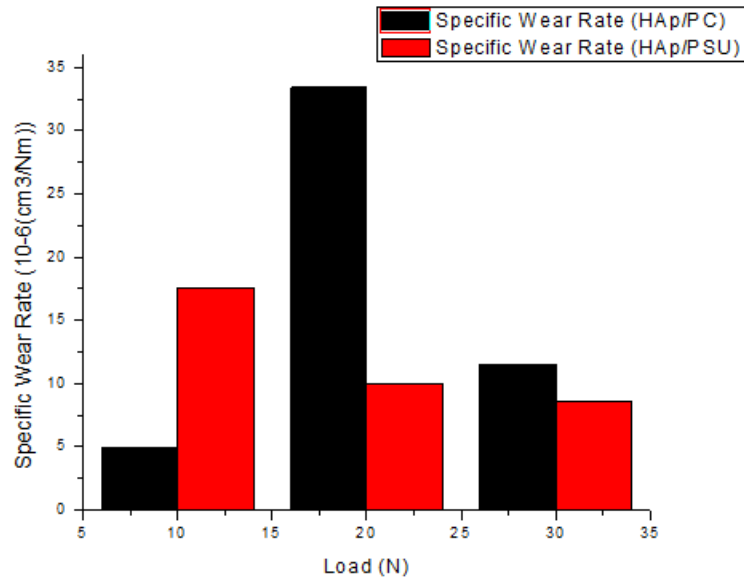


Figure 5.20 Specific wear rate vs. Load (at 10 vol. % at 400 grit size paper)

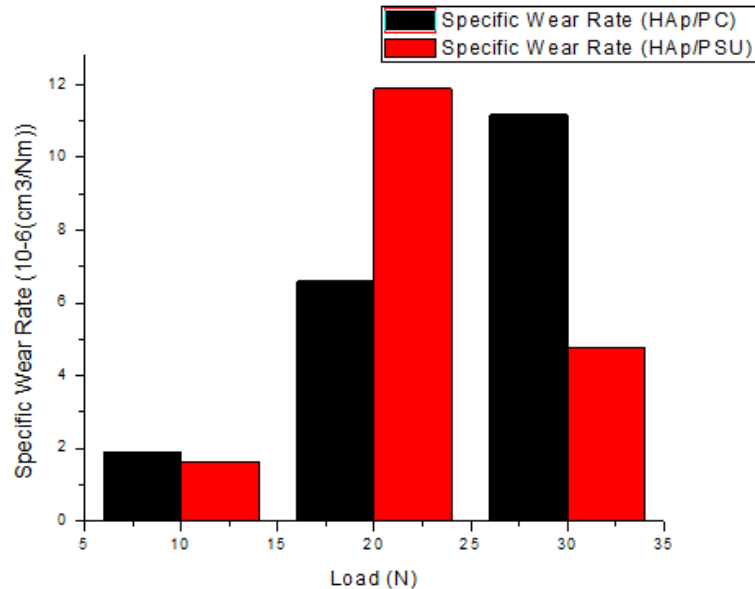


Figure 5.21 Specific wear rate vs. Load (at 20 vol. % at 400 grit size paper)

It can be observed from Figure 5.20 that specific wear rate increases when load increases for 10 N to 20 N and then decreases at 30 N for HAp/PC composite whereas specific wear rate decreases for load 10 N to 30 N for HAp/PSU composite at 10 vol. % and 400 grit size paper. It can be observed from Figure 5.21 that specific wear rate increases when load increases for 10 N to 30 N for HAp/PC composite whereas specific wear rate increases when load increases for 10 N to 20 N and then decreases at 30 N for HAp/PSU composite at 20 vol. % and 400 grit size paper. It can be observed from Figure 5.22 that co-efficient of friction decreases when sliding distance increases for both HAp/PC and HAp/PSU composites at 400 grit size paper.

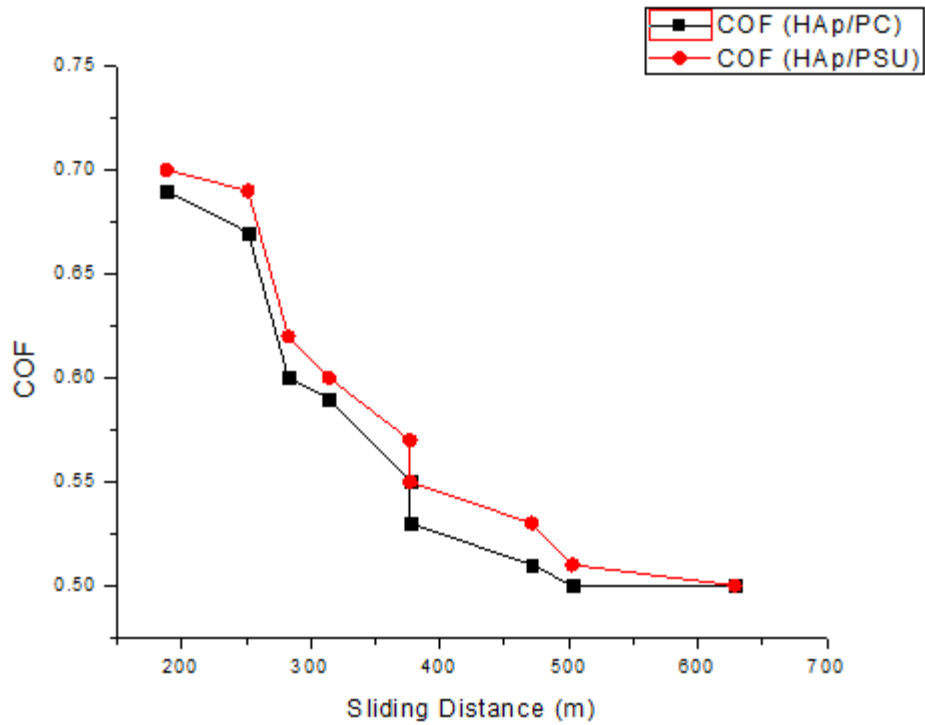


Figure 5.22 Sliding Distance vs. COF (at 400 grit size paper)

Similarly, the experimental data for HAp/PC composite conducted at 600 grit size paper is shown in Table 5.8.

Table 5.8 Experimental data for HAp/PC composite conducted at 600 grit size paper

Experiment No.	Factor A (HAp Volume) %	Factor B (Load Applied) N	Factor C (Sliding Speed) RPM	Factor D (Track Radius) mm	Wear Loss (gm)	S/N ratio (Lower The Better)
1	0	10	300	20	0.013	37.721
2	0	10	300	20	0.011	39.172
3	0	10	300	20	0.012	38.416
4	0	20	400	30	0.055	25.192
5	0	20	400	30	0.055	25.192
6	0	20	400	30	0.057	24.882
7	0	30	500	40	0.080	21.938
8	0	30	500	40	0.081	21.830
9	0	30	500	40	0.082	21.723
10	10	10	400	40	0.294	10.633
11	10	10	400	40	0.293	10.662
12	10	10	400	40	0.292	10.692
13	10	20	500	20	0.248	12.110
14	10	20	500	20	0.250	12.041
15	10	20	500	20	0.249	12.076
16	10	30	300	30	0.116	18.710
17	10	30	300	30	0.114	18.861
18	10	30	300	30	0.115	18.786
19	20	10	500	30	0.101	19.913
20	20	10	500	30	0.102	19.827
21	20	10	500	30	0.103	19.743
22	20	20	300	40	0.054	25.352
23	20	20	300	40	0.058	24.731
24	20	20	300	40	0.057	24.882
25	20	30	400	20	0.097	20.264
26	20	30	400	20	0.096	20.354
27	20	30	400	20	0.099	20.087

The ANOVA table for S/N ratio of HAp/PC composite is shown in Table 5.9.

Table 5.9 ANOVA table for S/N ratio of HAp/PC composite

Source	DF value	Seq SS	Adj SS	Adj MS	F value	P value	Percentage Contribution
A	2	962.34	962.34	481.17	6111.56	0.000	60.498
B	2	37.60	37.60	18.80	238.76	0.000	2.363
C	2	501.24	501.24	250.62	3183.22	0.000	31.510
D	2	88.11	88.11	44.05	559.54	0.000	5.539
Error	18	1.42	1.42	0.08			
Total	26	1590.69					

S = 0.280591, R-Sq = 99.91%, and R-Sq(adj) = 99.87%

From percentage contribution, it can be concluded here that significance of factors is in the order of Factor A, C, D and B.

Main effects plot for means of S/N ratio, normal probability plot and interaction plot are shown in Figure 5.23, 5.24 and 5.25 respectively.

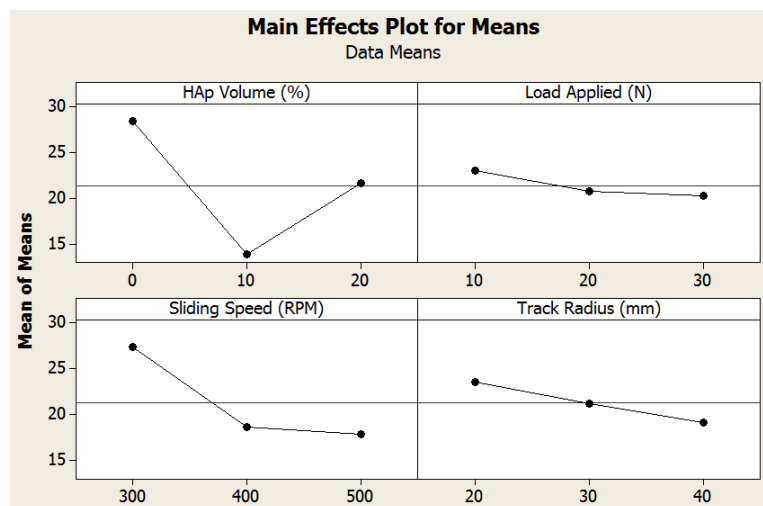


Figure 5.23 Main effects plot for means of S/N ratio

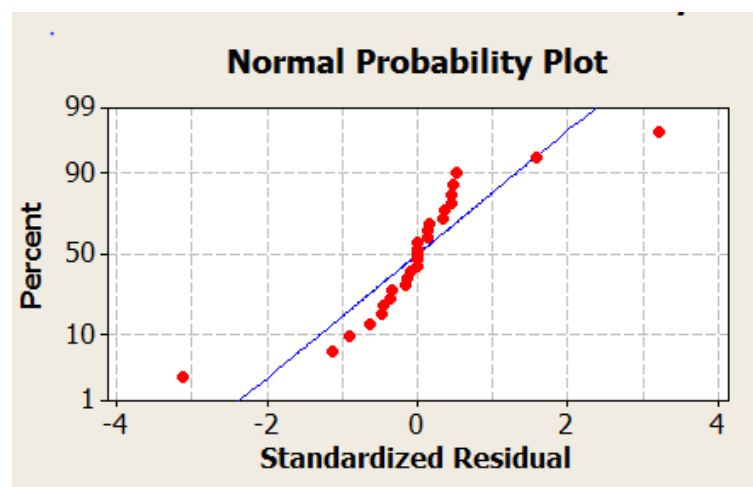


Figure 5.24 Normal probability plot for S/N ratio

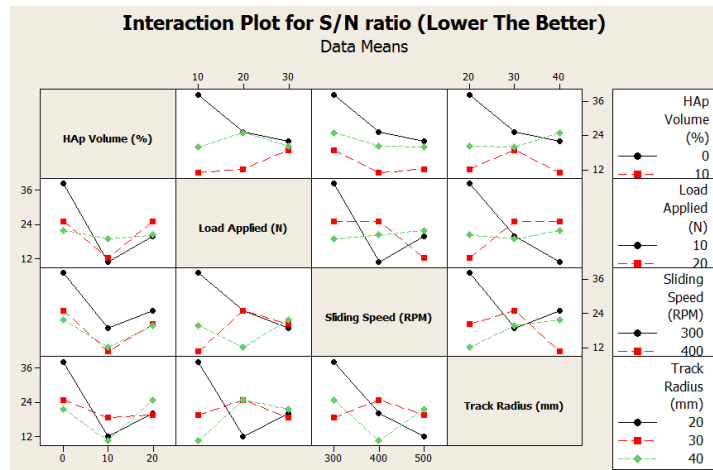


Figure 5.25 Interaction plot for S/N ratio

According to Figure 5.23, it is concluded that the optimal parametric combination is  $A_1B_1C_1D_1$ . When HAp volume is 0 vol. %, Load is 10 N, Sliding speed is 300 RPM and Track radius is 20 mm then minimum abrasive wear can be obtained. Referring to Figure 5.24, it can be concluded that the ANOVA proceeds in a satisfactory manner as the residuals follow a normal distribution. Figure 5.25 shows that two factor interaction of controllable factors seems to exist. However, the interaction of factors has not been considered for the sake of simplicity.

Table 5.10 shows the calculation data for HAp/PC composite conducted at 600 grit size paper in terms of volume loss, sliding distance, wear rate and specific wear rate

Table 5.10 Calculation data for HAp/PC composite conducted at 600 grit size paper

Experiment No.	Weight Loss (gm)	Volume Loss (cm <sup>3</sup> )	Sliding Distance (m)	Wear Rate 10 <sup>-6</sup> (cm <sup>3</sup> /m)	Specific Wear Rate 10 <sup>-6</sup> (cm <sup>3</sup> /Nm)
1	0.013	0.011	188.495	58.356	5.835
2	0.011	0.009	188.495	47.746	4.774
3	0.012	0.010	188.495	53.051	5.305
4	0.055	0.045	376.991	119.366	5.968
5	0.055	0.045	376.991	119.366	5.968
6	0.057	0.047	376.991	124.671	6.233
7	0.080	0.066	628.318	105.042	3.502
8	0.081	0.067	628.318	106.633	3.554
9	0.082	0.068	628.318	108.225	3.607
10	0.294	0.245	502.654	487.412	48.741
11	0.293	0.244	502.654	485.423	48.542
12	0.292	0.243	502.654	483.433	48.343
13	0.248	0.207	314.159	658.902	32.945
14	0.250	0.208	314.159	662.085	33.104
15	0.249	0.207	314.159	658.902	32.945
16	0.116	0.097	282.743	343.067	11.435
17	0.114	0.095	282.743	335.994	11.199
18	0.115	0.096	282.743	339.530	11.317
19	0.101	0.084	471.238	178.253	17.825
20	0.102	0.085	471.238	180.375	18.037
21	0.103	0.086	471.238	182.498	18.249
22	0.054	0.045	376.991	119.366	5.968
23	0.058	0.048	376.991	127.323	6.366
24	0.057	0.047	376.991	124.671	6.233
25	0.097	0.081	251.327	322.289	10.743
26	0.096	0.080	251.327	318.310	10.611
27	0.099	0.083	251.327	330.247	11.008



Similarly, the experimental data for HAp/PSU composite conducted at 600 grit size paper is shown in Table 5.11.

Table 5.11 Experimental data for HAp/PSU composite conducted at 600 grit size paper

Experiment No.	Factor A (HAp Volume) %	Factor B (Load Applied) N	Factor C (Sliding Speed) RPM	Factor D (Track Radius) mm	Wear Loss (gm)	S/N ratio (Lower The Better)
1	0	10	300	20	0.018	34.894
2	0	10	300	20	0.017	35.391
3	0	10	300	20	0.020	33.979
4	0	20	400	30	0.037	28.635
5	0	20	400	30	0.036	28.873
6	0	20	400	30	0.035	29.118
7	0	30	500	40	0.080	21.938
8	0	30	500	40	0.081	21.830
9	0	30	500	40	0.082	21.723
10	10	10	400	40	0.106	19.493
11	10	10	400	40	0.107	19.412
12	10	10	400	40	0.106	19.493
13	10	20	500	20	0.072	22.853
14	10	20	500	20	0.075	22.498
15	10	20	500	20	0.073	22.733
16	10	30	300	30	0.086	21.310
17	10	30	300	30	0.085	21.411
18	10	30	300	30	0.089	21.012
19	20	10	500	30	0.090	20.915
20	20	10	500	30	0.091	20.819
21	20	10	500	30	0.092	20.724
22	20	20	300	40	0.108	19.331
23	20	20	300	40	0.107	19.412
24	20	20	300	40	0.109	19.251
25	20	30	400	20	0.040	27.958
26	20	30	400	20	0.041	27.744
27	20	30	400	20	0.040	27.958

The ANOVA table for S/N ratio of HAp/PSU composite is shown in Table 5.12.

Table 5.12 ANOVA table for S/N ratio of HAp/PSU composite

Source	DF value	Seq SS	Adj SS	Adj MS	F value	P value	Percentage Contribution
A	2	270.486	270.486	135.243	1760.02	0.000	40.726
B	2	11.256	11.256	5.628	73.24	0.000	1.694
C	2	72.993	72.993	36.497	474.96	0.000	10.990
D	2	308.033	308.033	154.016	2004.34	0.000	46.379
Error	18	1.383	1.383	0.077			
Total	26	664.151					

S = 0.277203, R-Sq = 99.79%, and R-Sq(adj) = 99.70%

From percentage contribution, it can be concluded here that significance of factors is in the order of Factor D, A, C and B.

Main effects plot for means of S/N ratio, normal probability plot and interaction plot are shown in Figure 5.26, 5.27 and 5.28 respectively.

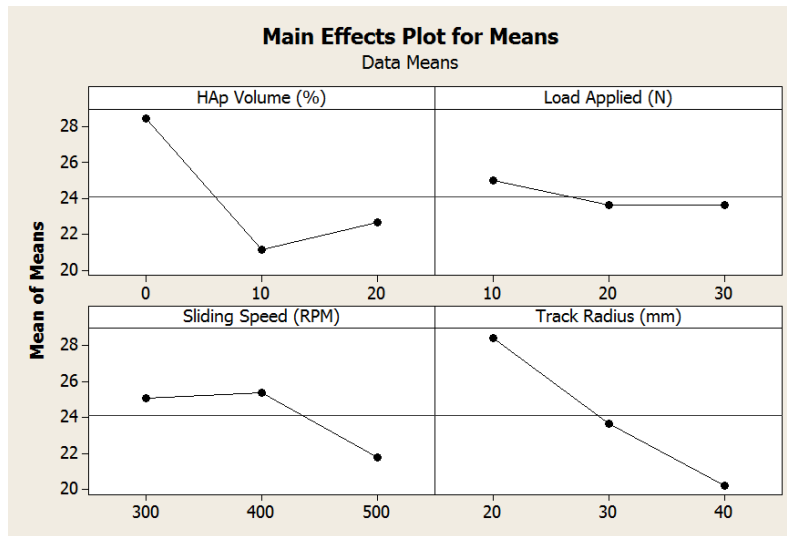


Figure 5.26 Main effects plot for means of S/N ratio

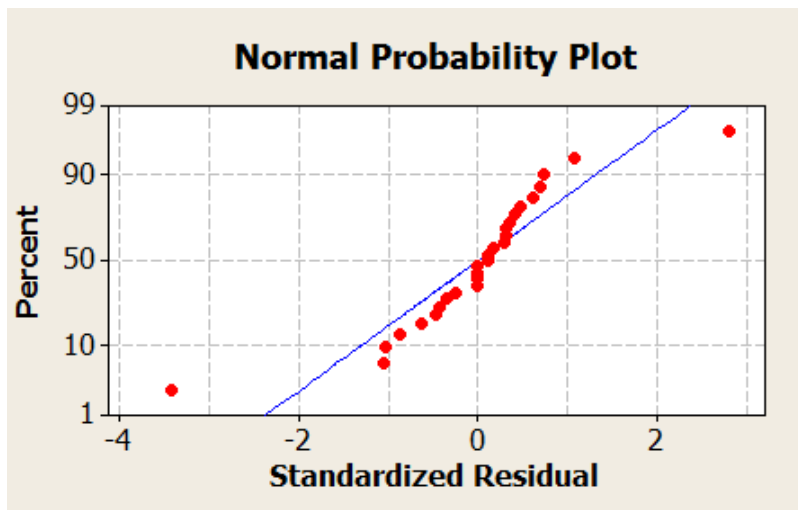


Figure 5.27 Normal probability plot for S/N ratio

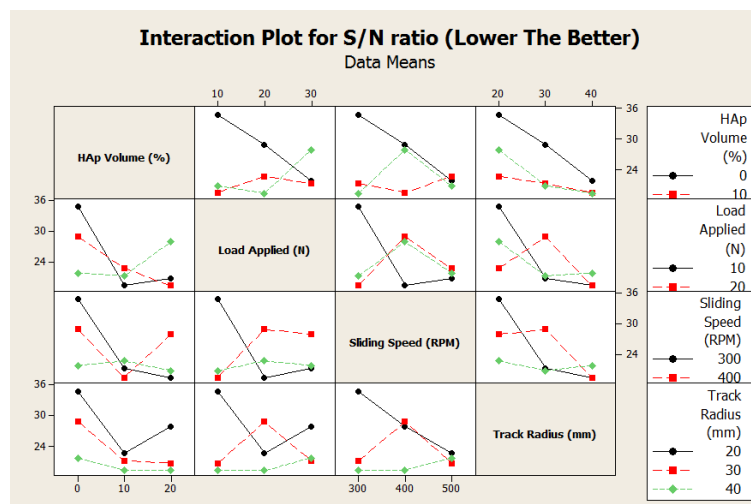


Figure 5.28 Interaction plot for S/N ratio

According to Figure 5.26, it is concluded that the optimal parametric combination is  $A_1B_1C_2D_1$ . When HAp volume is 0 vol. %, Load is 10 N, Sliding speed is 400 RPM and Track radius is 20 mm then minimum abrasive wear can be obtained. Referring to Figure 5.27, it can be concluded that the ANOVA proceeds in a satisfactory manner as the residuals follow a normal distribution. Figure 5.28 shows that two factor interaction of controllable factors seems to exist. However, the interaction of factors has not been considered for the sake of simplicity.

Table 5.13 shows the calculation data for HAp/PSU composite conducted at 600 grit size paper in terms of volume loss, sliding distance, wear rate and specific wear rate

Table 5.13 Calculation data for HAp/PSU composite conducted at 600 grit size paper

Experiment No.	Weight Loss (gm)	Volume Loss (cm <sup>3</sup> )	Sliding Distance (m)	Wear Rate 10 <sup>-6</sup> (cm <sup>3</sup> /m)	Specific Wear Rate 10 <sup>-6</sup> (cm <sup>3</sup> /Nm)
1	0.018	0.015	188.495	79.577	7.957
2	0.017	0.014	188.495	74.272	7.427
3	0.020	0.016	188.495	84.882	8.488
4	0.037	0.029	376.991	76.924	3.846
5	0.036	0.029	376.991	76.924	3.846
6	0.035	0.028	376.991	74.272	3.714
7	0.080	0.064	628.318	101.859	3.395
8	0.081	0.065	628.318	103.450	3.448
9	0.082	0.066	628.318	105.042	3.501
10	0.106	0.085	502.654	169.102	16.910
11	0.107	0.086	502.654	171.091	17.109
12	0.106	0.085	502.654	169.102	16.910
13	0.072	0.058	314.159	184.619	9.230
14	0.075	0.060	314.159	190.986	9.549
15	0.073	0.058	314.159	184.619	9.231
16	0.086	0.069	282.743	244.037	8.134
17	0.085	0.068	282.743	240.501	8.016
18	0.089	0.071	282.743	251.111	8.370
19	0.090	0.072	471.238	152.789	15.278
20	0.091	0.073	471.238	154.911	15.491
21	0.092	0.074	471.238	157.033	15.703
22	0.108	0.087	376.991	230.774	11.538
23	0.107	0.086	376.991	228.122	11.406
24	0.109	0.087	376.991	230.774	11.538
25	0.040	0.032	251.327	127.324	4.244
26	0.041	0.033	251.327	131.303	4.376
27	0.040	0.032	251.327	127.324	4.244

It can be observed from Figure 5.29 that wear loss increases for HAp/PC composite when load increases for load 10 N to 30 N whereas for HAp/PSU composite, wear loss increases for load 10 N to 20 N and then it decreases at 30 N at 300 rpm and 600 grit size paper. It can be observed from Figure 5.30 that wear loss decreases when load increases for 10 N to 20 N and then increases at 30 N for both HAp/PC and HAp/PSU composites at 400 rpm and 600 grit size paper.

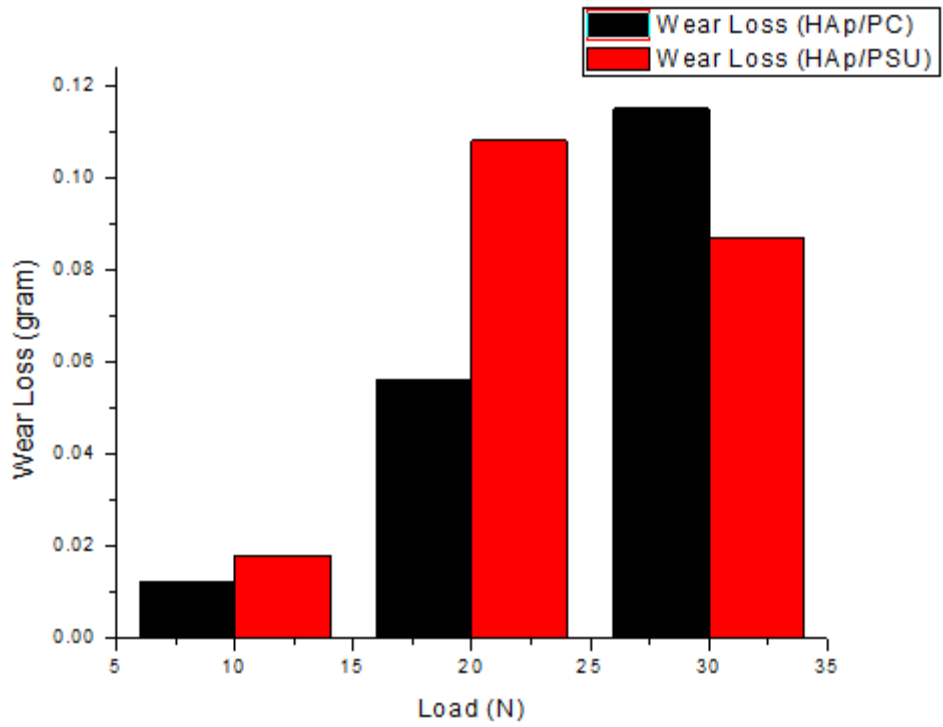


Figure 5.29 Load vs Wear loss (at 300 rpm on 600 grit size paper)

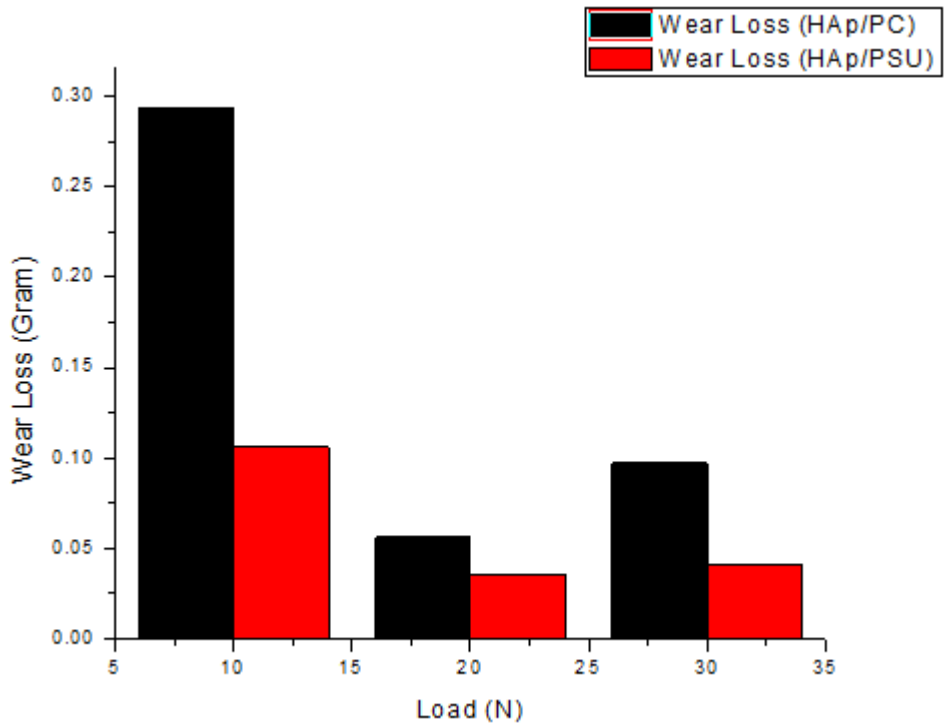


Figure 5.30 Load vs Wear loss (at 400 rpm on 600 grit size paper)

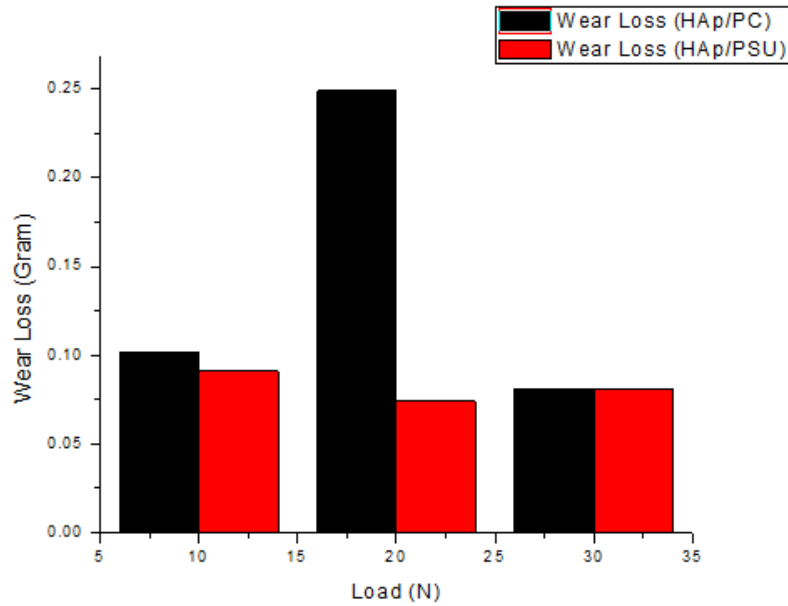


Figure 5.31 Load vs Wear loss (at 500 rpm on 600 grit size paper)

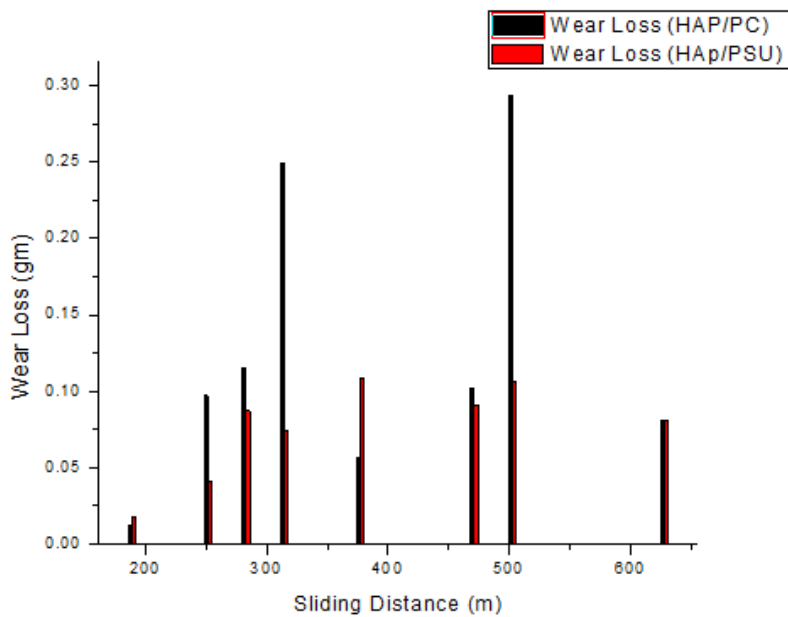


Figure 5.32 Sliding distance vs Wear loss (at 600 grit size paper)

It can be observed from Figure 5.31 that wear loss increases when load increases for load 10 N to 20 N and then decreases at 30 N for HAp/PC composite whereas for HAp/PSU composite wear loss decreases for load 10 N to 20 N and then increases at 30 N at 500 rpm and 600 grit size paper. It can be observed from Figure 5.32 that wear loss increases and decreases manner for both HAp/PC and HAp/PSU composites when sliding distance increases for 188.495 m to 628.318 m at 600 grit size paper.

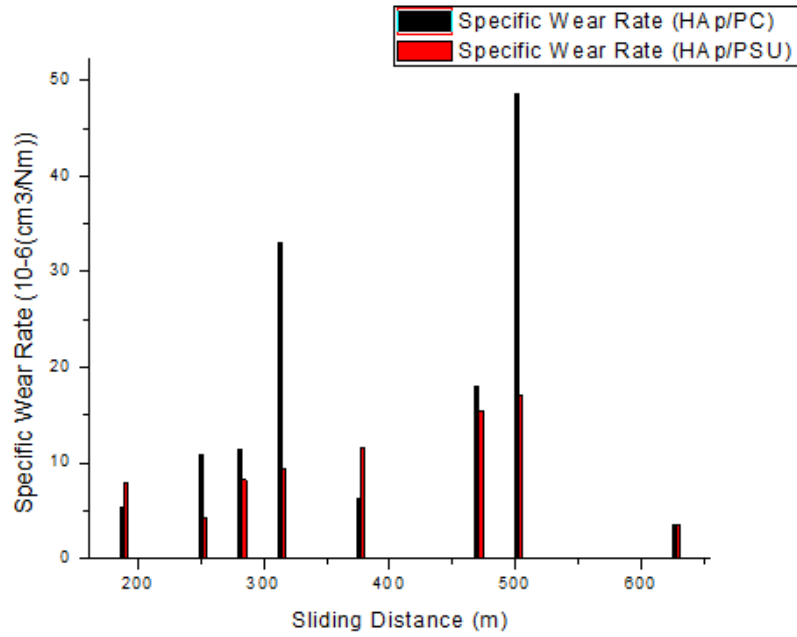


Figure 5.33 Sliding distance vs Specific wear rate (at 600 grit size paper)

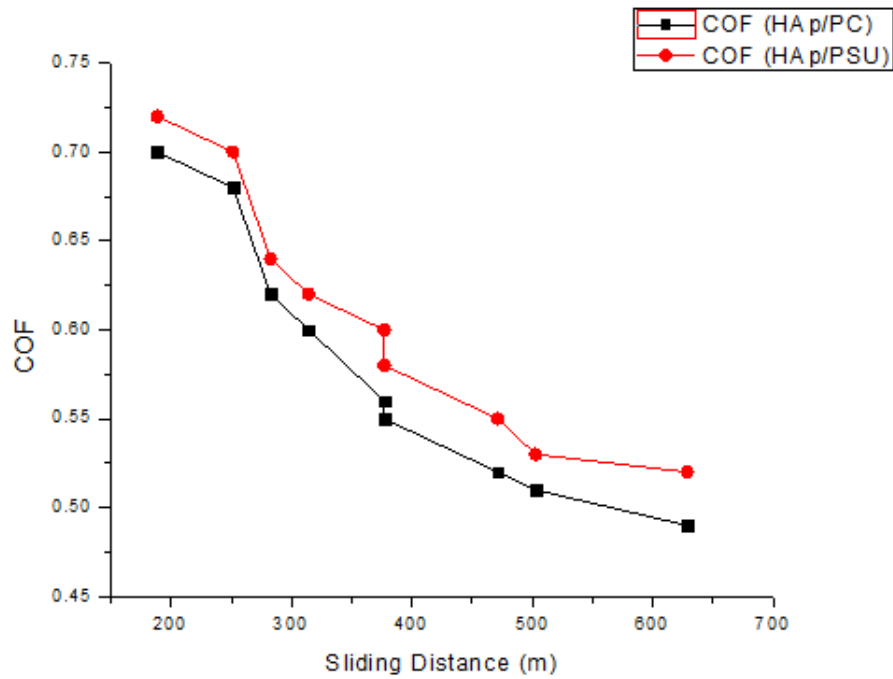


Figure 5.34 Sliding Distance vs. COF (at 600 grit size paper)

It can be observed from Figure 5.33 that specific wear rate for both HAp/PC and HAp/PSU composites increases and decreases manner when sliding distance increases for 188.495 m to 628.318 m at 600 grit size paper. It can be observed from Figure 5.34 that for both HAp/PC and HAp/PSU composites, co-efficient of friction decreases when sliding distance increases at 600 grit size paper.

Similarly, the experimental data for HAp/PC composite conducted at 1000 grit size paper is shown in Table 5.14.

Table 5.14 Experimental data for HAp/PC composite conducted at 1000 grit size paper

Experiment No.	Factor A (HAp Volume) %	Factor B (Load Applied) N	Factor C (Sliding Speed) RPM	Factor D (Track Radius) mm	Wear Loss (gm)	S/N ratio (Lower The Better)
1	0	10	300	20	0.010	40
2	0	10	300	20	0.007	43.098
3	0	10	300	20	0.009	40.915
4	0	20	400	30	0.050	26.020
5	0	20	400	30	0.051	25.848
6	0	20	400	30	0.052	25.679
7	0	30	500	40	0.076	22.383
8	0	30	500	40	0.077	22.270
9	0	30	500	40	0.078	22.158
10	10	10	400	40	0.290	10.752
11	10	10	400	40	0.288	10.812
12	10	10	400	40	0.286	10.872
13	10	20	500	20	0.245	12.216
14	10	20	500	20	0.246	12.181
15	10	20	500	20	0.243	12.287
16	10	30	300	30	0.111	19.093
17	10	30	300	30	0.110	19.172
18	10	30	300	30	0.111	19.093
19	20	10	500	30	0.097	20.264
20	20	10	500	30	0.096	20.354
21	20	10	500	30	0.100	20
22	20	20	300	40	0.051	25.848
23	20	20	300	40	0.053	25.514
24	20	20	300	40	0.054	25.352
25	20	30	400	20	0.093	20.630
26	20	30	400	20	0.092	20.724
27	20	30	400	20	0.095	20.445

The ANOVA table for S/N ratio of HAp/PC composite is shown in Table 5.15.

Table 5.15 ANOVA table for S/N ratio of HAp/PC composite

Source	DF value	Seq SS	Adj SS	Adj MS	F value	P value	Percentage Contribution
A	2	1118.75	1118.75	559.38	1863.42	0.000	58.493
B	2	62.01	62.01	31.01	103.29	0.000	3.242
C	2	605.10	605.10	302.55	1007.88	0.000	31.637
D	2	121.32	121.32	60.66	202.08	0.000	6.343
Error	18	5.40	5.40	0.30			
Total	26	1912.59					

S = 0.547893, R-Sq = 99.72%, and R-Sq(adj) = 99.59%

From percentage contribution, it can be concluded here that significance of factors is in the order of Factor A, C, D and B.

Main effects plot for means of S/N ratio, normal probability plot and interaction plot are shown in Figure 5.35, 5.36 and 5.37 respectively.

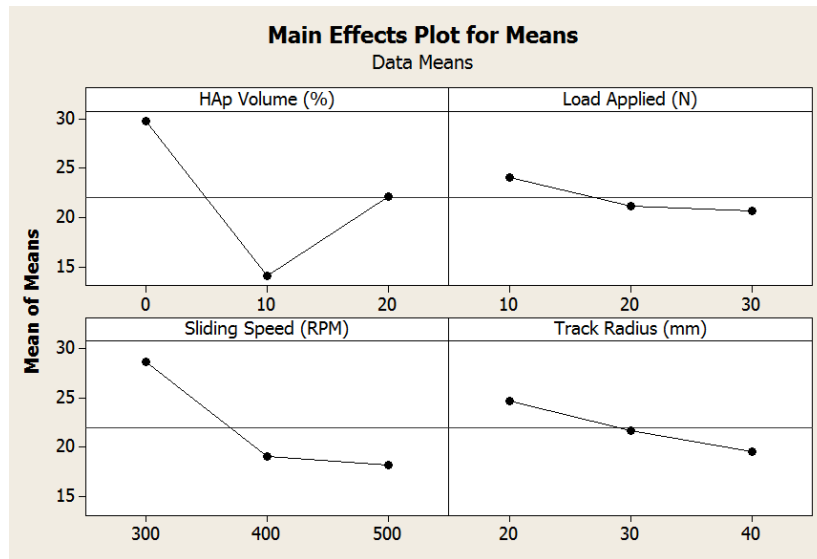


Figure 5.35 Main effects plot for means of S/N ratio

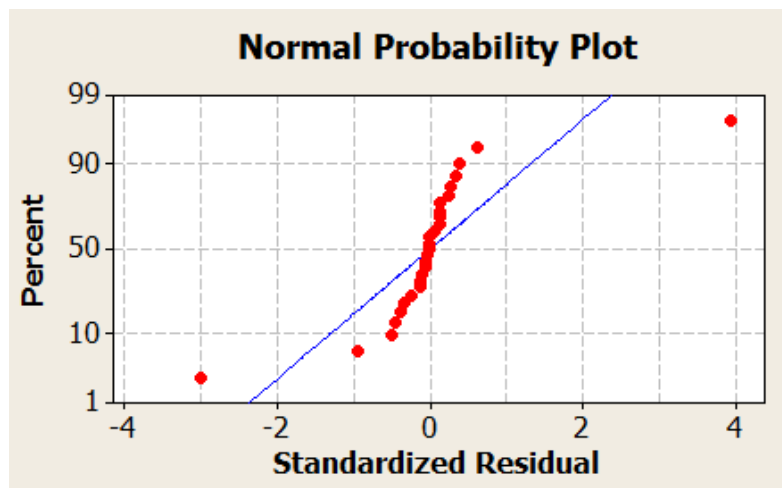


Figure 5.36 Normal probability plot for S/N ratio

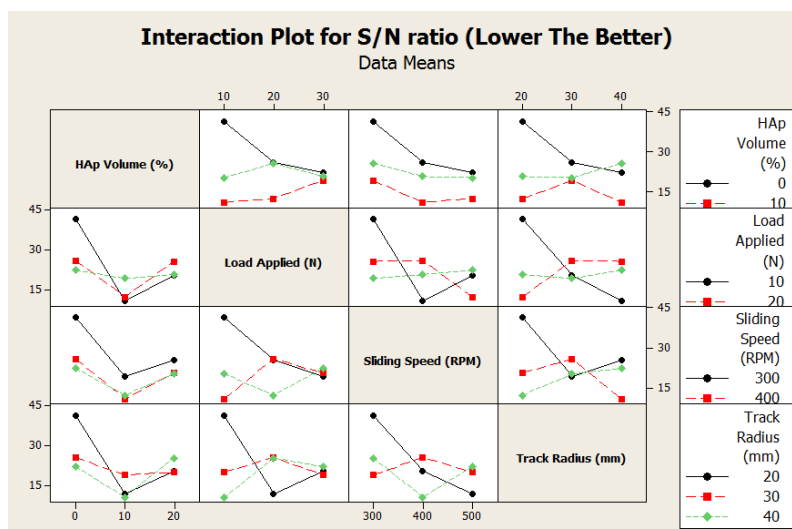


Figure 5.37 Interaction plot for S/N ratio



According to Figure 5.35, it is concluded that the optimal parametric combination is A<sub>1</sub>B<sub>1</sub>C<sub>1</sub>D<sub>1</sub>. When HAp volume is 0 vol. %, Load is 10 N, Sliding speed is 300 RPM and Track radius is 20 mm then minimum abrasive wear can be obtained. Referring to Figure 5.36, it can be concluded that the ANOVA proceeds in a satisfactory manner as the residuals follow a normal distribution. Figure 5.37 shows that two factor interaction of controllable factors seems to exist. However, the interaction of factors has not been considered for the sake of simplicity.

Table 5.16 shows the calculation data for HAp/PC composite conducted at 1000 grit size paper in terms of volume loss, sliding distance, wear rate and specific wear rate

Table 5.16 Calculation data for HAp/PC composite conducted at 1000 grit size paper

Experiment No.	Weight Loss (gm)	Volume Loss (cm <sup>3</sup> )	Sliding Distance (m)	Wear Rate 10 <sup>-6</sup> (cm <sup>3</sup> /m)	Specific Wear Rate 10 <sup>-6</sup> (cm <sup>3</sup> /Nm)
1	0.010	0.008	188.495	42.441	4.244
2	0.007	0.005	188.495	26.525	2.652
3	0.009	0.007	188.495	37.136	3.713
4	0.050	0.041	376.991	108.755	5.437
5	0.051	0.042	376.991	111.408	5.570
6	0.052	0.043	376.991	114.061	5.703
7	0.076	0.063	628.318	100.267	3.342
8	0.077	0.064	628.318	101.859	3.395
9	0.078	0.065	628.318	103.450	3.448
10	0.290	0.241	502.654	479.455	47.945
11	0.288	0.240	502.654	477.465	47.746
12	0.286	0.238	502.654	473.486	47.348
13	0.245	0.204	314.159	649.352	32.467
14	0.246	0.205	314.159	652.535	32.626
15	0.243	0.202	314.159	642.986	32.149
16	0.111	0.092	282.743	325.383	10.846
17	0.110	0.091	282.743	321.847	10.728
18	0.111	0.092	282.743	325.383	10.846
19	0.097	0.080	471.238	169.765	16.976
20	0.096	0.080	471.238	169.765	16.976
21	0.100	0.083	471.238	176.131	17.613
22	0.051	0.042	376.991	111.408	5.570
23	0.053	0.044	376.991	116.713	5.835
24	0.054	0.045	376.991	119.366	5.968
25	0.093	0.077	251.327	306.373	10.212
26	0.092	0.076	251.327	302.394	10.079
27	0.095	0.079	251.327	314.331	10.477

Similarly, the experimental data for HAp/PSU composite conducted at 1000 grit size paper is shown in Table 5.17.

Table 5.17 Experimental data for HAp/PSU composite conducted at 1000 grit size paper

Experiment No.	Factor A (HAp Volume) %	Factor B (Load Applied) N	Factor C (Sliding Speed) RPM	Factor D (Track Radius) mm	Wear Loss (gm)	S/N ratio (Lower The Better)
1	0	10	300	20	0.014	37.077
2	0	10	300	20	0.013	37.721
3	0	10	300	20	0.017	35.391
4	0	20	400	30	0.035	29.118
5	0	20	400	30	0.032	29.897
6	0	20	400	30	0.030	30.457
7	0	30	500	40	0.075	22.498
8	0	30	500	40	0.076	22.383
9	0	30	500	40	0.077	22.270
10	10	10	400	40	0.102	19.827
11	10	10	400	40	0.103	19.743
12	10	10	400	40	0.101	19.913
13	10	20	500	20	0.067	23.478
14	10	20	500	20	0.070	23.098
15	10	20	500	20	0.069	23.223
16	10	30	300	30	0.081	21.830
17	10	30	300	30	0.082	21.723
18	10	30	300	30	0.084	21.514
19	20	10	500	30	0.087	21.209
20	20	10	500	30	0.086	21.310
21	20	10	500	30	0.087	21.209
22	20	20	300	40	0.103	19.743
23	20	20	300	40	0.102	19.827
24	20	20	300	40	0.104	19.659
25	20	30	400	20	0.036	28.873
26	20	30	400	20	0.037	28.635
27	20	30	400	20	0.038	28.404

The ANOVA table for S/N ratio of HAp/PSU composite is shown in Table 5.18.

Table 5.18 ANOVA table for S/N ratio of HAp/PSU composite

Source	DF value	Seq SS	Adj SS	Adj MS	F value	P value	Percentage Contribution
A	2	326.634	326.634	163.317	717.37	0.000	41.168
B	2	16.864	16.864	8.432	37.04	0.000	2.125
C	2	85.628	85.628	42.814	188.06	0.000	10.792
D	2	360.179	360.179	180.090	791.05	0.000	45.396
Error	18	4.098	4.098	0.228			
Total	26	793.402					

$S = 0.477138$ ,  $R\text{-Sq} = 99.48\%$ , and  $R\text{-Sq}(\text{adj}) = 99.25\%$

From percentage contribution, it can be concluded here that significance of factors is in the order of Factor D, A, C and B.

Main effects plot for means of S/N ratio, normal probability plot and interaction plot are shown in Figure 5.38, 5.39 and 5.40 respectively.

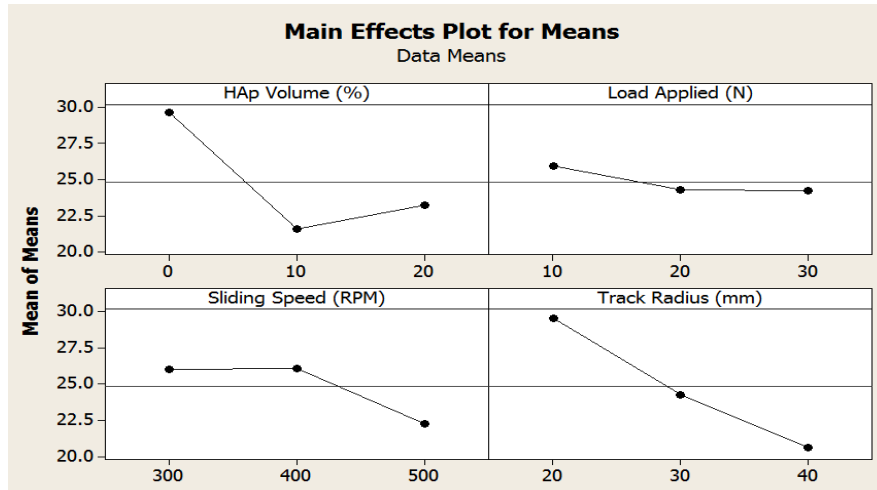


Figure 5.38 Main effects plot for means of S/N ratio

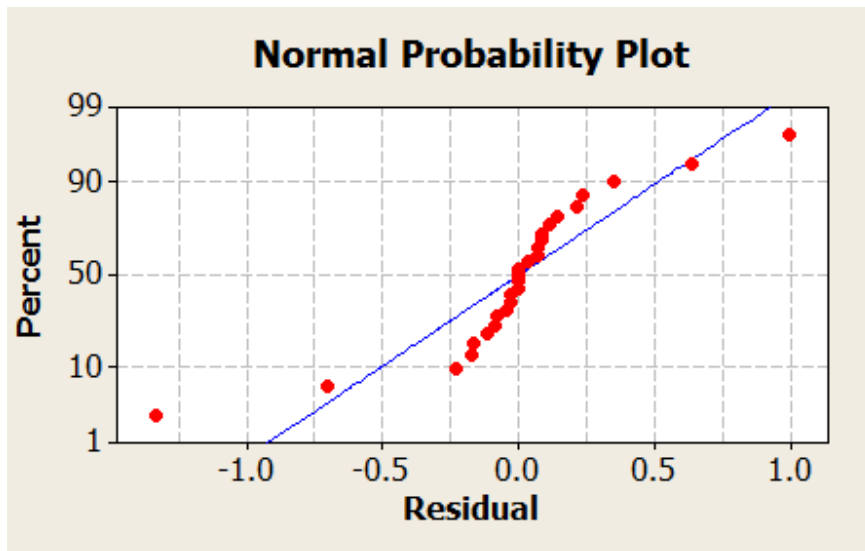


Figure 5.39 Normal probability plot for S/N ratio

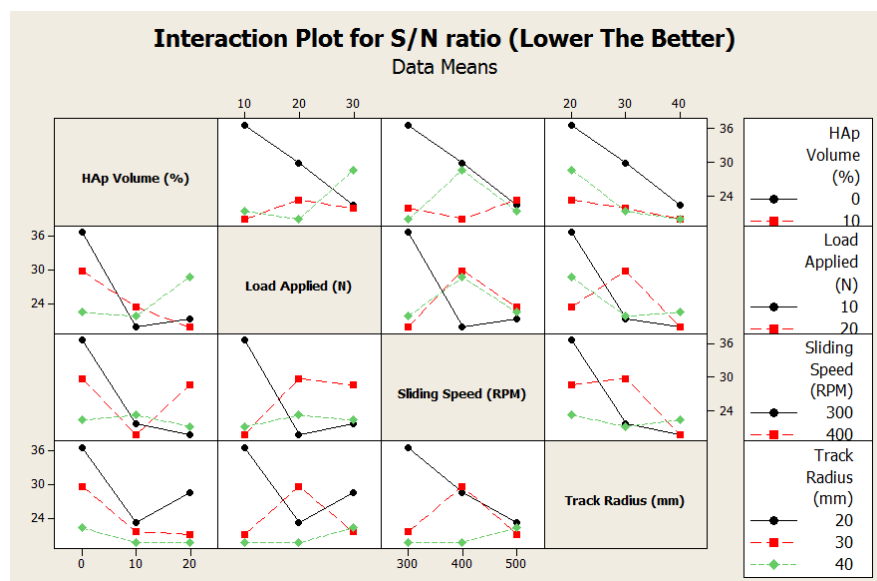


Figure 5.40 Interaction plot for S/N ratio

According to Figure 5.38, it is concluded that the optimal parametric combination is  $A_1B_1C_2D_1$ . When HAp volume is 0 vol. %, Load is 10 N, Sliding speed is 400 RPM and Track radius is 20 mm then minimum abrasive wear can be obtained. Referring to Figure 5.39, it can be concluded that the ANOVA proceeds in a satisfactory manner as the residuals follow a normal distribution. Figure 5.40 shows that two factor interaction of controllable factors seems to exist. However, the interaction of factors has not been considered for the sake of simplicity.

Table 5.19 shows the calculation data for HAp/PSU composite conducted at 1000 grit size paper in terms of volume loss, sliding distance, wear rate and specific wear rate

Table 5.19 Calculation data for HAp/PSU composite conducted at 1000 grit size paper

Experiment No.	Weight Loss (gm)	Volume Loss (cm <sup>3</sup> )	Sliding Distance (m)	Wear Rate 10 <sup>-6</sup> (cm <sup>3</sup> /m)	Specific Wear Rate 10 <sup>-6</sup> (cm <sup>3</sup> /Nm)
1	0.014	0.011	188.495	58.356	5.835
2	0.013	0.010	188.495	53.051	5.305
3	0.017	0.013	188.495	68.967	6.896
4	0.035	0.028	376.991	74.272	3.713
5	0.032	0.025	376.991	66.314	3.315
6	0.030	0.024	376.991	63.661	3.183
7	0.075	0.060	628.318	95.493	3.183
8	0.076	0.061	628.318	97.084	3.236
9	0.077	0.062	628.318	98.676	3.289
10	0.102	0.082	502.654	163.134	16.313
11	0.103	0.083	502.654	165.123	16.512
12	0.101	0.081	502.654	161.144	16.144
13	0.067	0.054	314.159	171.887	8.594
14	0.070	0.056	314.159	178.253	8.912
15	0.069	0.055	314.159	175.070	8.753
16	0.081	0.065	282.743	229.890	7.663
17	0.082	0.066	282.743	233.427	7.780
18	0.084	0.067	282.743	236.964	7.898
19	0.087	0.070	471.238	148.544	14.854
20	0.086	0.069	471.238	146.422	14.642
21	0.087	0.070	471.238	148.544	14.854
22	0.103	0.083	376.991	220.164	11.008
23	0.102	0.082	376.991	217.511	10.875
24	0.104	0.083	376.991	220.164	11.008
25	0.036	0.029	251.327	115.387	3.846
26	0.037	0.029	251.327	115.387	3.846
27	0.038	0.030	251.327	119.366	3.978

Load versus wear loss at (300, 400, and 500 rpm), sliding distance versus wear loss, sliding distance versus specific wear rate, sliding distance versus co-efficient of friction at 600 grit size paper are shown in Figure 5.41 to Figure 5.46 respectively.

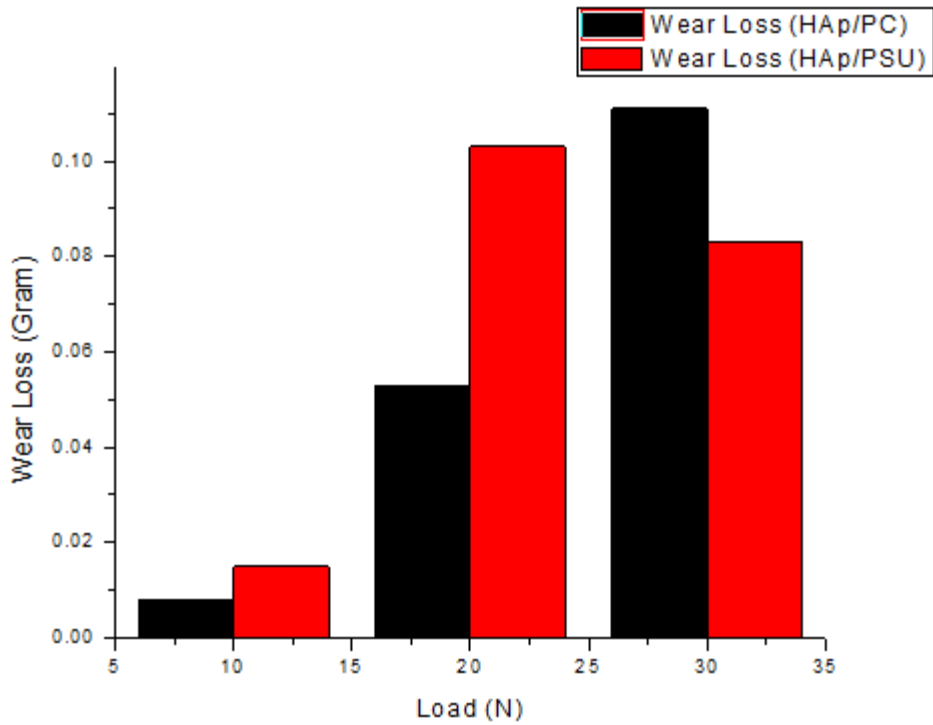


Figure 5.41 Load vs Wear loss (at 300 rpm on 1000 grit size paper)

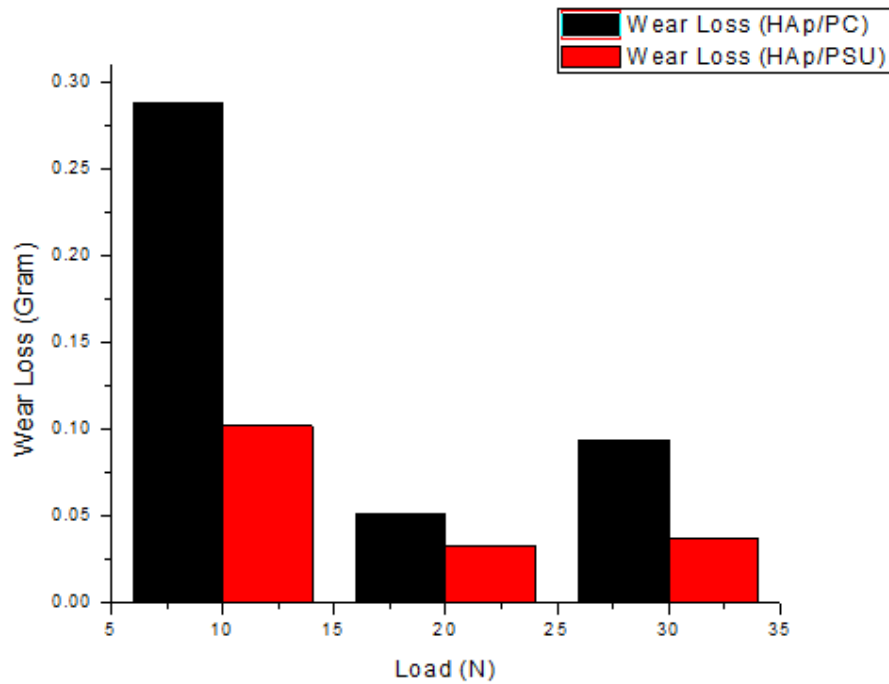


Figure 5.42 Load vs Wear loss (at 400 rpm on 1000 grit size paper)

It can be observed from Figure 5.41 that wear loss increases for load 10 N to 30 N for HAp/PC composite whereas for HAp/PSU composite wear loss increases for 10 N to 20 N and then decreases at 30 N at 300 rpm and 1000 grit size paper. It can be observed from Figure 5.42 that wear loss decreases for load 10 N to 20 N and then increases at 30 N for both HAp/PC and HAp/PSU composites at 400 rpm and 1000 grit size paper.

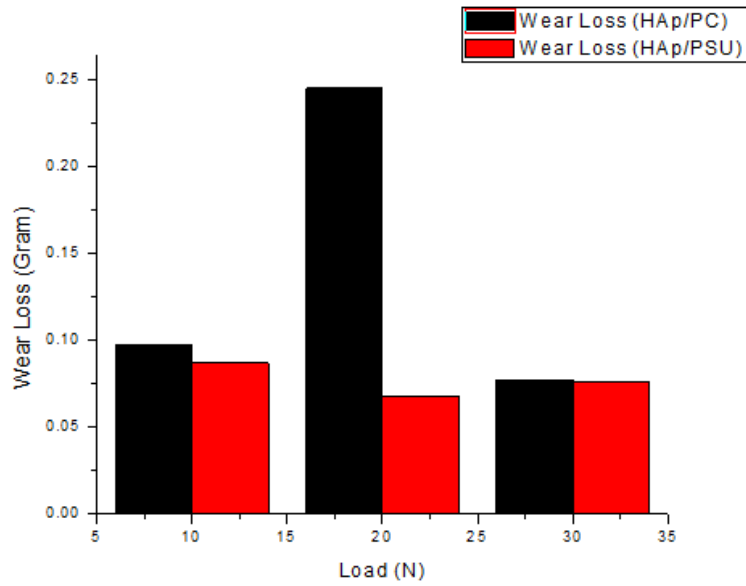


Figure 5.43 Load vs Wear loss (at 500 rpm on 1000 grit size paper)

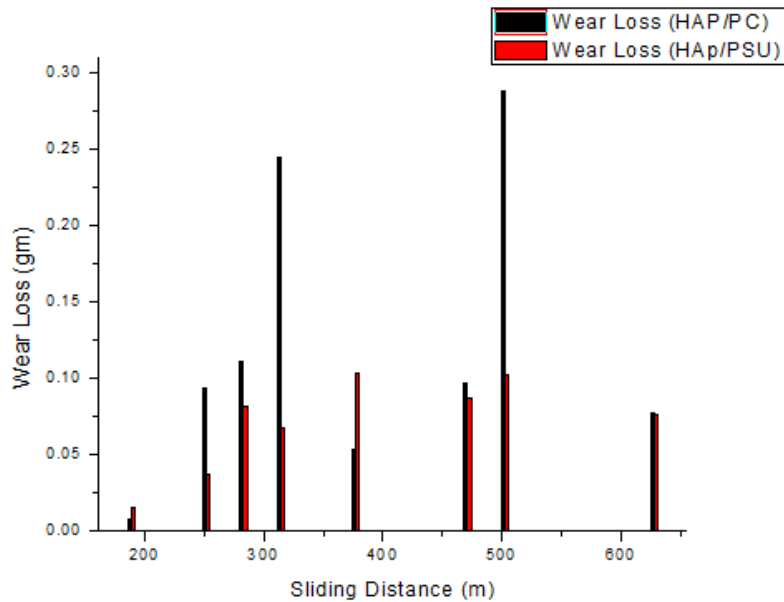


Figure 5.44 Sliding distance vs Wear loss (at 1000 grit size paper)

It can be observed from Figure 5.43 that wear loss increases for load 10 N to 20 N and then decreases at 30 N for HAp/PC composite whereas wear loss decreases for load 10 N to 20 N and then increases at 30 N for HAp/PSU composite at 500 rpm and 1000 grit size paper. It can be observed from Figure 5.44 that wear loss showing increases and decreases manner when sliding distance increases for 188.495 m to 628.318 m for both HAp/PC and HAp/PSU composites at 1000 grit size paper.

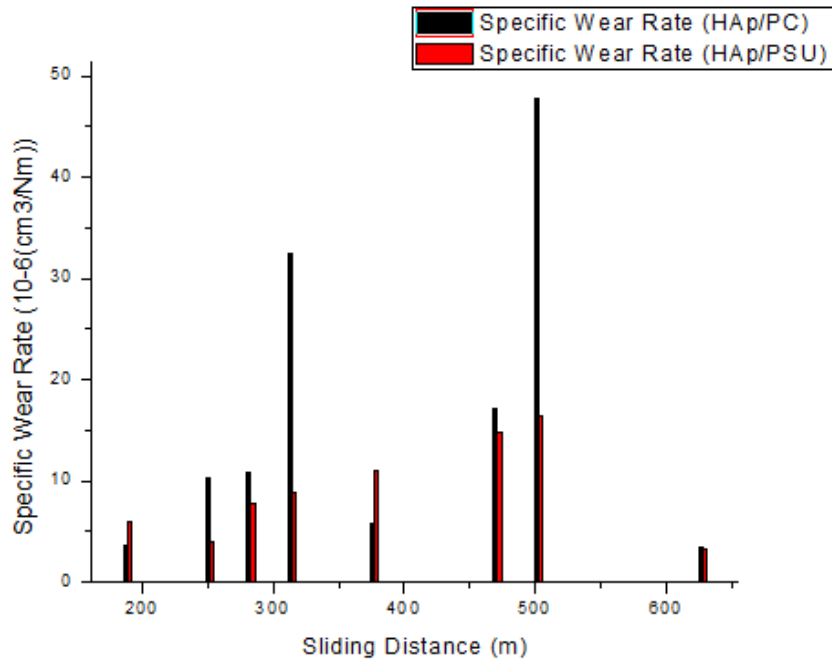


Figure 5.45 Sliding distance vs Specific wear rate (at 1000 grit size paper)

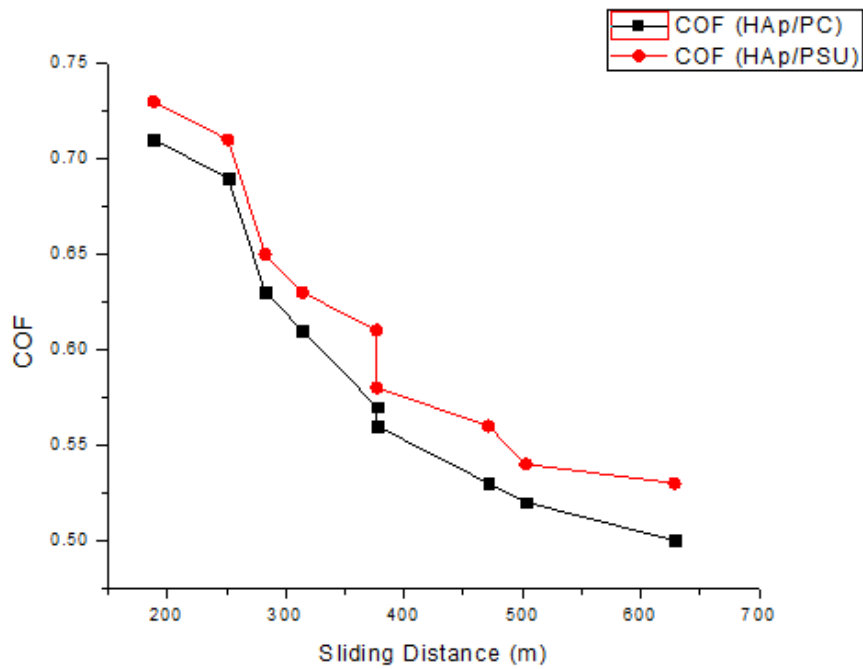


Figure 5.46 Sliding Distance vs. COF (at 1000 grit size paper)

It can be observed from Figure 5.45 that specific wear rate showing increases and decreases manner when sliding distance increases for 188.495 m to 628.318 m for both HAp/PC and HAp/PSU composites at 1000 grit size paper. It can be observed from Figure 5.46 that co-efficient of friction decreases for both HAp/PC and HAp/PSU composites when sliding distance increases at 1000 grit size paper.

### 5.2.1.1 Prediction of abrasive wear behaviour of composites

#### 5.2.1.1.1 Adaptive neuro fuzzy inference system (ANFIS) methodology used for HAp/PC composite (at 400 grit size paper)

(According to Younesi et al. [166]) Adaptive neuro-fuzzy inference system (ANFIS) is an inference system which is coupled between neural network and fuzzy inference system. Basically, ANFIS is a modified form of neural network that is based on Tagaki-Sugeno fuzzy inference system which maps inputs through input membership functions and output through output membership functions. Neural network are not easy to implement the results as it can learn from the data which is present in the form of input and output pairs however on the other hand fuzzy inference system are easy to implement the results as it requires only IF-THEN rules. So, to predict the results with a very high accuracy it is necessary to build the novel model which is based on both neural network and fuzzy inference system. A typical architecture of ANFIS system is shown in Figure 5.47. The ANFIS system is divided into five layers i.e. input fuzzification layer, fuzzy set database construction layer, fuzzy rule database construction layer, decision-making layer and finally output defuzzification layer.

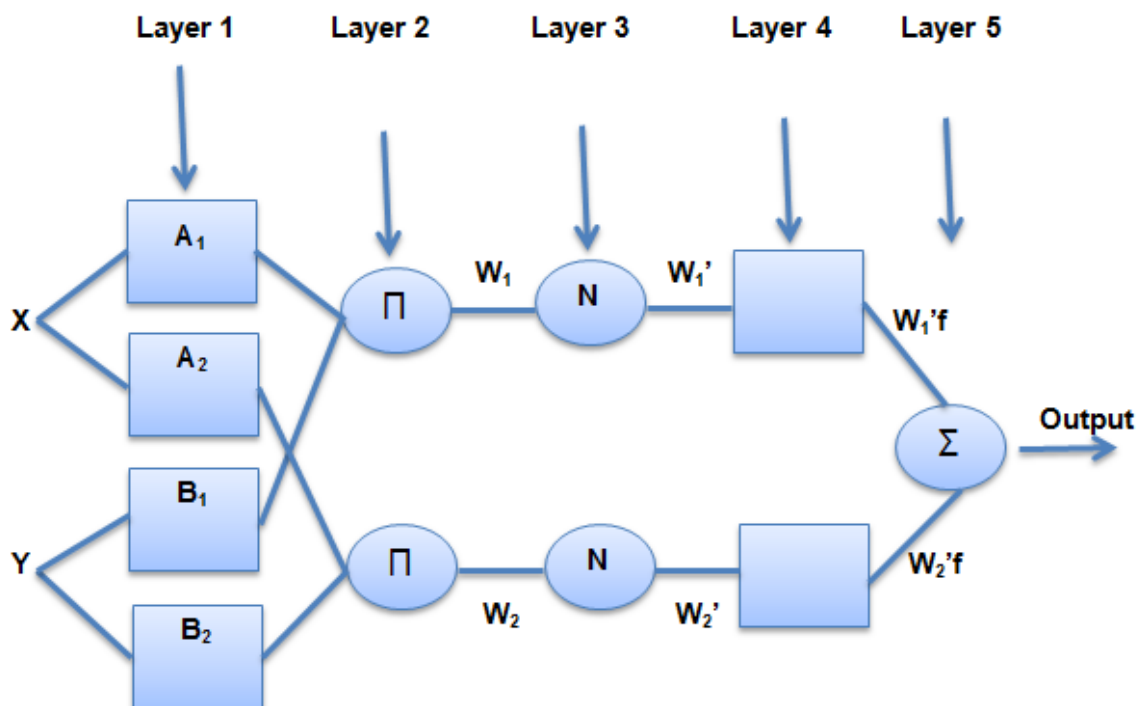


Figure 5.47 A typical architecture of ANFIS system

It consists of number of nodes connected through directional links. Each node is characterized by a node function with fixed or adjustable parameters. By considering a first order Tagaki, Sugeno and Kang (TSK) fuzzy inference system, a fuzzy model consisting of two rules (Sugeno and Kang, 1988)



Rule 1: If x is  $A_1$  and y is  $B_1$  then  $f_1 = p_1x+q_1y+r_1$

Rule 2: If x is  $A_2$  and y is  $B_2$  then  $f_2 = p_2x+q_2y+r_2$

If  $f_1$  and  $f_2$  are constants instead of linear equations we have zero order TSK fuzzy model. Node functions in the same layer are of the same function family as described below. It is to be noted that  $O_i^j$  denotes the output of the  $i$ th node in layer  $j$ .

Layer 1: Each node in this layer generates a membership grade of a linguistic label. For example, the node function of the  $i$ th node might be

$$O_i^j = \mu A_i(x) = \frac{1}{1+\left[\left(\frac{x-c_i}{a_i}\right)^2\right]^{b_i}} \quad (5.6)$$

where  $x$  is the input to the node  $i$ , and  $A_i$  is the linguistic label (small, large) associated with this node; and  $\{a_i, b_i, c_i\}$  is the parameter set that changes the shapes of the membership function. Parameters in this layer are referred to as the “premise parameters”.

Layer 2: Each node in this layer calculates the firing strength of each rule via multiplication:

$$O_i^2 = W_i = \mu A_i(x) \times \mu B_i(y) \quad i = 1, 2. \quad (5.7)$$

Layer 3: The  $i$ th node in this layer calculates the ratio of the  $i$ th rule’s firing strength to the sum of all rule’s firing strengths:

$$O_i^3 = W_i' = \frac{W_i}{W_1+W_2} \quad i = 1, 2. \quad (5.8)$$

Layer 4: Every node in this layer is a squared node with a node function

$$O_i^4 = W_i' f_i = W_i'(p_i x + q_i y + r_i) \quad (5.9)$$

where  $W_i'$  is the output of layer 3.

Layer 5: The single circle node computes the overall output as the summation of all incoming signals i.e.

$$O_i^5 = \text{Overall output} = \sum W_i' f_i = \frac{\sum W_i' f_i}{\sum W_i'} \quad (5.10)$$

Entire experimental data set is divided into training set and testing set. A total of 27 data sets are used out of which 20 are considered as training data and 7 as testing data.

During training, a five layered ANFIS model is constructed as discussed. The number of nodes in the 2<sup>nd</sup> layer increased gradually during training starting with two. It was observed that the error is converged (decreasing) by increasing the nodes up to three. Hence, the number of nodes in second layer is fixed to three and further analysis is carried out. The five layers are known as one input, three hidden and one output layer. The network was run on MATLAB platform using HP Compaq LE1902x desktop computer. Three triangular type membership functions (trimf) are chosen for input and constant type membership function is used for output during generating FIS. The function goes steadily due to faster hybrid learning rule which concluded that the model parameters are matched. After that 7 data are used for testing to verify the accuracy of the proposed model. The Figure 5.48 shows the procedure for developing the ANFIS model.

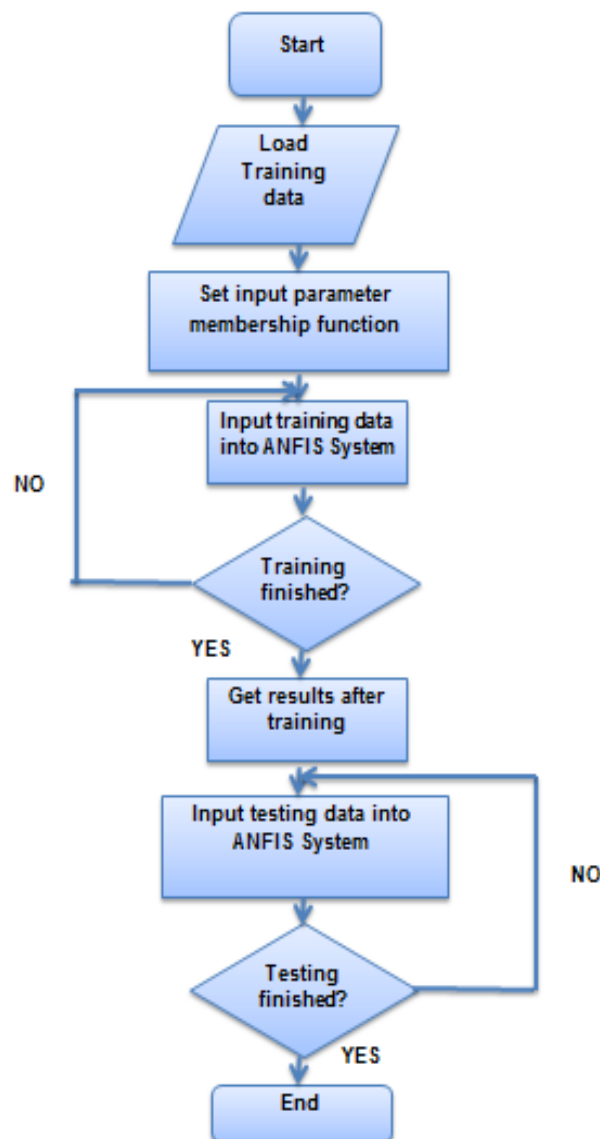


Figure 5.48 Flow chart of ANFIS model

The FIS editor for input parameters of both HAp/PC and HAp/PSU composites, and membership function editor for output parameter of HAp/PC composite at 400 grit size are shown in Figure 5.49 to Figure 5.54 respectively.

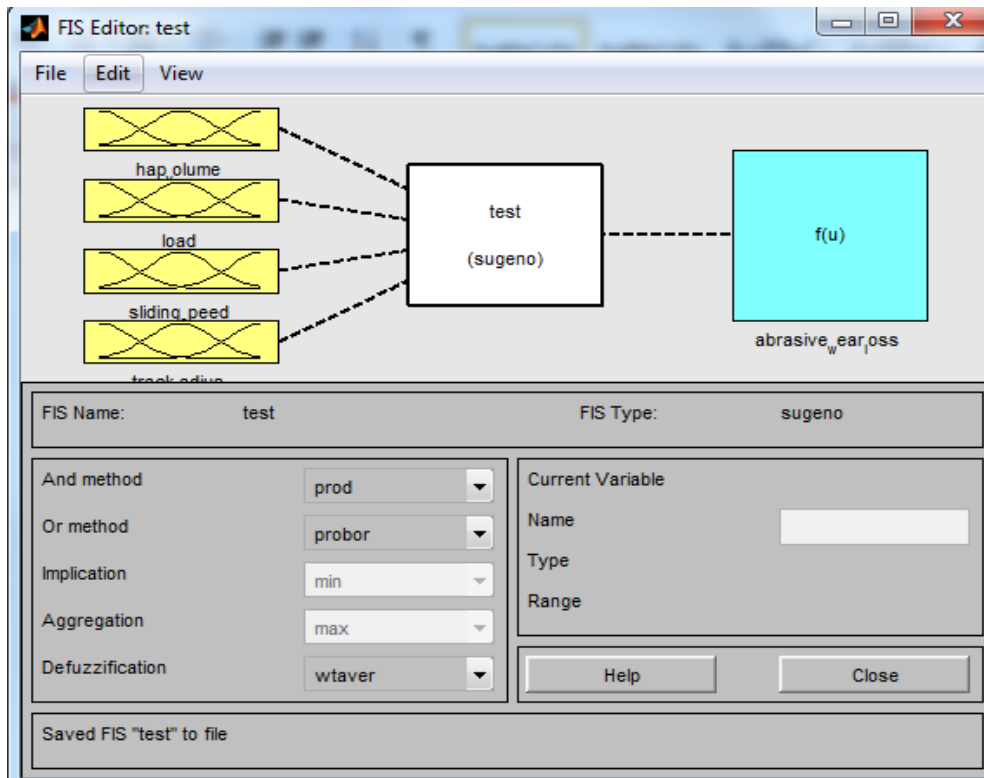


Figure 5.49 FIS editor

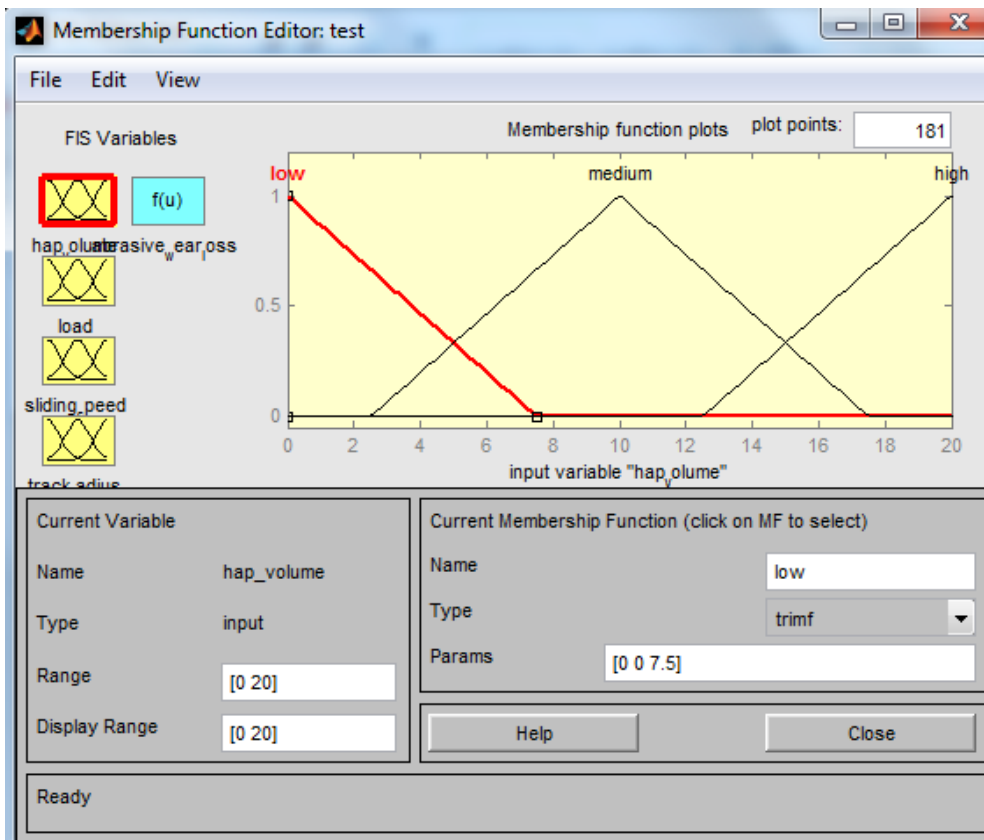


Figure 5.50 Membership function editor of Input 1

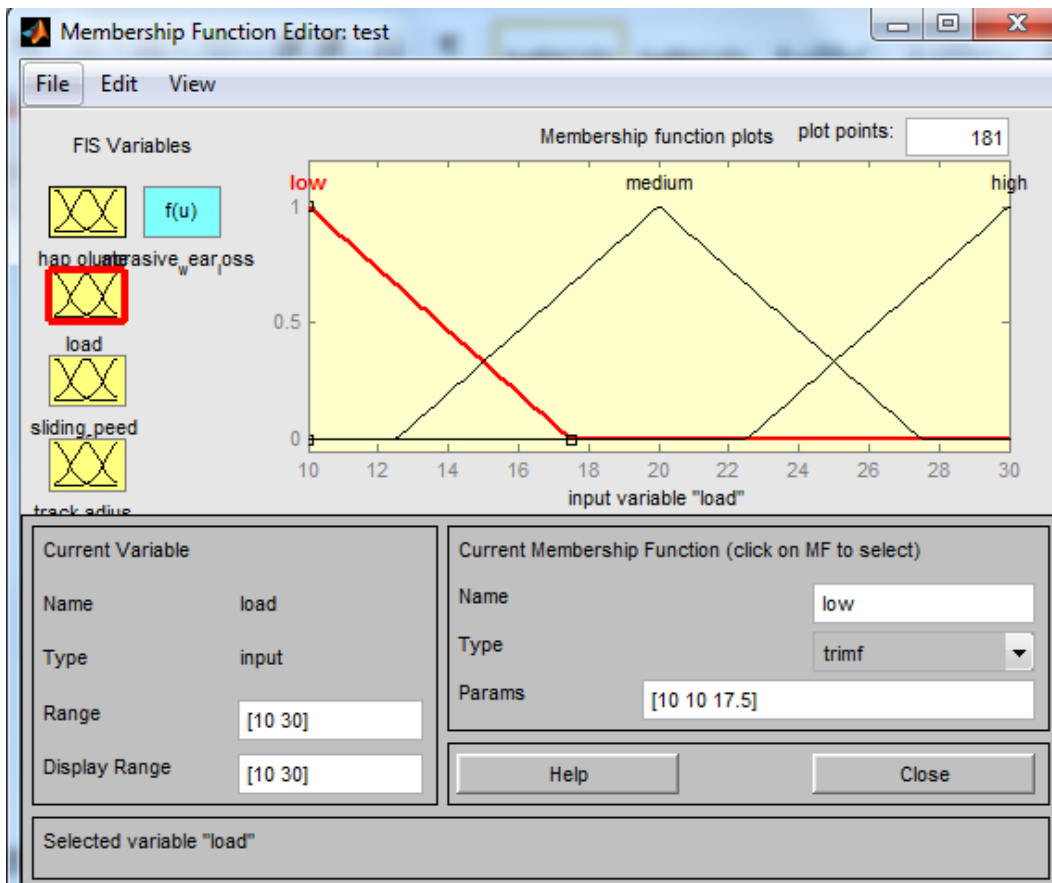


Figure 5.51 Membership function editor of Input 2

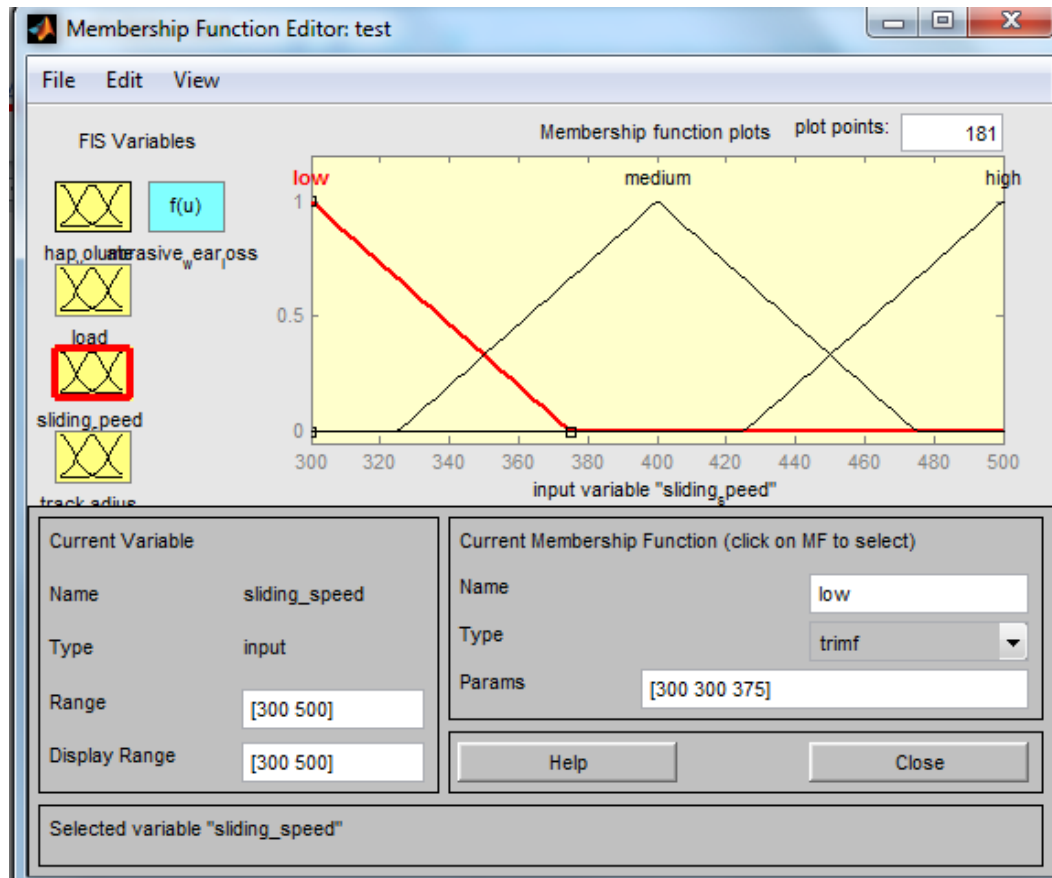


Figure 5.52 Membership function editor of Input 3

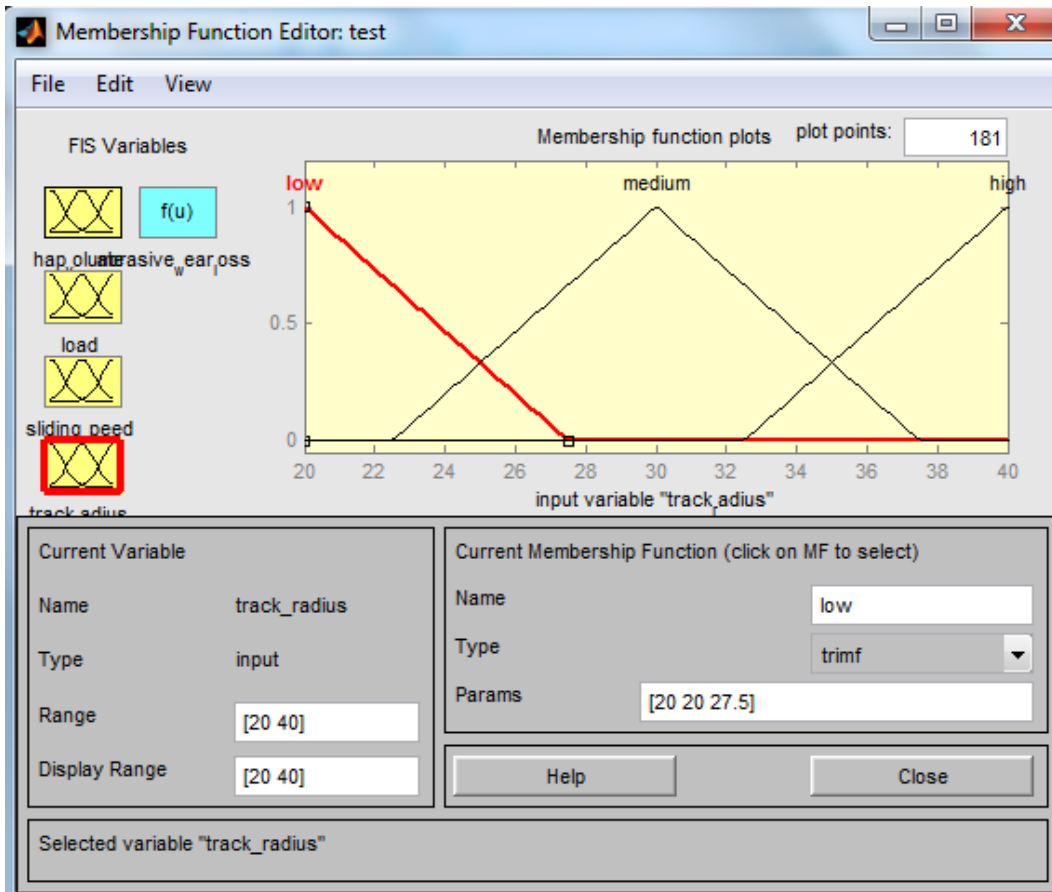


Figure 5.53 Membership function editor of Input 4

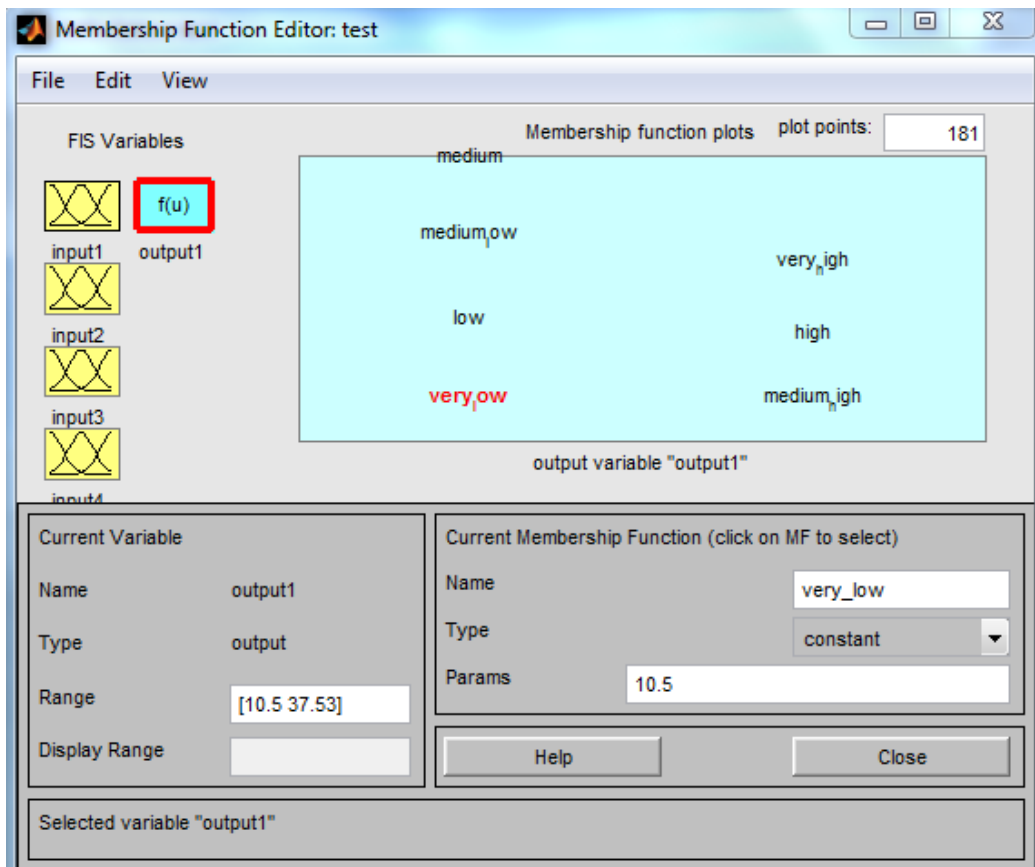


Figure 5.54 Membership function editor for output of HAp/PC composite

The ANFIS model structure of HAp/PC and HAp/PSU composites regarding abrasive wear, while ANFIS editor for both training and testing data, rule editor and rule viewer of HAp/PC composite are shown in Figure 5.55 to Figure 5.59.

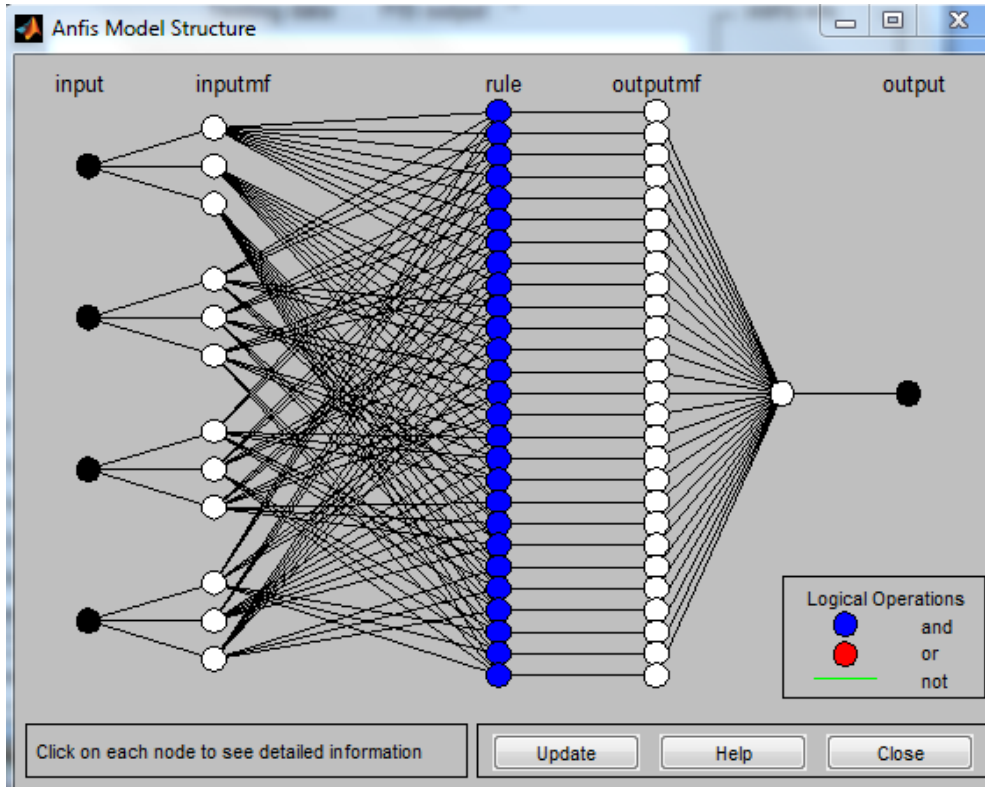


Figure 5.55 ANFIS model structure

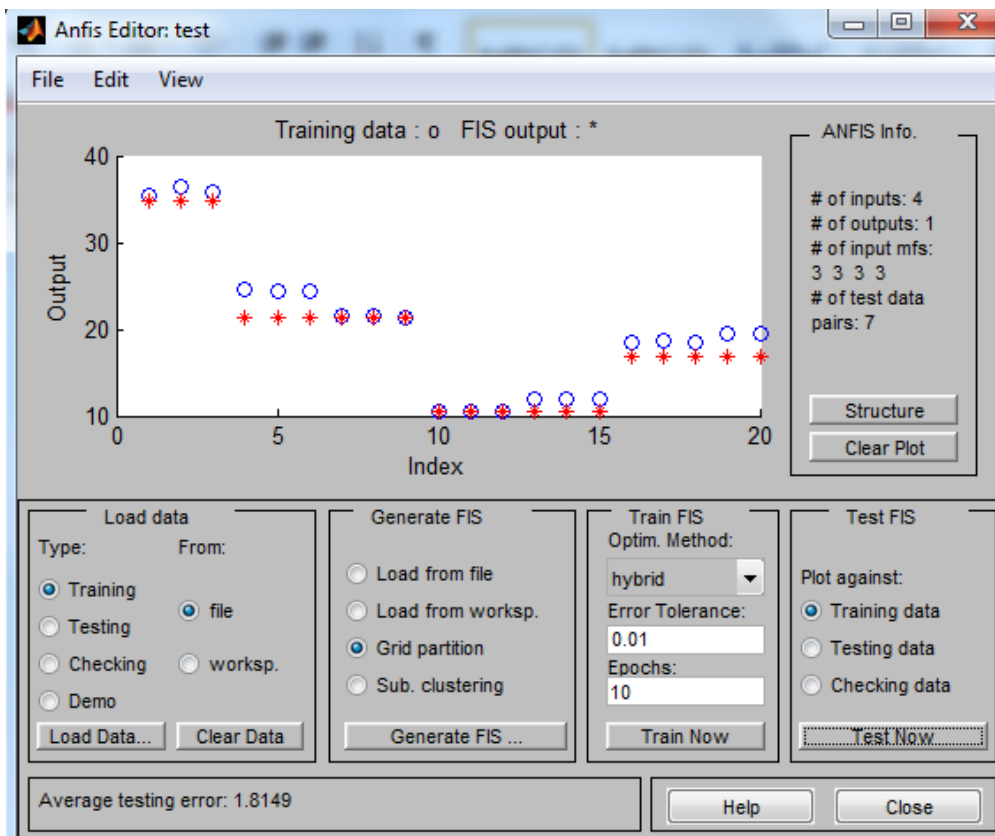


Figure 5.56 Distribution of predicted and actual data (Training)

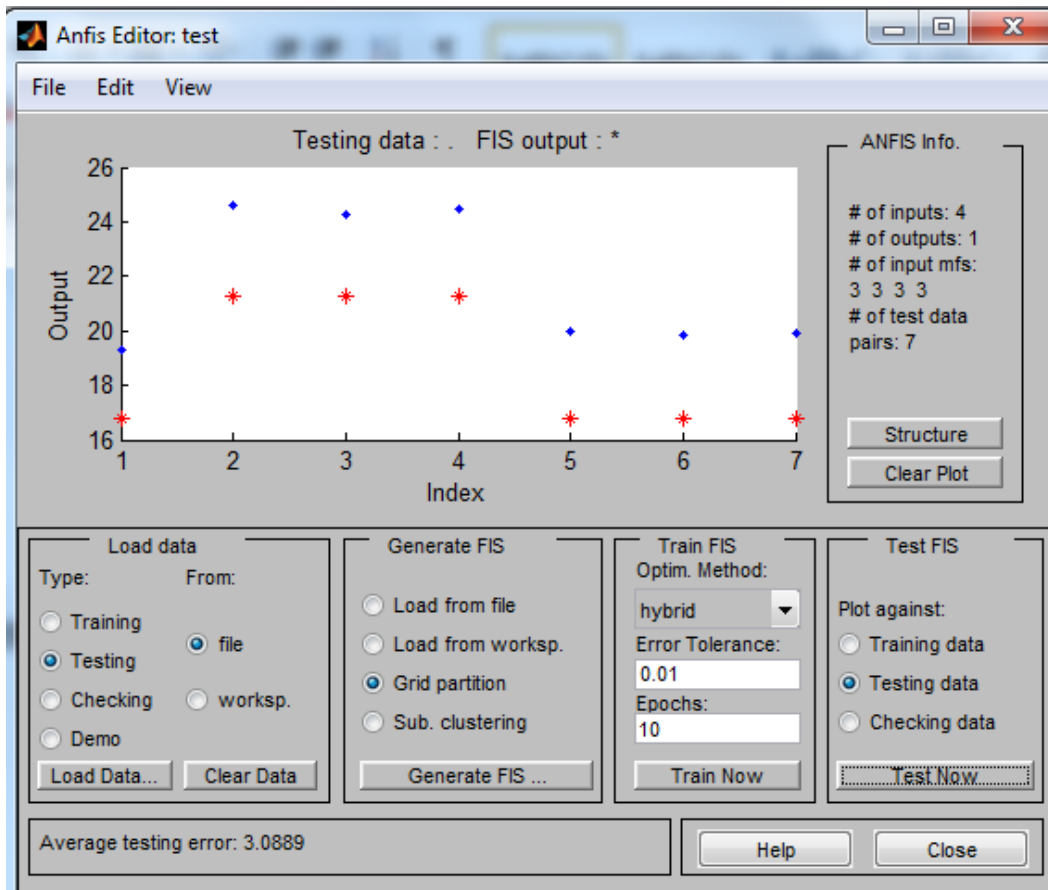


Figure 5.57 Distribution of predicted and actual data (Testing)

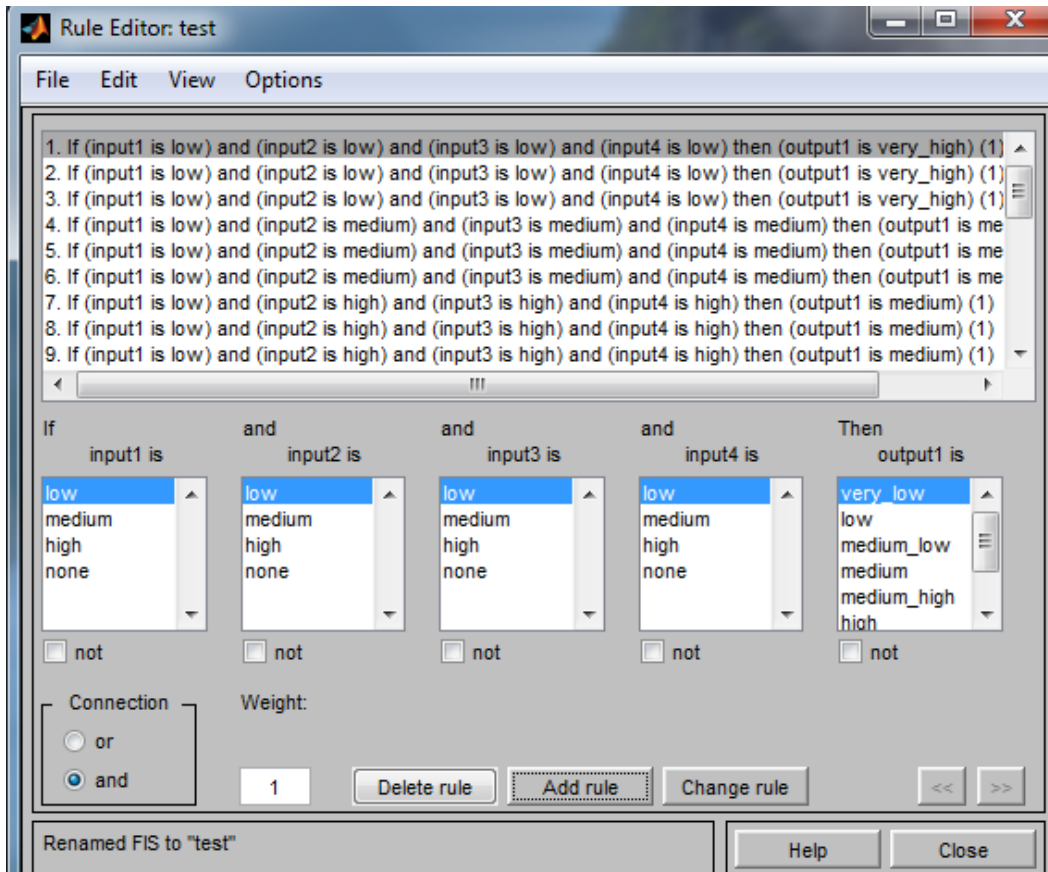


Figure 5.58 Rule editor

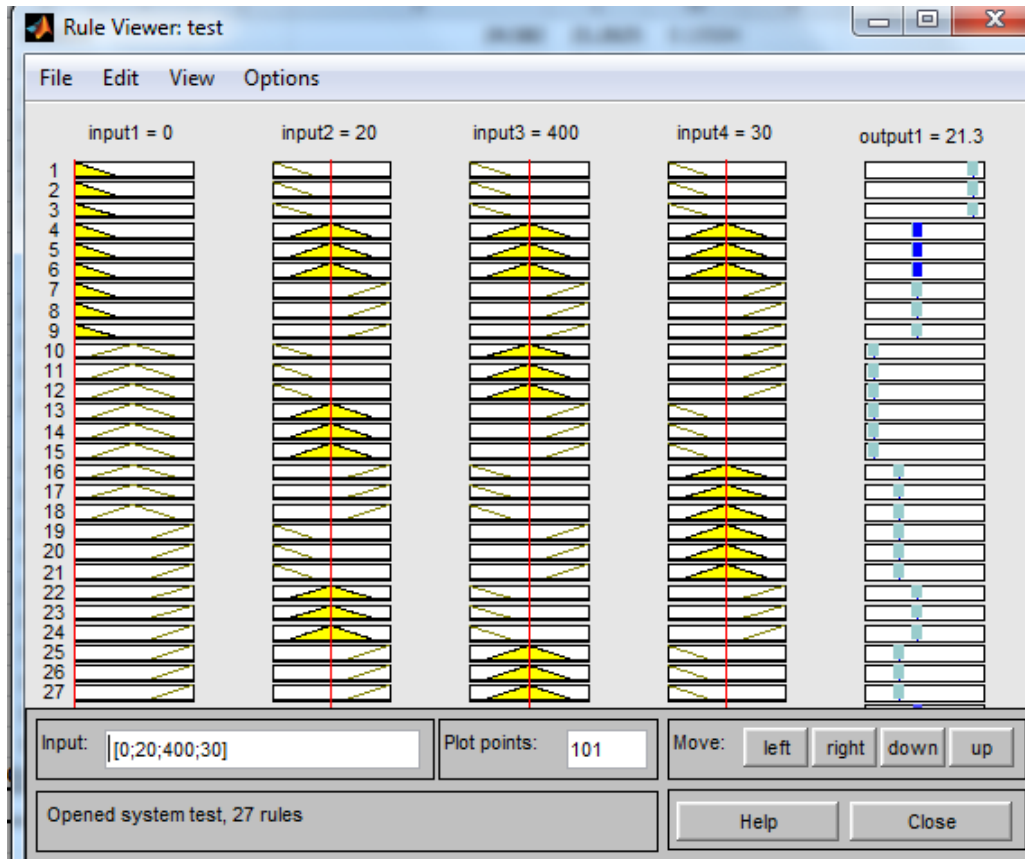


Figure 5.59 Rule viewer

The input and output experimental value with ANFIS predicted value of HAp/PC composite at 400 grit size for training purpose is shown in Table 5.20.

Table 5.20 Input and output data with ANFIS predicted value of HAp/PC composite at 400 grit size

No.	Factor A (HAp Volume) %	Factor B (Load Applied) N	Factor C (Sliding Speed) RPM	Factor D (Track Radius) mm	Wear Loss (gm)	S/N ratio of Experimental value	ANFIS output predicted value
1	0	10	300	20	0.017	35.391	34.7775
2	0	10	300	20	0.015	36.478	34.7775
3	0	10	300	20	0.016	35.917	34.7775
4	0	20	400	30	0.059	24.582	21.2625
5	0	20	400	30	0.060	24.436	21.2625
6	0	20	400	30	0.061	24.293	21.2625
7	0	30	500	40	0.084	21.514	21.2625
8	0	30	500	40	0.083	21.618	21.2625
9	0	30	500	40	0.085	21.411	21.2625
10	10	10	400	40	0.297	10.544	10.5
11	10	10	400	40	0.296	10.574	10.5
12	10	10	400	40	0.296	10.574	10.5
13	10	20	500	20	0.251	12.006	10.5
14	10	20	500	20	0.253	11.937	10.5
15	10	20	500	20	0.252	11.971	10.5
16	10	30	300	30	0.119	18.489	16.7575
17	10	30	300	30	0.117	18.636	16.7575
18	10	30	300	30	0.118	18.562	16.7575
19	20	10	500	30	0.106	19.493	16.7575
20	20	10	500	30	0.107	19.412	16.7575



The input and output data with ANFIS predicted value of HAp/PC composite at 400 grit size for testing purpose is shown in Table 5.21.

Table 5.21 Input and output data with ANFIS predicted value of HAp/PC composite at 400 grit size

No.	Factor A (HAp Volume) %	Factor B (Load Applied) N	Factor C (Sliding Speed) RPM	Factor D (Track Radius) mm	Wear Loss (gm)	S/N ratio of Experimental value	ANFIS output predicted value
1	20	10	500	30	0.108	19.331	16.7575
2	20	20	300	40	0.059	24.582	21.2625
3	20	20	300	40	0.061	24.293	21.2625
4	20	20	300	40	0.060	24.436	21.2625
5	20	30	400	20	0.100	20.000	16.7575
6	20	30	400	20	0.102	19.827	16.7575
7	20	30	400	20	0.101	19.913	16.7575

By calculating we get the mean relative percentage error for training and testing of HAp/PC composite conducted at 400 grit size paper is 7.38% and 14.26% respectively.

#### 5.2.1.1.2 Adaptive neuro fuzzy inference system (ANFIS) methodology used for HAp/PSU composite (at 400 grit size paper)

The membership function editor for output parameter of HAp/PSU composite at 400 grit size is shown in Figure 5.60.

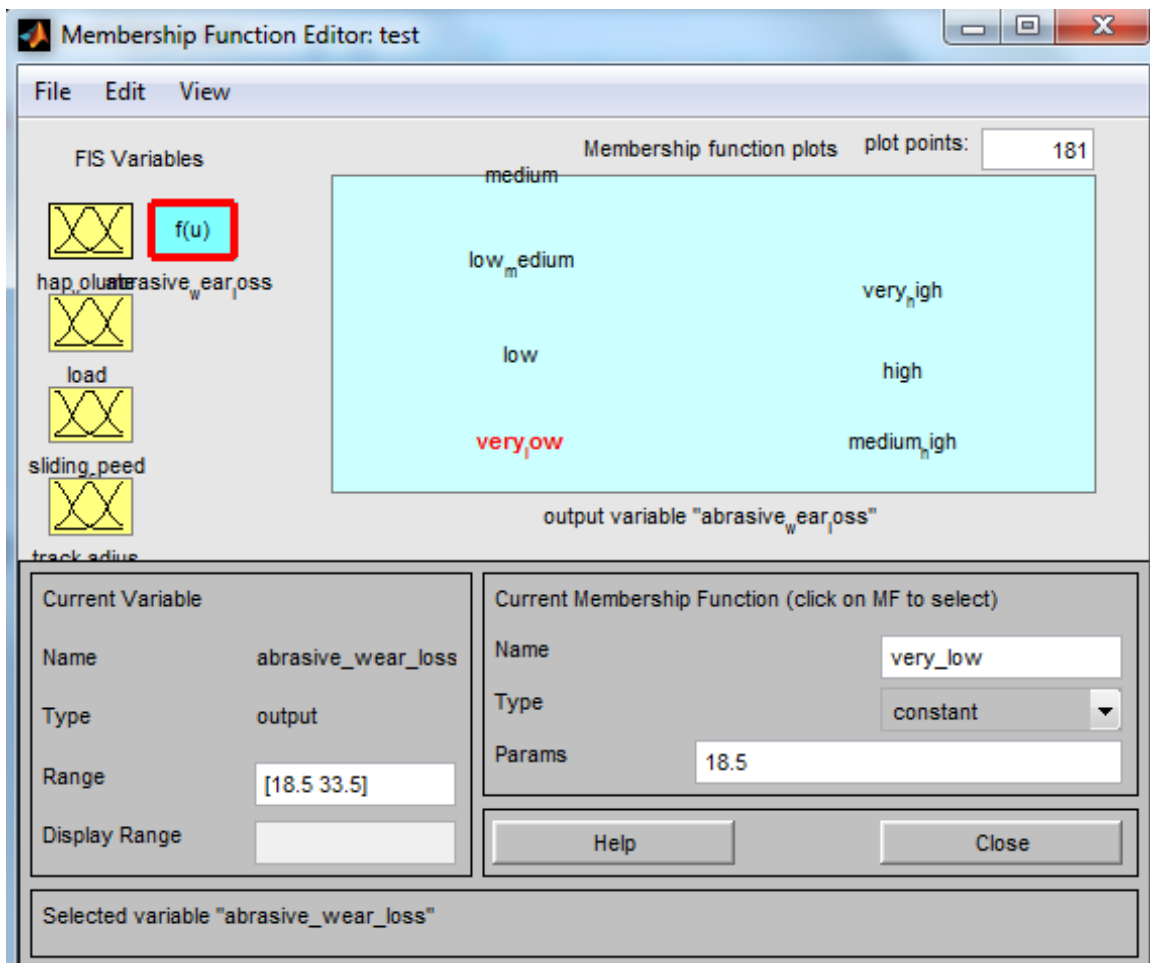


Figure 5.60 Membership function editor for output of HAp/PSU composite

The ANFIS editor for both training and testing data, rule editor and rule viewer of HAp/PSU composite are shown in Figure 5.61 to Figure 5.64.

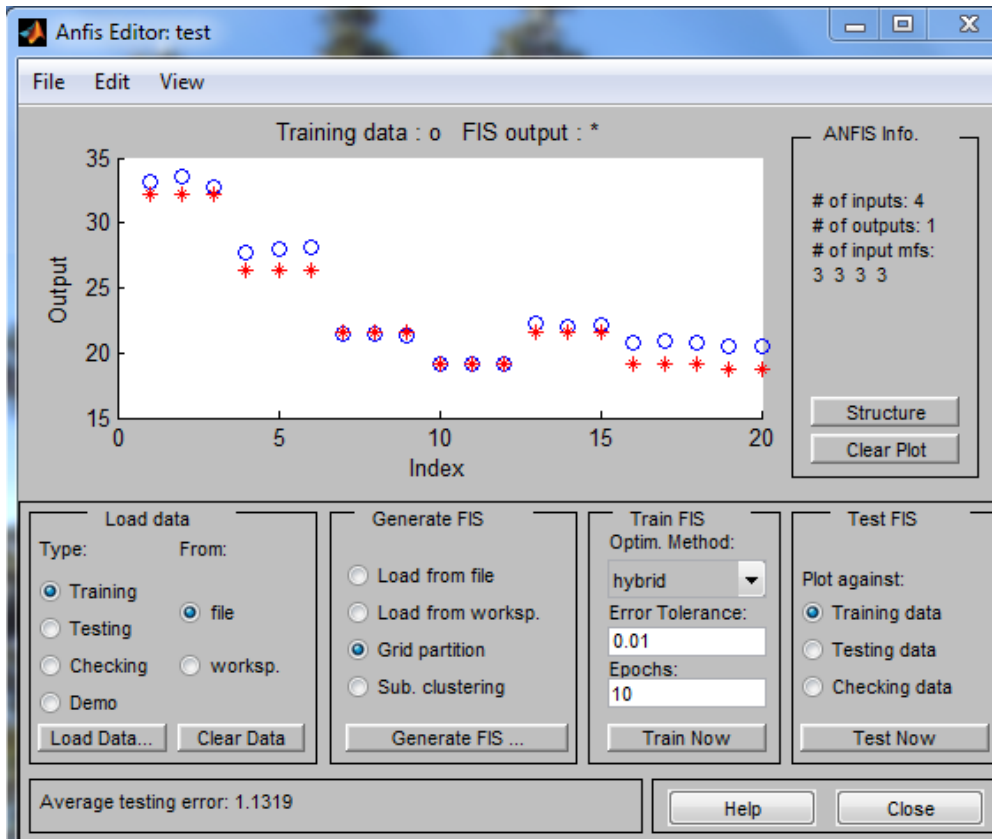


Figure 5.61 Distribution of predicted and actual data (Training)

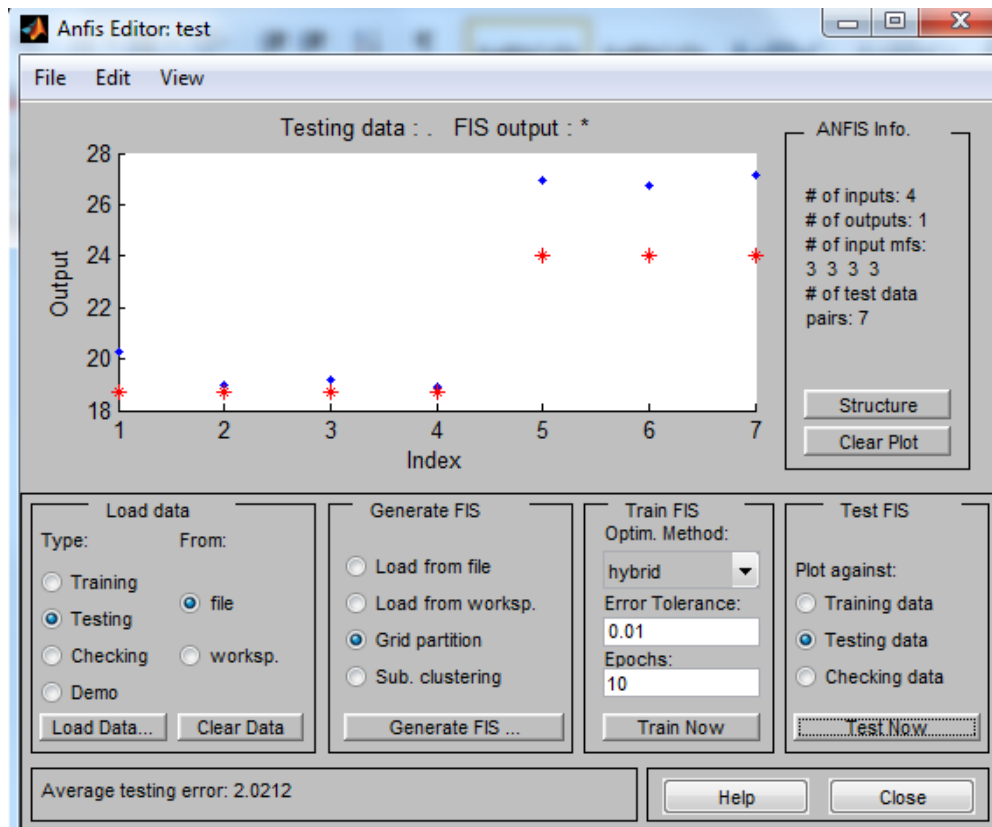


Figure 5.62 Distribution of predicted and actual data (Testing)

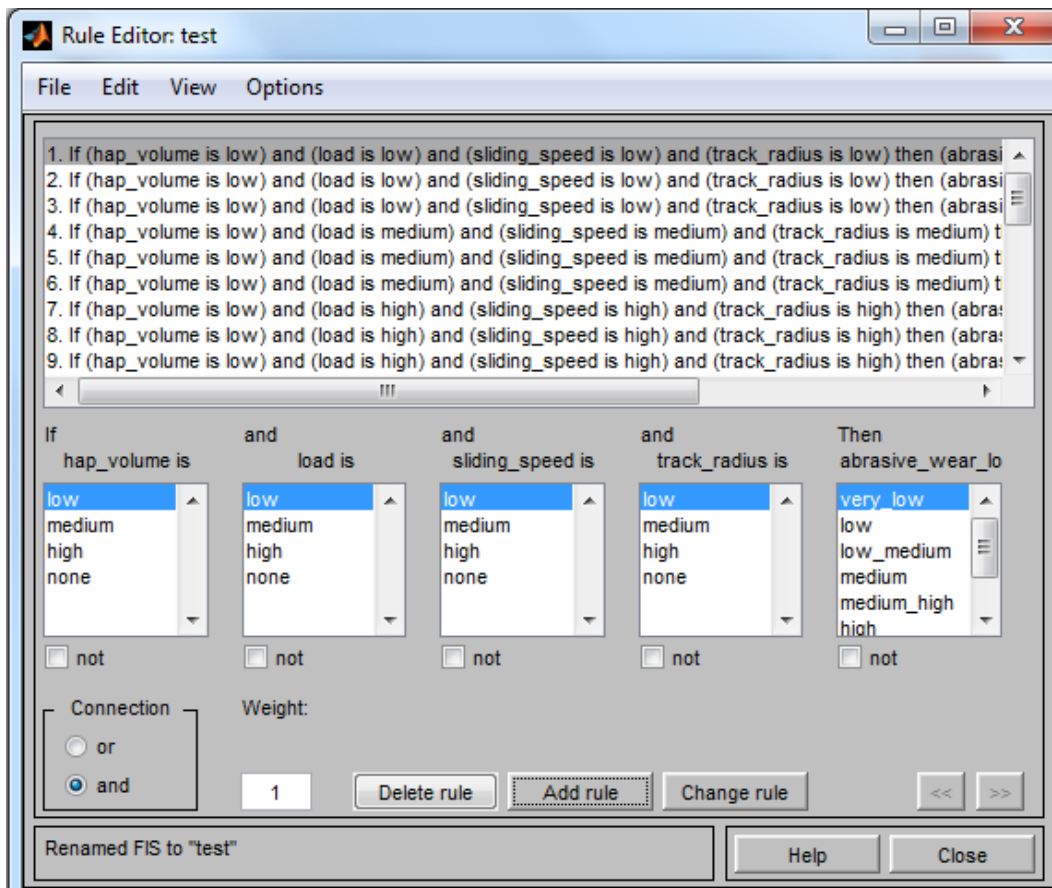


Figure 5.63 Rule editor

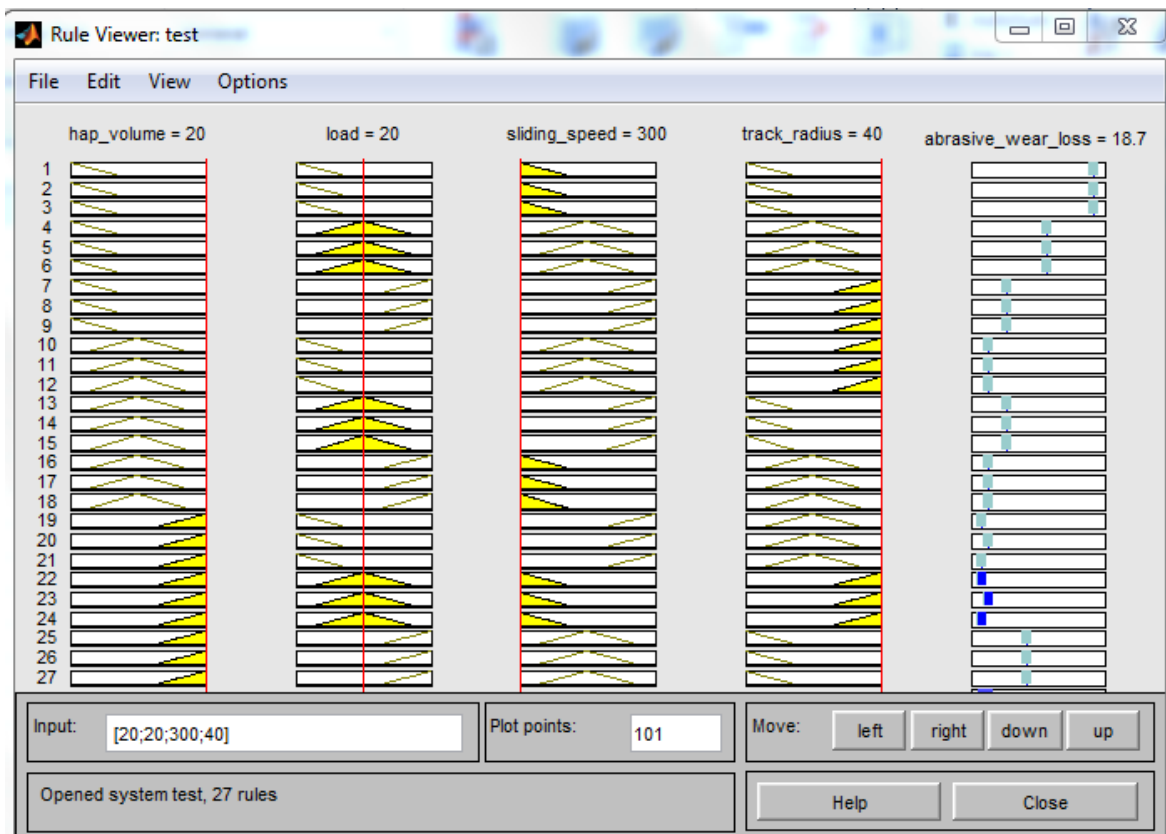


Figure 5.64 Rule viewer

The input and output experimental value with ANFIS predicted value of HAp/PSU composite at 400 grit size for training purpose is shown in Table 5.22.

Table 5.22 Input and output data with ANFIS predicted value of HAp/PSU composite at 400 grit size

No.	Factor A (HAp Volume) %	Factor B (Load Applied) N	Factor C (Sliding Speed) RPM	Factor D (Track Radius) mm	Wear Loss (gm)	S/N ratio of Experimental value	ANFIS output predicted value
1	0	10	300	20	0.022	33.151	32.2
2	0	10	300	20	0.021	33.555	32.2
3	0	10	300	20	0.023	32.765	32.2
4	0	20	400	30	0.041	27.744	26.4
5	0	20	400	30	0.040	27.958	26.4
6	0	20	400	30	0.039	28.178	26.4
7	0	30	500	40	0.085	21.411	21.6
8	0	30	500	40	0.084	21.514	21.6
9	0	30	500	40	0.086	21.310	21.6
10	10	10	400	40	0.110	19.172	19.2
11	10	10	400	40	0.111	19.093	19.2
12	10	10	400	40	0.110	19.172	19.2
13	10	20	500	20	0.077	22.270	21.6
14	10	20	500	20	0.079	22.047	21.6
15	10	20	500	20	0.078	22.158	21.6
16	10	30	300	30	0.091	20.819	19.2
17	10	30	300	30	0.090	20.915	19.2
18	10	30	300	30	0.092	20.724	19.2
19	20	10	500	30	0.095	20.445	18.7333
20	20	10	500	30	0.094	20.537	18.7333

The input and output data with ANFIS predicted value of HAp/PSU composite at 400 grit size for testing purpose is shown in Table 5.23.

Table 5.23 Input and output data with ANFIS predicted value of HAp/PSU composite at 400 grit size

No.	Factor A (HAp Volume) %	Factor B (Load Applied) N	Factor C (Sliding Speed) RPM	Factor D (Track Radius) mm	Wear Loss (gm)	S/N ratio of Experimental value	ANFIS output predicted value
1	20	10	500	30	0.097	20.264	18.7333
2	20	20	300	40	0.112	19.015	18.7333
3	20	20	300	40	0.110	19.172	18.7333
4	20	20	300	40	0.113	18.938	18.7333
5	20	30	400	20	0.045	26.935	24
6	20	30	400	20	0.046	26.744	24
7	20	30	400	20	0.044	27.130	24

By calculating we get the mean relative percentage error for training and testing of HAp/PSU composite conducted at 400 grit size paper is 3.80% and 6.30% respectively.

### 5.2.1.1.3 Adaptive neuro fuzzy inference system (ANFIS) methodology used for HAp/PC composite (at 600 grit size paper)

The membership function editor for output parameter of HAp/PC composite at 600 grit size is shown in Figure 5.65.

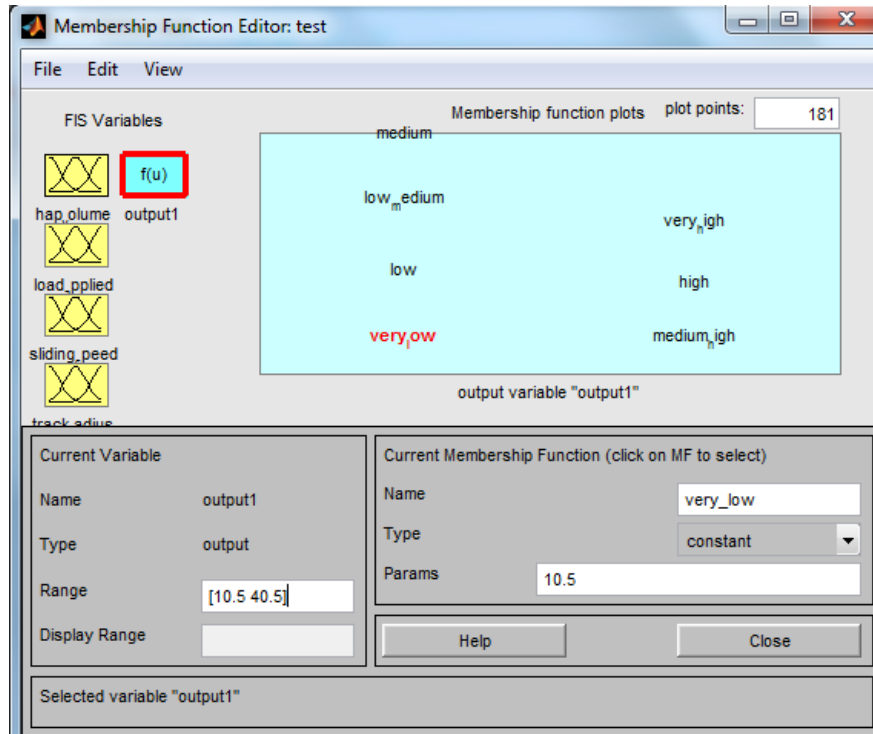


Figure 5.65 Membership function editor for output of HAp/PC composite

The ANFIS editor for both training and testing data, rule editor and rule viewer of HAp/PC composite are shown in Figure 5.66 to Figure 5.69 respectively.

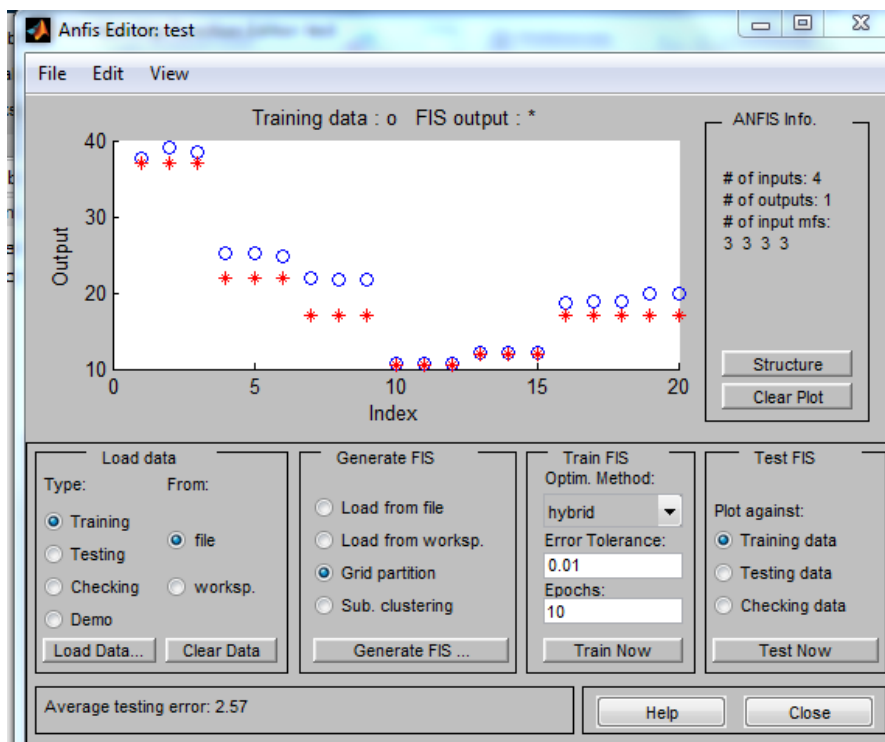


Figure 5.66 Distribution of predicted and actual data (Training)

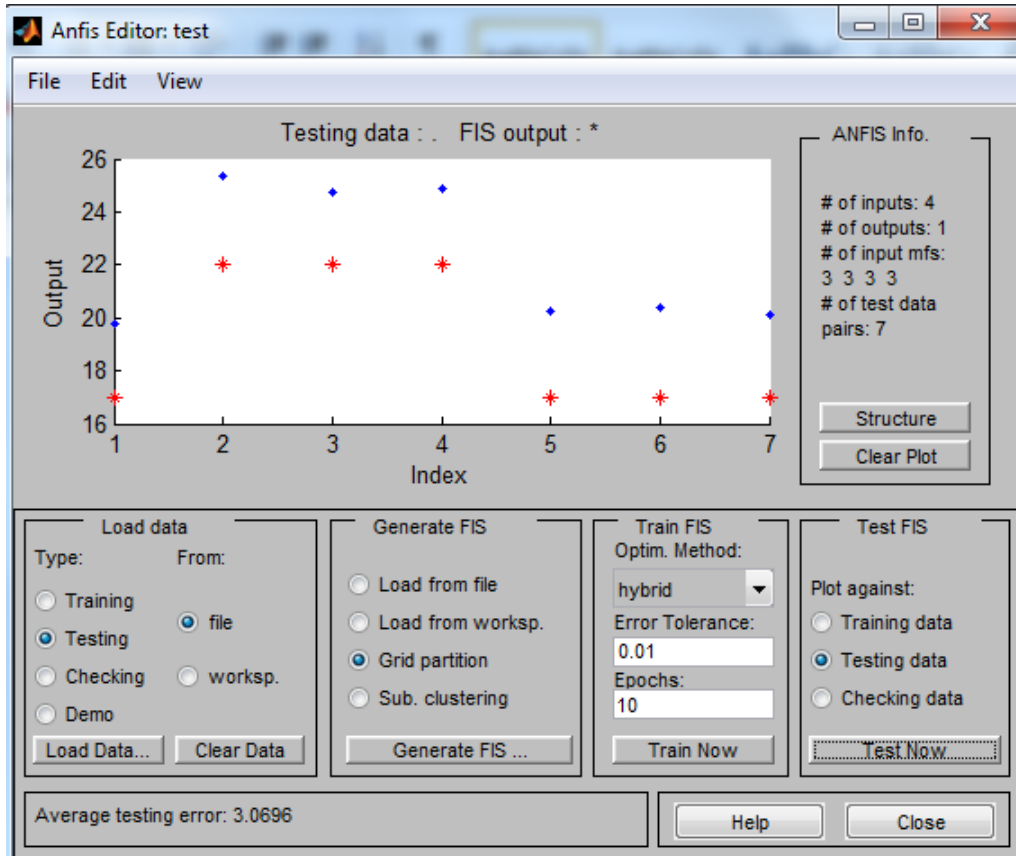


Figure 5.67 Distribution of predicted and actual data (Testing)

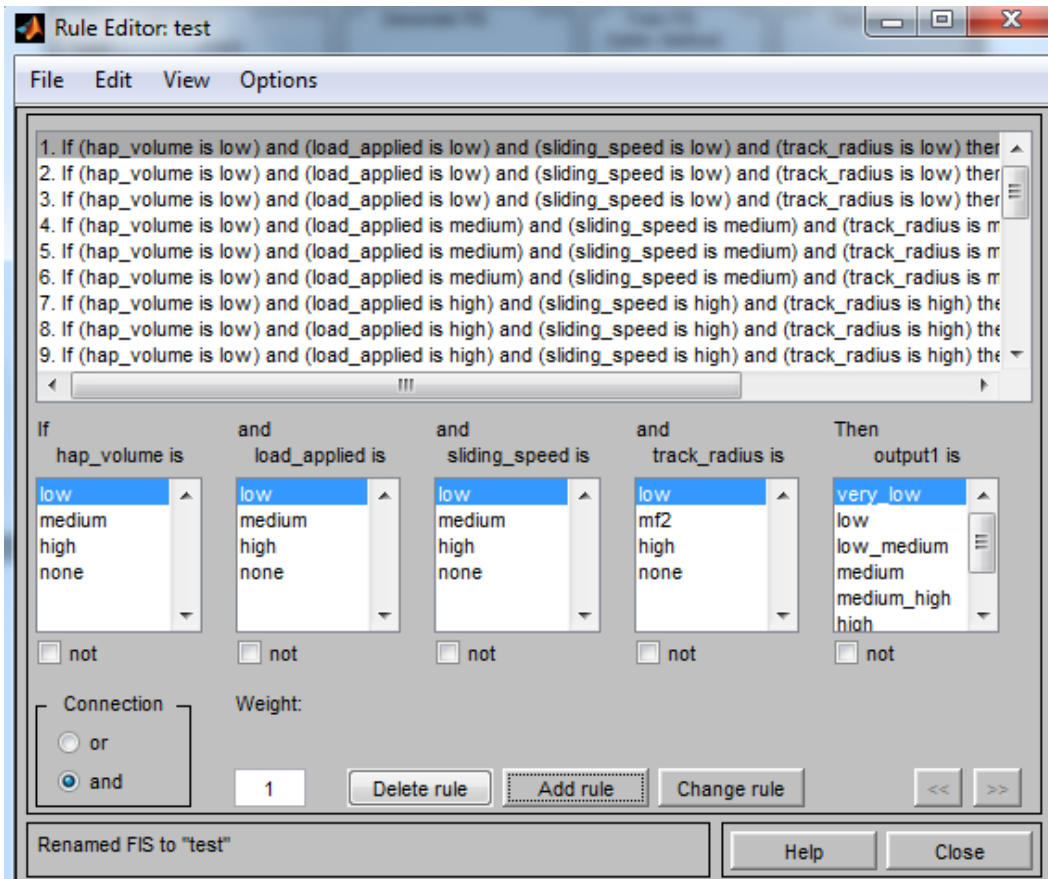


Figure 5.68 Rule editor

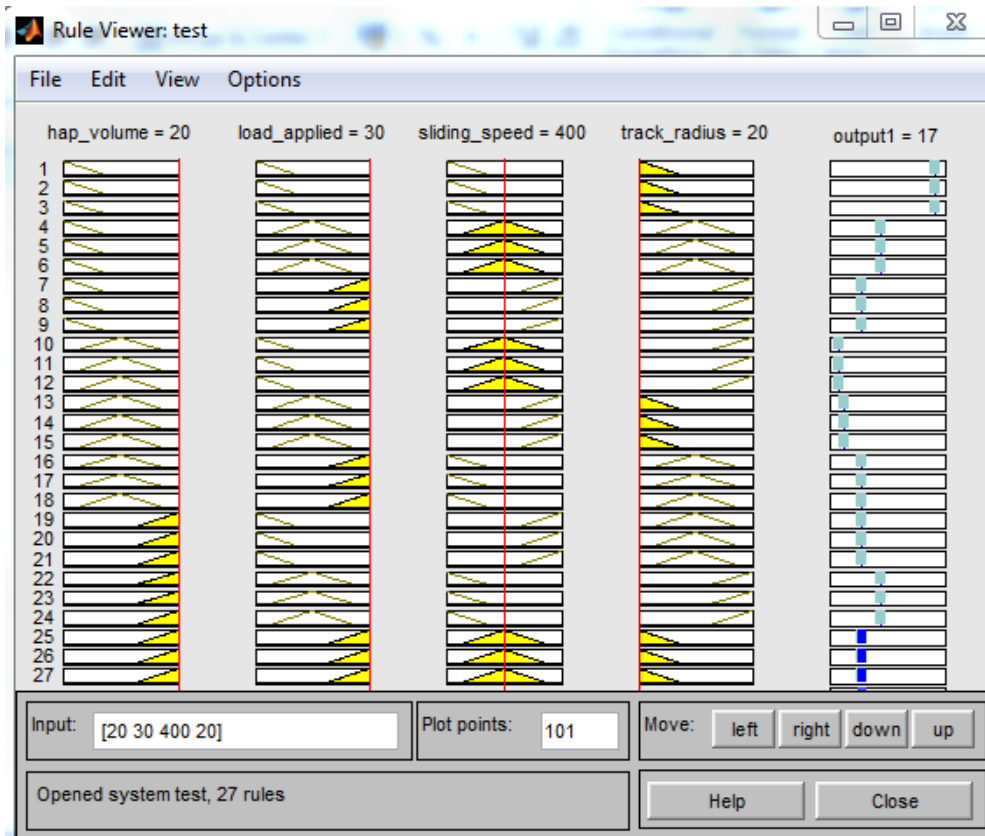


Figure 5.69 Rule viewer

The input and output experimental value with ANFIS predicted value of HAp/PC composite at 600 grit size for training purpose is shown in Table 5.24.

Table 5.24 Input and output data with ANFIS predicted value of HAp/PC composite at 600 grit size

No.	Factor A (HAp Volume) %	Factor B (Load Applied) N	Factor C (Sliding Speed) RPM	Factor D (Track Radius) mm	Wear Loss (gm)	S/N ratio of Experimental value	ANFIS output predicted value
1	0	10	300	20	0.013	37.721	37
2	0	10	300	20	0.011	39.172	37
3	0	10	300	20	0.012	38.416	37
4	0	20	400	30	0.055	25.192	22
5	0	20	400	30	0.055	25.192	22
6	0	20	400	30	0.057	24.882	22
7	0	30	500	40	0.080	21.938	17
8	0	30	500	40	0.081	21.830	17
9	0	30	500	40	0.082	21.723	17
10	10	10	400	40	0.294	10.633	10.5
11	10	10	400	40	0.293	10.662	10.5
12	10	10	400	40	0.292	10.692	10.5
13	10	20	500	20	0.248	12.110	12
14	10	20	500	20	0.250	12.041	12
15	10	20	500	20	0.249	12.076	12
16	10	30	300	30	0.116	18.710	17
17	10	30	300	30	0.114	18.861	17
18	10	30	300	30	0.115	18.786	17
19	20	10	500	30	0.101	19.913	17
20	20	10	500	30	0.102	19.827	17

The input and output data with ANFIS predicted value of HAp/PC composite at 400 grit size for testing purpose is shown in Table 5.25.

Table 5.25 Input and output data with ANFIS predicted value of HAp/PC composite at 600 grit size

No.	Factor A (HAp Volume) %	Factor B (Load Applied) N	Factor C (Sliding Speed) RPM	Factor D (Track Radius) mm	Wear Loss (gm)	S/N ratio of Experimental value	ANFIS output predicted value
1	20	10	500	30	0.103	19.743	17
2	20	20	300	40	0.054	25.352	22
3	20	20	300	40	0.058	24.731	22
4	20	20	300	40	0.057	24.882	22
5	20	30	400	20	0.097	20.264	17
6	20	30	400	20	0.096	20.354	17
7	20	30	400	20	0.099	20.087	17

By calculating we get the mean relative percentage error for training and testing of HAp/PC composite conducted at 600 grit size paper is 8.80% and 13.90% respectively.

#### 5.2.1.1.4 Adaptive neuro fuzzy inference system (ANFIS) methodology used for HAp/PSU composite (at 600 grit size paper)

The membership function editor for output parameter of HAp/PSU composite at 600 grit size is shown in Figure 5.70.

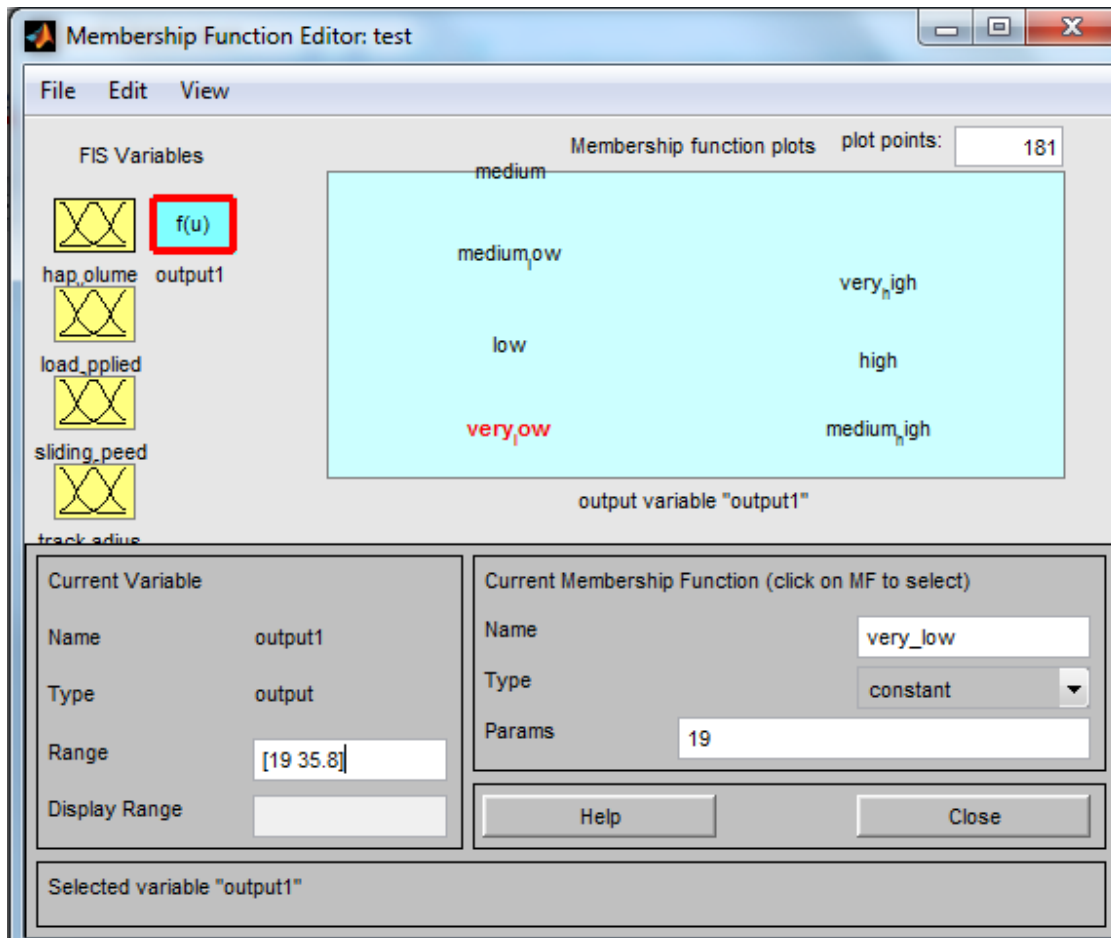


Figure 5.70 Membership function editor for output of HAp/PSU composite



The ANFIS editor for both training and testing data, rule editor and rule viewer of HAp/PSU composite are shown in Figure 5.71 to Figure 5.74 respectively.

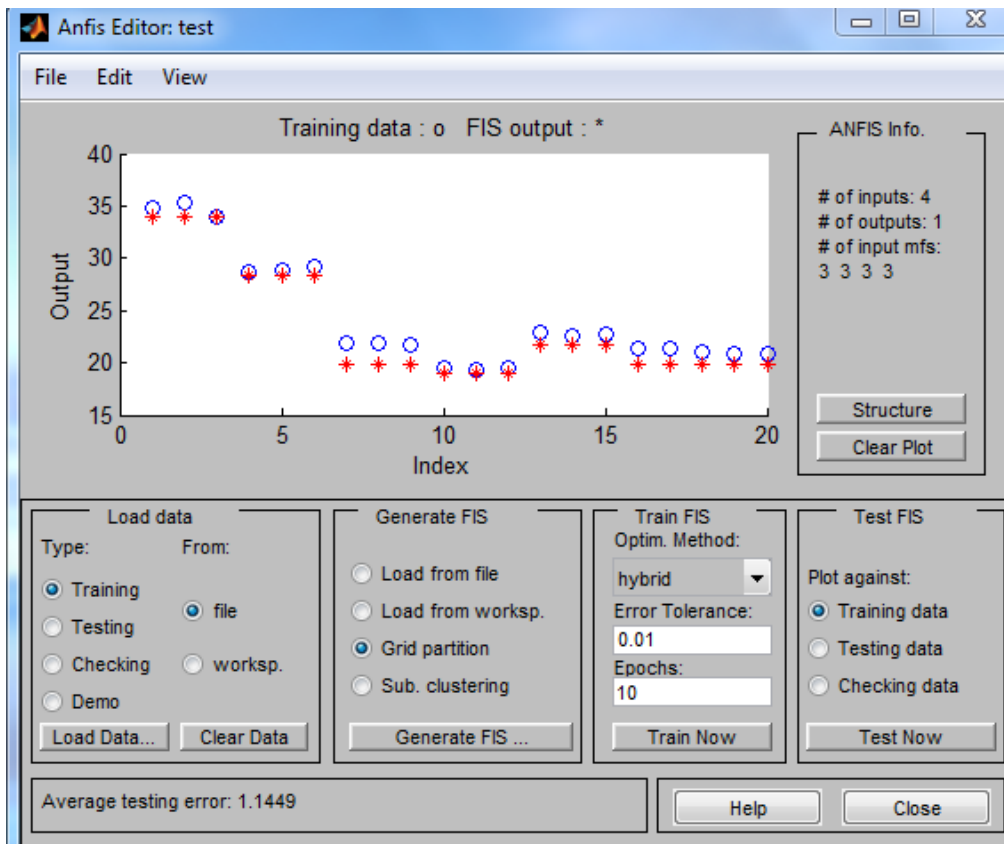


Figure 5.71 Distribution of predicted and actual data (Training)

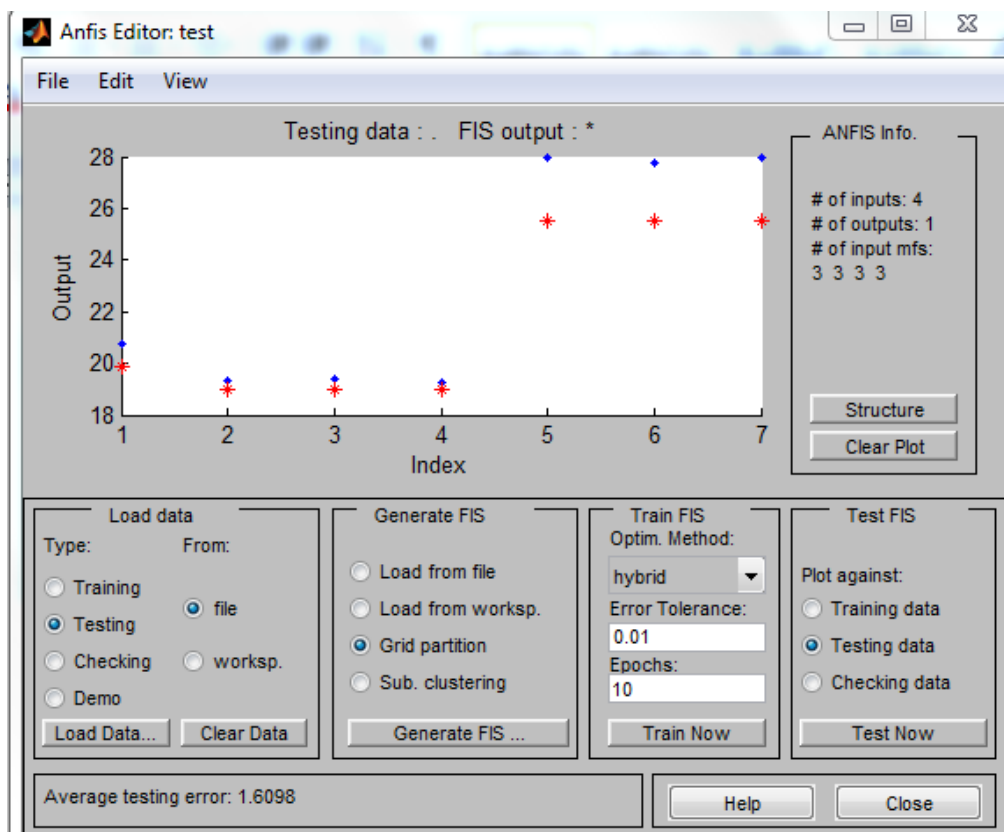


Figure 5.72 Distribution of predicted and actual data (Testing)

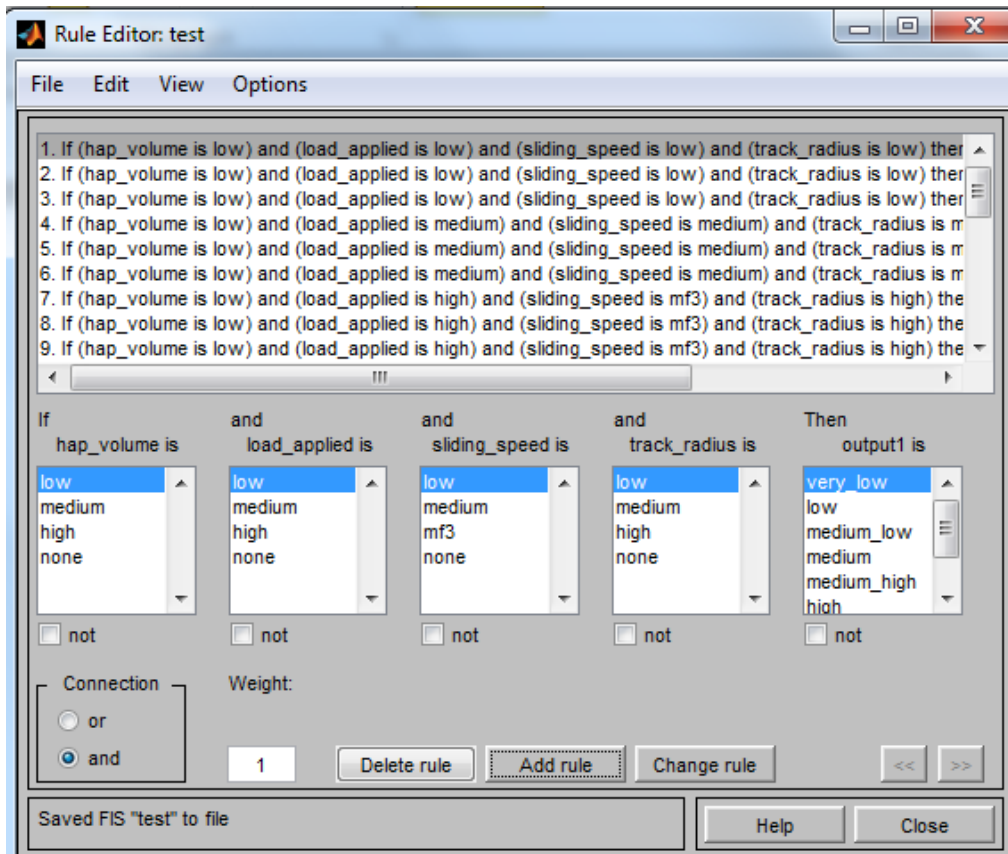


Figure 5.73 Rule editor

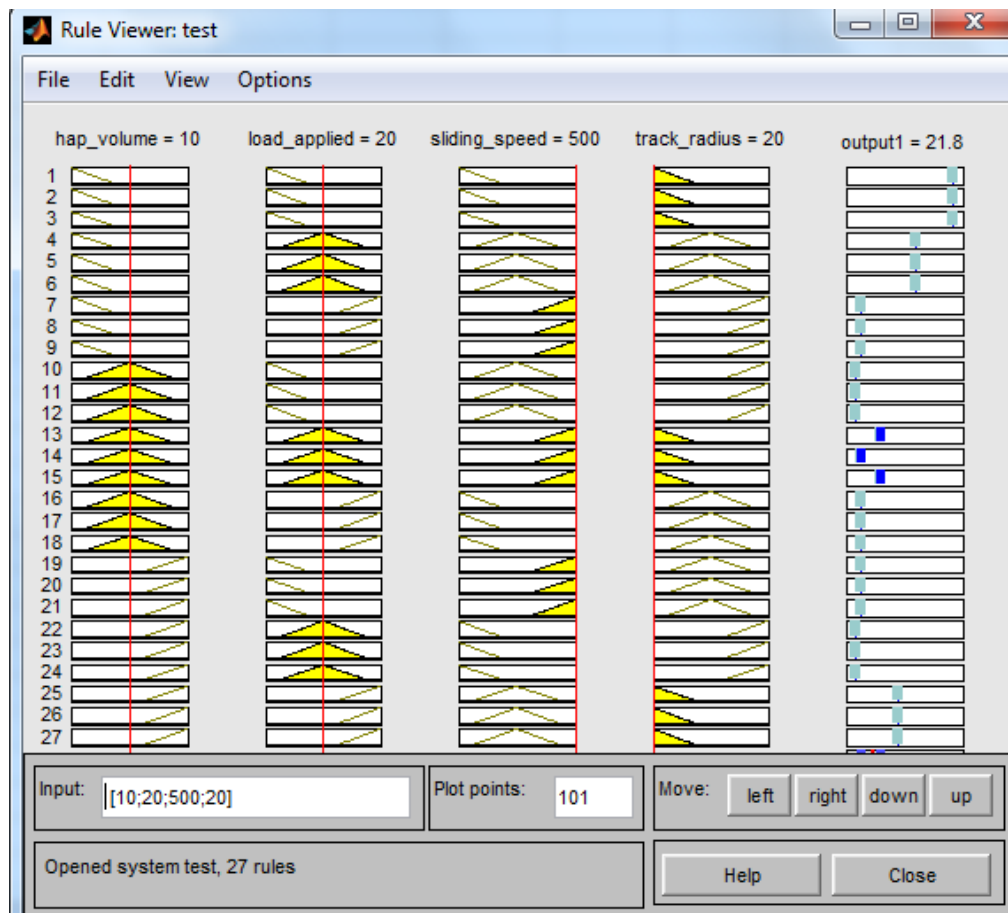


Figure 5.74 Rule viewer

The input and output experimental value with ANFIS predicted value of HAp/PSU composite at 600 grit size for training purpose is shown in Table 5.26.

Table 5.26 Input and output data with ANFIS predicted value of HAp/PSU composite at 600 grit size

No.	Factor A (HAp Volume) %	Factor B (Load Applied) N	Factor C (Sliding Speed) RPM	Factor D (Track Radius) mm	Wear Loss (gm)	S/N ratio of Experimental value	ANFIS output predicted value
1	0	10	300	20	0.018	34.894	33.9
2	0	10	300	20	0.017	35.391	33.9
3	0	10	300	20	0.020	33.979	33.9
4	0	20	400	30	0.037	28.635	28.3
5	0	20	400	30	0.036	28.873	28.3
6	0	20	400	30	0.035	29.118	28.3
7	0	30	500	40	0.080	21.938	19.9
8	0	30	500	40	0.081	21.830	19.9
9	0	30	500	40	0.082	21.723	19.9
10	10	10	400	40	0.106	19.493	19
11	10	10	400	40	0.107	19.412	19
12	10	10	400	40	0.106	19.493	19
13	10	20	500	20	0.072	22.853	21.7667
14	10	20	500	20	0.075	22.498	21.7667
15	10	20	500	20	0.073	22.733	21.7667
16	10	30	300	30	0.086	21.310	19.9
17	10	30	300	30	0.085	21.411	19.9
18	10	30	300	30	0.089	21.012	19.9
19	20	10	500	30	0.090	20.915	19.9
20	20	10	500	30	0.091	20.819	19.9

The input and output data with ANFIS predicted value of HAp/PSU composite at 600 grit size for testing purpose is shown in Table 5.27.

Table 5.27 Input and output data with ANFIS predicted value of HAp/PSU composite at 600 grit size

No.	Factor A (HAp Volume) %	Factor B (Load Applied) N	Factor C (Sliding Speed) RPM	Factor D (Track Radius) mm	Wear Loss (gm)	S/N ratio of Experimental value	ANFIS output predicted value
1	20	10	500	30	0.092	20.724	19.9
2	20	20	300	40	0.108	19.331	19
3	20	20	300	40	0.107	19.412	19
4	20	20	300	40	0.109	19.251	19
5	20	30	400	20	0.040	27.958	25.5
6	20	30	400	20	0.041	27.744	25.5
7	20	30	400	20	0.040	27.958	25.5

By calculating we get the mean relative percentage error for training and testing of HAp/PSU composite conducted at 600 grit size paper is 4.32% and 4.91% respectively.

**5.2.1.1.5 Adaptive neuro fuzzy inference system (ANFIS) methodology used for HAp/PC composite (at 1000 grit size paper)**

The membership function editor for output parameter of HAp/PC composite at 1000 grit size is shown in Figure 5.75.

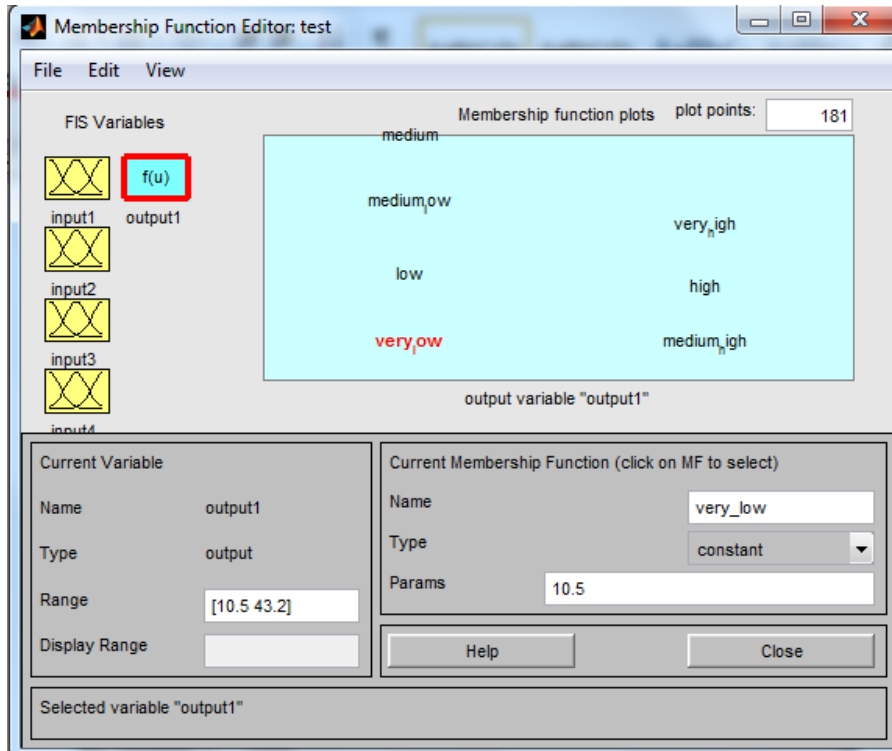


Figure 5.75 Membership function editor for output of HAp/PC composite

The ANFIS editor for both training and testing data, rule editor and rule viewer of HAp/PC composite are shown in Figure 5.76 to Figure 5.79 respectively.

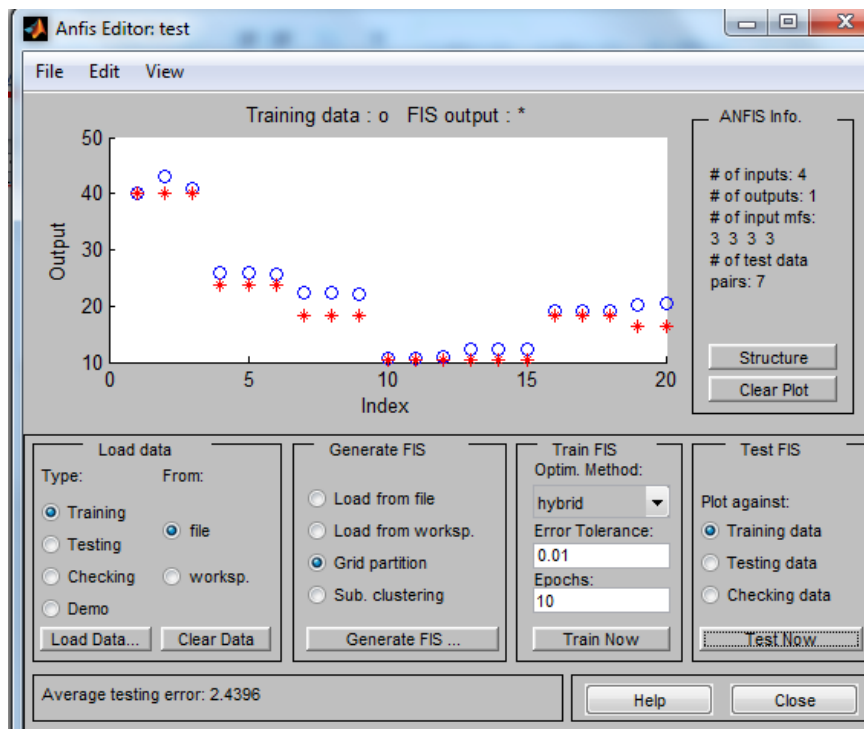


Figure 5.76 Distribution of predicted and actual data (Training)

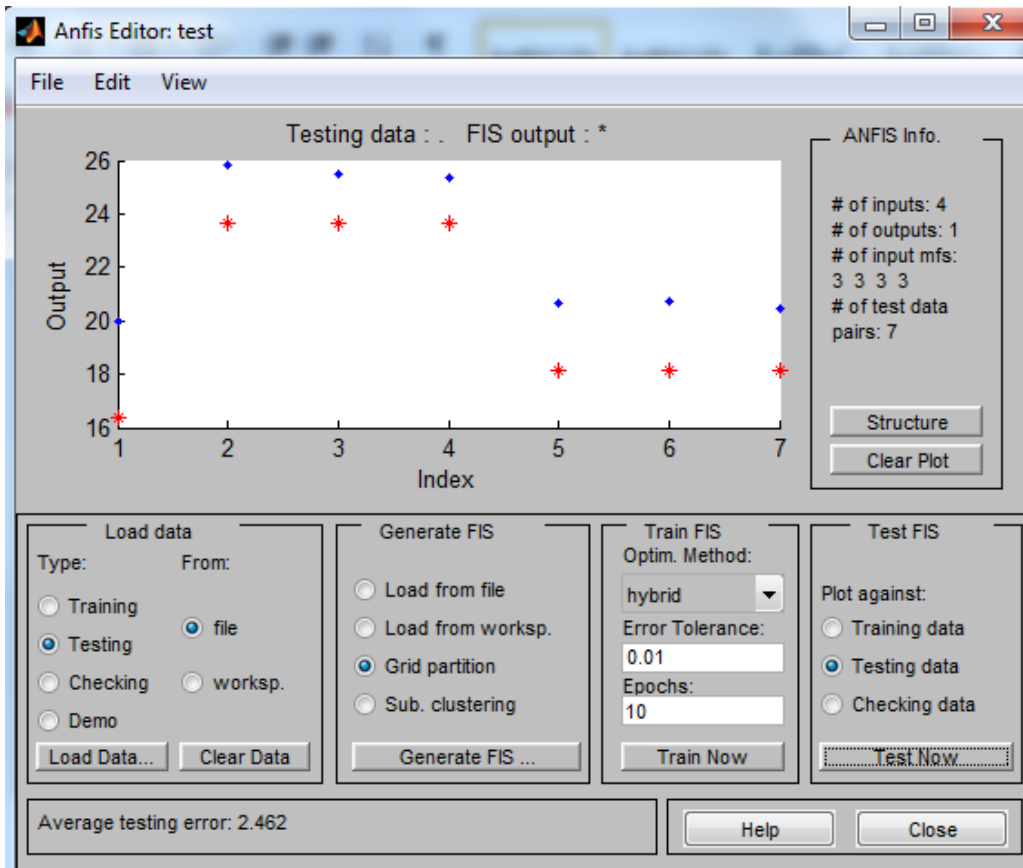


Figure 5.77 Distribution of predicted and actual data (Testing)

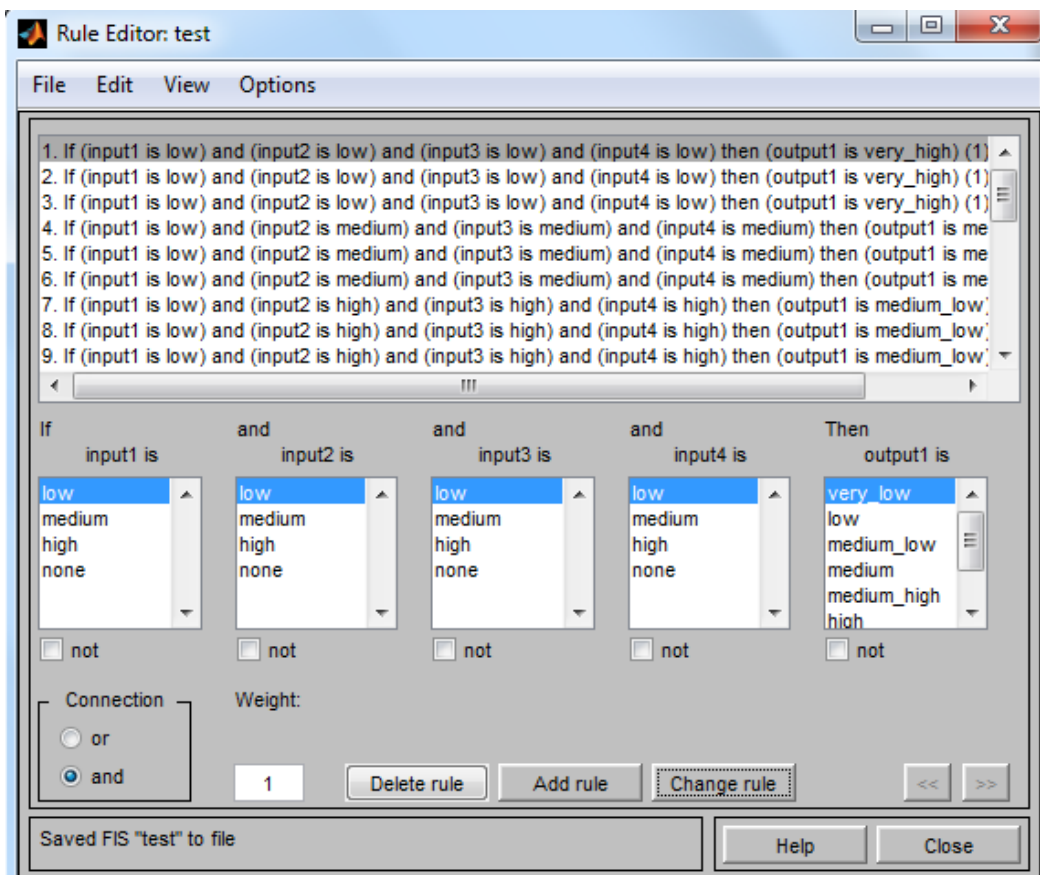


Figure 5.78 Rule editor

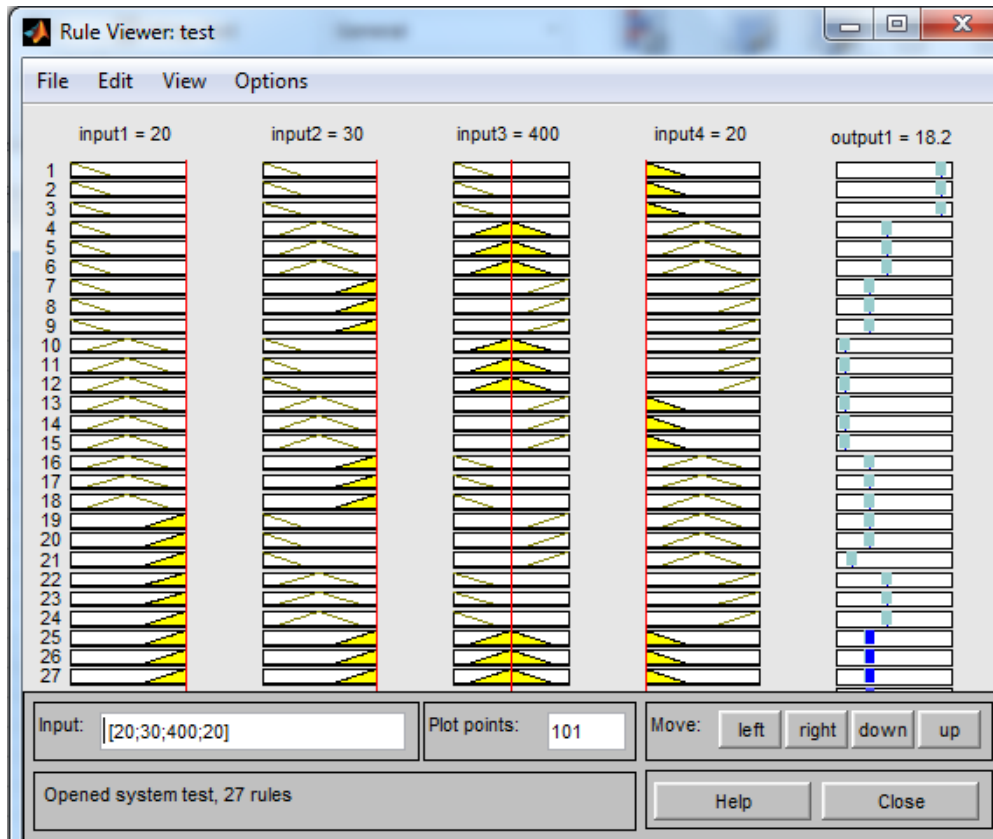


Figure 5.79 Rule viewer

The input and output experimental value with ANFIS predicted value of HAp/PC composite at 1000 grit size for training purpose is shown in Table 5.28.

Table 5.28 Input and output data with ANFIS predicted value of HAp/PC composite at 1000 grit size

No.	Factor A (HAp Volume) %	Factor B (Load Applied) N	Factor C (Sliding Speed) RPM	Factor D (Track Radius) mm	Wear Loss (gm)	S/N ratio of Experimental value	ANFIS output predicted value
1	0	10	300	20	0.010	40	39.975
2	0	10	300	20	0.007	43.098	39.975
3	0	10	300	20	0.009	40.915	39.975
4	0	20	400	30	0.050	26.020	23.625
5	0	20	400	30	0.051	25.848	23.625
6	0	20	400	30	0.052	25.679	23.625
7	0	30	500	40	0.076	22.383	18.175
8	0	30	500	40	0.077	22.270	18.175
9	0	30	500	40	0.078	22.158	18.175
10	10	10	400	40	0.290	10.752	10.5
11	10	10	400	40	0.288	10.812	10.5
12	10	10	400	40	0.286	10.872	10.5
13	10	20	500	20	0.245	12.216	10.5
14	10	20	500	20	0.246	12.181	10.5
15	10	20	500	20	0.243	12.287	10.5
16	10	30	300	30	0.111	19.093	18.175
17	10	30	300	30	0.110	19.172	18.175
18	10	30	300	30	0.111	19.093	18.175
19	20	10	500	30	0.097	20.264	16.3583
20	20	10	500	30	0.096	20.354	16.3583

The input and output data with ANFIS predicted value of HAp/PC composite at 1000 grit size for testing purpose is shown in Table 5.29.

Table 5.29 Input and output data with ANFIS predicted value of HAp/PC composite at 1000 grit size

No.	Factor A (HAp Volume) %	Factor B (Load Applied) N	Factor C (Sliding Speed) RPM	Factor D (Track Radius) mm	Wear Loss (gm)	S/N ratio of Experimental value	ANFIS output predicted value
1	20	10	500	30	0.100	20	16.3583
2	20	20	300	40	0.051	25.848	23.625
3	20	20	300	40	0.053	25.514	23.625
4	20	20	300	40	0.054	25.352	23.625
5	20	30	400	20	0.093	20.630	18.175
6	20	30	400	20	0.092	20.724	18.175
7	20	30	400	20	0.095	20.445	18.175

By calculating we get the mean relative percentage error for training and testing of HAp/PC composite conducted at 1000 grit size paper is 9.77% and 10.90% respectively.

#### 5.2.1.1.6 Adaptive neuro fuzzy inference system (ANFIS) methodology used for HAp/PSU composite (at 1000 grit size paper)

The membership function editor for output parameter of HAp/PSU composite at 1000 grit size is shown in Figure 5.80.

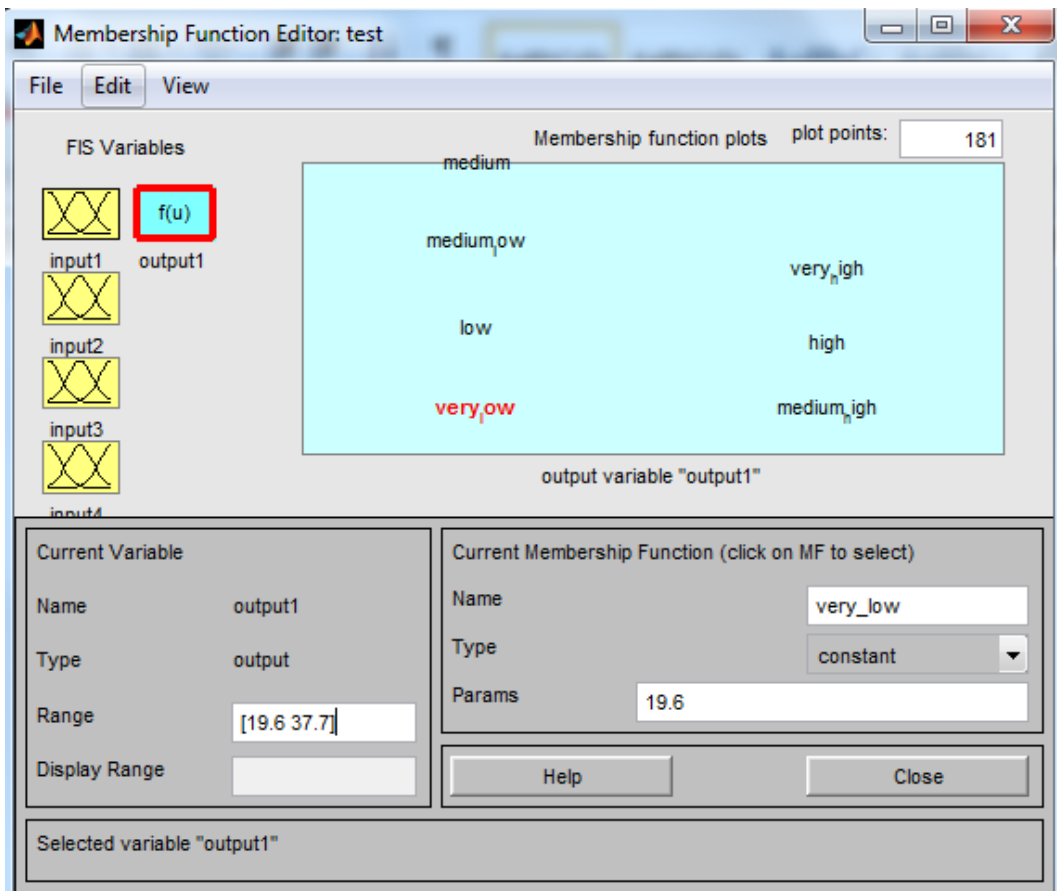


Figure 5.80 Membership function editor for output of HAp/PSU composite

The ANFIS editor for both training and testing data, rule editor and rule viewer of HAp/PSU composite are shown in Figure 5.81 to Figure 5.84 respectively.

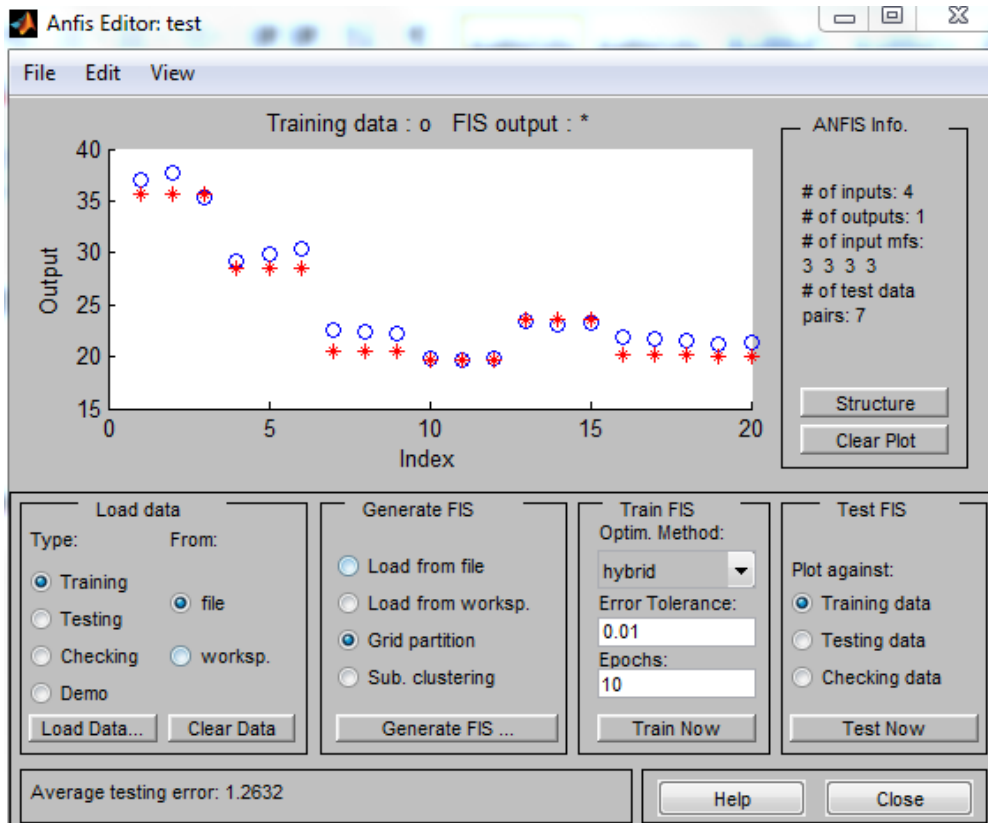


Figure 5.81 Distribution of predicted and actual data (Training)

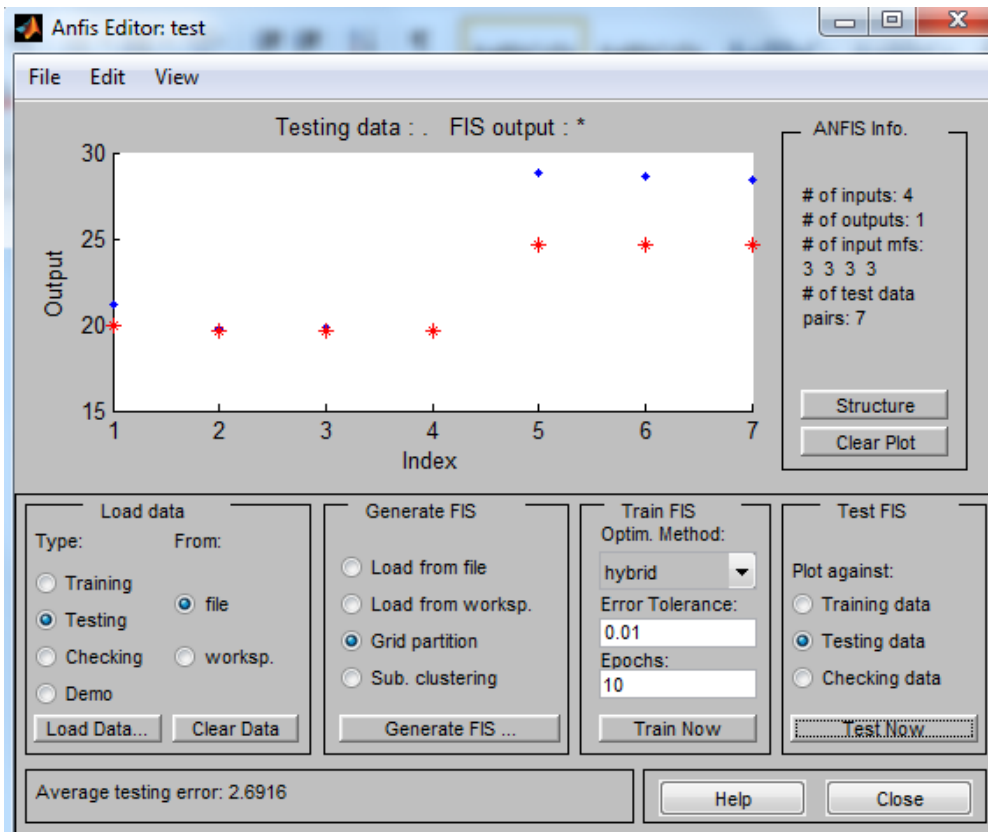


Figure 5.82 Distribution of predicted and actual data (Testing)



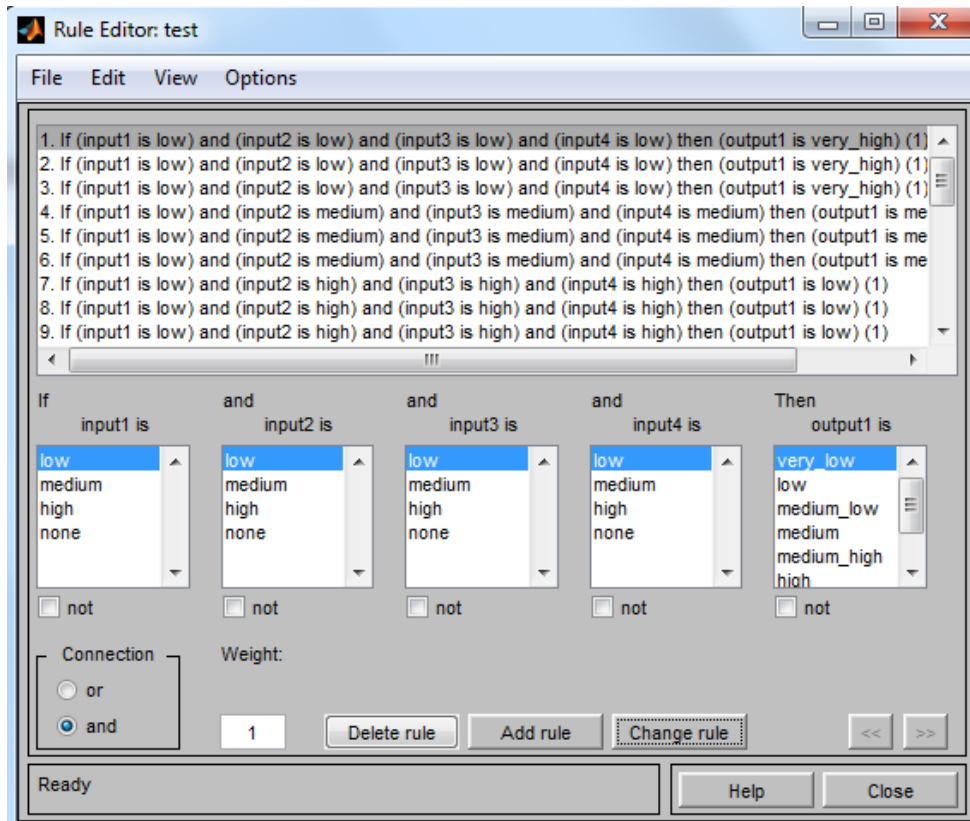


Figure 5.83 Rule editor

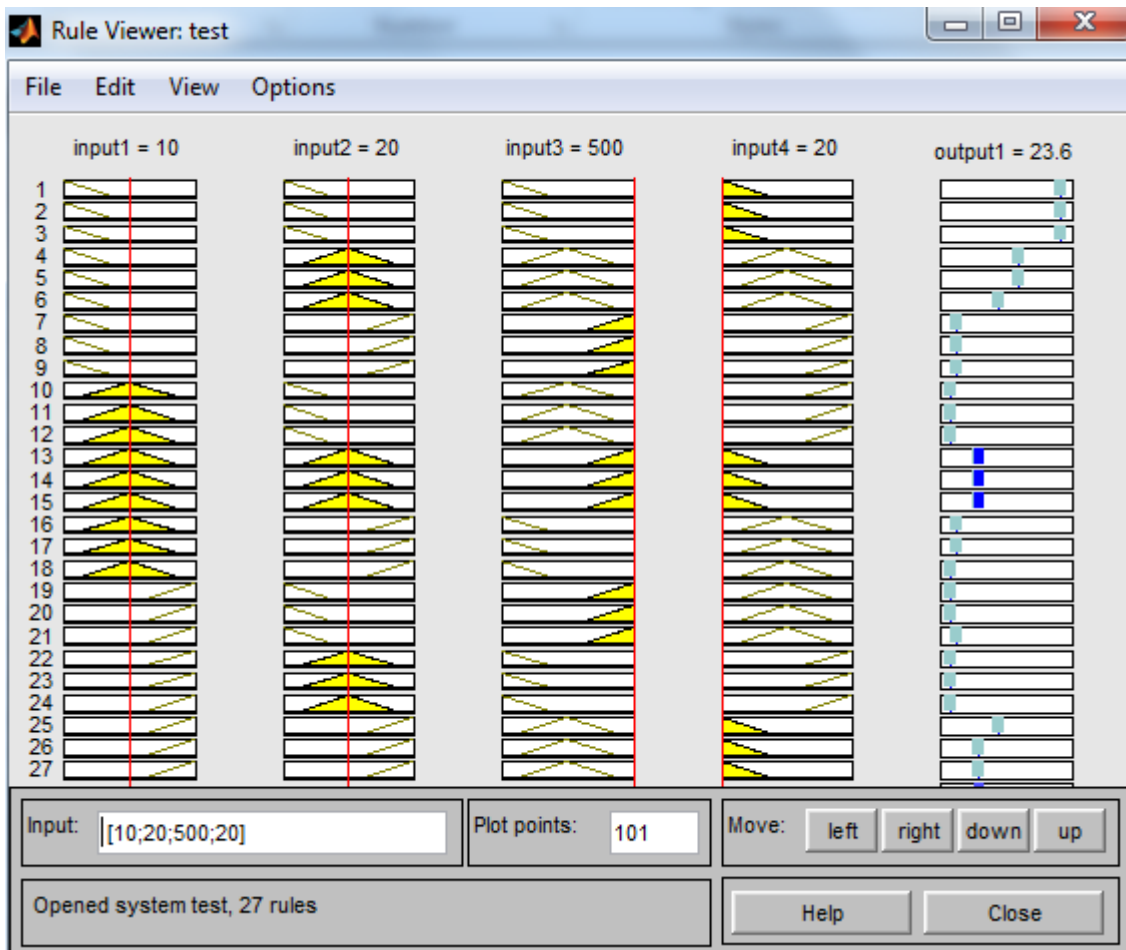


Figure 5.84 Rule viewer

The input and output experimental value with ANFIS predicted value of HAp/PSU composite at 1000 grit size for training purpose is shown in Table 5.30.

Table 5.30 Input and output data with ANFIS predicted value of HAp/PSU composite at 1000 grit size

No.	Factor A (HAp Volume) %	Factor B (Load Applied) N	Factor C (Sliding Speed) RPM	Factor D (Track Radius) mm	Wear Loss (gm)	S/N ratio of Experimental value	ANFIS output predicted value
1	0	10	300	20	0.014	37.077	35.6
2	0	10	300	20	0.013	37.721	35.6
3	0	10	300	20	0.017	35.391	35.6
4	0	20	400	30	0.035	29.118	28.6
5	0	20	400	30	0.032	29.897	28.6
6	0	20	400	30	0.030	30.457	28.6
7	0	30	500	40	0.075	22.498	20.6
8	0	30	500	40	0.076	22.383	20.6
9	0	30	500	40	0.077	22.270	20.6
10	10	10	400	40	0.102	19.827	19.6
11	10	10	400	40	0.103	19.743	19.6
12	10	10	400	40	0.101	19.913	19.6
13	10	20	500	20	0.067	23.478	23.6
14	10	20	500	20	0.070	23.098	23.6
15	10	20	500	20	0.069	23.223	23.6
16	10	30	300	30	0.081	21.830	20.2667
17	10	30	300	30	0.082	21.723	20.2667
18	10	30	300	30	0.084	21.514	20.2667
19	20	10	500	30	0.087	21.209	19.9333
20	20	10	500	30	0.086	21.310	19.9333

The input and output data with ANFIS predicted value of HAp/PSU composite at 1000 grit size for testing purpose is shown in Table 5.31.

Table 5.31 Input and output data with ANFIS predicted value of HAp/PSU composite at 1000 grit size

No.	Factor A (HAp Volume) %	Factor B (Load Applied) N	Factor C (Sliding Speed) RPM	Factor D (Track Radius) mm	Wear Loss (gm)	S/N ratio of Experimental value	ANFIS output predicted value
1	20	10	500	30	0.087	21.209	19.9333
2	20	20	300	40	0.103	19.743	19.6
3	20	20	300	40	0.102	19.827	19.6
4	20	20	300	40	0.104	19.659	19.6
5	20	30	400	20	0.036	28.873	24.6
6	20	30	400	20	0.037	28.635	24.6
7	20	30	400	20	0.038	28.404	24.6

By calculating we get the mean relative percentage error for training and testing of HAp/PSU composite conducted at 1000 grit size paper is 4.31% and 7.21% respectively.

### 5.2.1.2 Worn surface morphology

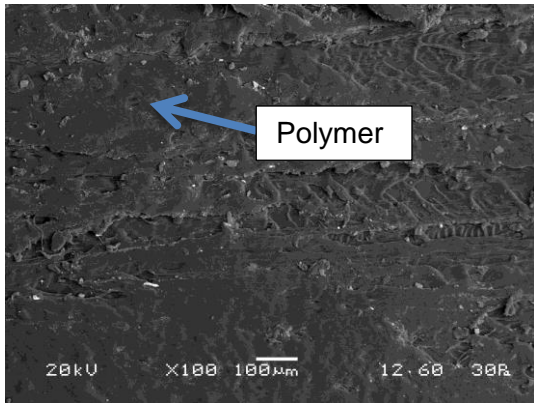


Figure 5.85 Wear of 0 vol. % HAp/PC (x100)

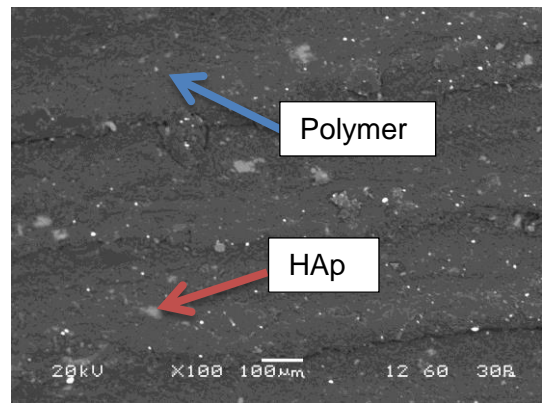


Figure 5.86 Wear of 10 vol. % HAp/PC (x100)

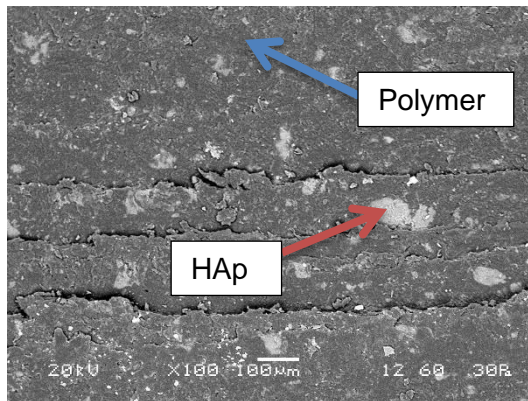


Figure 5.87 Wear of 20 vol. % HAp/PC (x100)

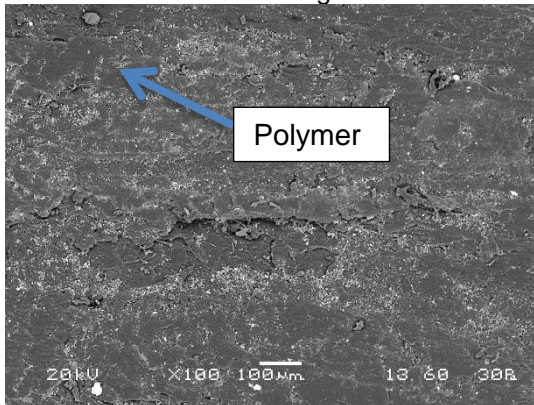


Figure 5.88 Wear of 0 vol. % HAp/PSU (x100)

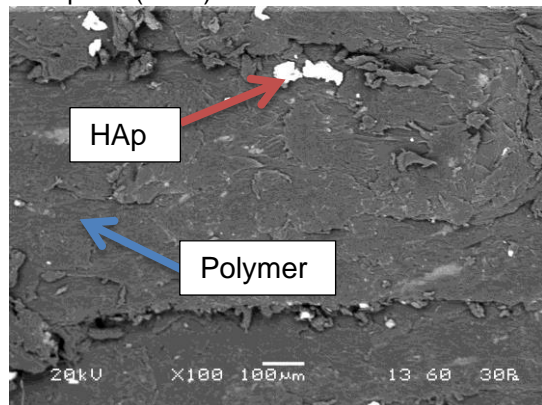


Figure 5.89 Wear of 10 vol. % HAp/PSU (x100)

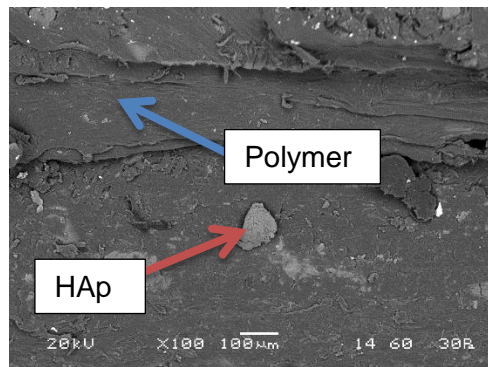


Figure 5.90 Wear of 20 vol. % HAp/PSU (x100)

SEM images of worn surfaces of both HAp/PC and HAp/PSU composite samples is shown from Figure 5.85 to Figure 5.90. According to Figure 5.85 to Figure 5.90, it is clearly seen that when HAp volume increases from 0 vol. % to 20 vol. %, scratches or wear increases in composite samples because of ceramic (HAp) particles (white colour, shown in Figure) slowly increasing in the polymer matrix (black colour, shown in Figure). Due to the hardness of HAp, this scratch occurs in the polymer matrix. According to Figure 5.93 and Figure 5.96, when HAp volume having 0 vol. %, there is no scratch in the polymer matrix because of absence of HAp particles. According to Figure 5.94 and Figure 5.97, when HAp volume having 10 vol. %, small scratches are seen clearly due to small percentage of HAp is mixing in the polymer matrix. Similarly, According to Figure 5.95 and Figure 5.98, when HAp volume having 20 vol. %, more scratches are shown in the polymer matrix due to percentage of HAp is more in the polymer matrix.

## 5.2.2 Experimental details of erosion wear behaviour of ceramic composites

(According to Basu and Kalin [167]) The erosion wear test of ceramic composites was performed on Air jet erosion test rig (ASTM G76) is shown in Figure 5.91. It consists of an air compressor (Figure 5.92), an air particle mixing chamber and accelerating chamber (Figure 5.93). Dry compressed air is mixed with the erodent particles which are fed at constant rate of  $10 \pm 1.0$  g/min from a sand flow control knob through the nozzle tube and then accelerated by passing the mixture through a convergent brass nozzle of 3mm internal diameter. These particles impact the specimen which can be held at different angles with respect to the direction of erodent flow using a swivel and adjustable clip. Square samples of 20mmx20mm are used for erosion wear test. In this study, dry silica sand (spherical) of different particle size of 300 $\mu$ m, 400 $\mu$ m and 500 $\mu$ m are used as erodent. The highest erosive wear loss was noticed at the specimens worn on 500 $\mu$ m erodent particle size as compared to both 300 $\mu$ m and 400 $\mu$ m erodent particle size. This is due to the larger size of the abrasive grains in 500 $\mu$ m causing greater damage to the specimen surface. The experimental data of erosion wear test showed that the wear behavior of the composite strongly depends on the erodent size of the silica sand.



Figure 5.91 Air jet erosion test rig



Figure 5.92 Air compressor



Figure 5.93 Accelerating chamber

The selected input parameters and their levels for all erodent size silica sand are shown in Table 5.32.

Table 5.32 Control parameters and their levels

S.No.	Factors	Symbol	Levels			Unit
			1	2	3	
1.	Pressure	A	1	2	3	Bar
2.	HAp volume	B	0	10	20	Vol.%
3.	Impingement angle	C	30	45	60	Degree

The experimental data for HAp/PC composite conducted at 300µm erodent particle size are shown in Table 5.33.

Table 5.33 Experimental data for HAp/PC composite conducted at 300µm erodent particle size

Experiment No.	Factor A Pressure (Bar)	Factor B HAp volume (%)	Factor C Impingement angle (Degree)	Erosion Wear Loss (gm)	S/N ratio (Lower The Better)
1	1	0	30	0.005	46.020
2	1	0	30	0.003	50.457
3	1	0	30	0.002	53.979
4	1	10	45	0.008	41.938
5	1	10	45	0.007	43.098
6	1	10	45	0.005	46.020
7	1	20	60	0.012	38.416
8	1	20	60	0.009	40.915
9	1	20	60	0.011	39.172
10	2	0	45	0.052	25.679
11	2	0	45	0.050	26.020
12	2	0	45	0.048	26.375
13	2	10	60	0.055	25.192
14	2	10	60	0.053	25.514
15	2	10	60	0.051	25.848
16	2	20	30	0.060	24.436
17	2	20	30	0.058	24.731
18	2	20	30	0.057	24.882
19	3	0	60	0.020	33.979
20	3	0	60	0.017	35.391
21	3	0	60	0.015	36.478
22	3	10	30	0.035	29.118
23	3	10	30	0.031	30.172
24	3	10	30	0.033	29.629
25	3	20	45	0.048	26.375
26	3	20	45	0.050	26.020
27	3	20	45	0.047	26.558

The ANOVA Table for HAp/PC composite are shown in Table 5.34.

Table 5.34 ANOVA Table for S/N ratio of HAp/PC composite

Source	DF value	Seq SS	Adj SS	Adj MS	F value	P value	Percentage Contribution
A	2	1753.19	1753.19	876.59	197.45	0.000	83.472
B	2	222.66	222.66	111.33	25.08	0.000	10.60
C	2	35.68	35.68	17.84	4.02	0.034	1.698
Error	20	88.79	88.79	4.44			
Total	26	2100.31					

S = 2.10702, R-Sq = 95.77%, and R-Sq(adj) = 94.50%

From percentage contribution, it can be concluded here that significance of factors is in the order of Factor A, B and C.

Main effects plot for means of S/N ratio, normal probability plot and interaction plot are shown in Figure 5.94, 5.95 and 5.96 respectively.



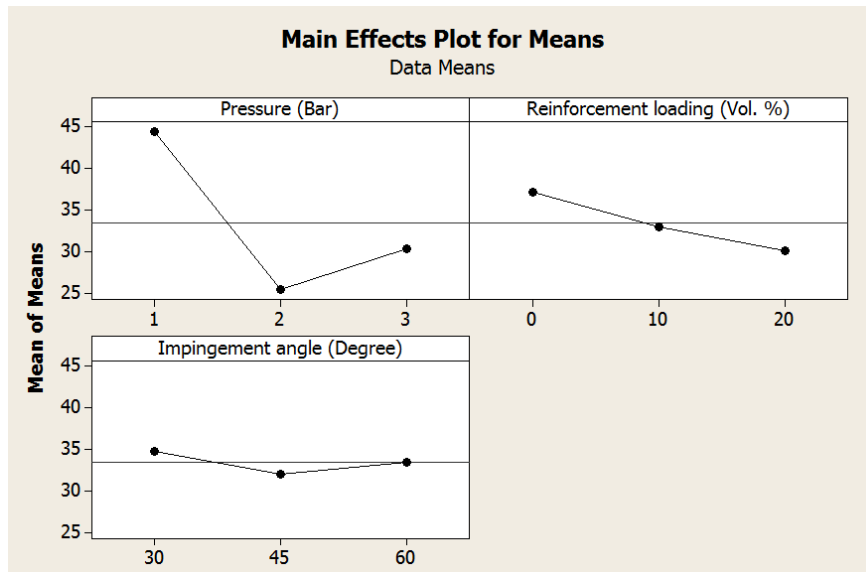


Figure 5.94 Main effects plot for means of S/N ratio

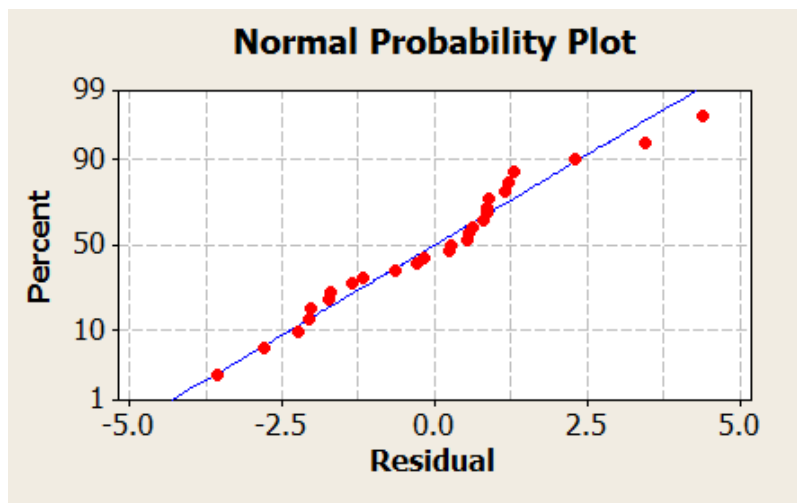


Figure 5.95 Normal probability plot for S/N ratio

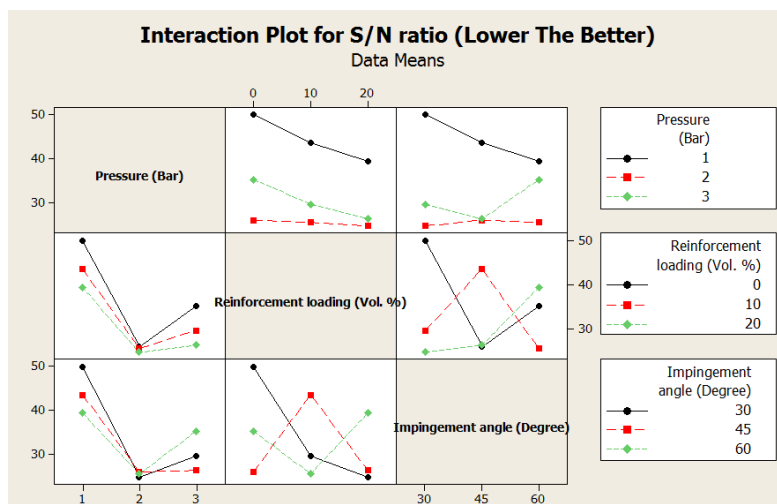


Figure 5.96 Interaction plot for S/N ratio

According to Figure 5.94, it is concluded that the optimal parametric combination is  $A_1B_1C_1$ . When pressure is 1 Bar, HAp volume is 0 vol.%, and impingement angle is 30

degree then minimum erosion wear can be obtained. Referring to Figure 5.95, it can be concluded that the ANOVA proceeds in a satisfactory manner as the residuals follow a normal distribution. Figure 5.96 shows that two factor interaction of controllable factors seems to exist. However, the interaction of factors has not been considered for the sake of simplicity.

Similarly, the experimental data for HAp/PSU composite conducted at 300µm erodent particle size are shown in Table 5.35.

Table 5.35 Experimental data for HAp/PSU composite conducted at 300µm erodent particle size

Experiment No.	Factor A Pressure (Bar)	Factor B HAp volume (%)	Factor C Impingement angle (Degree)	Erosion Wear Loss (gm)	S/N ratio (Lower The Better)
1	1	0	30	0.002	53.979
2	1	0	30	0.004	47.958
3	1	0	30	0.001	60.000
4	1	10	45	0.013	37.721
5	1	10	45	0.016	35.917
6	1	10	45	0.014	37.077
7	1	20	60	0.010	40.000
8	1	20	60	0.007	43.098
9	1	20	60	0.009	40.915
10	2	0	45	0.022	33.151
11	2	0	45	0.019	34.424
12	2	0	45	0.023	32.765
13	2	10	60	0.032	29.897
14	2	10	60	0.034	29.370
15	2	10	60	0.031	30.172
16	2	20	30	0.037	28.635
17	2	20	30	0.035	29.118
18	2	20	30	0.032	29.897
19	3	0	60	0.025	32.041
20	3	0	60	0.022	33.151
21	3	0	60	0.024	32.395
22	3	10	30	0.030	30.457
23	3	10	30	0.027	31.372
24	3	10	30	0.029	30.752
25	3	20	45	0.041	27.744
26	3	20	45	0.039	28.178
27	3	20	45	0.040	27.958

The ANOVA Table for HAp/PSU composite are shown in Table 5.36.

Table 5.36 ANOVA Table for S/N ratio of HAp/PSU composite

Source	DF value	Seq SS	Adj SS	Adj MS	F value	P value	Percentage Contribution
A	2	1083.84	1083.84	541.92	64.12	0.000	63.701
B	2	320.42	320.42	160.21	18.96	0.000	18.832
C	2	128.12	128.12	64.06	7.58	0.004	7.530
Error	20	169.02	169.02	8.45			
Total	26	1701.40					

$S = 2.90706$ ,  $R\text{-Sq} = 90.07\%$ , and  $R\text{-Sq}(\text{adj}) = 87.09\%$

From percentage contribution, it can be concluded here that significance of factors is in the order of Factor A, B and C.

Main effects plot for means of S/N ratio, normal probability plot and interaction plot are shown in Figure 5.97, 5.98 and 5.99 respectively.



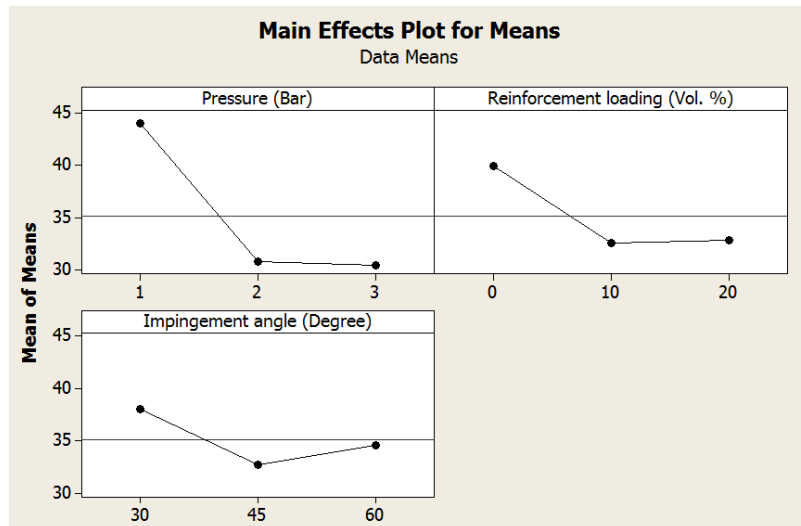


Figure 5.97 Main effects plot for means of S/N ratio

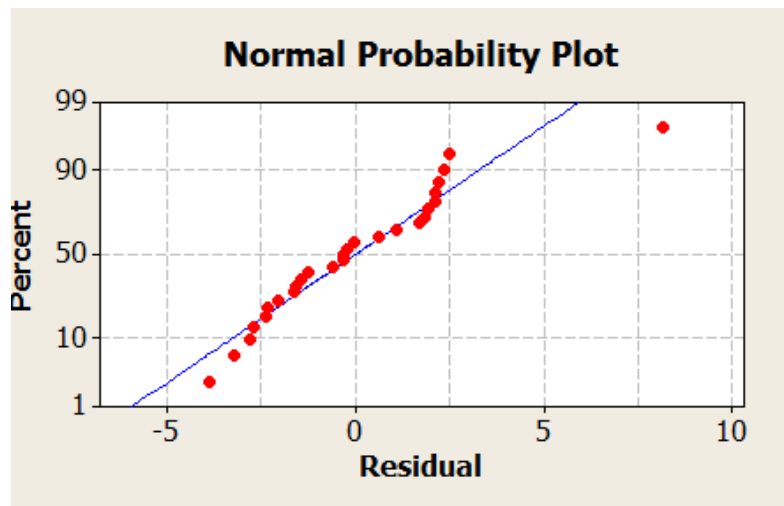


Figure 5.98 Normal probability plot for S/N ratio

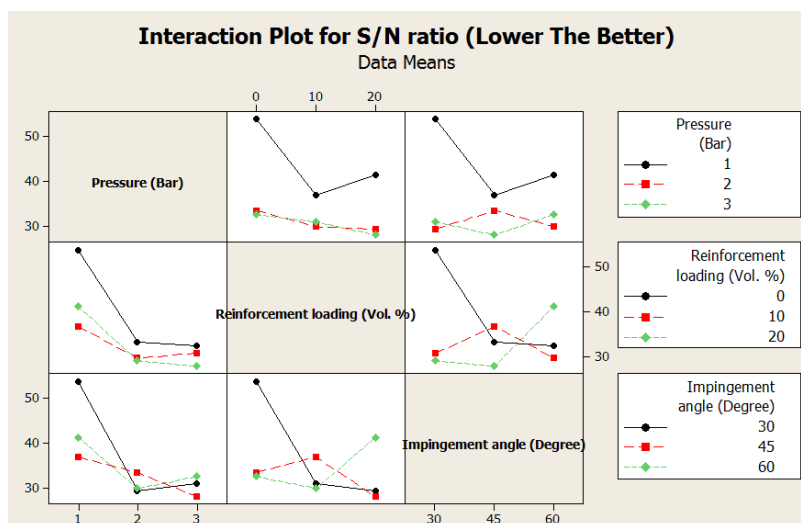


Figure 5.99 Interaction plot for S/N ratio

According to Figure 5.97, it is concluded that the optimal parametric combination is  $A_1B_1C_1$ . When pressure is 1 Bar, HAp volume is 0 vol. %, and impingement angle is 30

degree then minimum erosion wear can be obtained. Referring to Figure 5.98, it can be concluded that the ANOVA proceeds in a satisfactory manner as the residuals follow a normal distribution. Figure 5.99 shows that two factor interaction of controllable factors seems to exist. However, the interaction of factors has not been considered for the sake of simplicity.

The experimental data for HAp/PC composite conducted at 400µm erodent particle size are shown in Table 5.37.

Table 5.37 Experimental data for HAp/PC composite conducted at 400µm erodent particle size

Exp. No.	Factor A Pressure (Bar)	Factor B HAp volume (%)	Factor C Impingement angle (Degree)	Erosion Wear Loss (gm)	S/N ratio (Lower The Better)
1	1	0	30	0.008	41.938
2	1	0	30	0.005	46.020
3	1	0	30	0.004	47.958
4	1	10	45	0.011	39.172
5	1	10	45	0.010	40.000
6	1	10	45	0.007	43.098
7	1	20	60	0.015	36.478
8	1	20	60	0.014	37.077
9	1	20	60	0.016	35.917
10	2	0	45	0.056	25.036
11	2	0	45	0.055	25.192
12	2	0	45	0.052	25.679
13	2	10	60	0.057	24.882
14	2	10	60	0.058	24.731
15	2	10	60	0.056	25.036
16	2	20	30	0.066	23.609
17	2	20	30	0.063	24.013
18	2	20	30	0.061	24.923
19	3	0	60	0.025	32.041
20	3	0	60	0.021	33.555
21	3	0	60	0.020	33.979
22	3	10	30	0.040	27.958
23	3	10	30	0.036	28.873
24	3	10	30	0.038	28.404
25	3	20	45	0.053	25.514
26	3	20	45	0.056	25.036
27	3	20	45	0.052	25.679

The ANOVA Table for HAp/PC composite are shown in Table 5.38.

Table 5.38 ANOVA Table for S/N ratio of HAp/PC composite

Source	DF value	Seq SS	Adj SS	Adj MS	F value	P value	Percentage Contribution
A	2	1248.28	1248.28	624.14	192.67	0.000	83.708
B	2	157.48	157.48	78.74	24.31	0.000	10.560
C	2	20.68	20.68	10.34	3.19	0.063	1.386
Error	20	64.79	64.79	3.24			
Total	26	1491.23					

S = 1.79986, R-Sq = 95.66%, and R-Sq(adj) = 94.35%

From percentage contribution, it can be concluded here that significance of factors is in the order of Factor A, B and C.

Main effects plot for means of S/N ratio, normal probability plot and interaction plot are shown in Figure 5.100, 5.101 and 5.102 respectively.

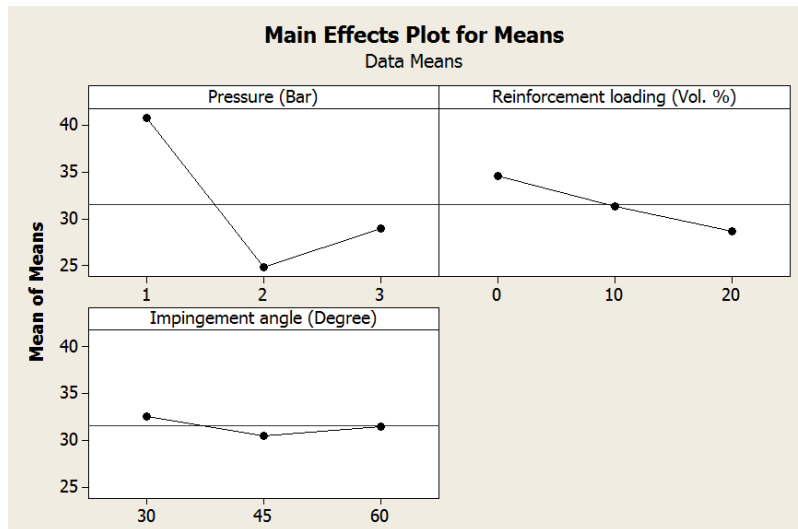


Figure 5.100 Main effects plot for means of S/N ratio

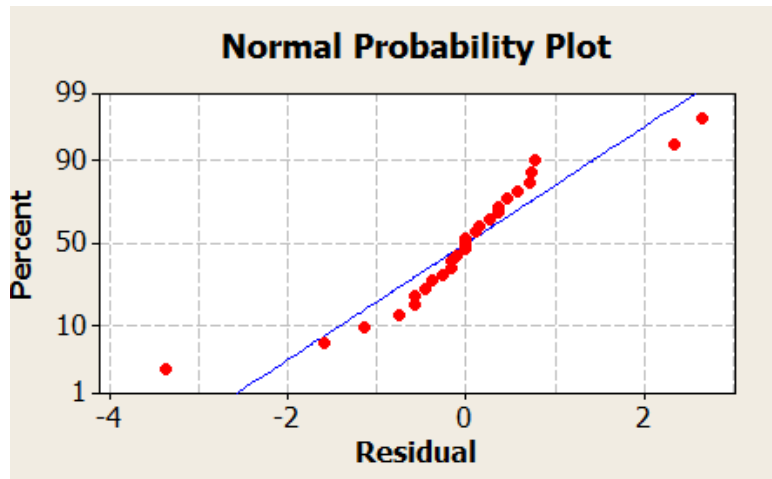


Figure 5.101 Normal probability plot for S/N ratio

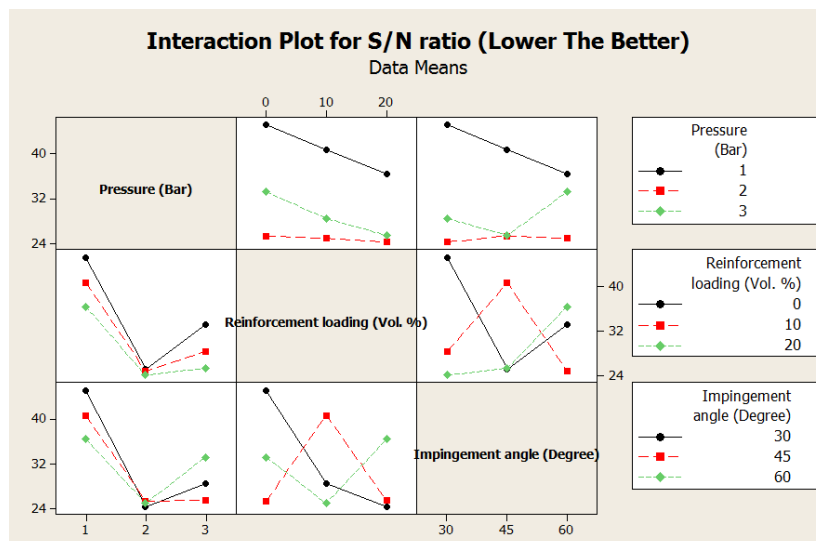


Figure 5.102 Interaction plot for S/N ratio

According to Figure 5.100, it is concluded that the optimal parametric combination is  $A_1B_1C_1$ . When pressure is 1 Bar, HAp volume is 0 vol. %, and impingement angle is 30 degree then minimum erosion wear can be obtained. Referring to Figure 5.101, it can be

concluded that the ANOVA proceeds in a satisfactory manner as the residuals follow a normal distribution. Figure 5.102 shows that two factor interaction of controllable factors seems to exist. However, the interaction of factors has not been considered for the sake of simplicity.

Similarly, the experimental data for HAp/PSU composite conducted at 400µm erodent particle size are shown in Table 5.39.

Table 5.39 Experimental data for HAp/PSU composite conducted at 400µm erodent particle size

Exp. No.	Factor A Pressure (Bar)	Factor B HAp volume (%)	Factor C Impingement angle (Degree)	Erosion Wear Loss (gm)	S/N ratio (Lower The Better)
1	1	0	30	0.006	44.436
2	1	0	30	0.008	41.938
3	1	0	30	0.006	44.436
4	1	10	45	0.018	34.894
5	1	10	45	0.022	33.151
6	1	10	45	0.019	34.424
7	1	20	60	0.015	36.478
8	1	20	60	0.012	38.416
9	1	20	60	0.013	37.721
10	2	0	45	0.027	31.372
11	2	0	45	0.025	32.041
12	2	0	45	0.028	31.056
13	2	10	60	0.036	28.873
14	2	10	60	0.040	27.958
15	2	10	60	0.039	28.178
16	2	20	30	0.044	27.130
17	2	20	30	0.040	27.958
18	2	20	30	0.037	28.635
19	3	0	60	0.031	30.172
20	3	0	60	0.030	30.457
21	3	0	60	0.031	30.172
22	3	10	30	0.036	28.873
23	3	10	30	0.033	29.629
24	3	10	30	0.036	28.873
25	3	20	45	0.047	26.558
26	3	20	45	0.048	26.375
27	3	20	45	0.049	26.196

The ANOVA Table for HAp/PSU composite are shown in Table 5.40.

Table 5.40 ANOVA Table for S/N ratio of HAp/PSU composite

Source	DF value	Seq SS	Adj SS	Adj MS	F value	P value	Percentage Contribution
A	2	545.22	545.22	272.61	162.46	0.000	73.728
B	2	124.05	124.05	62.03	36.96	0.000	16.764
C	2	37.12	37.12	18.56	11.06	0.001	5.016
Error	20	33.56	33.56	1.68			
Total	26	739.95					

$S = 1.29540$ ,  $R-Sq = 95.46\%$ , and  $R-Sq(adj) = 94.10\%$

From percentage contribution, it can be concluded here that significance of factors is in the order of Factor A, B and C.

Main effects plot for means of S/N ratio, normal probability plot and interaction plot are shown in Figure 5.103, 5.104 and 5.105 respectively.

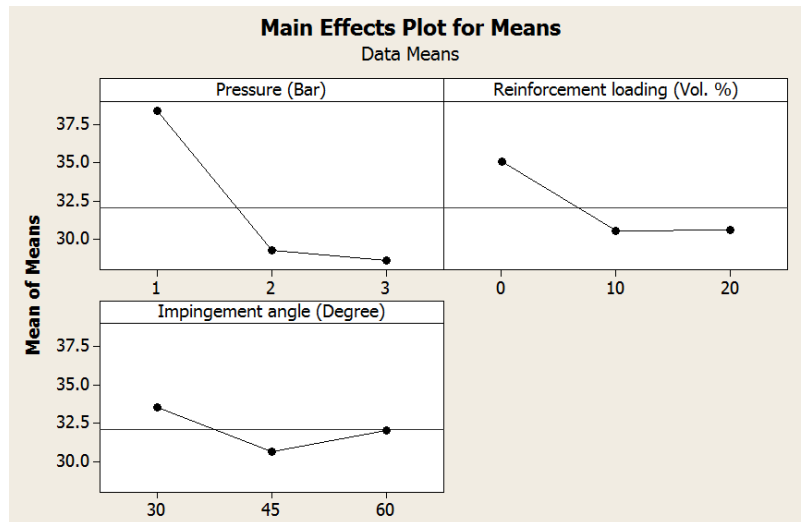


Figure 5.103 Main effects plot for means of S/N ratio

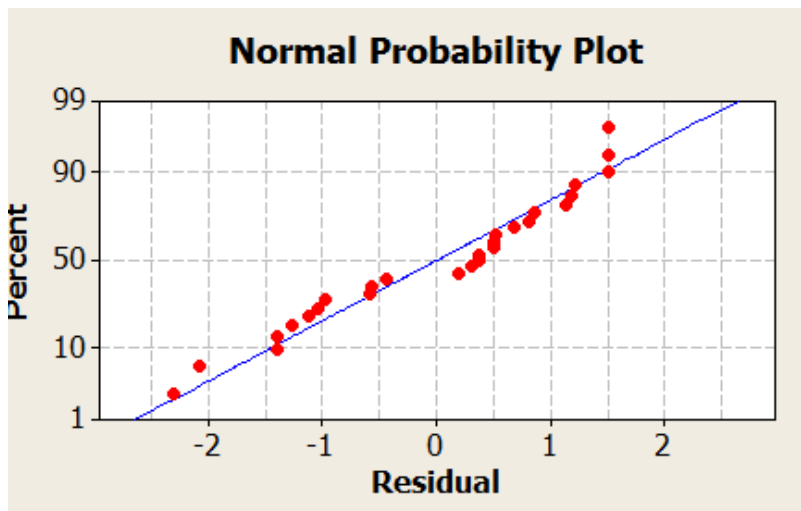


Figure 5.104 Normal probability plot for S/N ratio

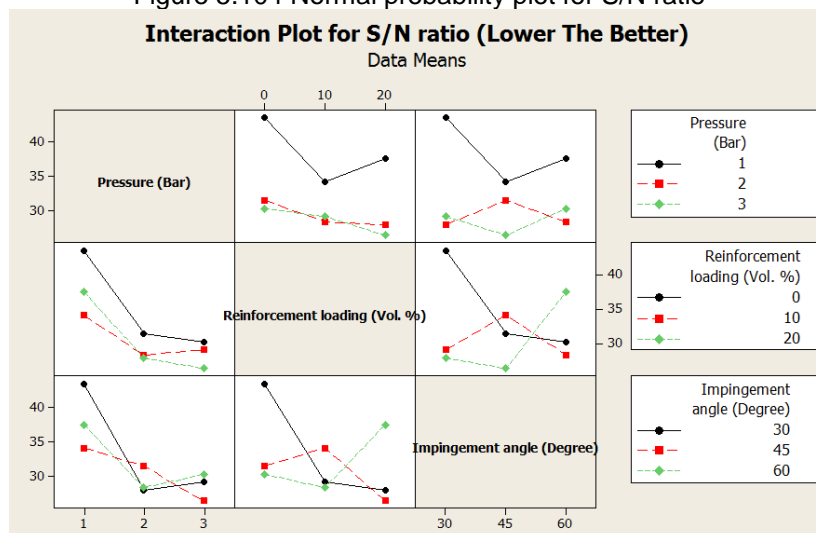


Figure 5.105 Interaction plot for S/N ratio

According to Figure 5.103, it is concluded that the optimal parametric combination is  $A_1B_1C_1$ . When pressure is 1 Bar, HAp volume is 0 vol. %, and impingement angle is 30

degree then minimum erosion wear can be obtained. Referring to Figure 5.104, it can be concluded that the ANOVA proceeds in a satisfactory manner as the residuals follow a normal distribution. Figure 5.105 shows that two factor interaction of controllable factors seems to exist. However, the interaction of factors has not been considered for the sake of simplicity.

The experimental data for HAp/PC composite conducted at 500µm erodent particle size are shown in Table 5.41.

Table 5.41 Experimental data for HAp/PC composite conducted at 500µm erodent particle size

Exp. No.	Factor A Pressure (Bar)	Factor B HAp volume (%)	Factor C Impingement angle (Degree)	Erosion Wear Loss (gm)	S/N ratio (Lower The Better)
1	1	0	30	0.012	38.416
2	1	0	30	0.010	40.000
3	1	0	30	0.009	40.915
4	1	10	45	0.015	36.478
5	1	10	45	0.013	37.721
6	1	10	45	0.011	39.172
7	1	20	60	0.019	34.424
8	1	20	60	0.018	34.894
9	1	20	60	0.021	33.555
10	2	0	45	0.061	24.293
11	2	0	45	0.059	24.582
12	2	0	45	0.057	24.882
13	2	10	60	0.063	24.013
14	2	10	60	0.062	24.152
15	2	10	60	0.060	24.436
16	2	20	30	0.071	22.974
17	2	20	30	0.069	23.223
18	2	20	30	0.066	23.609
19	3	0	60	0.030	30.457
20	3	0	60	0.026	31.700
21	3	0	60	0.027	31.372
22	3	10	30	0.046	26.744
23	3	10	30	0.042	27.535
24	3	10	30	0.042	27.535
25	3	20	45	0.058	24.731
26	3	20	45	0.060	24.436
27	3	20	45	0.055	25.192

The ANOVA Table for HAp/PC composite are shown in Table 5.42.

Table 5.42 ANOVA Table for S/N ratio of HAp/PC composite

Source	DF value	Seq SS	Adj SS	Adj MS	F value	P value	Percentage Contribution
A	2	842.89	842.89	421.44	296.64	0.000	87.441
B	2	87.10	87.10	43.55	30.65	0.000	9.035
C	2	5.55	5.55	2.78	1.95	0.168	0.575
Error	20	28.41	28.41	1.42			
Total	26	963.95					

S = 1.19195, R-Sq = 97.05%, and R-Sq(adj) = 96.17%

From percentage contribution, it can be concluded here that significance of factors is in the order of Factor A, B and C.

Main effects plot for means of S/N ratio, normal probability plot and interaction plot are shown in Figure 5.106, 5.107 and 5.108 respectively.

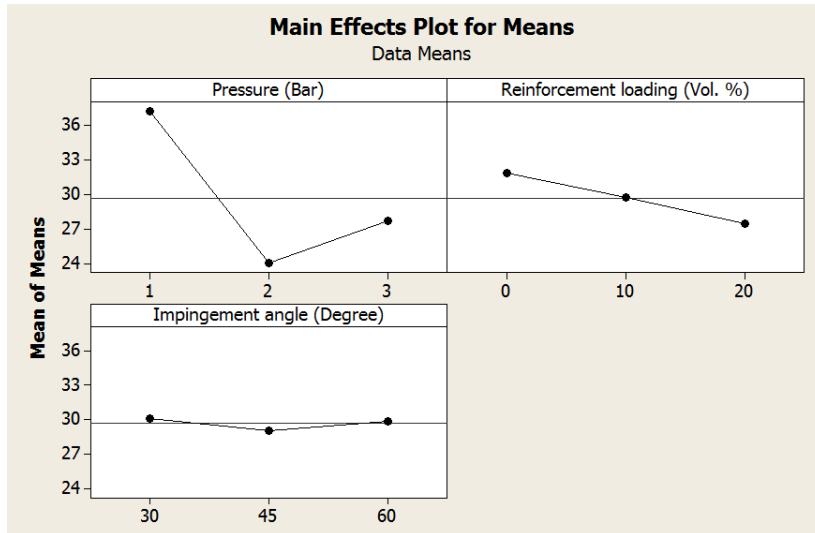


Figure 5.106 Main effects plot for means of S/N ratio

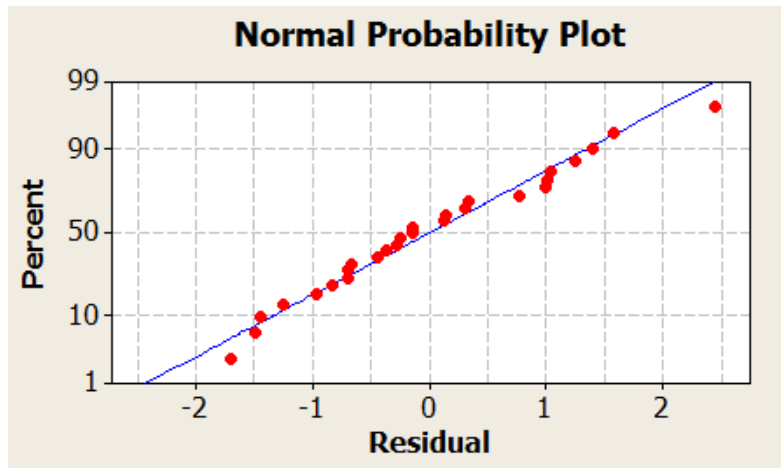


Figure 5.107 Normal probability plot for S/N ratio

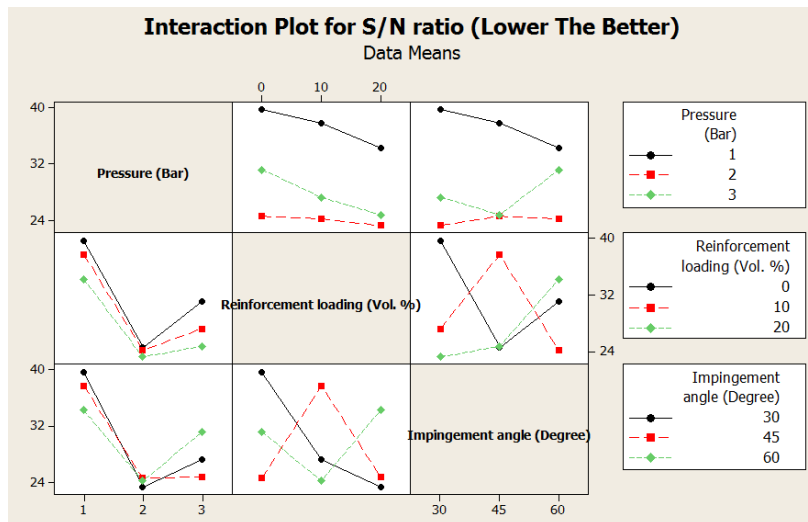


Figure 5.108 Interaction plot for S/N ratio

According to Figure 5.106, it is concluded that the optimal parametric combination is  $A_1B_1C_1$ . When pressure is 1 Bar, HAp volume is 0 vol. %, and impingement angle is 30

degree then minimum erosion wear can be obtained. Referring to Figure 5.107, it can be concluded that the ANOVA proceeds in a satisfactory manner as the residuals follow a normal distribution. Figure 5.108 shows that two factor interaction of controllable factors seems to exist. However, the interaction of factors has not been considered for the sake of simplicity.

Similarly, the experimental data for HAp/PSU composite conducted at 500µm erodent particle size are shown in Table 5.43.

Table 5.43 Experimental data for HAp/PSU composite conducted at 500µm erodent particle size

Exp. No.	Factor A Pressure (Bar)	Factor B HAp volume (%)	Factor C Impingement angle (Degree)	Erosion Wear Loss (gm)	S/N ratio (Lower The Better)
1	1	0	30	0.010	40.000
2	1	0	30	0.012	38.416
3	1	0	30	0.010	40.000
4	1	10	45	0.023	32.765
5	1	10	45	0.026	31.700
6	1	10	45	0.023	32.765
7	1	20	60	0.019	34.424
8	1	20	60	0.014	37.077
9	1	20	60	0.016	35.917
10	2	0	45	0.031	30.172
11	2	0	45	0.032	29.897
12	2	0	45	0.033	29.629
13	2	10	60	0.039	28.178
14	2	10	60	0.045	26.935
15	2	10	60	0.043	27.330
16	2	20	30	0.049	26.196
17	2	20	30	0.045	26.935
18	2	20	30	0.042	27.535
19	3	0	60	0.033	29.629
20	3	0	60	0.038	28.404
21	3	0	60	0.036	28.873
22	3	10	30	0.041	27.744
23	3	10	30	0.036	28.873
24	3	10	30	0.039	28.178
25	3	20	45	0.051	25.848
26	3	20	45	0.053	25.514
27	3	20	45	0.055	25.192

The ANOVA Table for HAp/PSU composite are shown in Table 5.44.

Table 5.44 ANOVA Table for S/N ratio of HAp/PSU composite

Source	DF value	Seq SS	Adj SS	Adj MS	F value	P value	Percentage Contribution
A	2	390.858	390.858	195.429	145.14	0.000	76.584
B	2	68.760	68.760	34.380	25.53	0.000	13.472
C	2	23.815	23.815	11.907	8.84	0.002	4.666
Error	20	26.929	26.929	1.346			
Total	26	510.362					

$S = 1.16037$ ,  $R\text{-Sq} = 94.72\%$ , and  $R\text{-Sq}(\text{adj}) = 93.14\%$

From percentage contribution, it can be concluded here that significance of factors is in the order of Factor A, B and C.

Main effects plot for means of S/N ratio, normal probability plot and interaction plot are shown in Figure 5.109, 5.110 and 5.111 respectively.



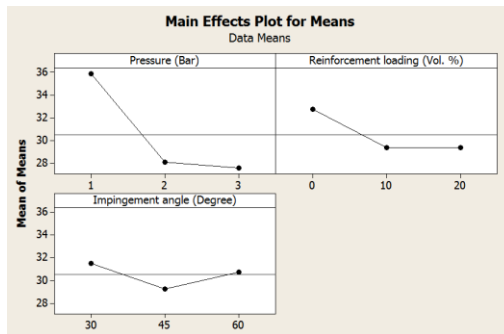


Figure 5.109 Main effects plot for means of S/N ratio

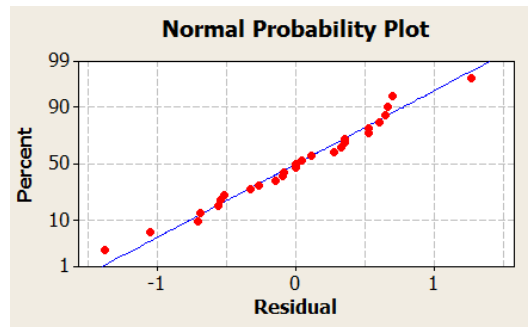


Figure 5.110 Normal probability plot for S/N ratio

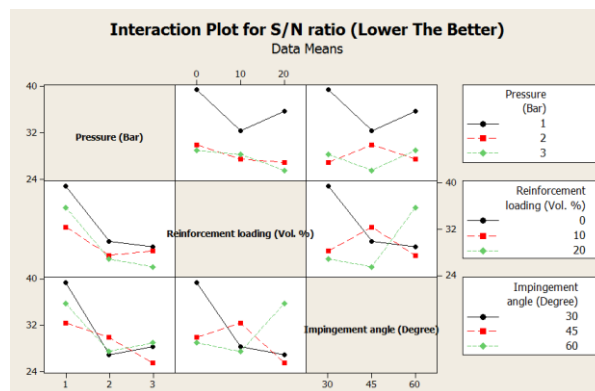


Figure 5.111 Interaction plot for S/N ratio

According to Figure 5.109, it is concluded that the optimal parametric combination is  $A_1B_1C_1$ . When pressure is 1 Bar, HAp volume is 0 vol. %, and impingement angle is 30 degree then minimum erosion wear can be obtained. Referring to Figure 5.110, it can be concluded that the ANOVA proceeds in a satisfactory manner as the residuals follow a normal distribution. Figure 5.111 shows that two factor interaction of controllable factors seems to exist. However, the interaction of factors has not been considered for the sake of simplicity.

## 5.2.2.1 Prediction of erosive wear behaviour of composites

### 5.2.2.1.1 Adaptive neuro fuzzy inference system (ANFIS) methodology used for HAp/PC composite (at 300 micron size)

The FIS editor for input parameters of both HAp/PC and HAp/PSU composites, and membership function editor for output parameter of HAp/PC composite at 300 micron size are shown in Figure 5.112 to Figure 5.116 respectively.

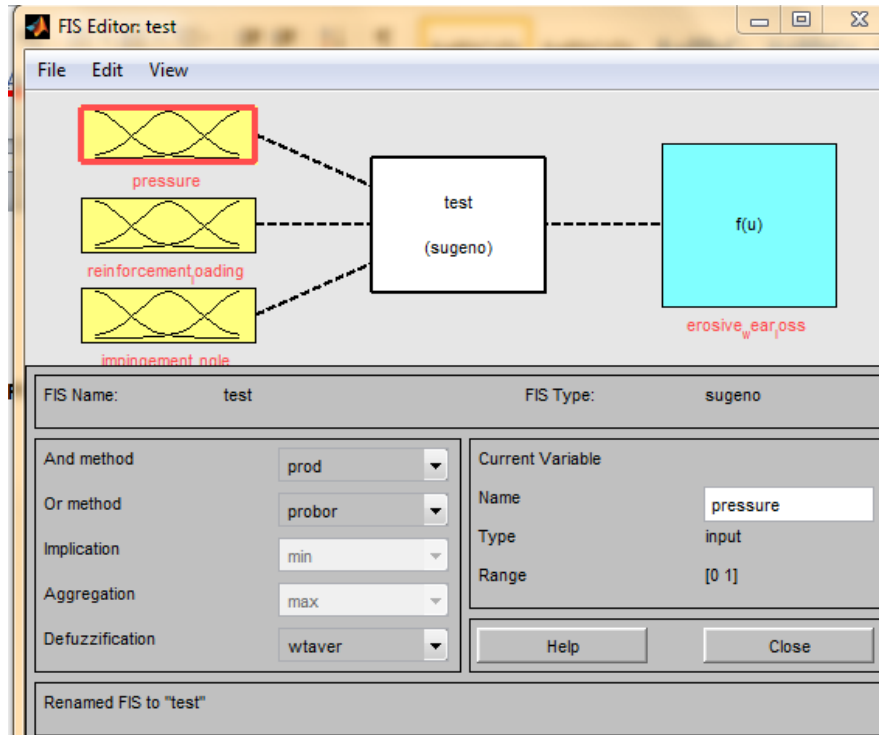


Figure 5.112 FIS editor

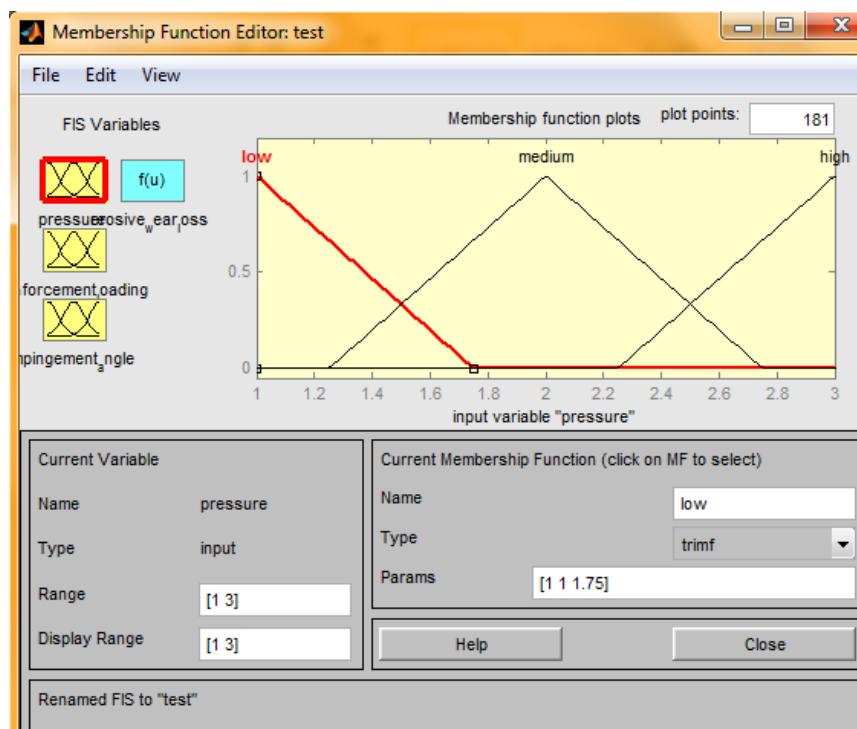


Figure 5.113 Membership function editor of Input 1

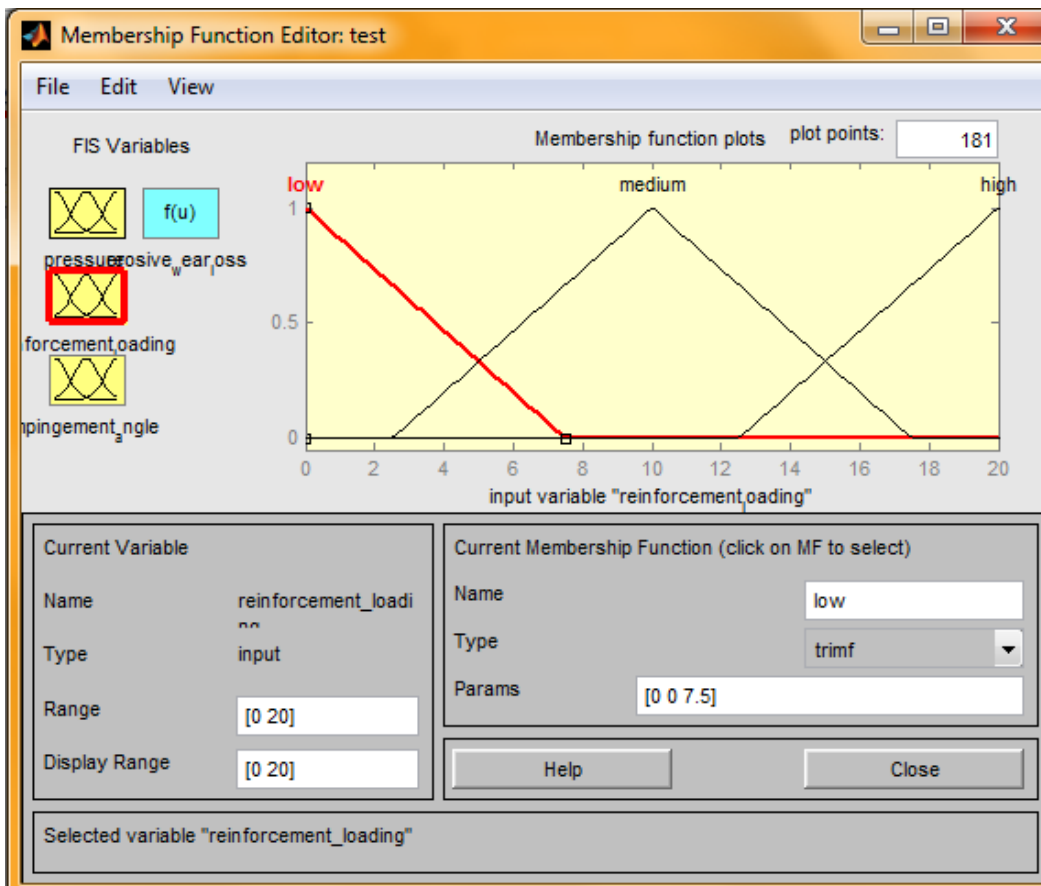


Figure 5.114 Membership function editor of Input 2

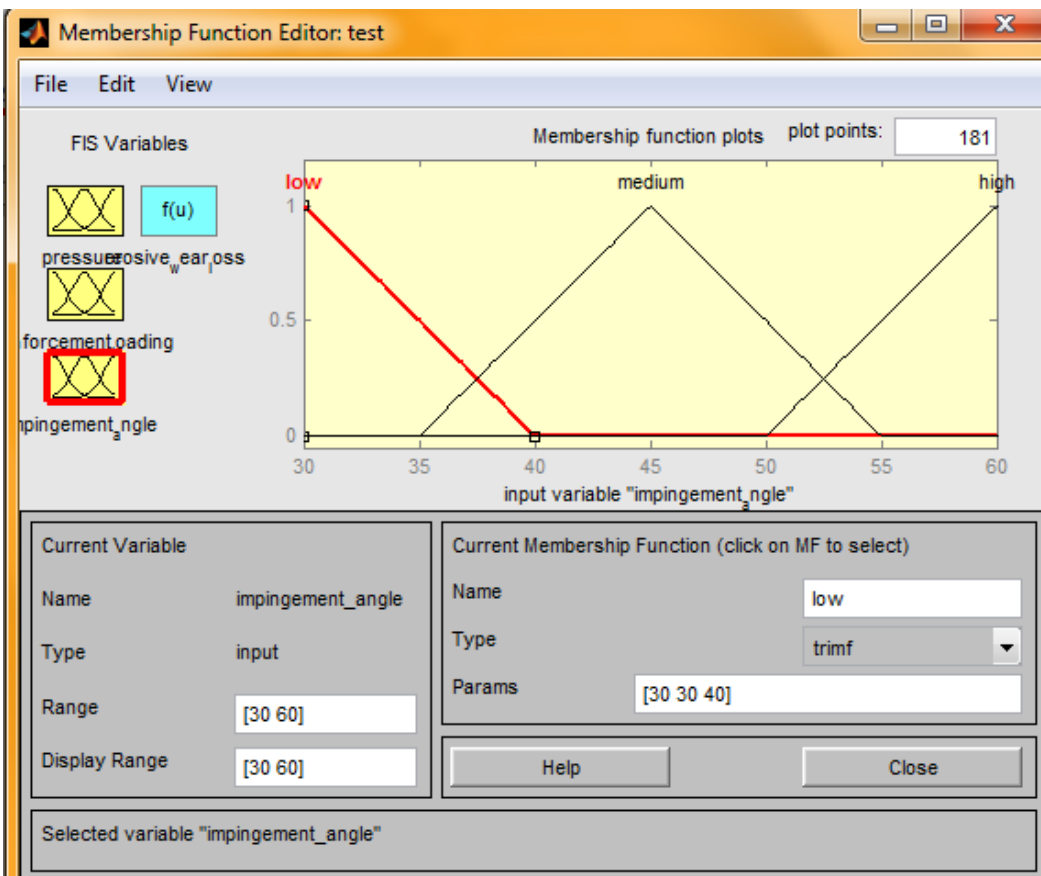


Figure 5.115 Membership function editor of Input 3

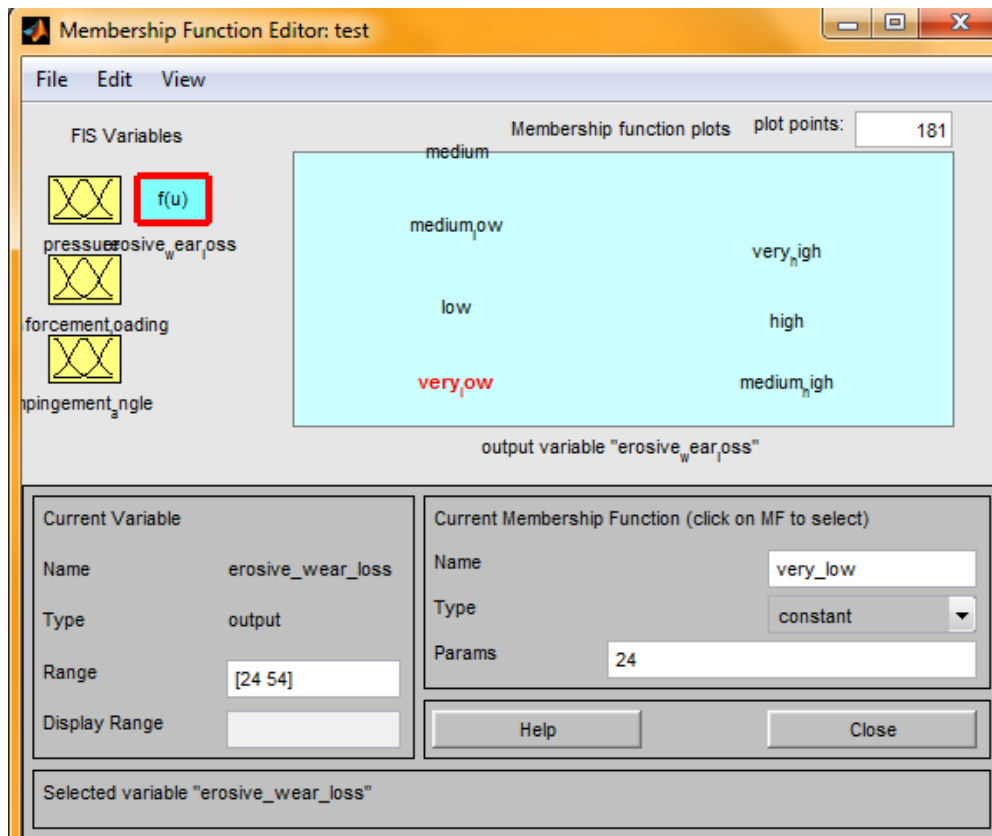


Figure 5.116 Membership function editor for output of HAp/PC composite

The ANFIS model structure of HAp/PC and HAp/PSU composites regarding erosive wear, while ANFIS editor for both training and testing data, rule editor and rule viewer of HAp/PC composite are shown in Figure 5.117 to Figure 5.121 respectively.

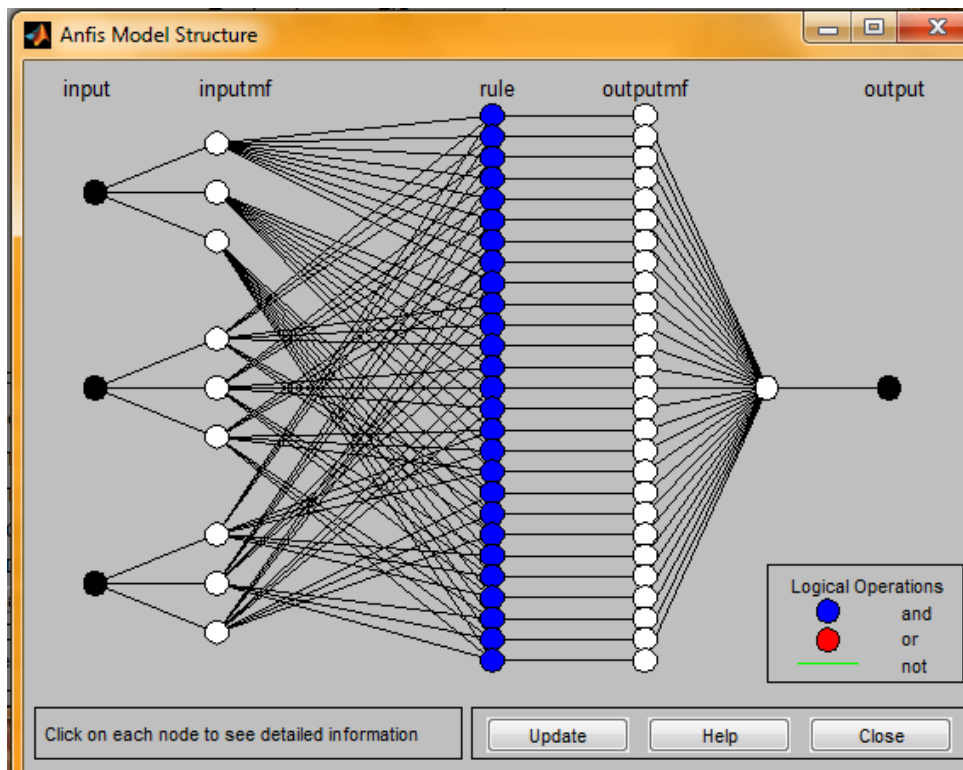


Figure 5.117 ANFIS model structure

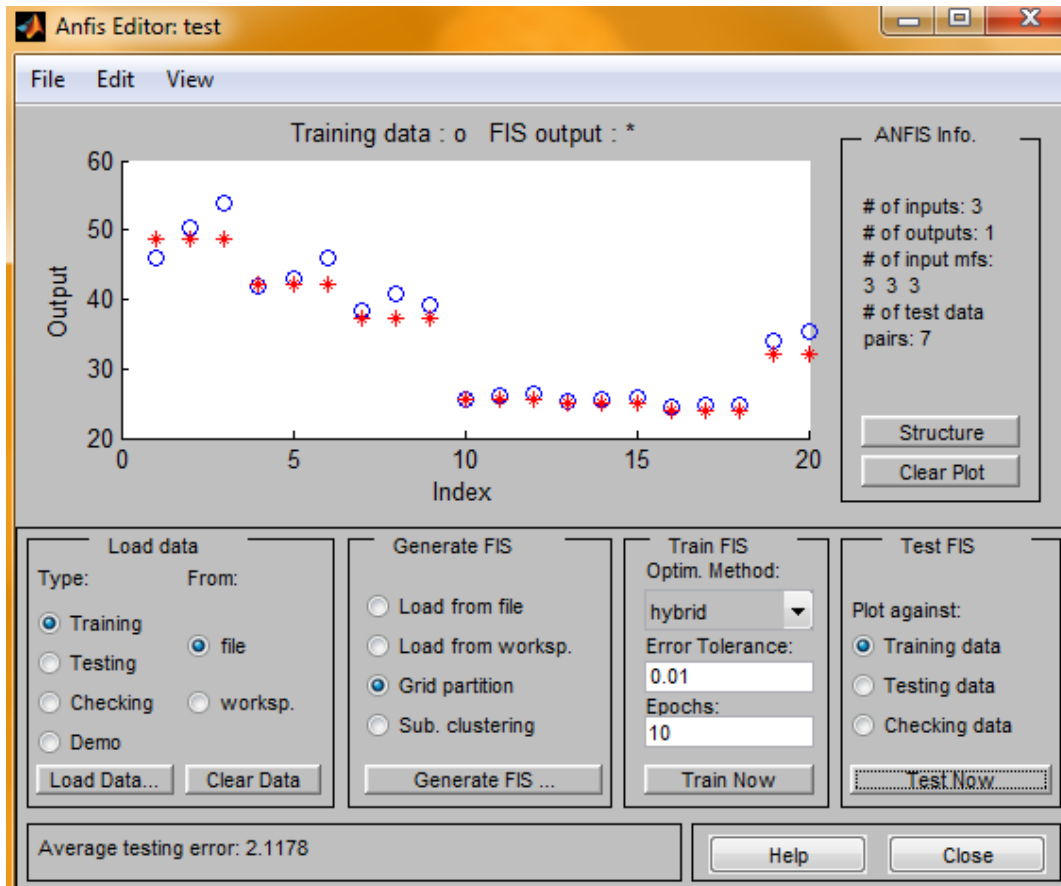


Figure 5.118 Distribution of predicted and actual data (Training)

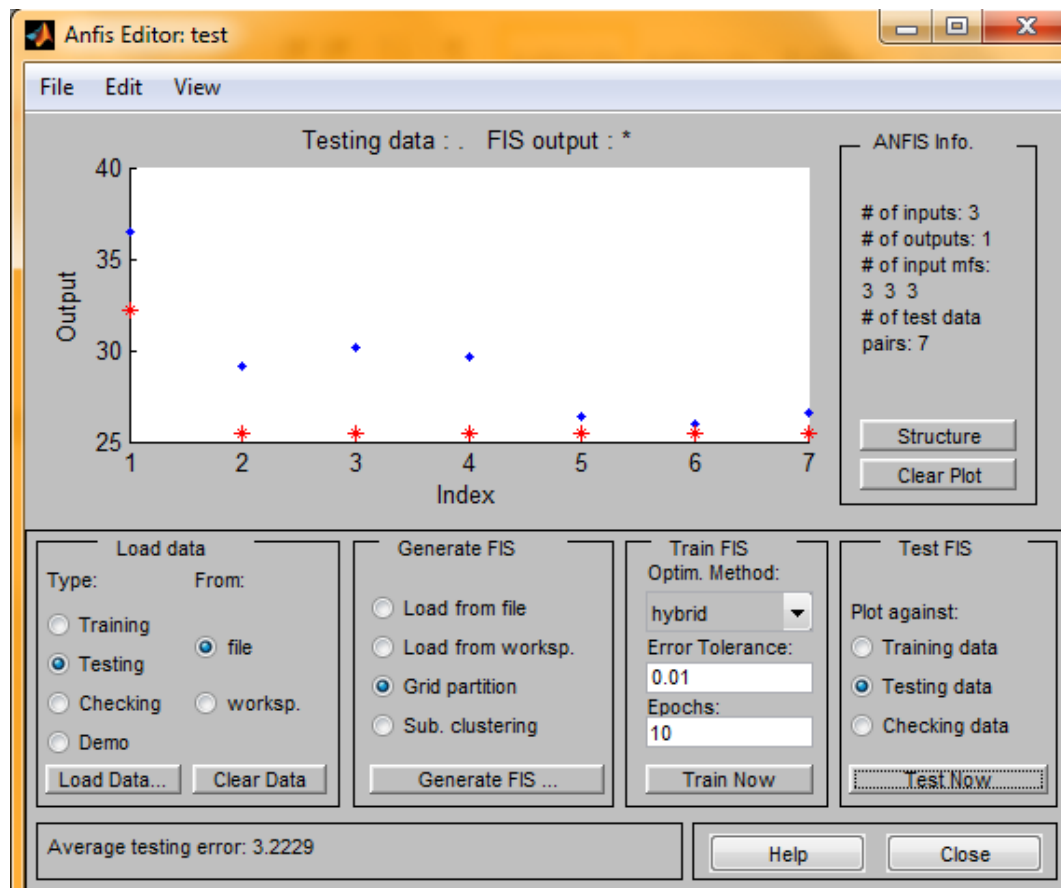


Figure 5.119 Distribution of predicted and actual data (Testing)

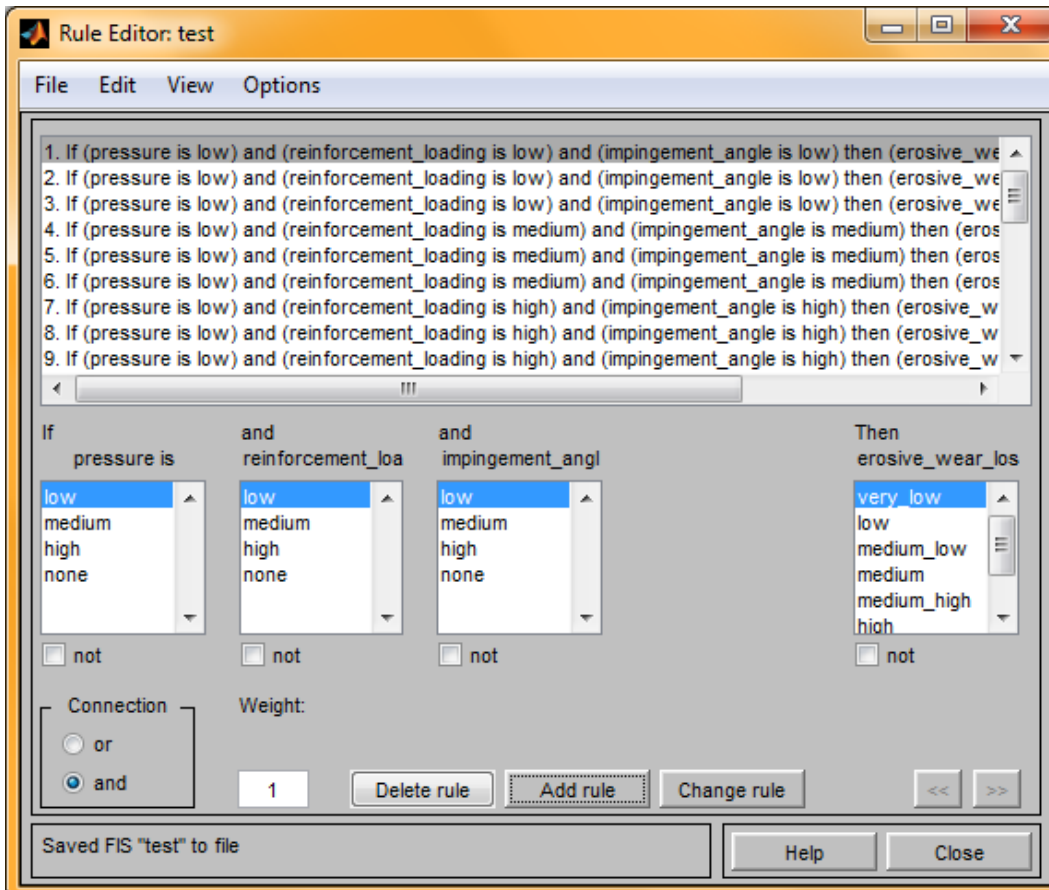


Figure 5.120 Rule editor

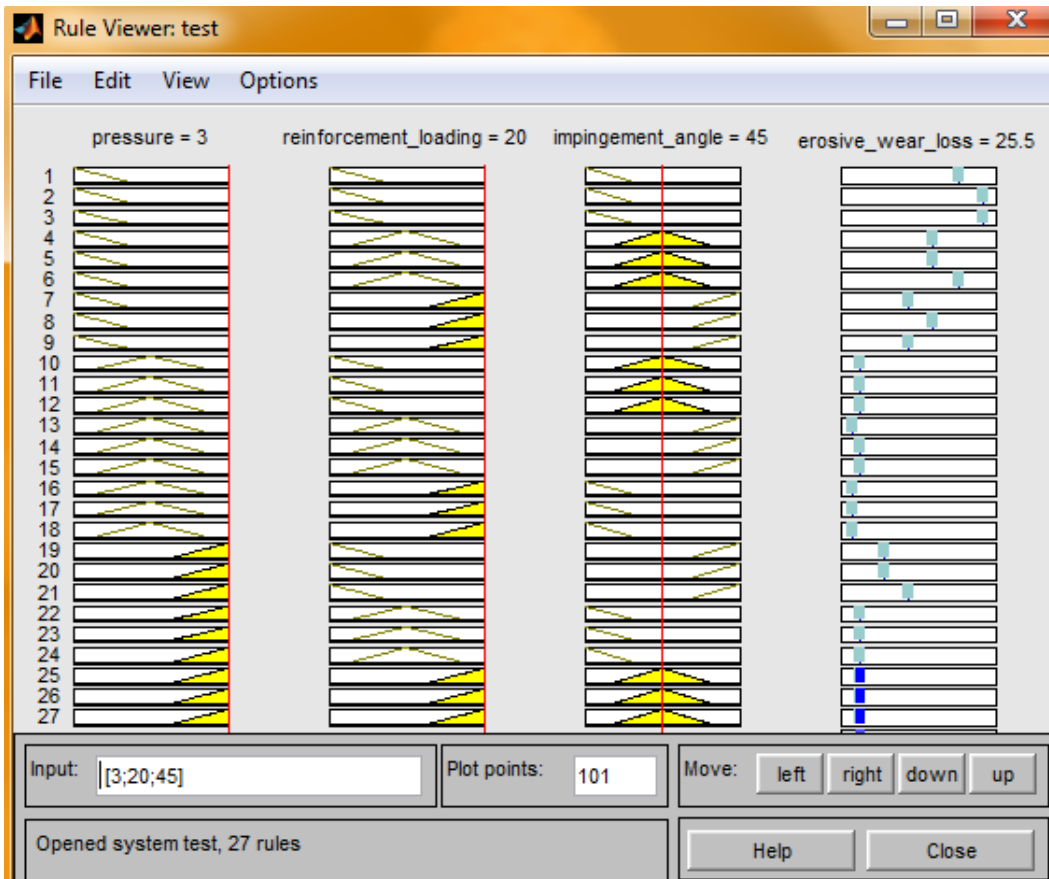


Figure 5.121 Rule viewer

The input and output experimental value with ANFIS predicted value of HAp/PC composite at 300 micron size for training purpose is shown in Table 5.45.

Table 5.45 Input and output data with ANFIS predicted value of HAp/PC composite at 300 micron size

No.	Factor A Pressure (Bar)	Factor B HAp volume (%)	Factor C Impingement angle (Degree)	Wear Loss (gm)	S/N ratio of Exp. value	ANFIS output predicted value
1	1	0	30	0.005	46.020	48.8333
2	1	0	30	0.003	50.457	48.8333
3	1	0	30	0.002	53.979	48.8333
4	1	10	45	0.008	41.938	42.1667
5	1	10	45	0.007	43.098	42.1667
6	1	10	45	0.005	46.020	42.1667
7	1	20	60	0.012	38.416	37.1667
8	1	20	60	0.009	40.915	37.1667
9	1	20	60	0.011	39.172	37.1667
10	2	0	45	0.052	25.679	25.5
11	2	0	45	0.050	26.020	25.5
12	2	0	45	0.048	26.375	25.5
13	2	10	60	0.055	25.192	25
14	2	10	60	0.053	25.514	25
15	2	10	60	0.051	25.848	25
16	2	20	30	0.060	24.436	24
17	2	20	30	0.058	24.731	24
18	2	20	30	0.057	24.882	24
19	3	0	60	0.020	33.979	32.1667
20	3	0	60	0.017	35.391	32.1667

The input and output data with ANFIS predicted value of HAp/PC composite at 300 micron size for testing purpose is shown in Table 5.46.

Table 5.46 Input and output data with ANFIS predicted value of HAp/PC composite at 300 micron size

No.	Factor A Pressure (Bar)	Factor B HAp volume (%)	Factor C Impingement angle (Degree)	Wear Loss (gm)	S/N ratio of Exp. value	ANFIS output predicted value
1	3	0	60	0.015	36.478	32.1667
2	3	10	30	0.035	29.118	25.5
3	3	10	30	0.031	30.172	25.5
4	3	10	30	0.033	29.629	25.5
5	3	20	45	0.048	26.375	25.5
6	3	20	45	0.050	26.020	25.5
7	3	20	45	0.047	26.558	25.5

By calculating we get the mean relative percentage error for training and testing of HAp/PC composite conducted at 300 micron size is 4.11% and 9.00% respectively.

### 5.2.2.1.2 Adaptive neuro fuzzy inference system (ANFIS) methodology used for HAp/PSU composite (at 300 micron size)

The membership function editor for output parameter of HAp/PSU composite at 300 micron size is shown in Figure 5.122.

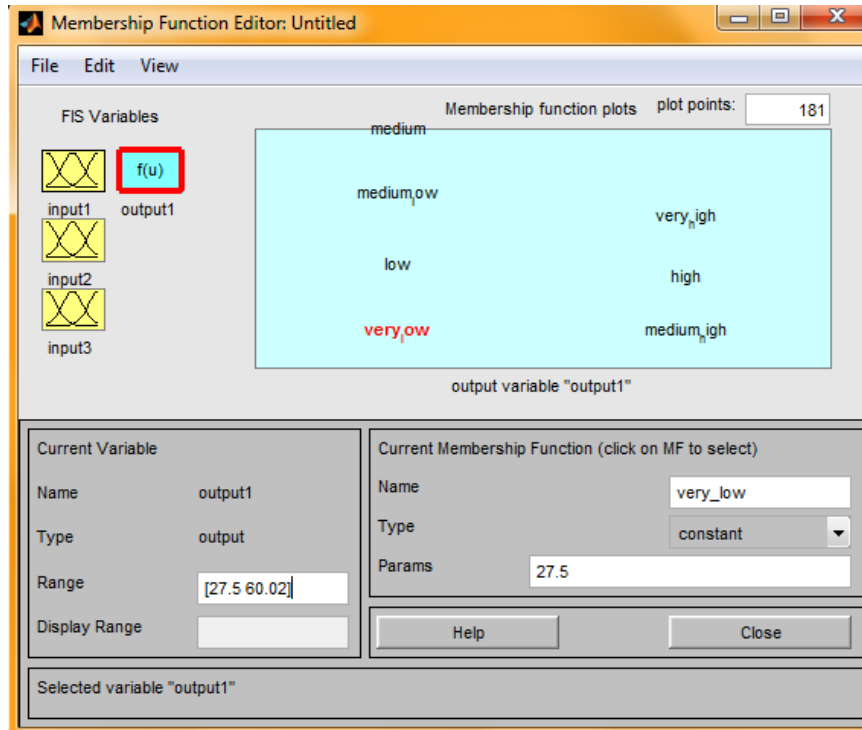


Figure 5.122 Membership function editor for output of HAp/PSU composite

The ANFIS editor for both training and testing data, rule editor and rule viewer of HAp/PSU composite are shown in Figure 5.123 to Figure 5.126 respectively.

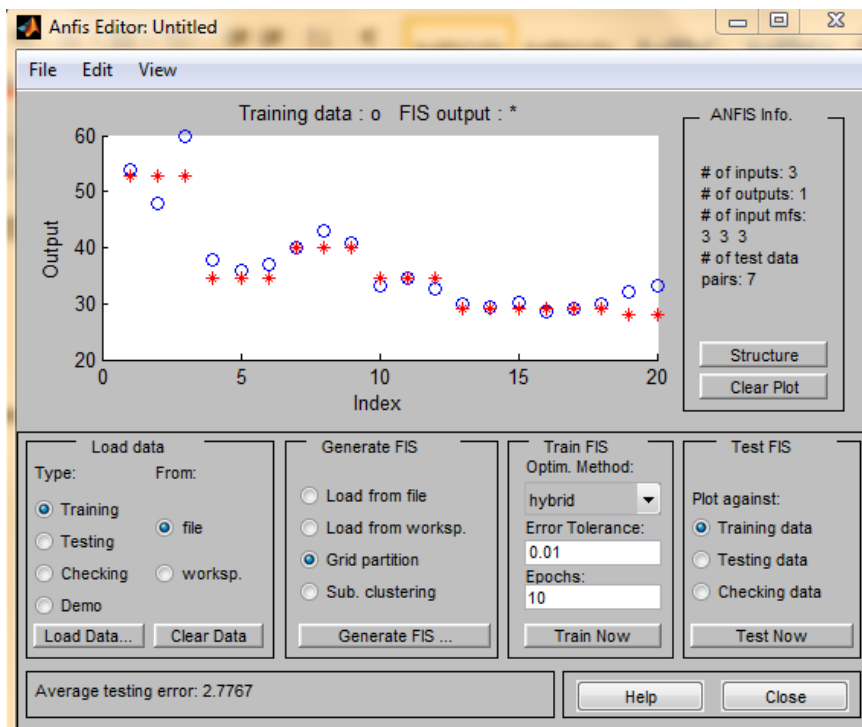


Figure 5.123 Distribution of predicted and actual data (Training)



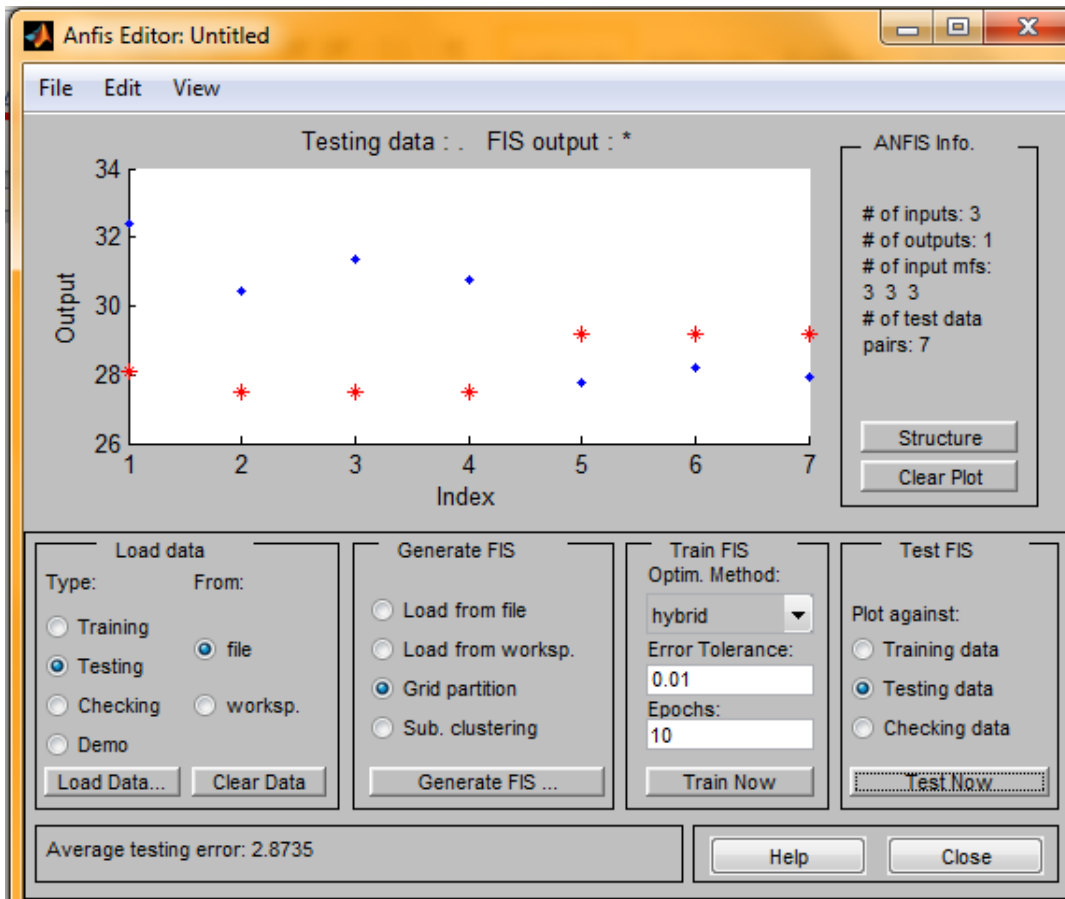


Figure 5.124 Distribution of predicted and actual data (Testing)

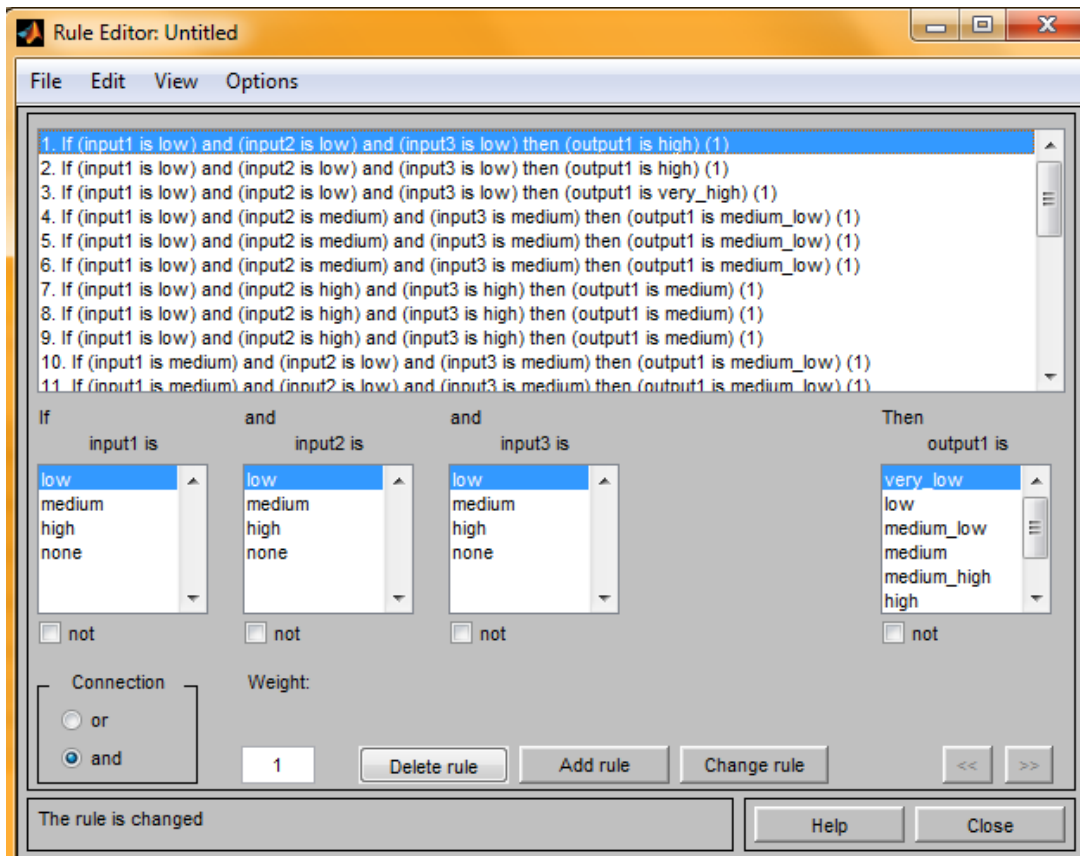


Figure 5.125 Rule editor

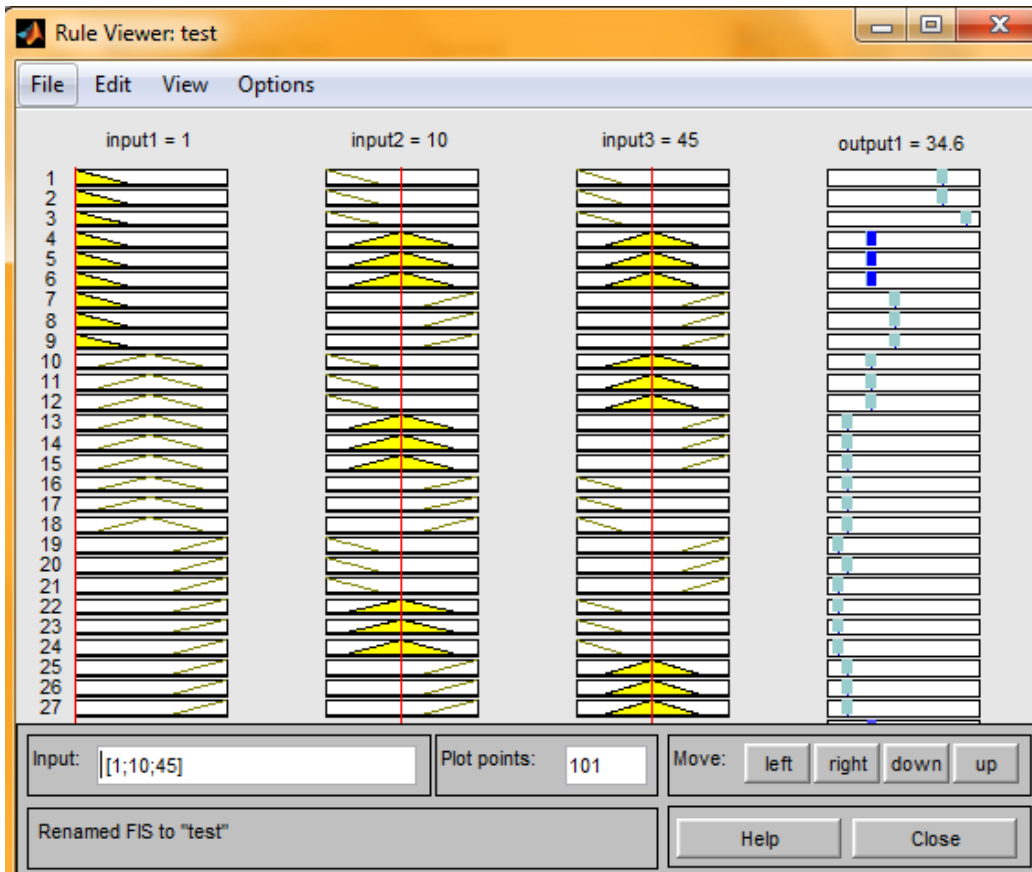


Figure 5.126 Rule viewer

The input and output experimental value with ANFIS predicted value of HAp/PSU composite at 300 micron size for training purpose is shown in Table 5.47.

Table 5.47 Input and output data with ANFIS predicted value of HAp/PSU composite at 300 micron size

No.	Factor A Pressure (Bar)	Factor B HAp volume (%)	Factor C Impingement angle (Degree)	Wear Loss (gm)	S/N ratio of Exp. value	ANFIS output predicted value
1	1	0	30	0.002	53.979	52.6967
2	1	0	30	0.004	47.958	52.6967
3	1	0	30	0.001	60.000	52.6967
4	1	10	45	0.013	37.721	34.63
5	1	10	45	0.016	35.917	34.63
6	1	10	45	0.014	37.077	34.63
7	1	20	60	0.010	40.000	40.05
8	1	20	60	0.007	43.098	40.05
9	1	20	60	0.009	40.915	40.05
10	2	0	45	0.022	33.151	34.63
11	2	0	45	0.019	34.424	34.63
12	2	0	45	0.023	32.765	34.63
13	2	10	60	0.032	29.897	29.21
14	2	10	60	0.034	29.370	29.21
15	2	10	60	0.031	30.172	29.21
16	2	20	30	0.037	28.635	29.21
17	2	20	30	0.035	29.118	29.21
18	2	20	30	0.032	29.897	29.21
19	3	0	60	0.025	32.041	28.07
20	3	0	60	0.022	33.151	28.07

The input and output data with ANFIS predicted value of HAp/PSU composite at 300 micron size for testing purpose is shown in Table 5.48.

Table 5.48 Input and output data with ANFIS predicted value of HAp/PSU composite at 300 micron size

No.	Factor A Pressure (Bar)	Factor B HAp volume (%)	Factor C Impingement angle (Degree)	Wear Loss (gm)	S/N ratio of Exp. value	ANFIS output predicted value
1	3	0	60	0.024	32.395	28.07
2	3	10	30	0.030	30.457	27.5
3	3	10	30	0.027	31.372	27.5
4	3	10	30	0.029	30.752	27.5
5	3	20	45	0.041	27.744	29.21
6	3	20	45	0.039	28.178	29.21
7	3	20	45	0.040	27.958	29.21

By calculating we get the mean relative percentage error for training and testing of HAp/PSU composite conducted at 300 micron size is 5.06% and 8.49% respectively.

### 5.2.2.1.3 Adaptive neuro fuzzy inference system (ANFIS) methodology used for HAp/PC composite (at 400 micron size)

The membership function editor for output parameter of HAp/PC composite at 400 micron size is shown in Figure 5.127.

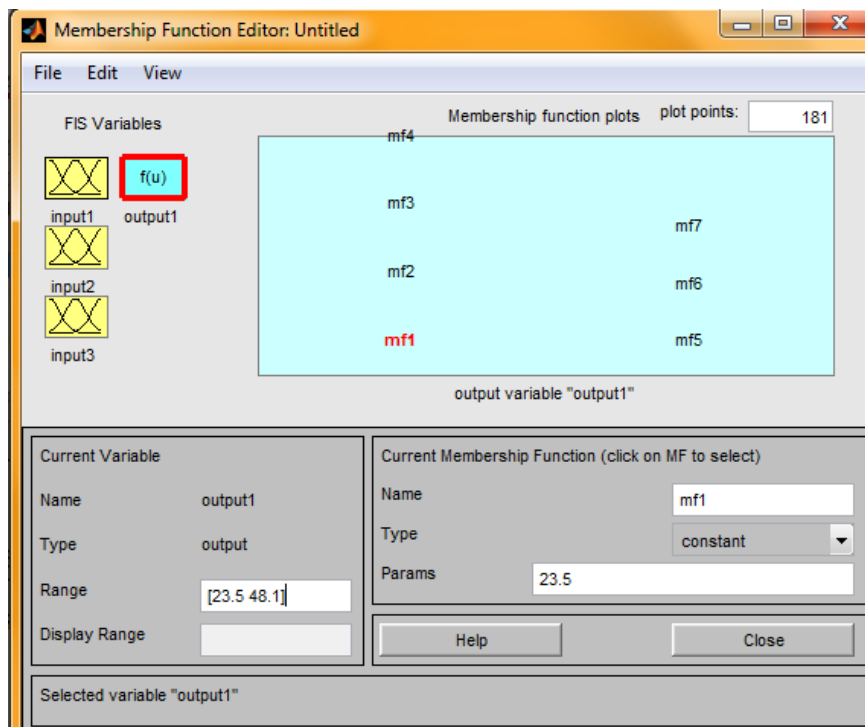


Figure 5.127 Membership function editor for output of HAp/PC composite

The ANFIS editor for both training and testing data, rule editor and rule viewer of HAp/PC composite are shown in Figure 5.128 to Figure 5.131.

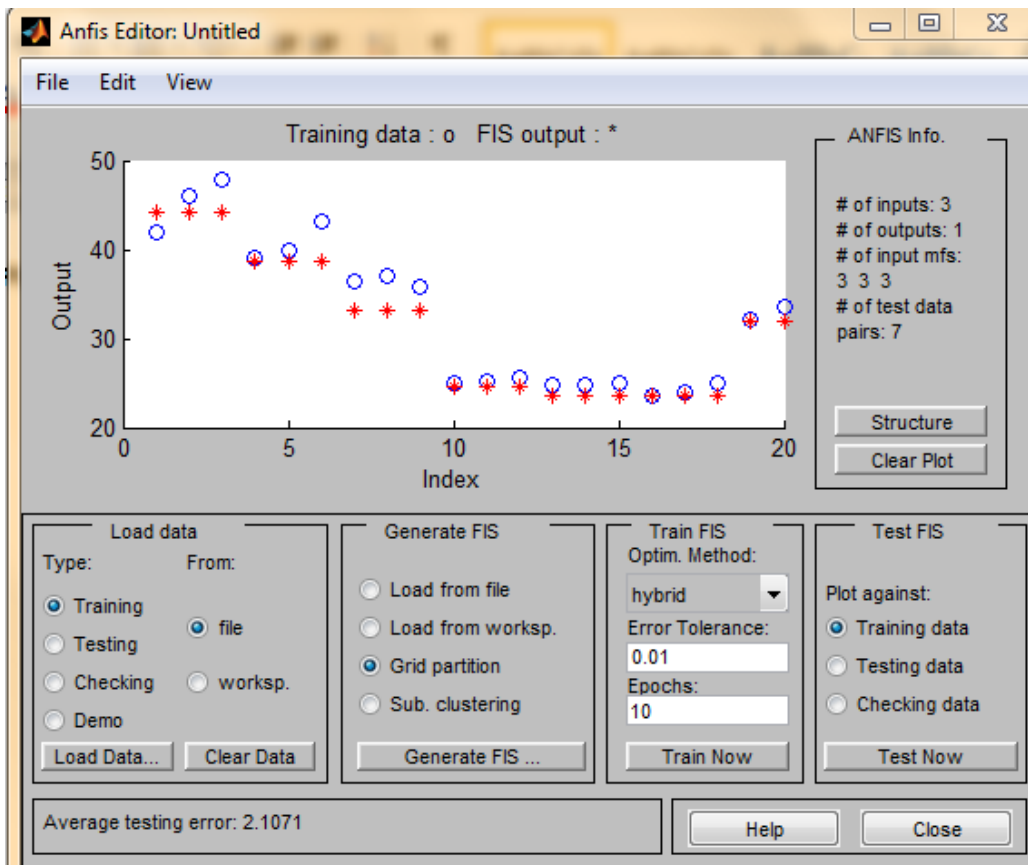


Figure 5.128 Distribution of predicted and actual data (Training)

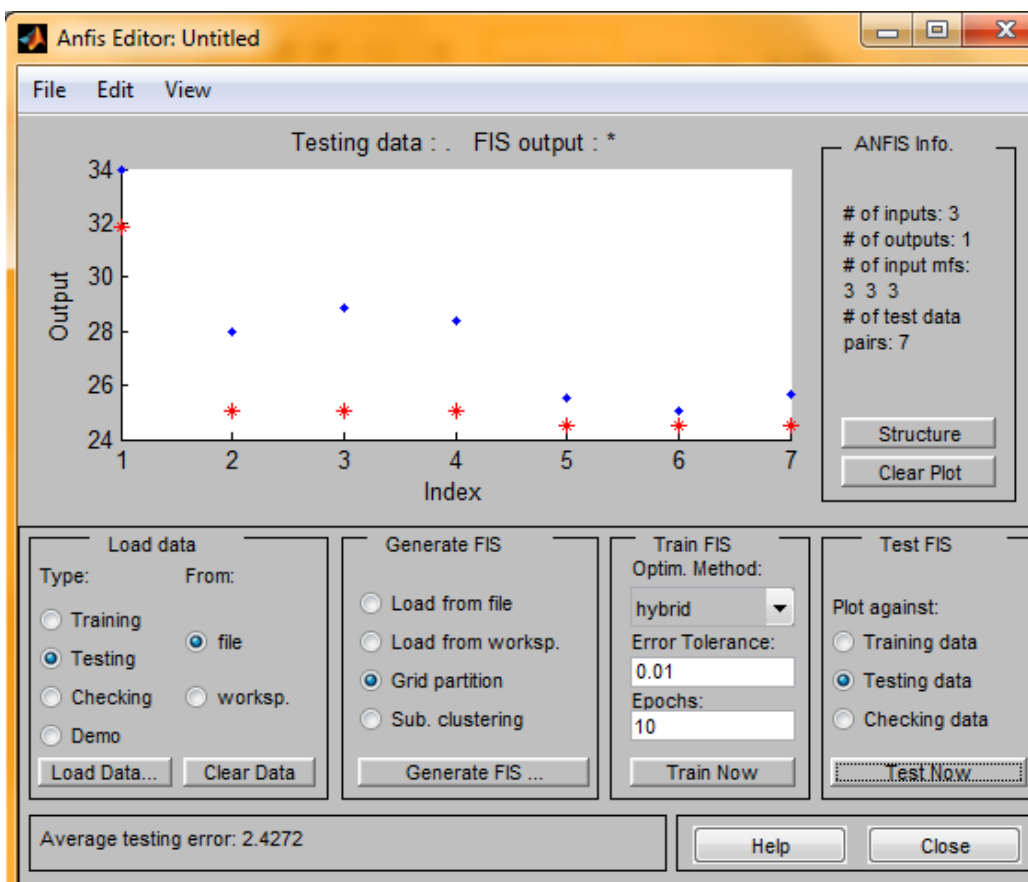


Figure 5.129 Distribution of predicted and actual data (Testing)

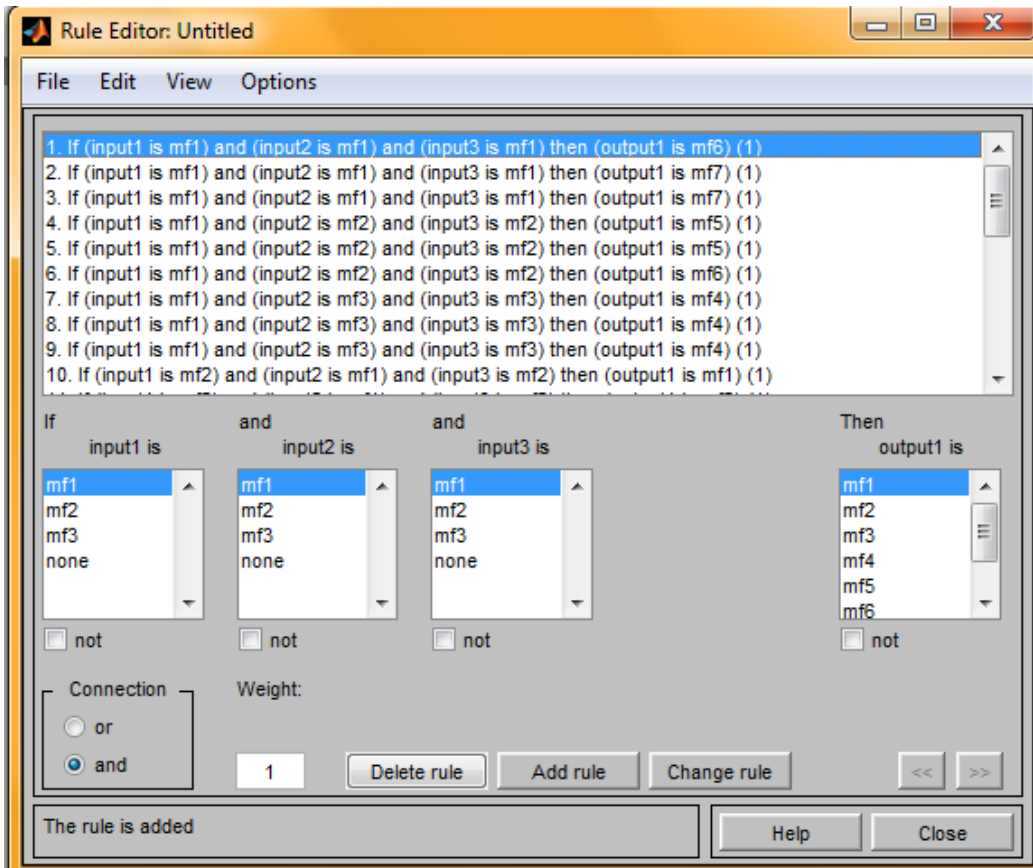


Figure 5.130 Rule editor

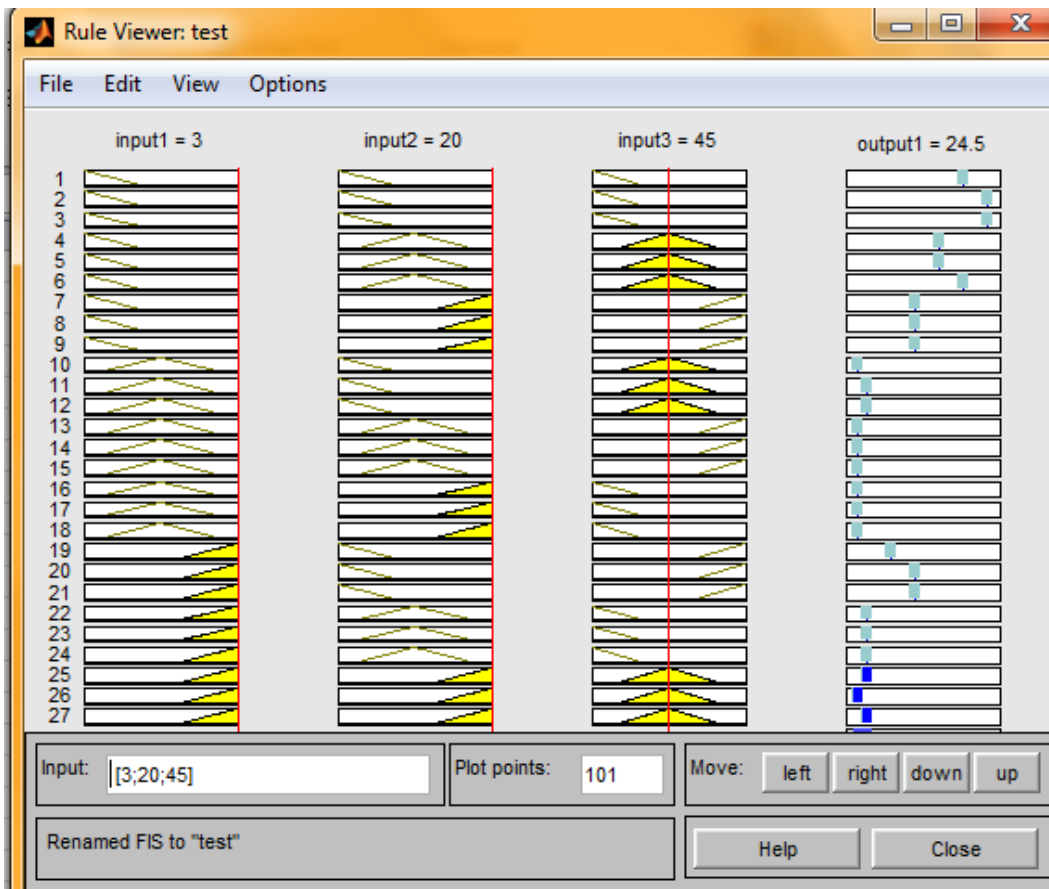


Figure 5.131 Rule viewer

The input and output experimental value with ANFIS predicted value of HAp/PC composite at 400 micron size for training purpose is shown in Table 5.49.

Table 5.49 Input and output data with ANFIS predicted value of HAp/PC composite at 400 micron size

No.	Factor A Pressure (Bar)	Factor B HAp volume (%)	Factor C Impingement angle (Degree)	Wear Loss (gm)	S/N ratio of Exp. value	ANFIS output predicted value
1	1	0	30	0.008	41.938	44.1833
2	1	0	30	0.005	46.020	44.1833
3	1	0	30	0.004	47.958	44.1833
4	1	10	45	0.011	39.172	38.7167
5	1	10	45	0.010	40.000	38.7167
6	1	10	45	0.007	43.098	38.7167
7	1	20	60	0.015	36.478	33.25
8	1	20	60	0.014	37.077	33.25
9	1	20	60	0.016	35.917	33.25
10	2	0	45	0.056	25.036	24.5333
11	2	0	45	0.055	25.192	24.5333
12	2	0	45	0.052	25.679	24.5333
13	2	10	60	0.057	24.882	23.5
14	2	10	60	0.058	24.731	23.5
15	2	10	60	0.056	25.036	23.5
16	2	20	30	0.066	23.609	23.5
17	2	20	30	0.063	24.013	23.5
18	2	20	30	0.061	24.923	23.5
19	3	0	60	0.025	32.041	31.8833
20	3	0	60	0.021	33.555	31.8833

The input and output data with ANFIS predicted value of HAp/PC composite at 400 micron size for testing purpose is shown in Table 5.50.

Table 5.50 Input and output data with ANFIS predicted value of HAp/PC composite at 400 micron size

No.	Factor A Pressure (Bar)	Factor B HAp volume (%)	Factor C Impingement angle (Degree)	Wear Loss (gm)	S/N ratio of Exp. value	ANFIS output predicted value
1	3	0	60	0.020	33.979	31.8833
2	3	10	30	0.040	27.958	25.05
3	3	10	30	0.036	28.873	25.05
4	3	10	30	0.038	28.404	25.05
5	3	20	45	0.053	25.514	24.5333
6	3	20	45	0.056	25.036	24.5333
7	3	20	45	0.052	25.679	24.5333

By calculating we get the mean relative percentage error for training and testing of HAp/PC composite conducted at 400 micron size is 4.89% and 7.42% respectively.

#### 5.2.2.1.4 Adaptive neuro fuzzy inference system (ANFIS) methodology used for HAp/PSU composite (at 400 micron size)

The membership function editor for output parameter of HAp/PSU composite at 400 micron size is shown in Figure 5.132.

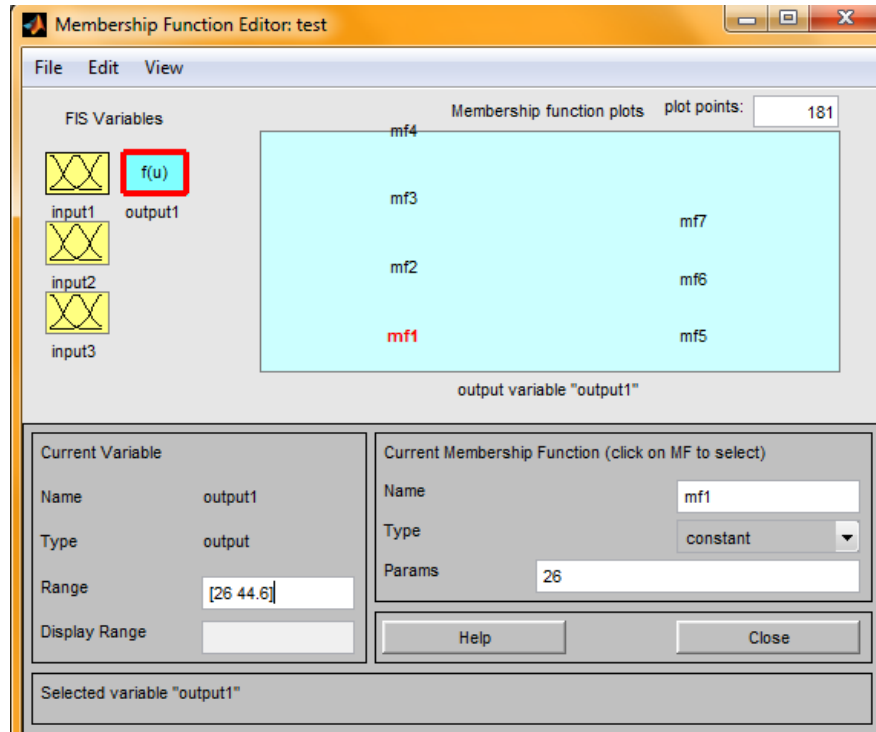


Figure 5.132 Membership function editor for output of HAp/PSU composite

The ANFIS editor for both training and testing data, rule editor and rule viewer of HAp/PSU composite are shown in Figure 5.133 to Figure 5.136 respectively.

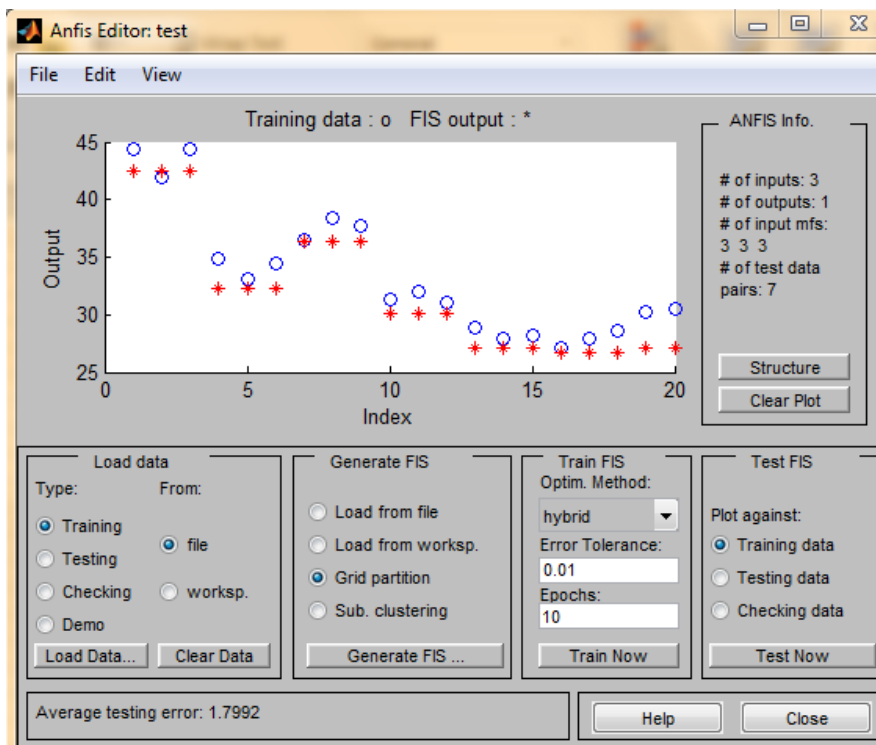


Figure 5.133 Distribution of predicted and actual data (Training)

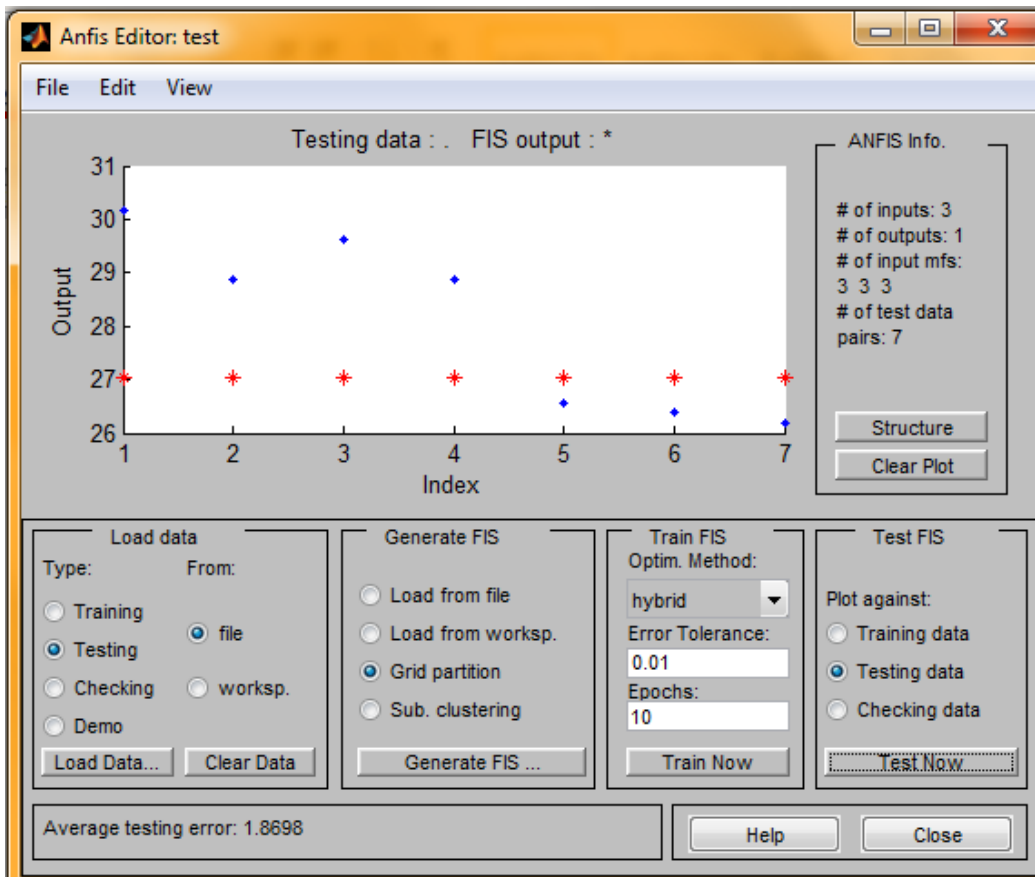


Figure 5.134 Distribution of predicted and actual data (Testing)

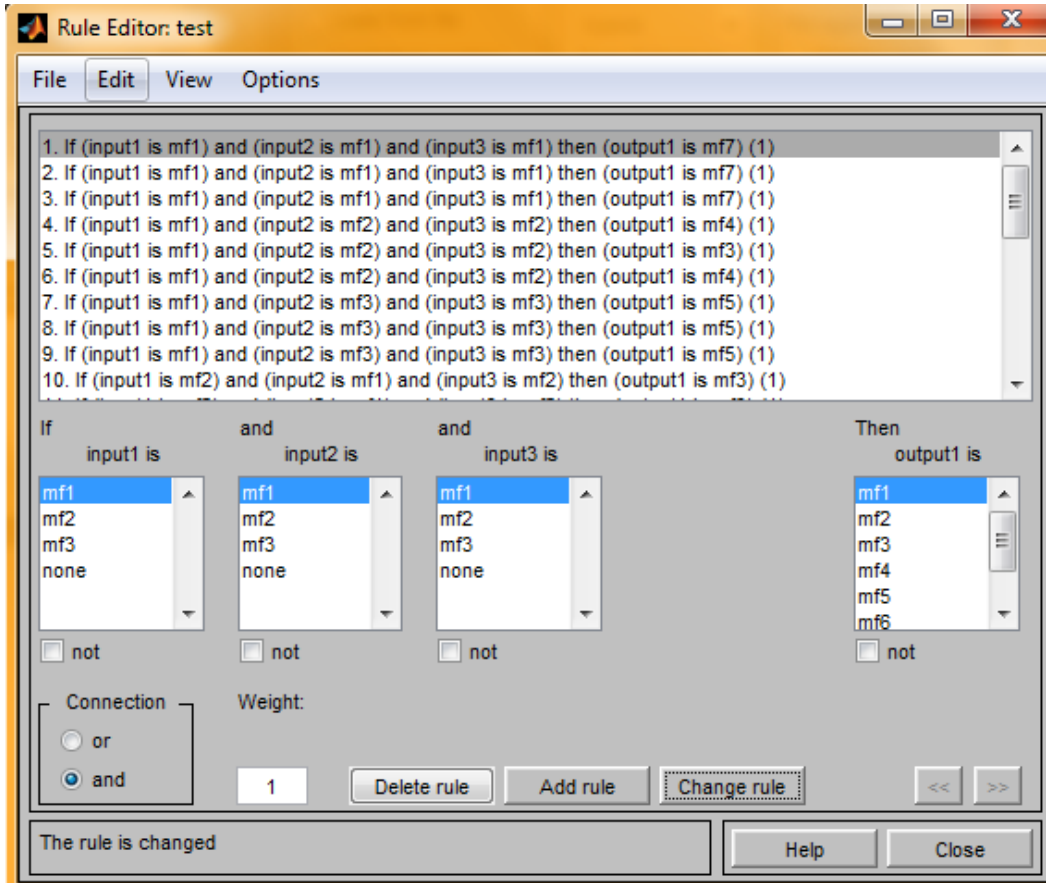


Figure 5.135 Rule editor



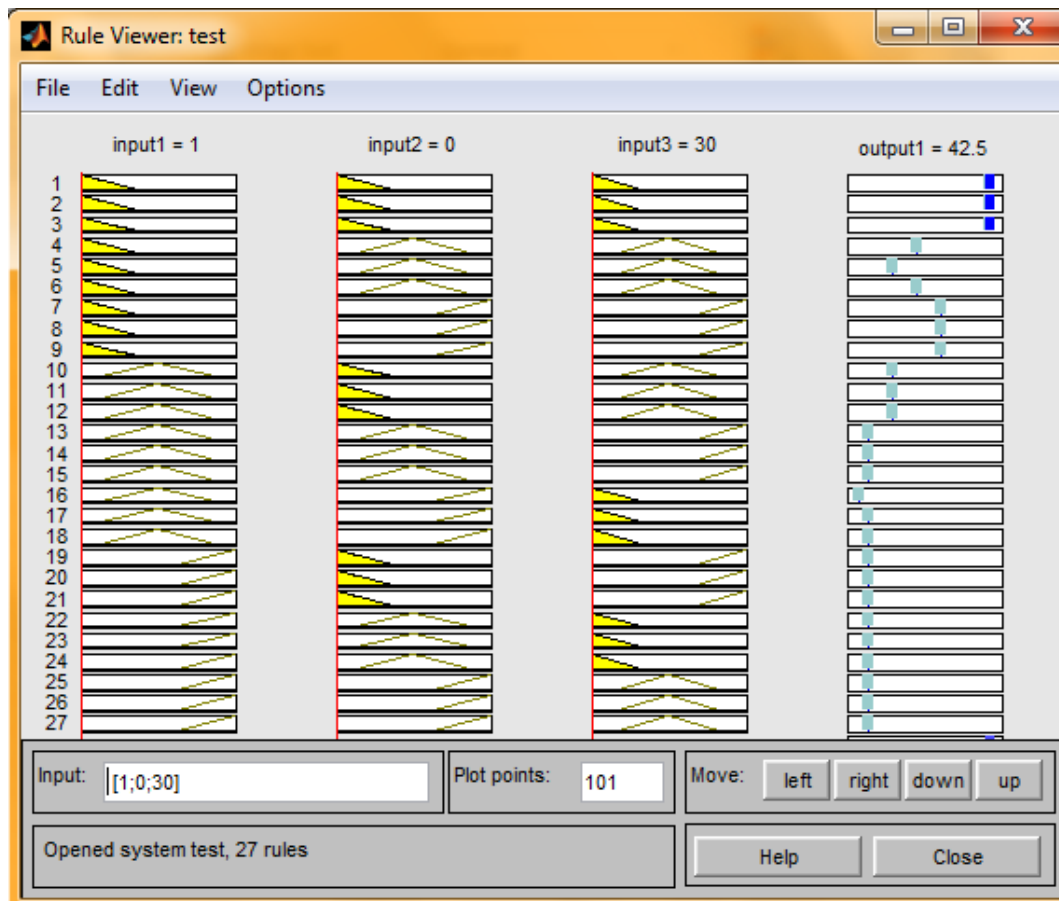


Figure 5.136 Rule viewer

The input and output experimental value with ANFIS predicted value of HAP/PSU composite at 400 micron size for training purpose is shown in Table 5.51.

Table 5.51 Input and output data with ANFIS predicted value of HAP/PSU composite at 400 micron size

No.	Factor A Pressure (Bar)	Factor B HAp volume (%)	Factor C Impingement angle (Degree)	Wear Loss (gm)	S/N ratio of Exp. value	ANFIS output predicted value
1	1	0	30	0.006	44.436	42.55
2	1	0	30	0.008	41.938	42.55
3	1	0	30	0.006	44.436	42.55
4	1	10	45	0.018	34.894	32.2167
5	1	10	45	0.022	33.151	32.2167
6	1	10	45	0.019	34.424	32.2167
7	1	20	60	0.015	36.478	36.35
8	1	20	60	0.012	38.416	36.35
9	1	20	60	0.013	37.721	36.35
10	2	0	45	0.027	31.372	30.15
11	2	0	45	0.025	32.041	30.15
12	2	0	45	0.028	31.056	30.15
13	2	10	60	0.036	28.873	27.05
14	2	10	60	0.040	27.958	27.05
15	2	10	60	0.039	28.178	27.05
16	2	20	30	0.044	27.130	26.7
17	2	20	30	0.040	27.958	26.7
18	2	20	30	0.037	28.635	26.7
19	3	0	60	0.031	30.172	27.05
20	3	0	60	0.030	30.457	27.05

The input and output data with ANFIS predicted value of HAp/PSU composite at 400 micron size for testing purpose is shown in Table 5.52.

Table 5.52 Input and output data with ANFIS predicted value of HAp/PSU composite at 400 micron size

No.	Factor A Pressure (Bar)	Factor B HAp volume (%)	Factor C Impingement angle (Degree)	Wear Loss (gm)	S/N ratio of Exp. value	ANFIS output predicted value
1	3	0	60	0.031	30.172	27.05
2	3	10	30	0.036	28.873	27.05
3	3	10	30	0.033	29.629	27.05
4	3	10	30	0.036	28.873	27.05
5	3	20	45	0.047	26.558	27.05
6	3	20	45	0.048	26.375	27.05
7	3	20	45	0.049	26.196	27.05

By calculating we get the mean relative percentage error for training and testing of HAp/PSU composite conducted at 400 micron size is 4.84% and 5.62% respectively.

#### 5.2.2.1.5 Adaptive neuro fuzzy inference system (ANFIS) methodology used for HAp/PC composite (at 500 micron size)

The membership function editor for output parameter of HAp/PC composite at 500 micron size is shown in Figure 5.137.

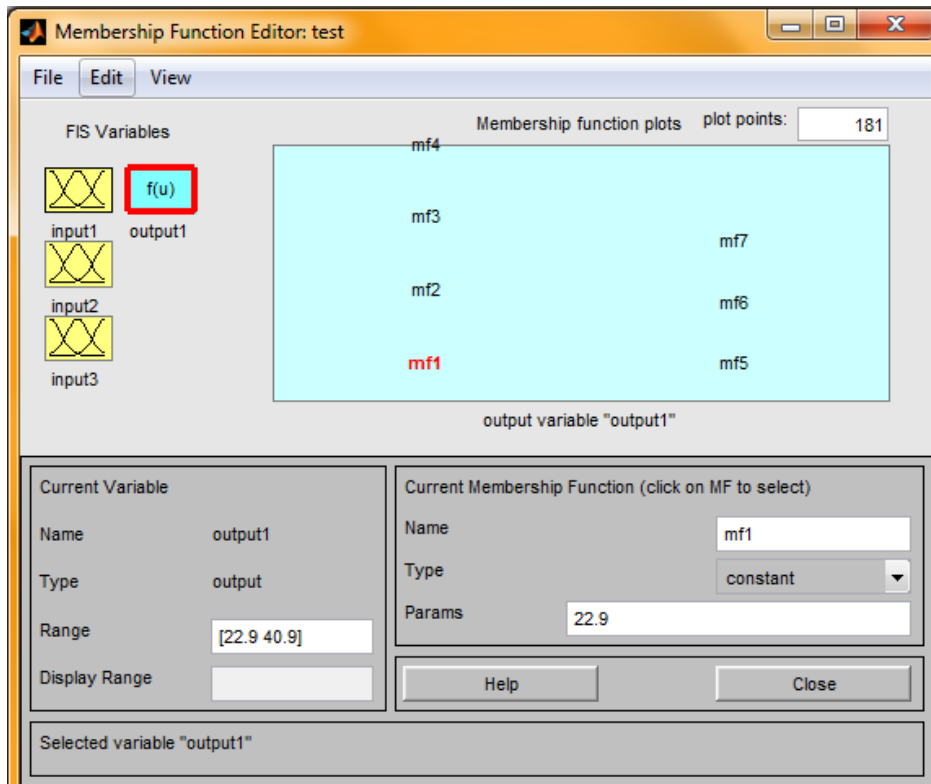


Figure 5.137 Membership function editor for output of HAp/PC composite

The ANFIS editor for both training and testing data, rule editor and rule viewer of HAp/PC composite are shown in Figure 5.138 to Figure 5.141 respectively.

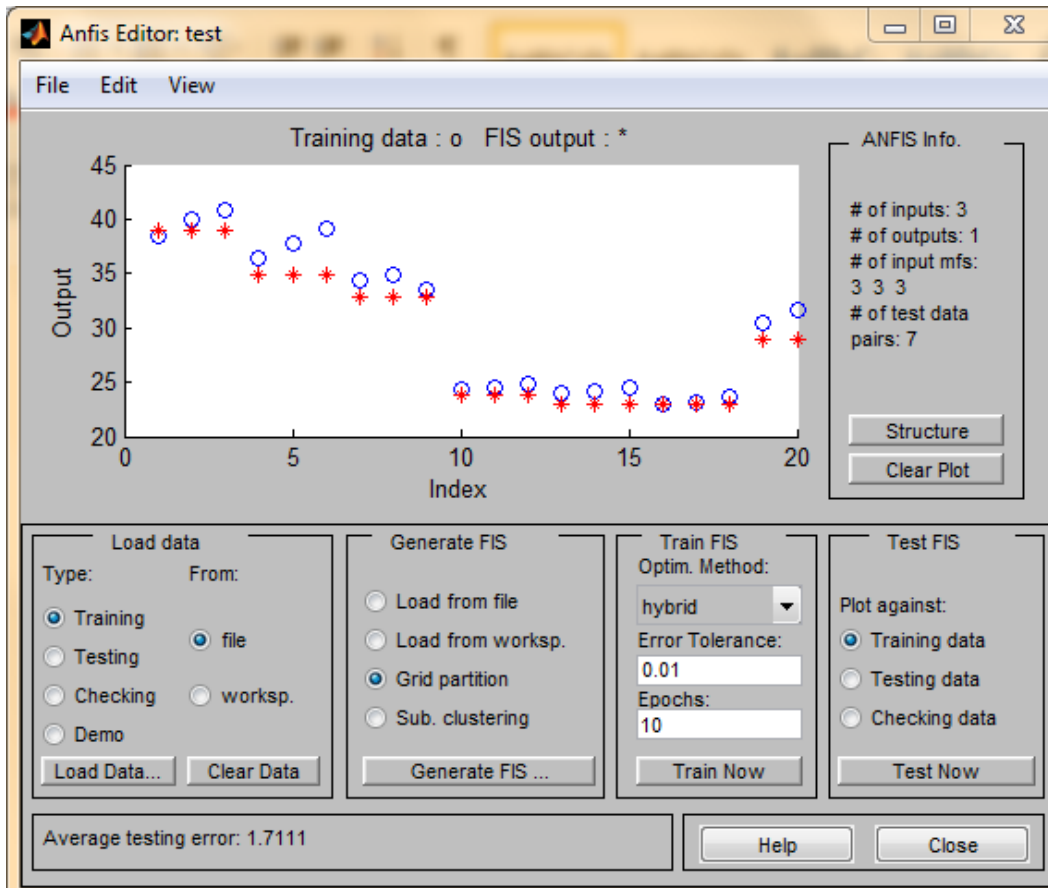


Figure 5.138 Distribution of predicted and actual data (Training)

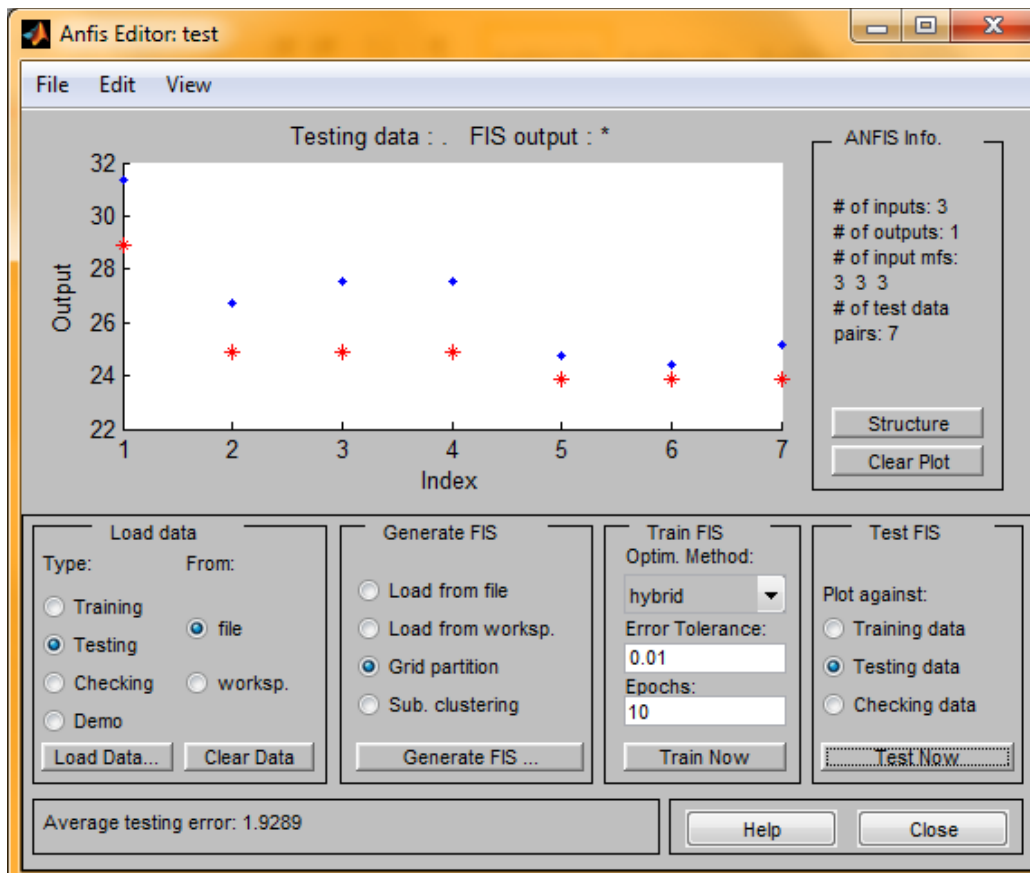


Figure 5.139 Distribution of predicted and actual data (Testing)

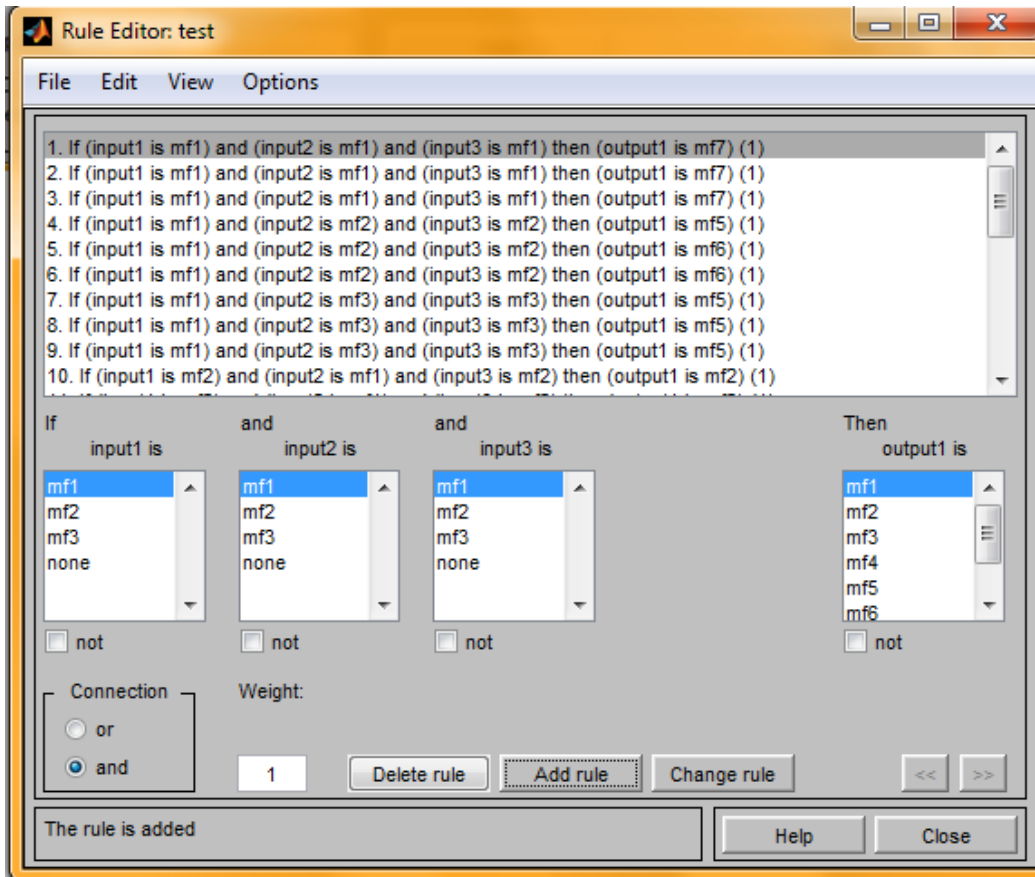


Figure 5.140 Rule editor

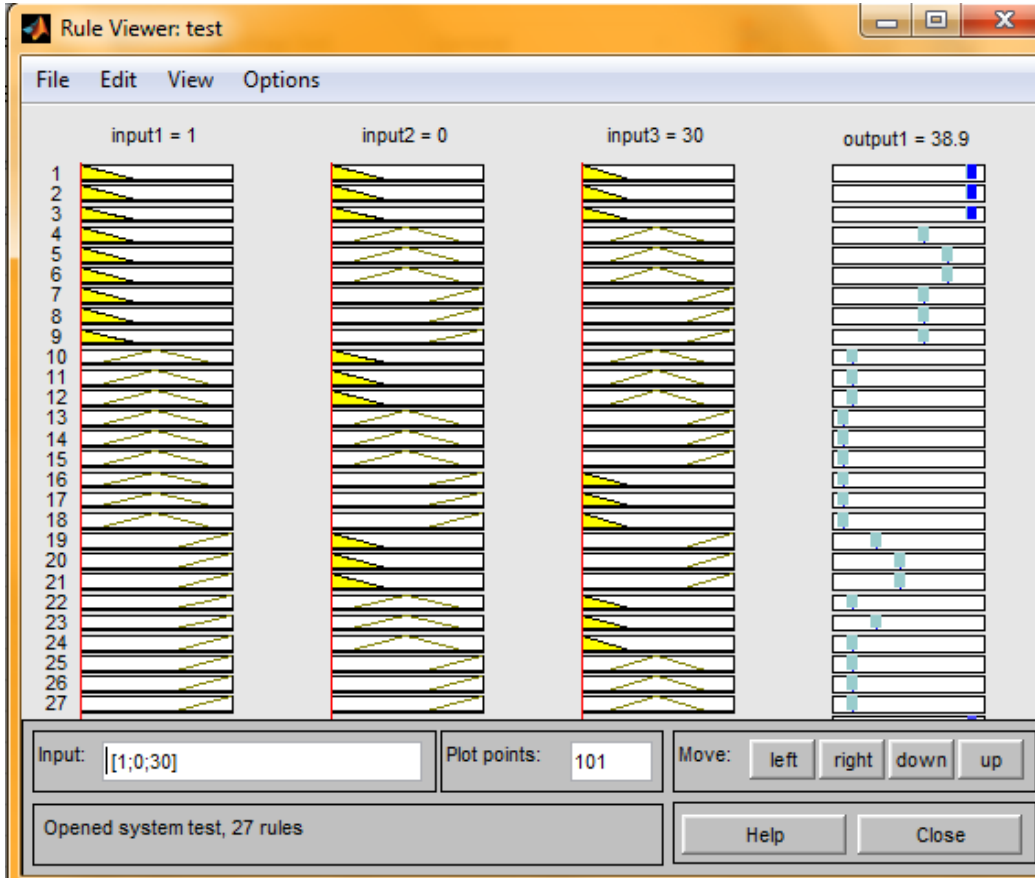


Figure 5.141 Rule viewer

The input and output experimental value with ANFIS predicted value of HAp/PC composite at 500 micron size for training purpose is shown in Table 5.53.

Table 5.53 Input and output data with ANFIS predicted value of HAp/PC composite at 500 micron size

No.	Factor A Pressure (Bar)	Factor B HAp volume (%)	Factor C Impingement angle (Degree)	Wear Loss (gm)	S/N ratio of Exp. value	ANFIS output predicted value
1	1	0	30	0.012	38.416	38.9
2	1	0	30	0.010	40.000	38.9
3	1	0	30	0.009	40.915	38.9
4	1	10	45	0.015	36.478	34.9
5	1	10	45	0.013	37.721	34.9
6	1	10	45	0.011	39.172	34.9
7	1	20	60	0.019	34.424	32.9
8	1	20	60	0.018	34.894	32.9
9	1	20	60	0.021	33.555	32.9
10	2	0	45	0.061	24.293	23.9
11	2	0	45	0.059	24.582	23.9
12	2	0	45	0.057	24.882	23.9
13	2	10	60	0.063	24.013	22.9
14	2	10	60	0.062	24.152	22.9
15	2	10	60	0.060	24.436	22.9
16	2	20	30	0.071	22.974	22.9
17	2	20	30	0.069	23.223	22.9
18	2	20	30	0.066	23.609	22.9
19	3	0	60	0.030	30.457	28.9
20	3	0	60	0.026	31.700	28.9

The input and output data with ANFIS predicted value of HAp/PC composite at 500 micron size for testing purpose is shown in Table 5.54.

Table 5.54 Input and output data with ANFIS predicted value of HAp/PC composite at 500 micron size

No.	Factor A Pressure (Bar)	Factor B HAp volume (%)	Factor C Impingement angle (Degree)	Wear Loss (gm)	S/N ratio of Exp. value	ANFIS output predicted value
1	3	0	60	0.027	31.372	28.9
2	3	10	30	0.046	26.744	24.9
3	3	10	30	0.042	27.535	24.9
4	3	10	30	0.042	27.535	24.9
5	3	20	45	0.058	24.731	23.9
6	3	20	45	0.060	24.436	23.9
7	3	20	45	0.055	25.192	23.9

By calculating we get the mean relative percentage error for training and testing of HAp/PC composite conducted at 500 micron size is 4.34% and 6.37% respectively.

### 5.2.2.1.6 Adaptive neuro fuzzy inference system (ANFIS) methodology used for HAp/PSU composite (at 500 micron size)

The membership function editor for output parameter of HAp/PSU composite at 500 micron size is shown in Figure 5.142.

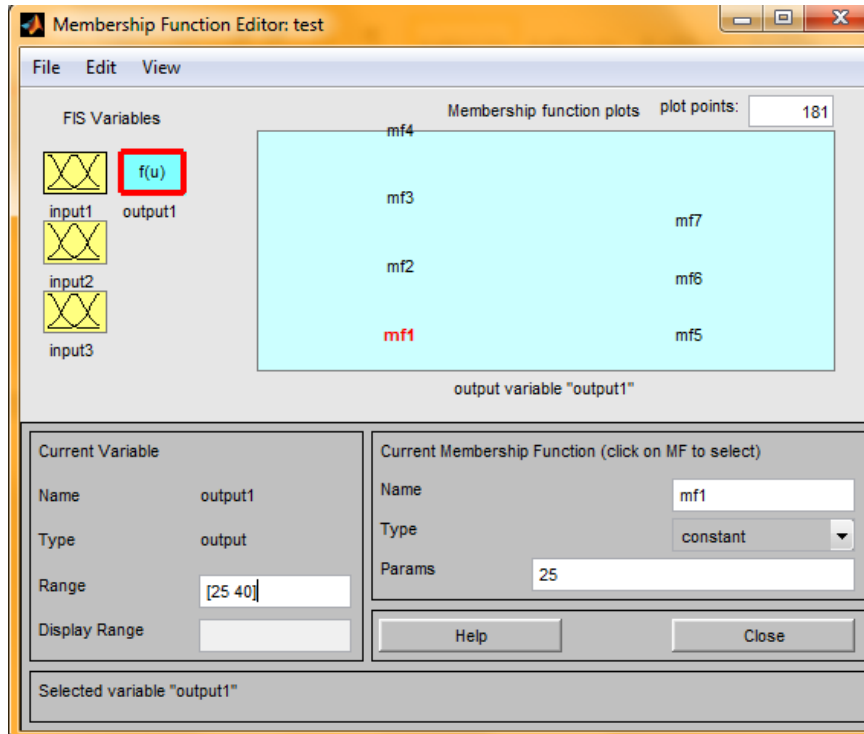


Figure 5.142 Membership function editor for output of HAp/PSU composite

The ANFIS editor for both training and testing data, rule editor and rule viewer of HAp/PSU composite are shown in Figure 5.143 to Figure 5.146 respectively.

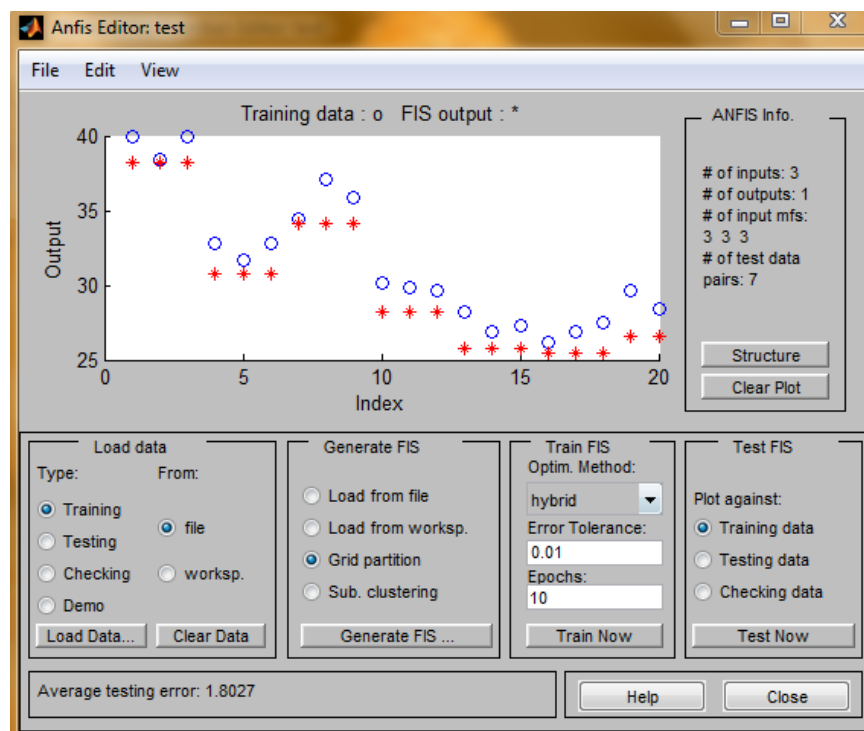


Figure 5.143 Distribution of predicted and actual data (Training)

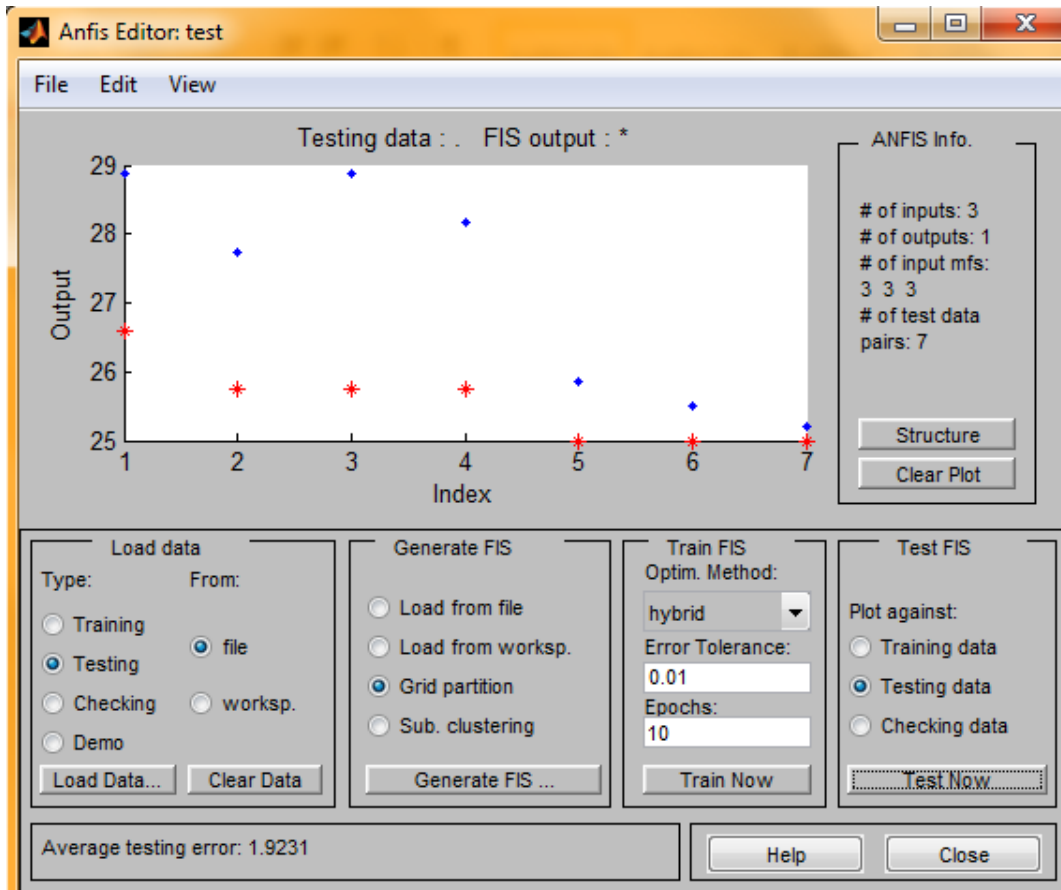


Figure 5.144 Distribution of predicted and actual data (Testing)

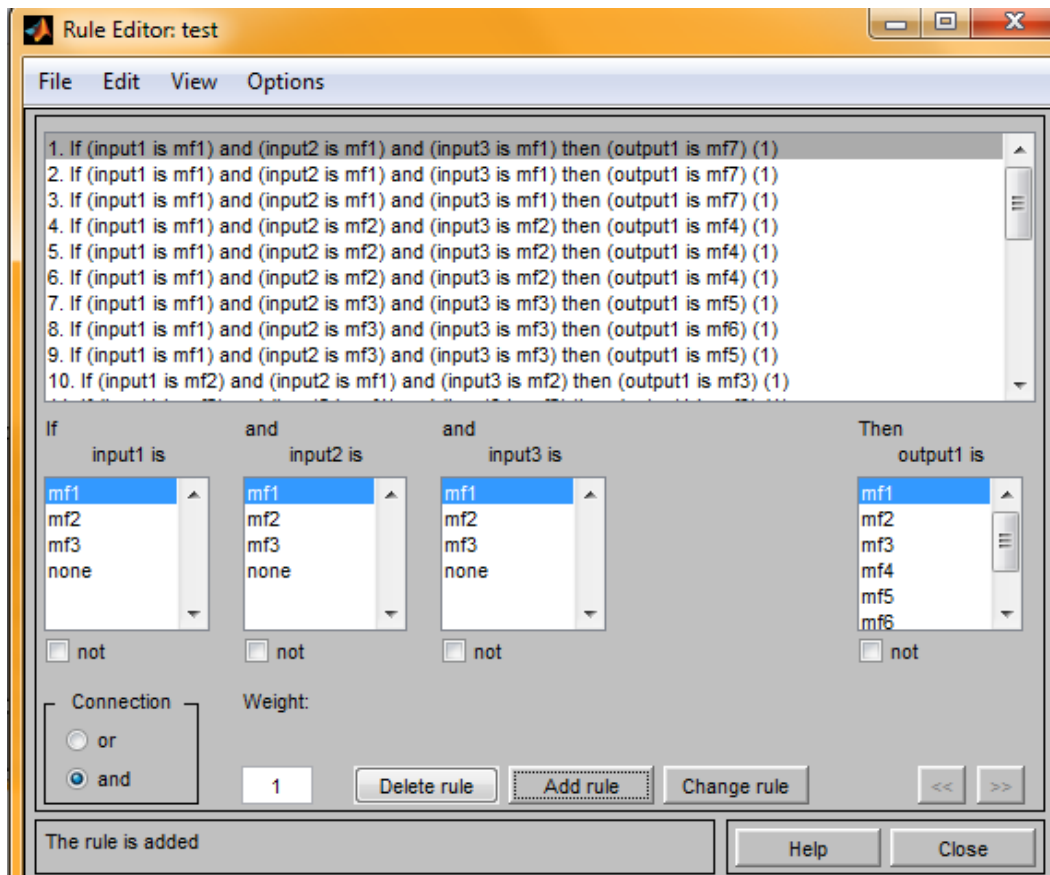


Figure 5.145 Rule editor

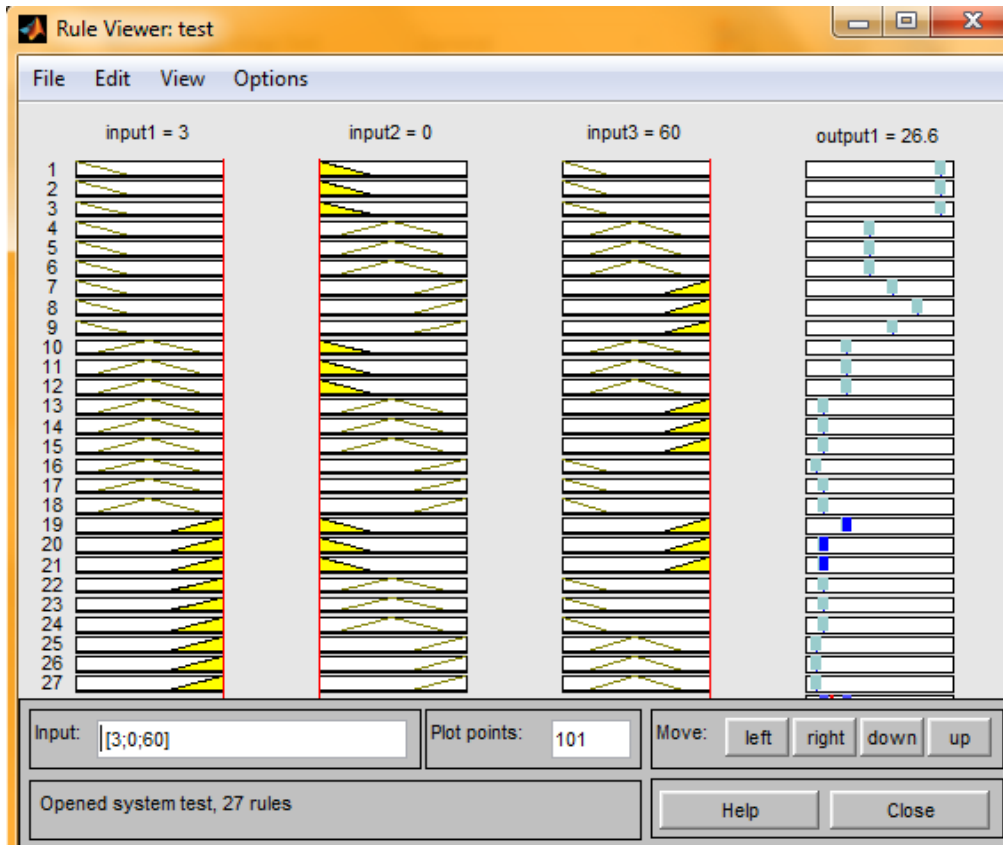


Figure 5.146 Rule viewer

The input and output experimental value with ANFIS predicted value of HAp/PSU composite at 500 micron size for training purpose is shown in Table 5.55.

Table 5.55 Input and output data with ANFIS predicted value of HAp/PSU composite at 500 micron size

No.	Factor A Pressure (Bar)	Factor B HAp volume (%)	Factor C Impingement angle (Degree)	Wear Loss (gm)	S/N ratio of Exp. value	ANFIS output predicted value
1	1	0	30	0.010	40.000	38.25
2	1	0	30	0.012	38.416	38.25
3	1	0	30	0.010	40.000	38.25
4	1	10	45	0.023	32.765	30.75
5	1	10	45	0.026	31.700	30.75
6	1	10	45	0.023	32.765	30.75
7	1	20	60	0.019	34.424	34.0833
8	1	20	60	0.014	37.077	34.0833
9	1	20	60	0.016	35.917	34.0833
10	2	0	45	0.031	30.172	28.25
11	2	0	45	0.032	29.897	28.25
12	2	0	45	0.033	29.629	28.25
13	2	10	60	0.039	28.178	25.75
14	2	10	60	0.045	26.935	25.75
15	2	10	60	0.043	27.330	25.75
16	2	20	30	0.049	26.196	25.5
17	2	20	30	0.045	26.935	25.5
18	2	20	30	0.042	27.535	25.5
19	3	0	60	0.033	29.629	26.5833
20	3	0	60	0.038	28.404	26.5833



The input and output data with ANFIS predicted value of HAp/PSU composite at 500 micron size for testing purpose is shown in Table 5.56.

Table 5.56 Input and output data with ANFIS predicted value of HAp/PSU composite at 500 micron size

No.	Factor A Pressure (Bar)	Factor B HAp volume (%)	Factor C Impingement angle (Degree)	Wear Loss (gm)	S/N ratio of Exp. value	ANFIS output predicted value
1	3	0	60	0.036	28.873	26.5833
2	3	10	30	0.041	27.744	25.75
3	3	10	30	0.036	28.873	25.75
4	3	10	30	0.039	28.178	25.75
5	3	20	45	0.051	25.848	25
6	3	20	45	0.053	25.514	25
7	3	20	45	0.055	25.192	25

By calculating we get the mean relative percentage error for training and testing of HAp/PSU composite conducted at 500 micron size is 5.30% and 5.80% respectively.

### 5.2.2.2 Worn surface morphology

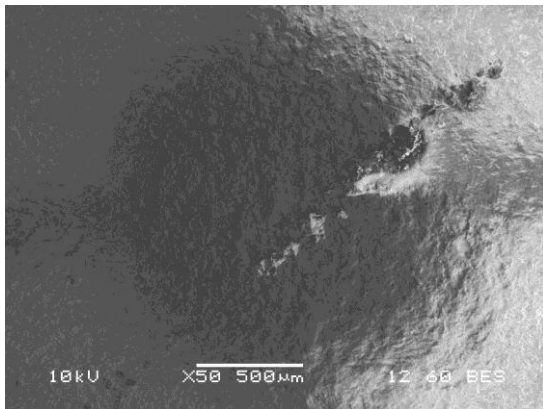


Figure 5.147 Wear of 0 vol. % HAp/PC (x50)

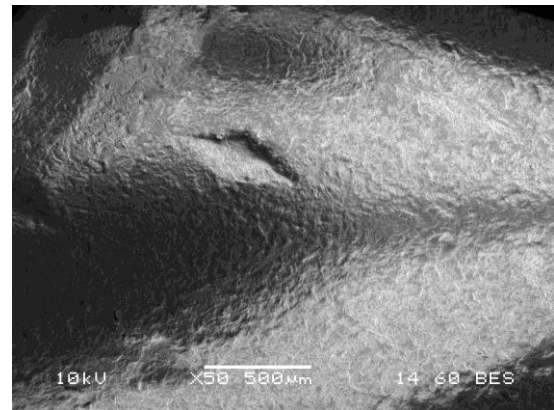


Figure 5.148 Wear of 10 vol. % HAp/PC (x50)

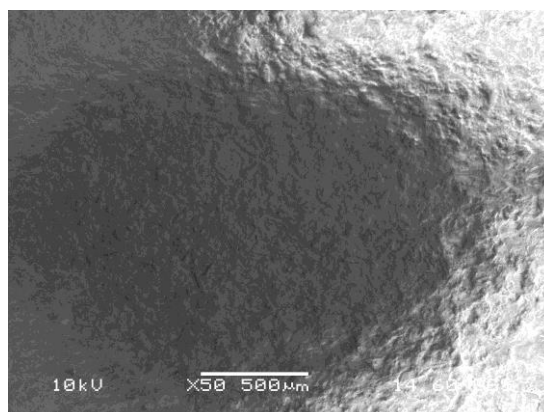


Figure 5.149 Wear of 20 vol. % HAp/PC (x50)

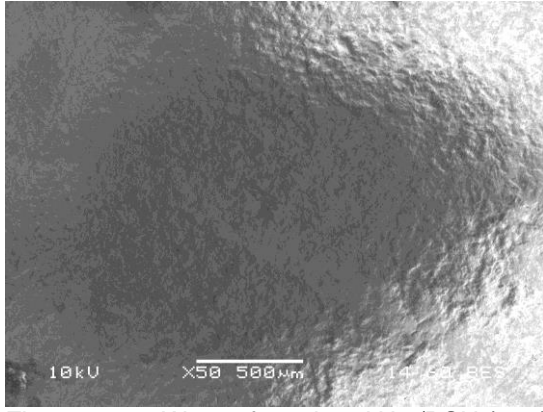


Figure 5.150 Wear of 0 vol. % HAp/PSU (x50)

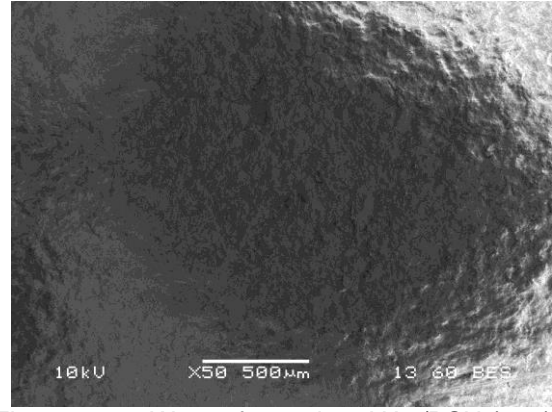


Figure 5.151 Wear of 10 vol. % HAp/PSU (x50)

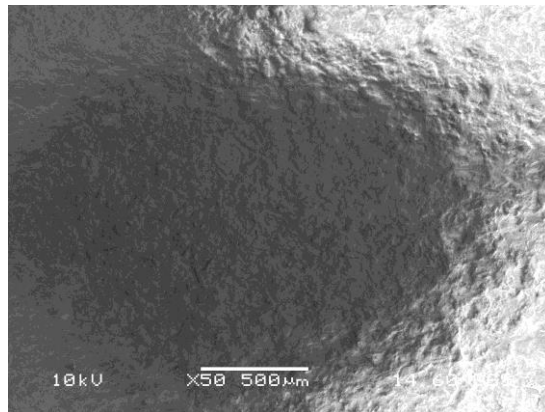


Figure 5.152 Wear of 20 vol. % HAp/PSU (x50)

SEM images of worn surfaces of both HAp/PC and HAp/PSU composite samples is shown from Figure 5.147 to Figure 5.152. According to Figure 5.147 to Figure 5.152, it is clearly shown that as HAp volume increases from 0 vol. % to 20 vol. %, wear also increases due to HAp particles increases in the polymer matrix. When HAp volume is 0 vol. %, no scratches or wear found in the polymer matrix due to absence of the HAp particles. When HAp volume is 10 vol. %, small scratches are generated due to less amount of HAp particles. But, when, HAp volume is 20 vol. %, more scratches or wear occurs in the polymer matrix.

### 5.2.3 Experimental details of sliding wear behavior of ceramic composites

(According to Galetz et al. [168]) The sliding wear test of ceramic composites was performed on ball on plate wear tester (Model No. TR-208-M1, DUCOM, Bangalore) (ASTM G194) is shown in Figure 5.153. The Diamond indenter is used in this test for indentation in the surface of the composite samples. Taguchi's  $L_{27}$  design was used to evaluate the tribological properties with three control variables such as HAp volume, load applied, and sliding speed each at three levels.



Figure 5.153 Ball on plate wear tester

The selected input parameters and their levels are shown in Table 5.57.

Table 5.57 Control parameters and their levels

S.No.	Factors	Symbol	Levels			Unit
			1	2	3	
1.	HAp volume	A	0	10	20	%
2.	Load applied	B	10	20	30	N
3.	Sliding speed	C	10	15	20	RPM

The experimental data for HAp/PC composite are shown in Table 5.58.

Table 5.58 Experimental data for HAp/PC composite

Exp. No.	Factor A HAp Volume (%)	Factor B Load applied (N)	Factor C Sliding speed (rpm)	Sliding wear loss (gm)	S/N ratio (Lower The Better)
1	0	10	10	0.006	44.436
2	0	10	10	0.007	43.098
3	0	10	10	0.006	44.436
4	0	20	15	0.008	41.938
5	0	20	15	0.007	43.098
6	0	20	15	0.009	40.915
7	0	30	20	0.010	40.000
8	0	30	20	0.011	39.172
9	0	30	20	0.009	40.915
10	10	10	15	0.005	46.020
11	10	10	15	0.006	44.436
12	10	10	15	0.007	43.098
13	10	20	20	0.008	41.938
14	10	20	20	0.007	43.098
15	10	20	20	0.006	44.436
16	10	30	10	0.009	40.915
17	10	30	10	0.011	39.172
18	10	30	10	0.010	40.000
19	20	10	20	0.006	44.436
20	20	10	20	0.007	43.098
21	20	10	20	0.006	44.436
22	20	20	10	0.009	40.915
23	20	20	10	0.010	40.000
24	20	20	10	0.008	41.938
25	20	30	15	0.011	39.172
26	20	30	15	0.012	38.416
27	20	30	15	0.013	37.721

The ANOVA Table for HAp/PC composite are shown in Table 5.59.

Table 5.59 ANOVA Table for S/N ratio of HAp/PC composite

Source	DF value	Seq SS	Adj SS	Adj MS	F value	P value
A	2	9.504	9.504	4.752	5.19	0.015
B	2	98.288	98.288	49.144	53.72	0.000
C	2	3.293	3.293	1.647	1.80	0.191
Error	20	18.297	18.297	0.915		
Total	26	129.382				

S = 0.956475, R-Sq = 85.86%, and R-Sq(adj) = 81.62%

It can be concluded here that significance of factors is in the order of Factor B, A and C.

Main effects plot for means of S/N ratio, normal probability plot and interaction plot are shown in Figure 5.154, 5.155 and 5.156 respectively.

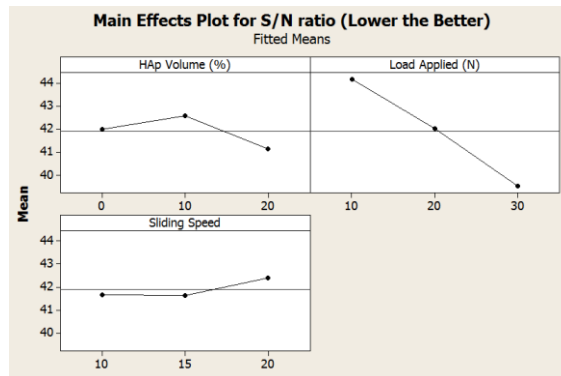


Figure 5.154 Main effects plot for means of S/N ratio

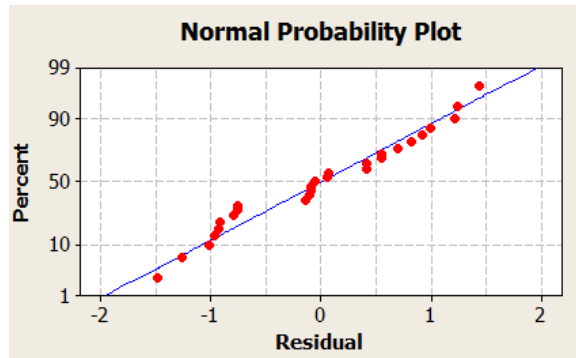


Figure 5.155 Normal probability plot for S/N ratio

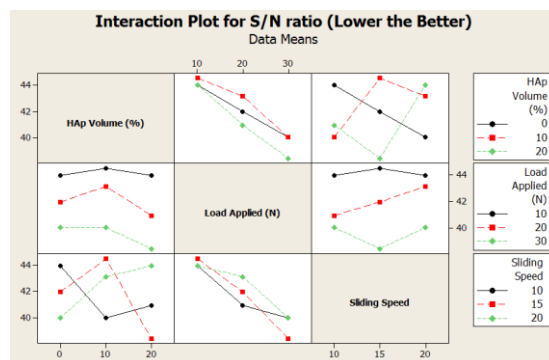


Figure 5.156 Interaction plot for S/N ratio

According to Figure 5.154, it is concluded that the optimal parametric combination is  $A_2B_1C_3$ . When HAp volume is 10 vol. %, load applied is 10 N, and sliding speed is 20 RPM then minimum sliding wear can be obtained. Referring to Figure 5.155, it can be concluded that the ANOVA proceeds in a satisfactory manner as the residuals follow a normal distribution. Figure 5.156 shows that two factor interaction of controllable factors seems to exist. However, the interaction of factors has not been considered for the sake of simplicity.

Similarly, the experimental data for HAp/PSU composite are shown in Table 5.60.

Table 5.60 Experimental data for HAp/PSU composite

Experiment No.	Factor A HAp Volume (%)	Factor B Load applied (N)	Factor C Sliding speed (rpm)	Sliding wear loss (gm)	S/N ratio (Lower The Better)
1	0	10	10	0.004	47.958
2	0	10	10	0.005	46.020
3	0	10	10	0.003	50.457
4	0	20	15	0.006	44.436
5	0	20	15	0.007	43.098
6	0	20	15	0.006	44.436
7	0	30	20	0.008	41.938
8	0	30	20	0.007	43.098
9	0	30	20	0.008	41.938
10	10	10	15	0.005	46.020
11	10	10	15	0.006	44.436
12	10	10	15	0.005	46.020
13	10	20	20	0.007	43.098
14	10	20	20	0.008	41.938
15	10	20	20	0.006	44.436
16	10	30	10	0.010	40.000
17	10	30	10	0.009	40.915
18	10	30	10	0.009	40.915
19	20	10	20	0.003	50.457
20	20	10	20	0.004	47.958
21	20	10	20	0.005	46.020
22	20	20	10	0.007	43.098
23	20	20	10	0.007	43.098
24	20	20	10	0.008	41.938
25	20	30	15	0.011	39.172
26	20	30	15	0.012	38.416
27	20	30	15	0.010	40.000

The ANOVA Table for HAp/PSU composite are shown in Table 5.61.

Table 5.61 ANOVA Table for S/N ratio of HAp/PSU composite

Source	DF value	Seq SS	Adj SS	Adj MS	F value	P value
A	2	15.699	15.699	7.849	4.80	0.020
B	2	196.021	196.021	98.010	59.92	0.000
C	2	12.312	12.312	6.156	3.76	0.041
Error	20	32.712	32.712	1.636		
Total	26	256.744				

$S = 1.27891$ ,  $R\text{-Sq} = 87.26\%$ , and  $R\text{-Sq}(\text{adj}) = 83.44\%$

It can be concluded here that significance of factors is in the order of Factor B, A and C.

Main effects plot for means of S/N ratio, normal probability plot and interaction plot are shown in Figure 5.157, 5.158 and 5.159 respectively.

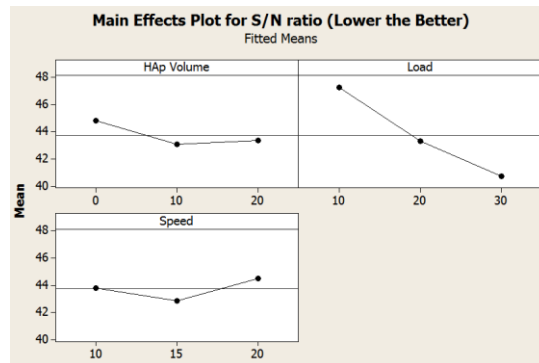


Figure 5.157 Main effects plot for means of S/N ratio

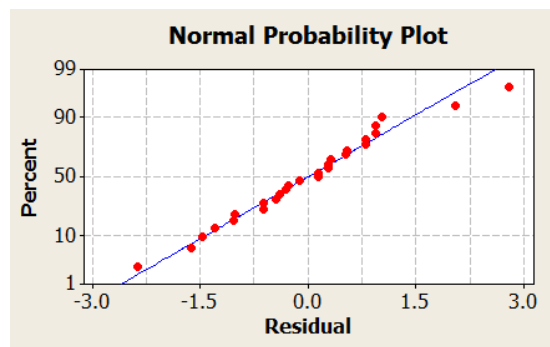


Figure 5.158 Normal probability plot for S/N ratio

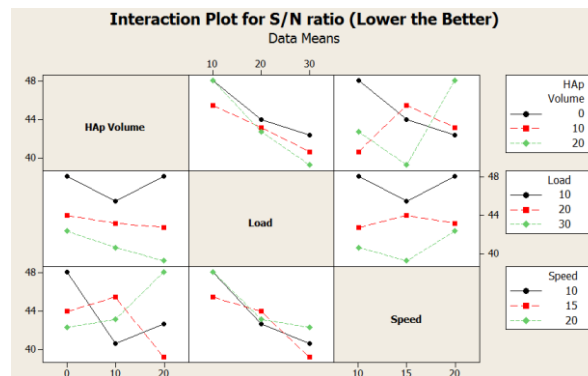


Figure 5.159 Interaction plot for S/N ratio

According to Figure 5.157, it is concluded that the optimal parametric combination is  $A_1B_1C_3$ . When HAp volume is 0 vol. %, load applied is 10 N, and sliding speed is 20 RPM then minimum sliding wear can be obtained. Referring to Figure 5.158, it can be concluded that the ANOVA proceeds in a satisfactory manner as the residuals follow a normal distribution. Figure 5.159 shows that two factor interaction of controllable factors seems to exist. However, the interaction of factors has not been considered for the sake of simplicity.

### 5.2.3.1 Prediction of sliding wear behaviour of composites

#### 5.2.3.1.1 Adaptive neuro fuzzy inference system (ANFIS) methodology used for HAp/PC composite

The FIS editor for input parameters of both HAp/PC and HAp/PSU composites, and membership function editor for output parameter of HAp/PC composite are shown in Figure 5.160 to Figure 5.164 respectively.

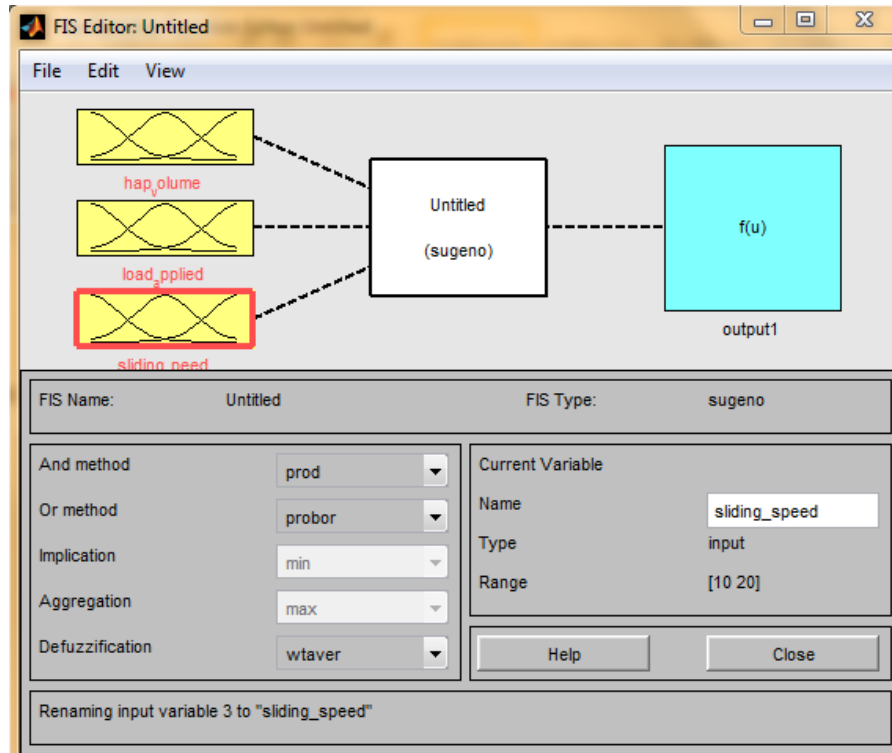


Figure 5.160 FIS editor

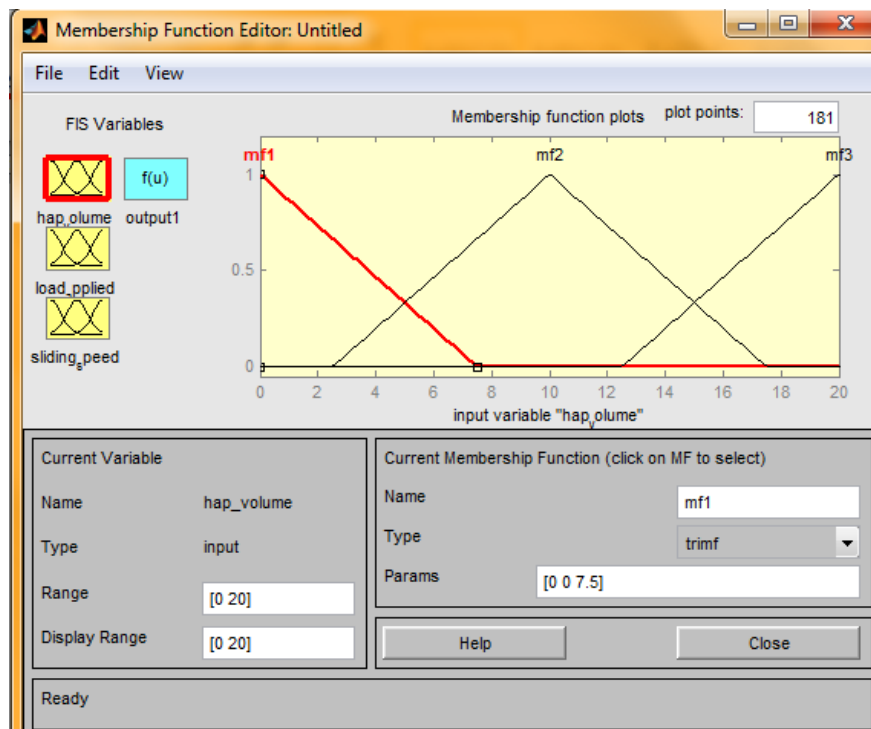


Figure 5.161 Membership function editor of Input 1

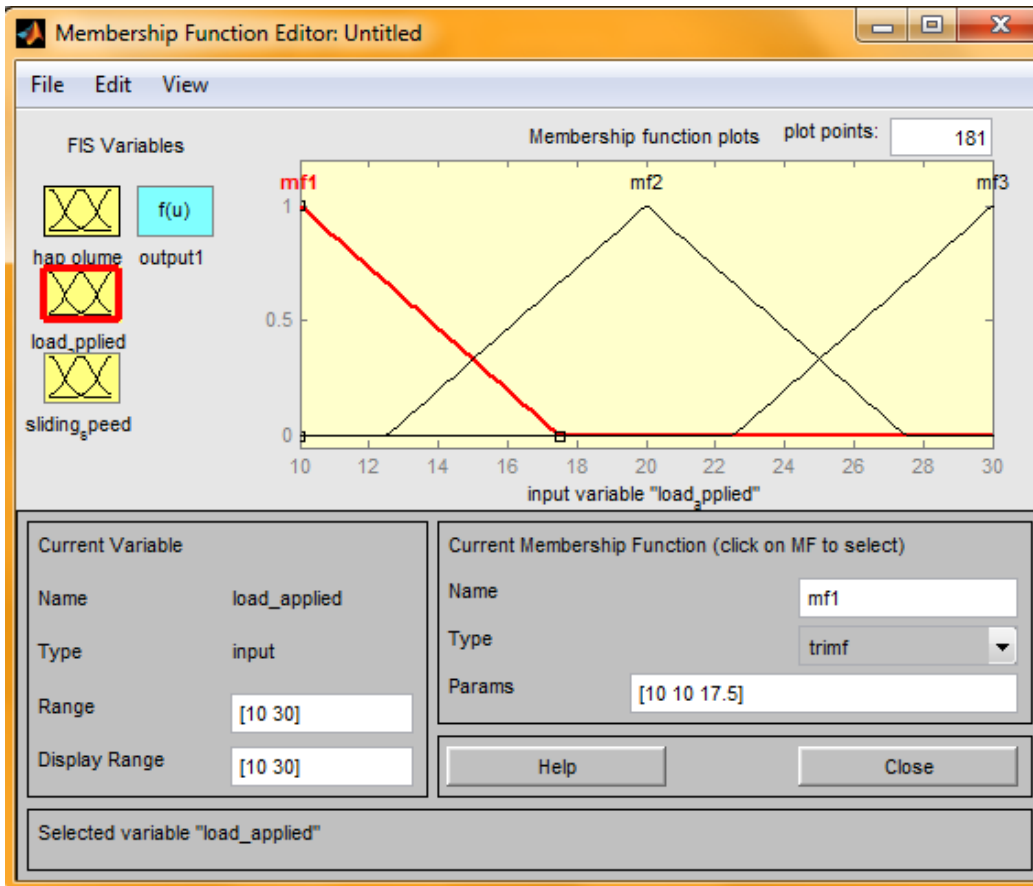


Figure 5.162 Membership function editor of Input 2

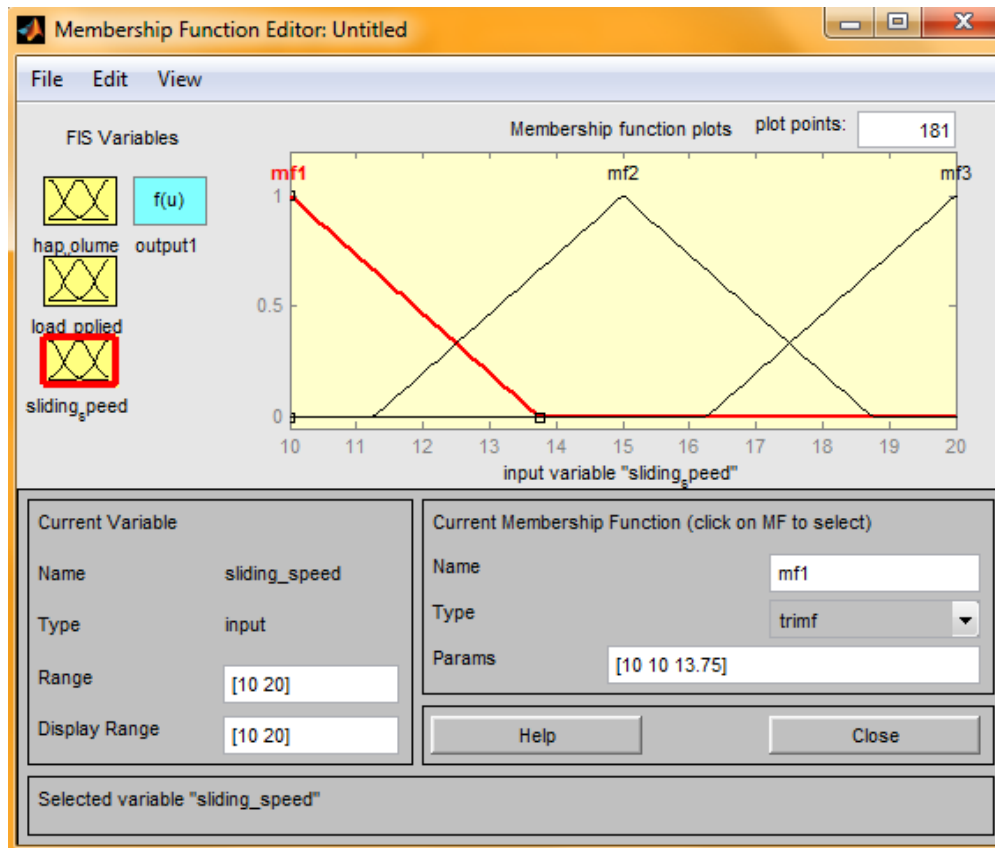


Figure 5.163 Membership function editor of Input 3



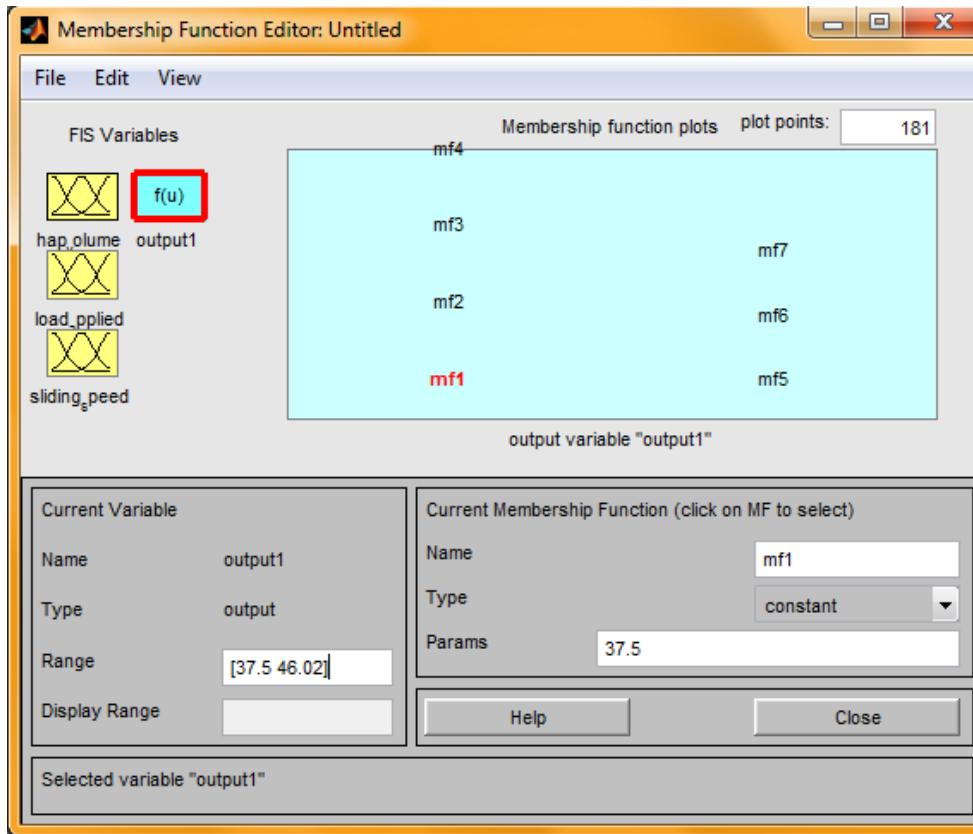


Figure 5.164 Membership function editor for output of HAP/PC composite

The ANFIS model structure of HAP/PC and HAP/PSU composites regarding sliding wear, while ANFIS editor for both training and testing data, rule editor and rule viewer of HAP/PC composite are shown in Figure 5.165 to Figure 5.169 respectively.

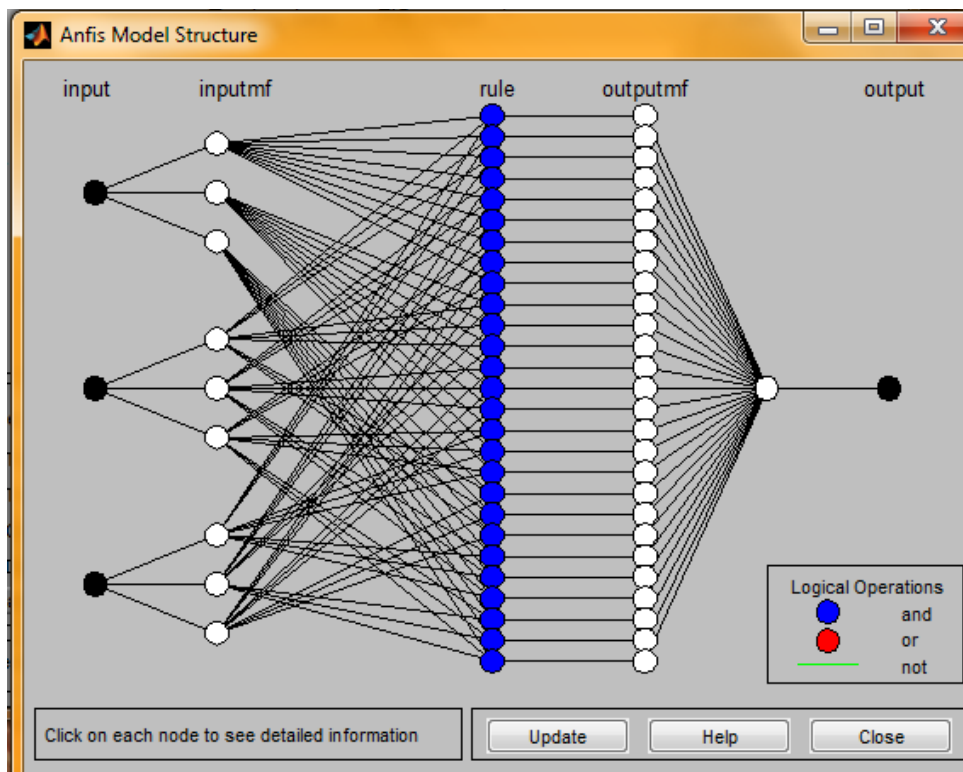


Figure 5.165 ANFIS model structure

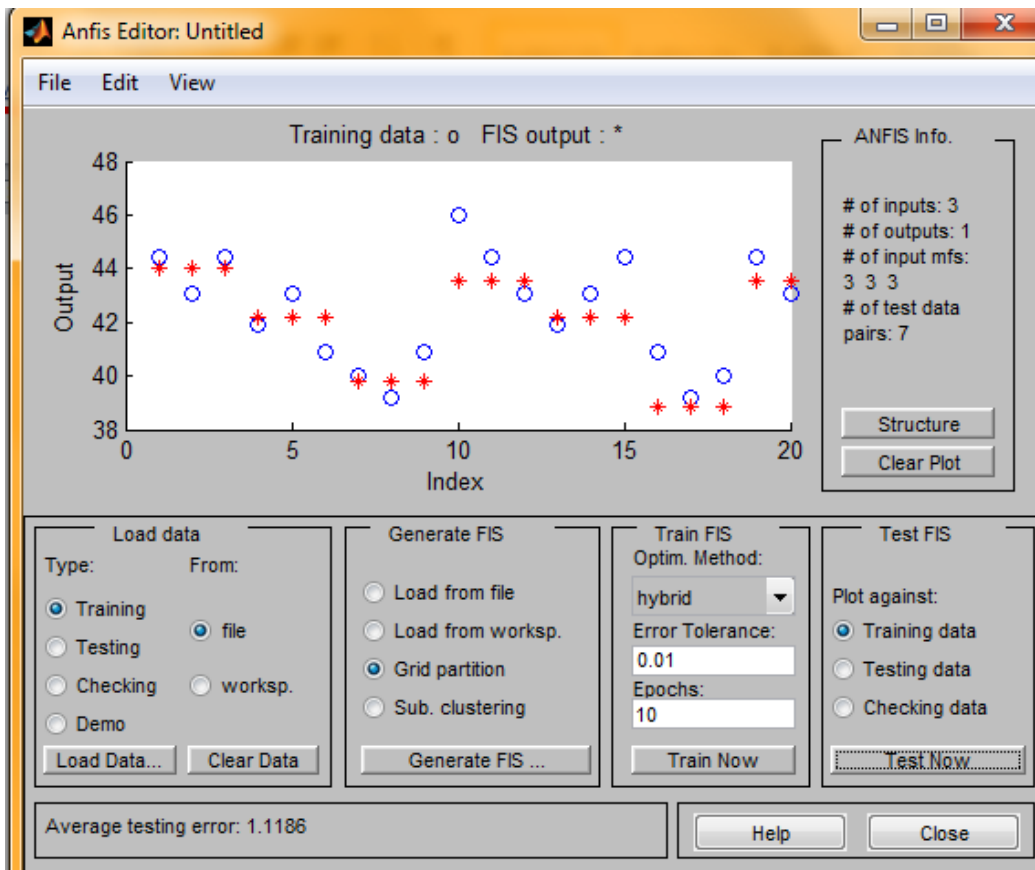


Figure 5.166 Distribution of predicted and actual data (Training)

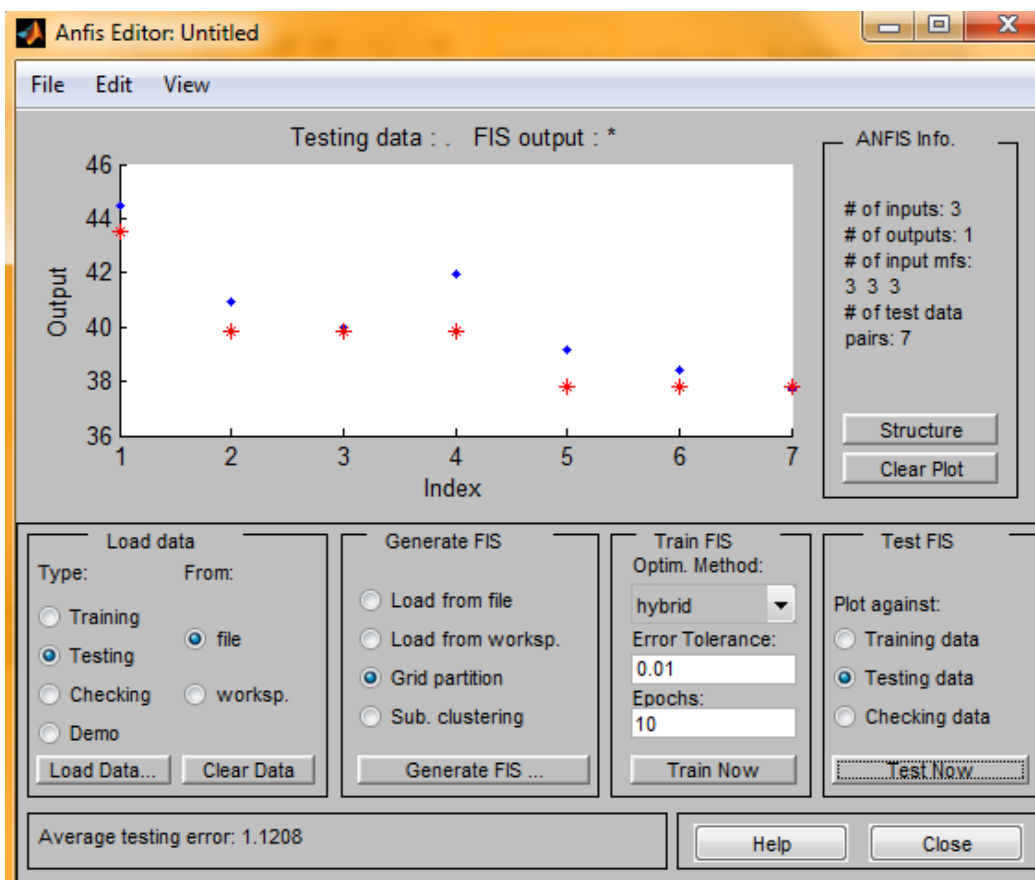


Figure 5.167 Distribution of predicted and actual data (Testing)

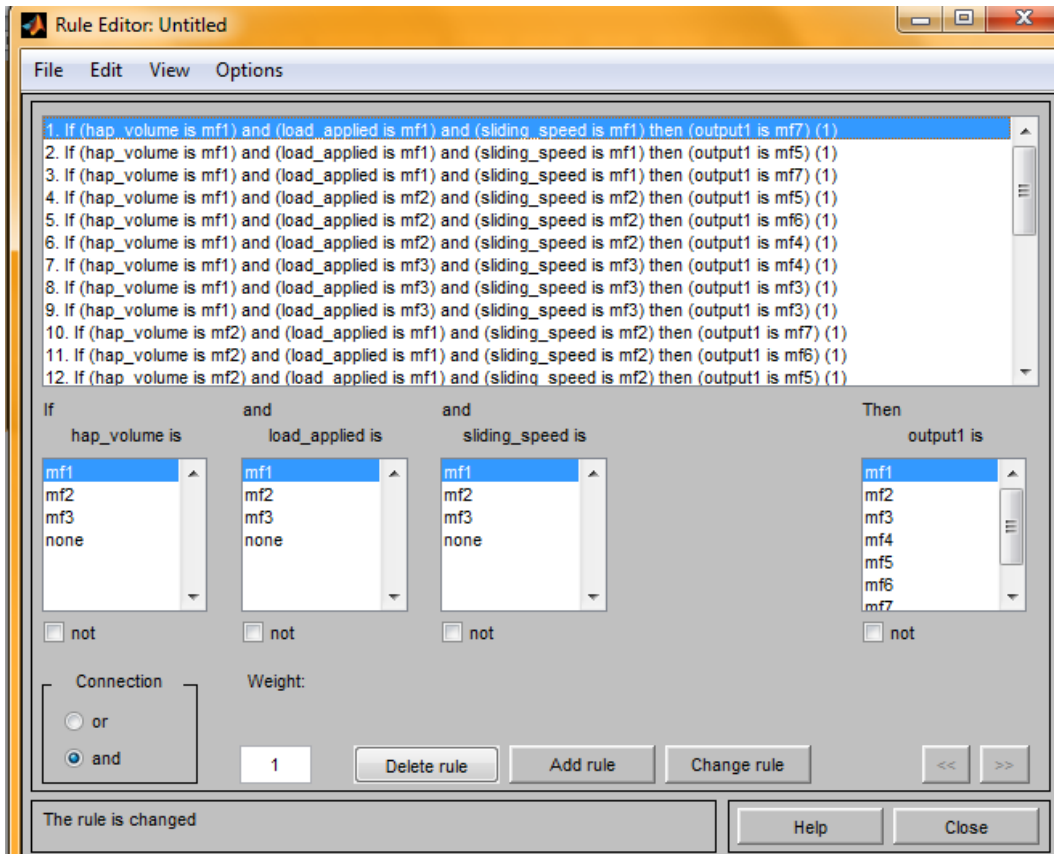


Figure 5.168 Rule editor

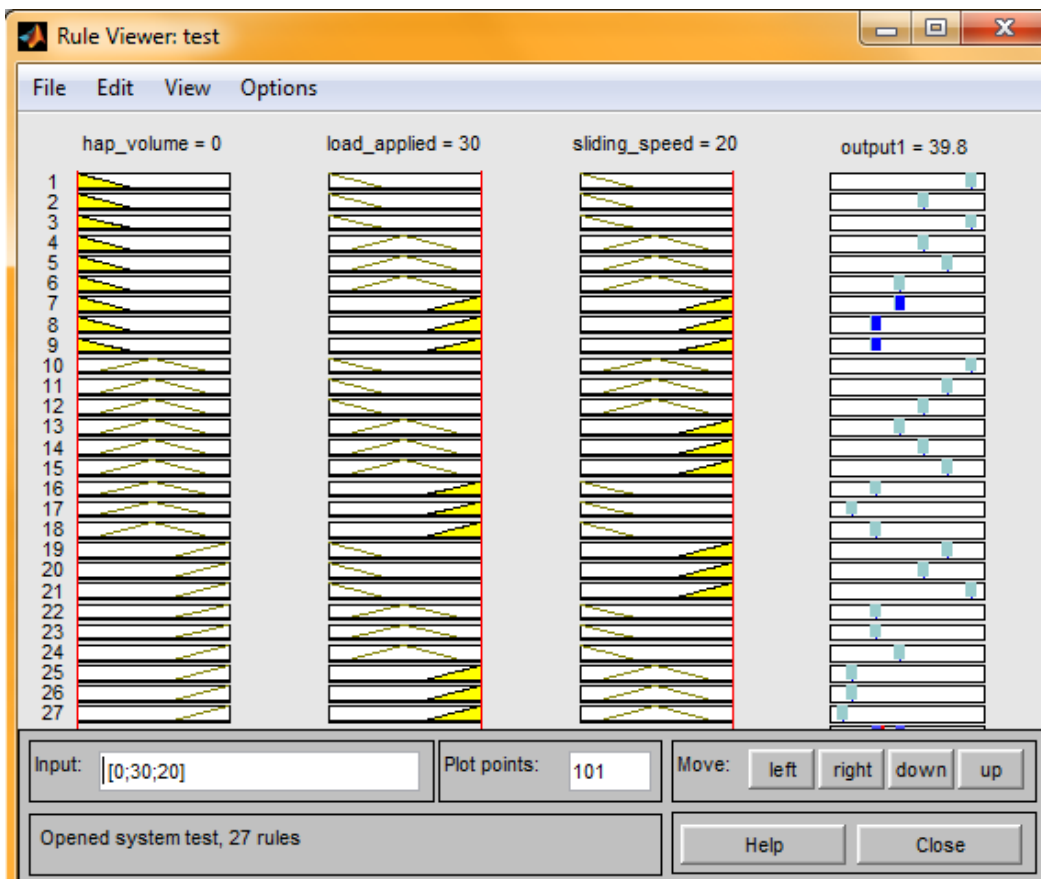


Figure 5.169 Rule viewer

The input and output experimental value with ANFIS predicted value of HAp/PC composite for training purpose is shown in Table 5.62.

Table 5.62 Input and output data with ANFIS predicted value of HAp/PC composite

No.	Factor A HAp Volume (%)	Factor B Load applied (N)	Factor C Sliding speed (rpm)	Wear Loss (gm)	S/N ratio of Exp. value	ANFIS output predicted value
1	0	10	10	0.006	44.436	44.0167
2	0	10	10	0.007	43.098	44.0167
3	0	10	10	0.006	44.436	44.0167
4	0	20	15	0.008	41.938	42.15
5	0	20	15	0.007	43.098	42.15
6	0	20	15	0.009	40.915	42.15
7	0	30	20	0.010	40.000	39.8167
8	0	30	20	0.011	39.172	39.8167
9	0	30	20	0.009	40.915	39.8167
10	10	10	15	0.005	46.020	43.55
11	10	10	15	0.006	44.436	43.55
12	10	10	15	0.007	43.098	43.55
13	10	20	20	0.008	41.938	42.15
14	10	20	20	0.007	43.098	42.15
15	10	20	20	0.006	44.436	42.15
16	10	30	10	0.009	40.915	38.8833
17	10	30	10	0.011	39.172	38.8833
18	10	30	10	0.010	40.000	38.8833
19	20	10	20	0.006	44.436	43.55
20	20	10	20	0.007	43.098	43.55

The input and output data with ANFIS predicted value of HAp/PC composite for testing purpose is shown in Table 5.63.

Table 5.63 Input and output data with ANFIS predicted value of HAp/PC composite

No.	Factor A HAp Volume (%)	Factor B Load applied (N)	Factor C Sliding speed (rpm)	Wear Loss (gm)	S/N ratio of Exp. value	ANFIS output predicted value
1	20	10	20	0.006	44.436	43.55
2	20	20	10	0.009	40.915	39.8167
3	20	20	10	0.010	40.000	39.8167
4	20	20	10	0.008	41.938	39.8167
5	20	30	15	0.011	39.172	37.8
6	20	30	15	0.012	38.416	37.8
7	20	30	15	0.013	37.721	37.8

By calculating we get the mean relative percentage error for training and testing of HAp/PC composite is 2.12% and 2.22% respectively.

### 5.2.3.1.2 Adaptive neuro fuzzy inference system (ANFIS) methodology used for HAp/PSU composite

The membership function editor for output parameter of HAp/PSU composite is shown in Figure 5.170.

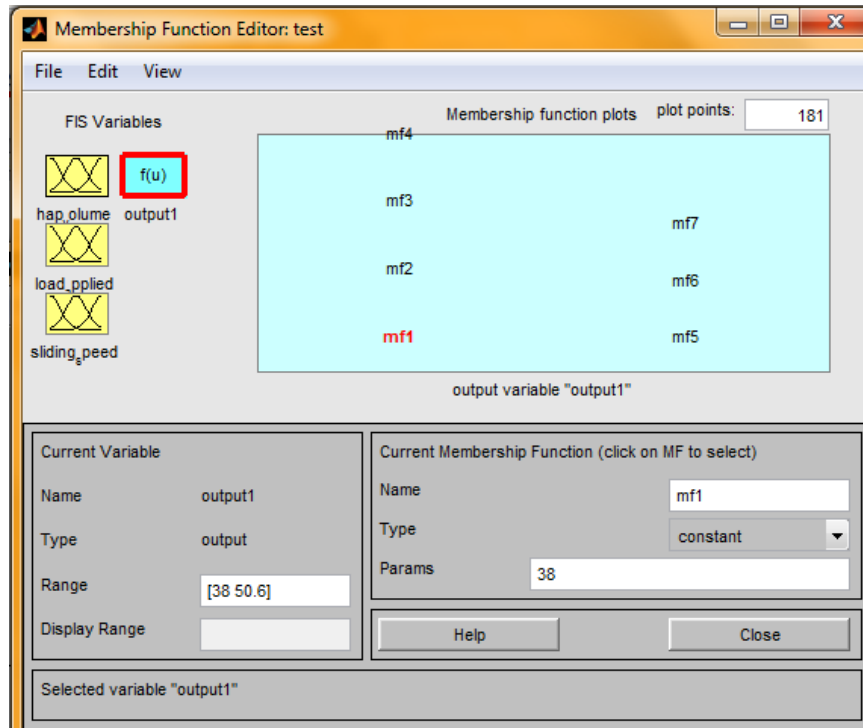


Figure 5.170 Membership function editor for output of HAp/PSU composite

The ANFIS editor for both training and testing data, rule editor and rule viewer of HAp/PSU composite are shown in Figure 5.171 to Figure 5.174 respectively.

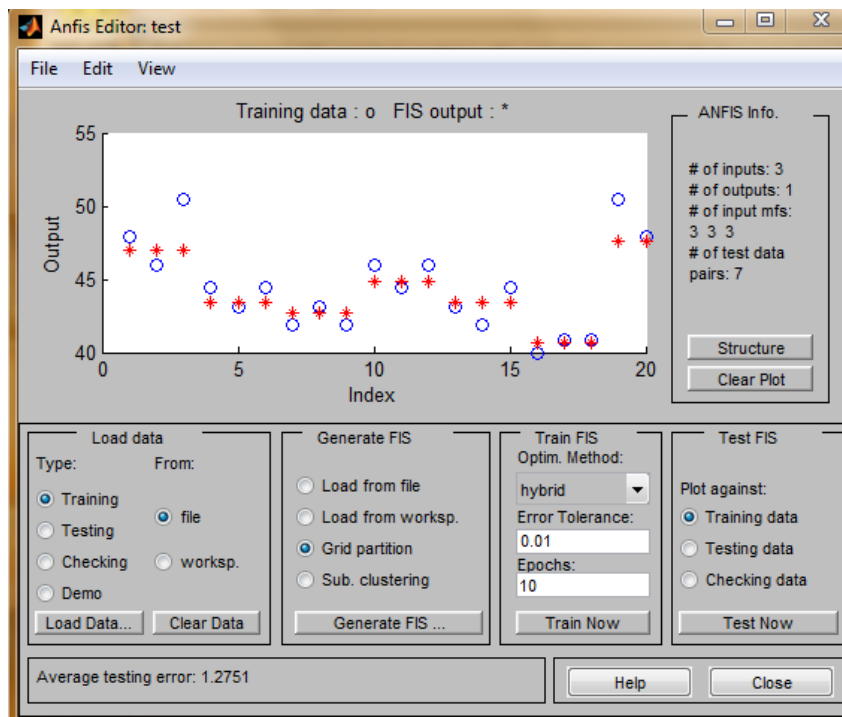


Figure 5.171 Distribution of predicted and actual data (Training)

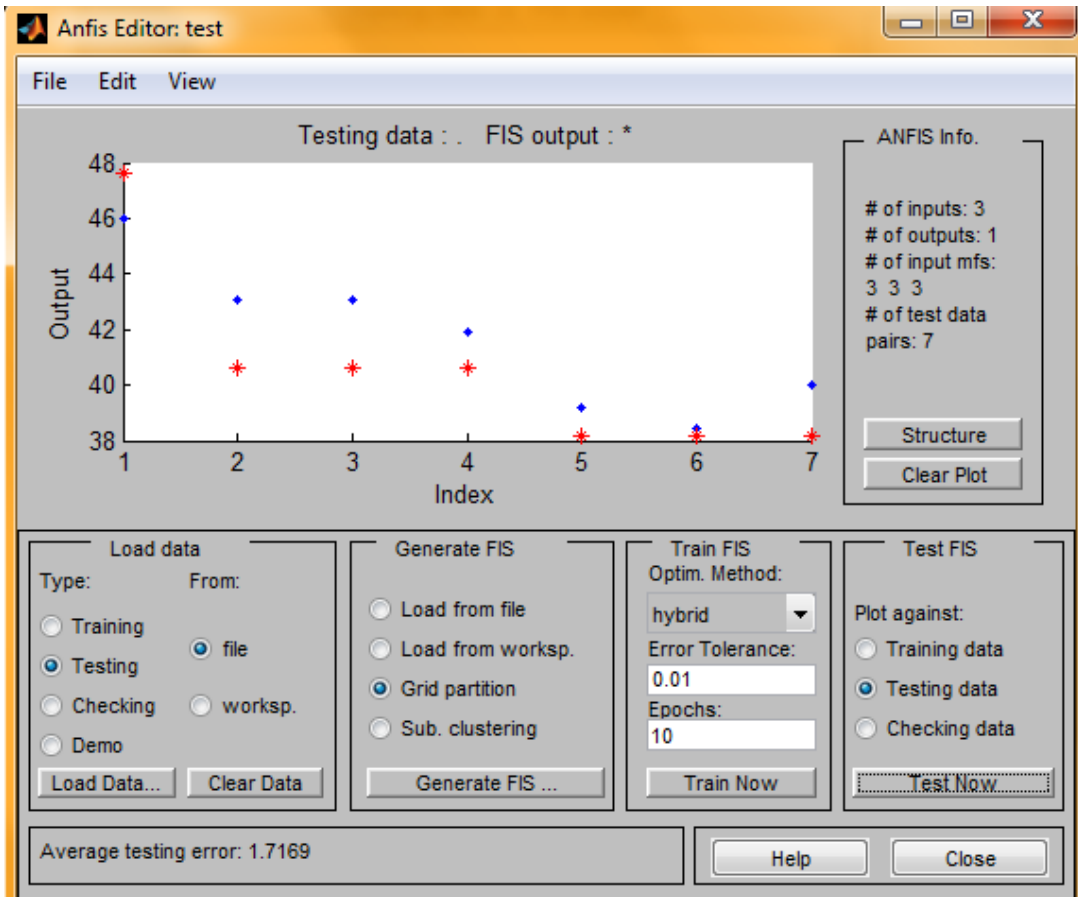


Figure 5.172 Distribution of predicted and actual data (Testing)

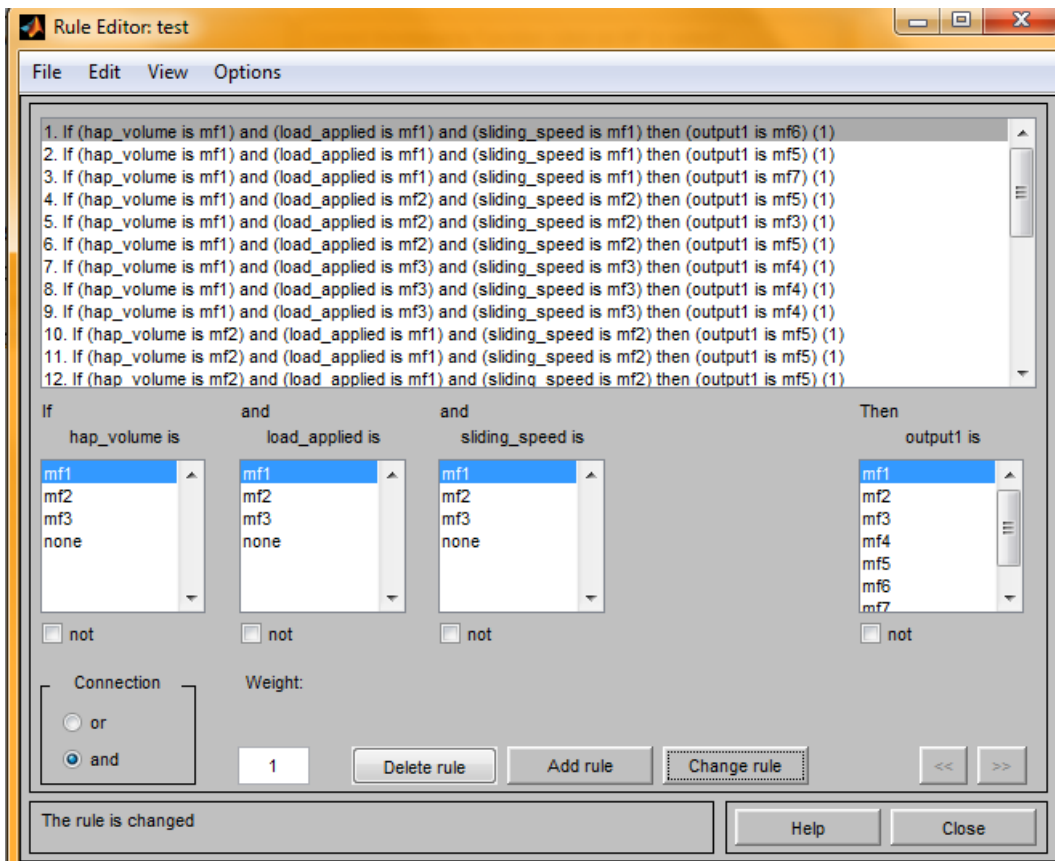


Figure 5.173 Rule editor

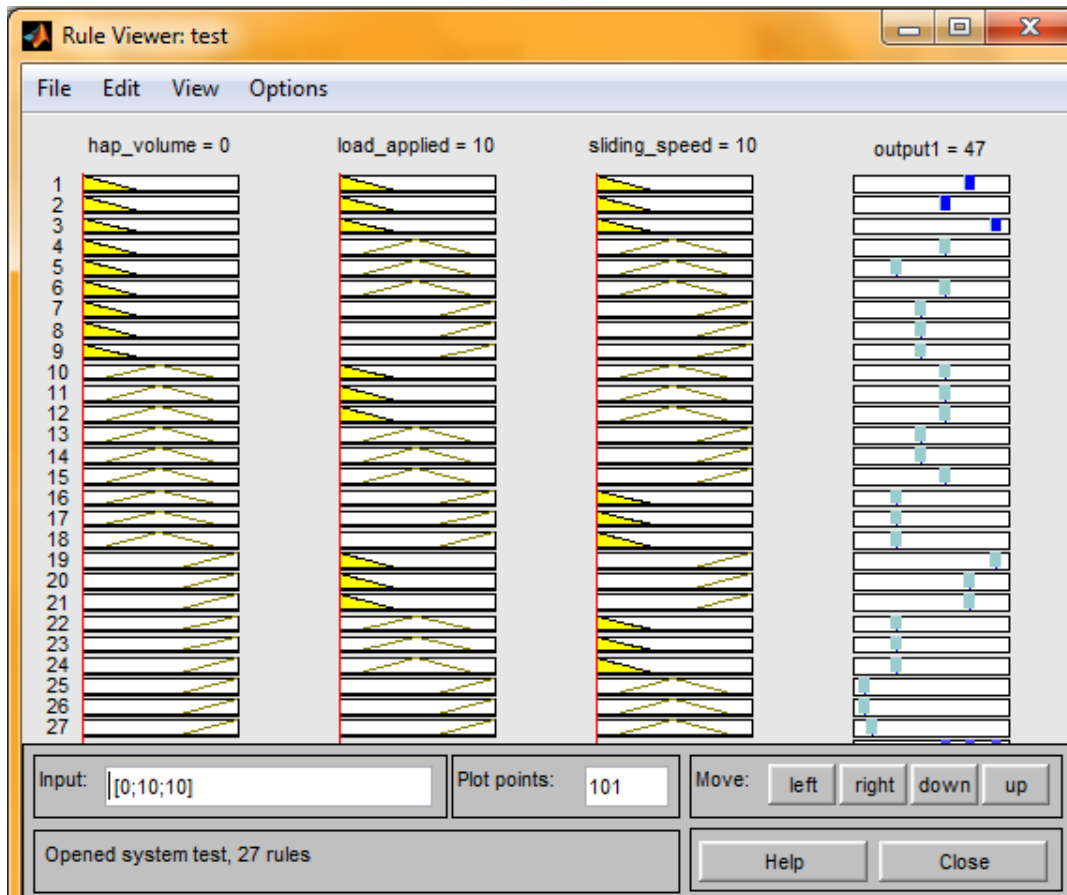


Figure 5.174 Rule viewer

The input and output experimental value with ANFIS predicted value of HAp/PSU composite for training purpose is shown in Table 5.64.

Table 5.64 Input and output data with ANFIS predicted value of HAp/PSU composite

No.	Factor A HAp Volume (%)	Factor B Load applied (N)	Factor C Sliding speed (rpm)	Wear Loss (gm)	S/N ratio of Exp. value	ANFIS output predicted value
1	0	10	10	0.004	47.958	46.95
2	0	10	10	0.005	46.020	46.95
3	0	10	10	0.003	50.457	46.95
4	0	20	15	0.006	44.436	43.45
5	0	20	15	0.007	43.098	43.45
6	0	20	15	0.006	44.436	43.45
7	0	30	20	0.008	41.938	42.75
8	0	30	20	0.007	43.098	42.75
9	0	30	20	0.008	41.938	42.75
10	10	10	15	0.005	46.020	44.85
11	10	10	15	0.006	44.436	44.85
12	10	10	15	0.005	46.020	44.85
13	10	20	20	0.007	43.098	43.45
14	10	20	20	0.008	41.938	43.45
15	10	20	20	0.006	44.436	43.45
16	10	30	10	0.010	40.000	40.65
17	10	30	10	0.009	40.915	40.65
18	10	30	10	0.009	40.915	40.65
19	20	10	20	0.003	50.457	47.65
20	20	10	20	0.004	47.958	47.65

The input and output data with ANFIS predicted value of HAp/PSU composite for testing purpose is shown in Table 5.65.

Table 5.65 Input and output data with ANFIS predicted value of HAp/PSU composite

No.	Factor A HAp Volume (%)	Factor B Load applied (N)	Factor C Sliding speed (rpm)	Wear Loss (gm)	S/N ratio of Exp. value	ANFIS output predicted value
1	20	10	20	0.005	46.020	47.65
2	20	20	10	0.007	43.098	40.65
3	20	20	10	0.007	43.098	40.65
4	20	20	10	0.008	41.938	40.65
5	20	30	15	0.011	39.172	38.1833
6	20	30	15	0.012	38.416	38.1833
7	20	30	15	0.010	40.000	38.1833

By calculating we get the mean relative percentage error for training and testing of HAp/PSU composite is 2.14% and 3.66% respectively.

### 5.2.3.2 Worn surface morphology

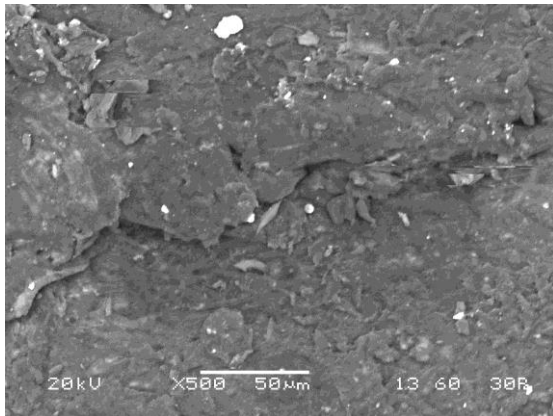


Figure 5.175 Wear of 0 vol. % HAp/PC (500x)

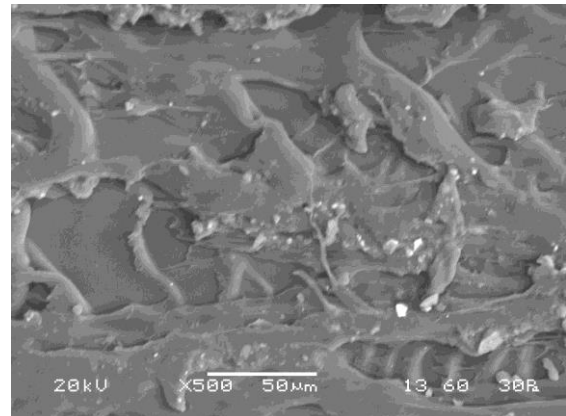


Figure 5.176 Wear of 10 vol. % HAp/PC (500x)

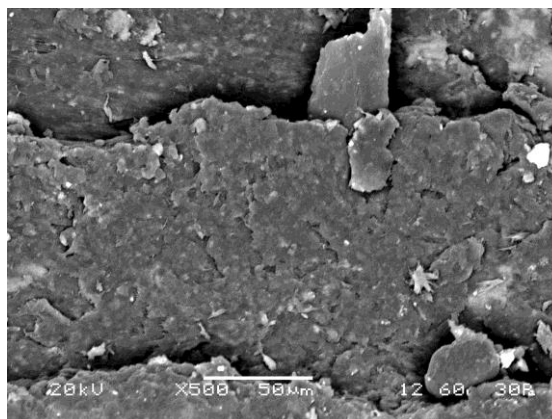


Figure 5.177 Wear of 20 vol. % HAp/PC (500x)



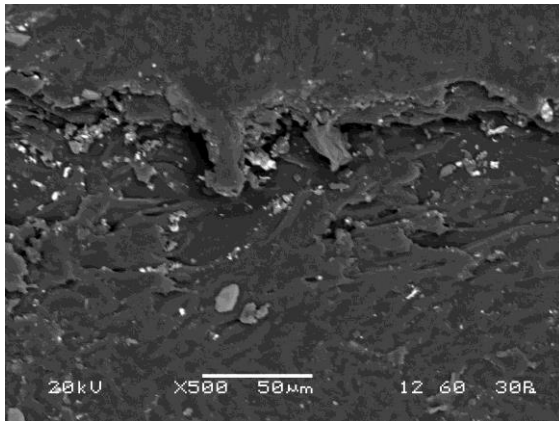


Figure 5.178 Wear of 0 vol. % HAp/PSU (500x)

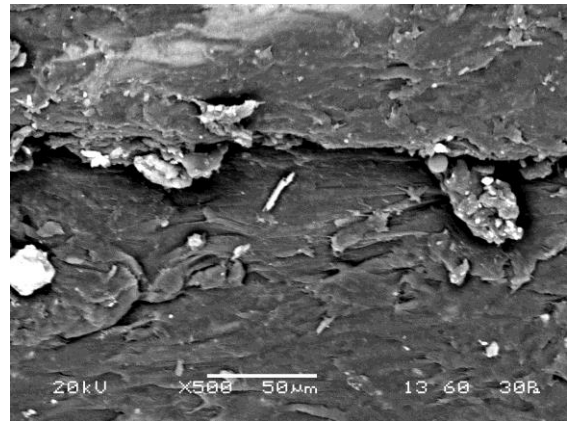


Figure 5.179 Wear of 10 vol. % HAp/PSU (500x)

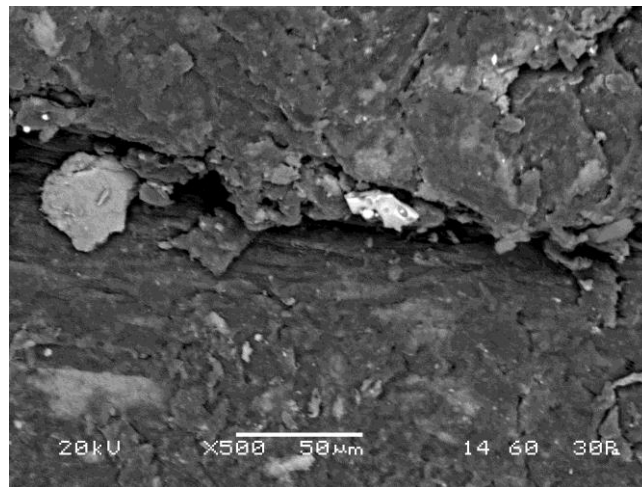


Figure 5.180 Wear of 20 vol. % HAp/PSU (500x)

SEM images of worn surfaces of both HAp/PC and HAp/PSU composite samples is shown from Figure 5.175 to 5.180. According to Figure 5.175 to 5.180, it is clearly shown that when HAp volume is increases from 0 vol. % to 20 vol. %, scratch or wear increases due to HAp particles increases in the polymer matrix. When HAp volume is 0 vol. %, no scratches or wear occurs due to absence of HAp particles. When, HAp volume is 10 vol. %, less scratch occurs in the polymer matrix. Similarly, when HAp volume is increases up to 20 vol. %, more scratches or wear occurs in the polymer matrix.

## 5.2.4 Experimental details of fretting wear behaviour of ceramic composites

The fretting wear test of ceramic composites was performed on high frequency reciprocating rig (HFRR) testing machine (TR-282, DUCOM, Bangalore) (ASTM D6079) and their parts are shown in Figure 5.181.

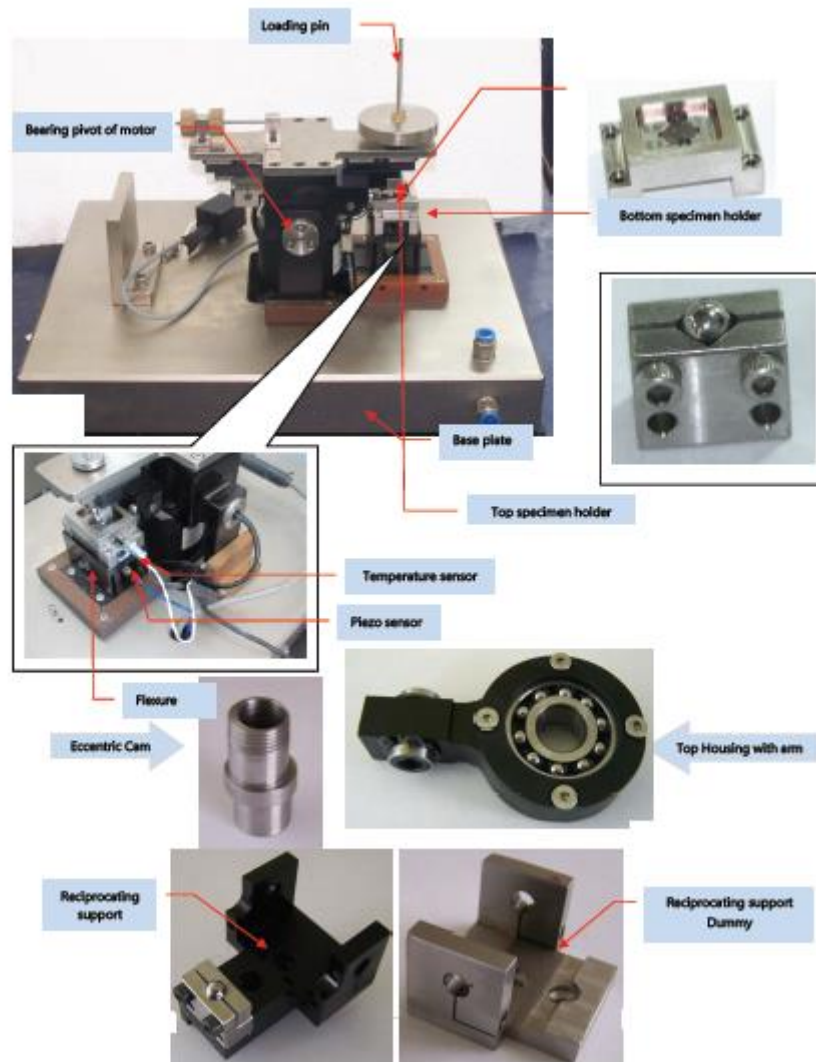


Figure 5.181 High frequency reciprocating rig (HFRR) and their parts

(According to Perumal et al. [169] to Yoon et al. [175]) Taguchi's  $L_{27}$  design was used to evaluate the tribological properties with three control variables such as HAp volume, load applied, and frequency each at three levels. The selected input parameters and their levels are shown in Table 5.66.

Table 5.66 Control parameters and their levels

S.No.	Factors	Symbol	Levels			Unit
			1	2	3	
1.	HAp volume	A	0	10	20	%
2.	Load applied	B	2	4	5	N
3.	Frequency	C	40	50	60	Hz

The experimental data for HAp/PC composite are shown in Table 5.67.

Table 5.67 Experimental data for HAp/PC composite

Exp. No.	Factor A HAp Volume (%)	Factor B Load (N)	Factor C Frequency (Hz)	Fretting wear loss (gm)	S/N ratio (Lower The Better)
1	0	2	40	0.002	53.979
2	0	2	40	0.001	60.000
3	0	2	40	0.003	50.457
4	0	4	50	0.004	47.958
5	0	4	50	0.003	50.457
6	0	4	50	0.005	46.020
7	0	5	60	0.006	44.436
8	0	5	60	0.007	43.098
9	0	5	60	0.005	46.020
10	10	2	50	0.003	50.457
11	10	2	50	0.004	47.958
12	10	2	50	0.003	50.457
13	10	4	60	0.005	46.020
14	10	4	60	0.004	47.958
15	10	4	60	0.003	50.457
16	10	5	40	0.007	43.098
17	10	5	40	0.008	41.938
18	10	5	40	0.006	44.436
19	20	2	60	0.002	53.979
20	20	2	60	0.003	50.457
21	20	2	60	0.003	50.457
22	20	4	40	0.006	44.436
23	20	4	40	0.005	46.020
24	20	4	40	0.004	47.958
25	20	5	50	0.007	43.098
26	20	5	50	0.009	40.915
27	20	5	50	0.008	41.938

The ANOVA Table for HAp/PC composite are shown in Table 5.68.

Table 5.68 ANOVA Table for S/N ratio of HAp/PC composite

Source	DF value	Seq SS	Adj SS	Adj MS	F value	P value
A	2	34.632	34.632	17.316	3.28	0.059
B	2	348.817	348.817	174.409	32.99	0.000
C	2	13.207	13.207	6.604	1.25	0.308
Error	20	105.744	105.744	5.287		
Total	26	502.401				

$S = 2.29939$ ,  $R\text{-Sq} = 78.95\%$ , and  $R\text{-Sq}(\text{adj}) = 72.64\%$

It can be concluded here that significance of factors is in the order of Factor B, A and C.

Main effects plot for means of S/N ratio, normal probability plot and interaction plot are shown in Figure 5.182, 5.183 and 5.184 respectively.

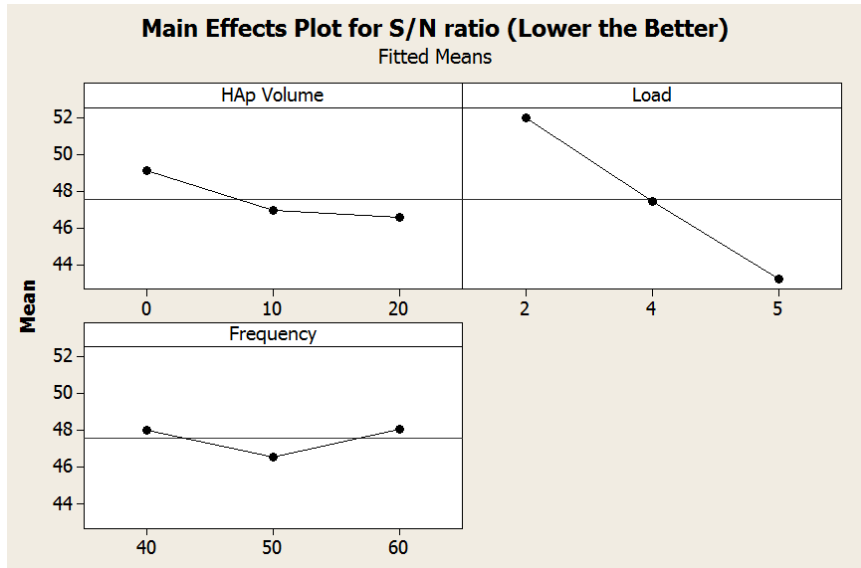


Figure 5.182 Main effects plot for means of S/N ratio

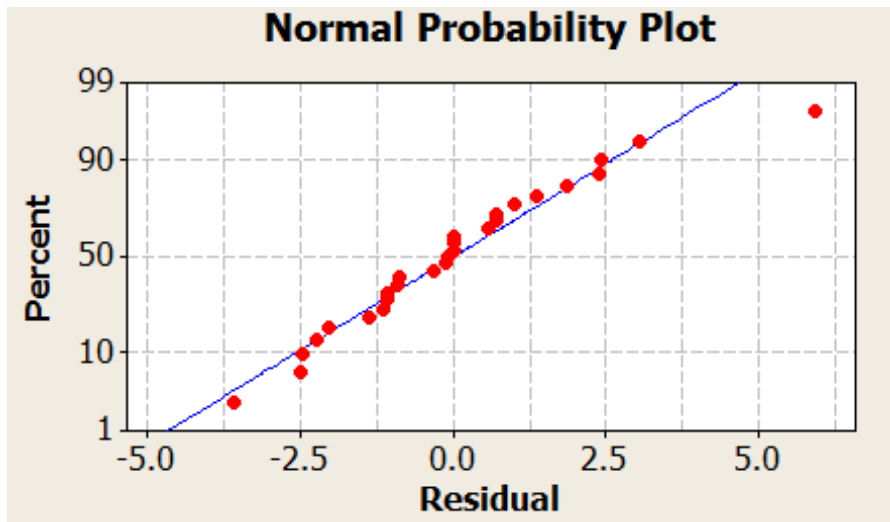


Figure 5.183 Normal probability plot for S/N ratio

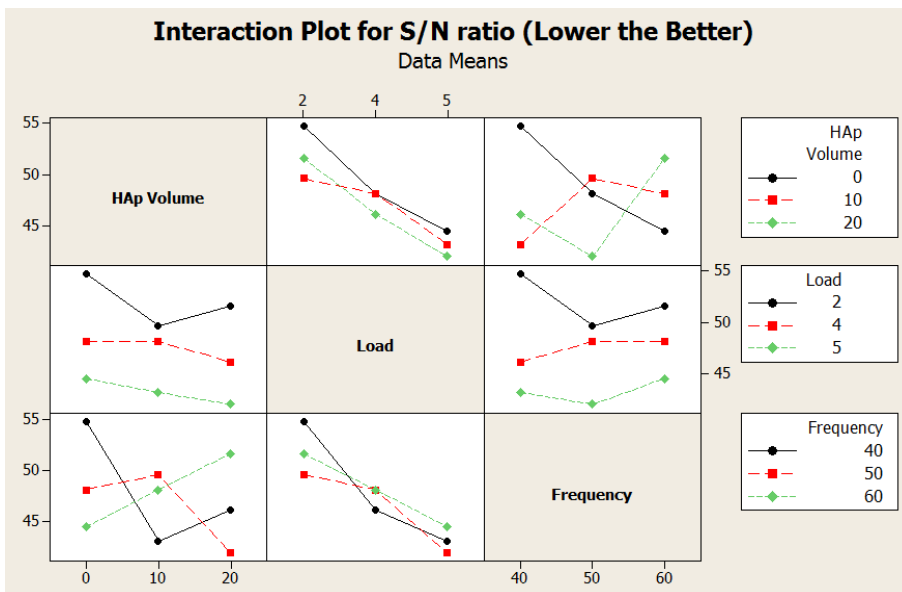


Figure 5.184 Interaction plot for S/N ratio

According to Figure 5.182, it is concluded that the optimal parametric combination is  $A_1B_1C_3$ . When HAp volume is 0 vol. %, load applied is 2 N, and frequency is 60 Hertz then minimum fretting wear can be obtained. Referring to Figure 5.183, it can be concluded that the ANOVA proceeds in a satisfactory manner as the residuals follow a normal distribution. Figure 5.184 shows that two factor interactions of controllable factors seems to exist. However, the interaction of factors has not been considered for the sake of simplicity.

Similarly, the experimental data for HAp/PSU composite are shown in Table 5.69.

Table 5.69 Experimental data for HAp/PSU composite

Exp. No.	Factor A HAp Volume (%)	Factor B Load (N)	Factor C Frequency (Hz)	Fretting wear loss (gm)	S/N ratio (Lower The Better)
1	0	2	40	0.001	60.000
2	0	2	40	0.002	53.979
3	0	2	40	0.001	60.000
4	0	4	50	0.003	50.457
5	0	4	50	0.002	53.979
6	0	4	50	0.003	50.457
7	0	5	60	0.004	47.958
8	0	5	60	0.005	46.020
9	0	5	60	0.005	46.020
10	10	2	50	0.002	53.979
11	10	2	50	0.001	60.000
12	10	2	50	0.003	50.457
13	10	4	60	0.004	47.958
14	10	4	60	0.003	50.457
15	10	4	60	0.002	53.979
16	10	5	40	0.004	47.958
17	10	5	40	0.003	50.457
18	10	5	40	0.004	47.958
19	20	2	60	0.001	60.000
20	20	2	60	0.002	53.979
21	20	2	60	0.002	53.979
22	20	4	40	0.005	46.020
23	20	4	40	0.004	47.958
24	20	4	40	0.003	50.457
25	20	5	50	0.005	46.020
26	20	5	50	0.004	47.958
27	20	5	50	0.006	44.436

The ANOVA Table for HAp/PSU composite are shown in Table 5.70.

Table 5.70 ANOVA Table for S/N ratio of HAp/PSU composite

Source	DF value	Seq SS	Adj SS	Adj MS	F value	P value
A	2	18.965	18.965	9.482	1.12	0.347
B	2	384.035	384.035	192.017	22.63	0.000
C	2	2.819	2.819	1.409	0.17	0.848
Error	20	169.728	169.728	8.486		
Total	26	575.545				

$S = 2.91314$ ,  $R\text{-Sq} = 70.51\%$ , and  $R\text{-Sq}(\text{adj}) = 61.66\%$

It can be concluded here that significance of factors is in the order of Factor B, A and C.

Main effects plot for means of S/N ratio, normal probability plot and interaction plot are shown in Figure 5.185, 5.186 and 5.187 respectively.

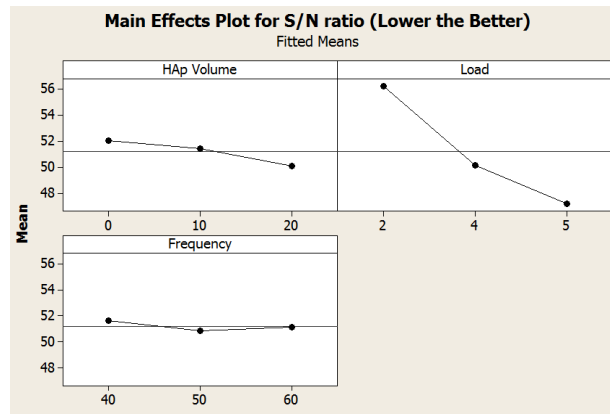


Figure 5.185 Main effects plot for means of S/N ratio

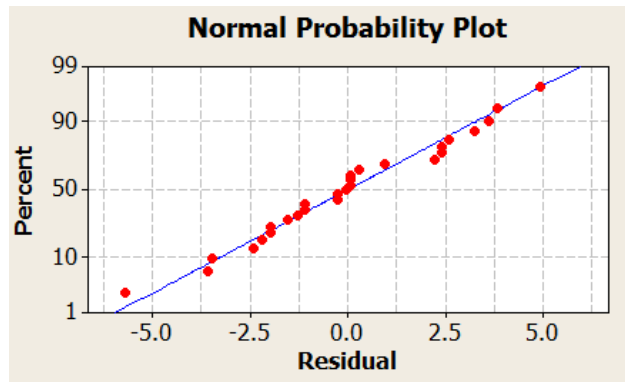


Figure 5.186 Normal probability plot for S/N ratio

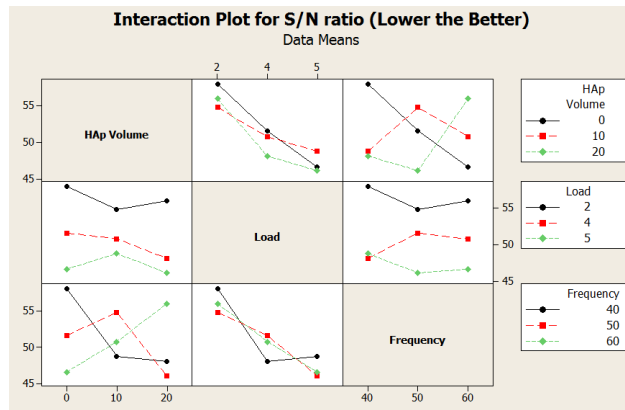


Figure 5.187 Interaction plot for S/N ratio

According to Figure 5.185, it is concluded that the optimal parametric combination is  $A_1B_1C_1$ . When HAp volume is 0 vol. %, load applied is 2 N, and frequency is 40 Hertz then minimum fretting wear can be obtained. Referring to Figure 5.186, it can be concluded that the ANOVA proceeds in a satisfactory manner as the residuals follow a normal distribution. Figure 5.187 shows that two factor interactions of controllable factors seems to exist. However, the interaction of Load of factors has not been considered for the sake of simplicity.

The values of coefficient of friction (COF) of each composition for HAp/PC and HAp/PSU composites are generated with the help of WINDUCOM 2010 software which are shown in Figure 5.188 to Figure 5.193 respectively.

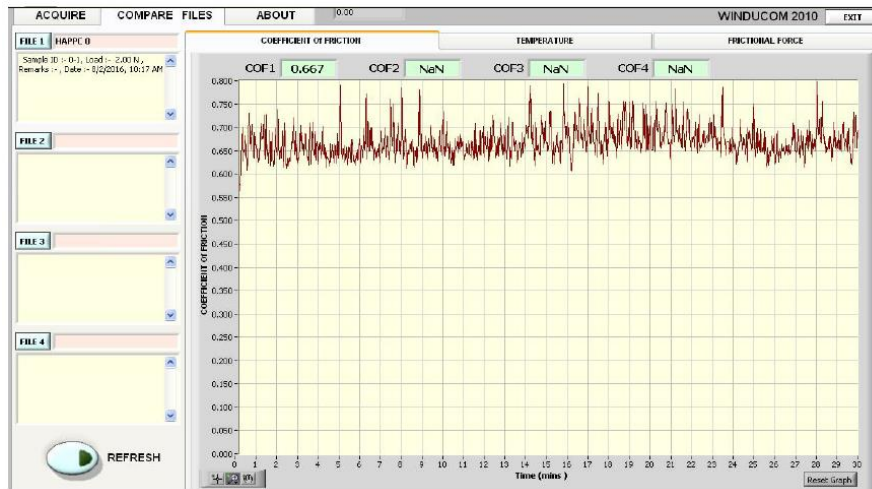


Figure 5.188 COF of 0 vol. % HAp/PC composite loaded at 2N and 60 Hz frequency



Figure 5.189 COF of 10 vol. % HAp/PC composite loaded at 4N and 50 Hz frequency

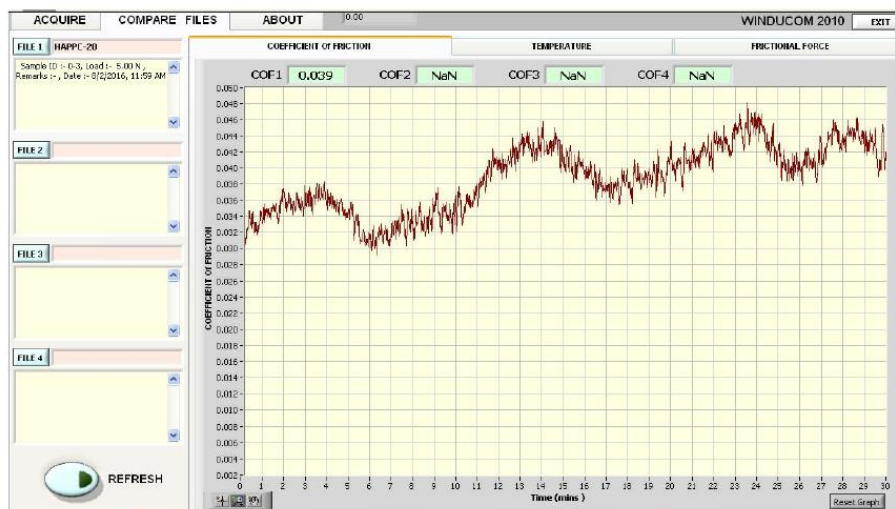


Figure 5.190 COF of 20 vol. % HAp/PC composite loaded at 5N and 40 Hz frequency



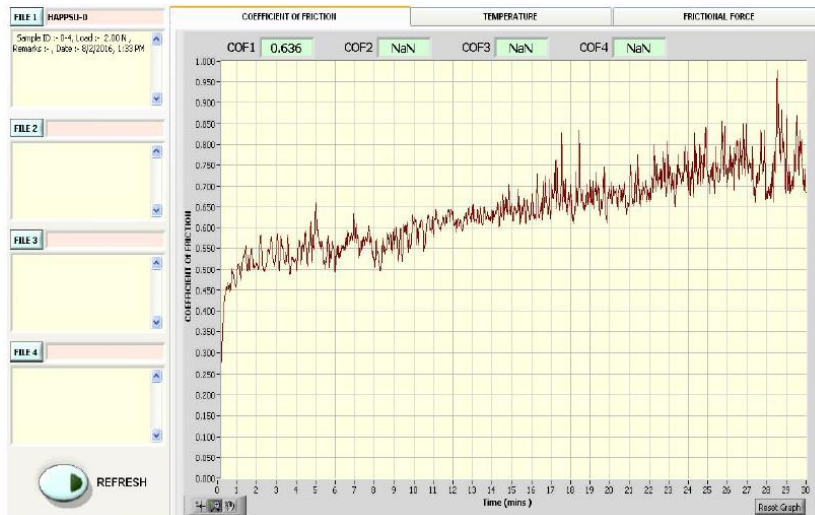


Figure 5.191 COF of 0 vol. % HAp/PSU composite loaded at 2N and 60 Hz frequency

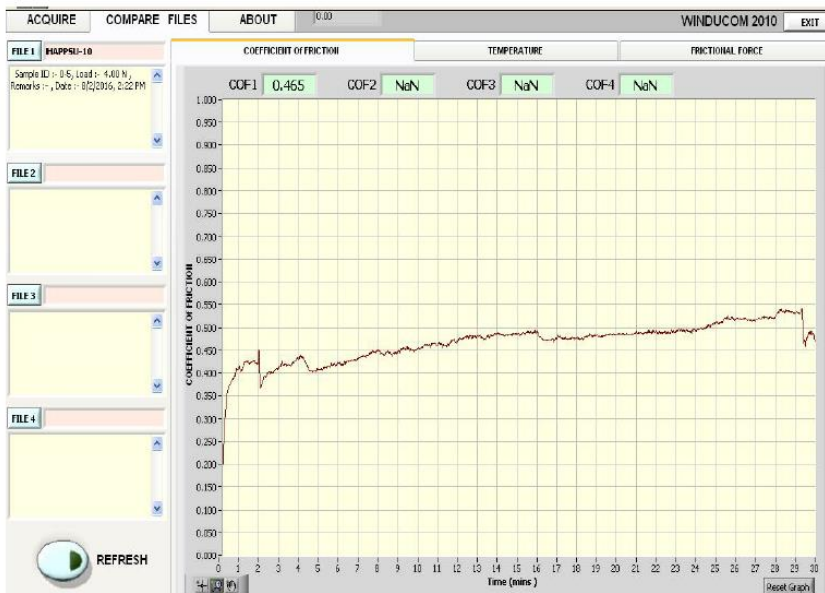


Figure 5.192 COF of 10 vol. % HAp/PSU composite loaded at 4N and 50 Hz frequency

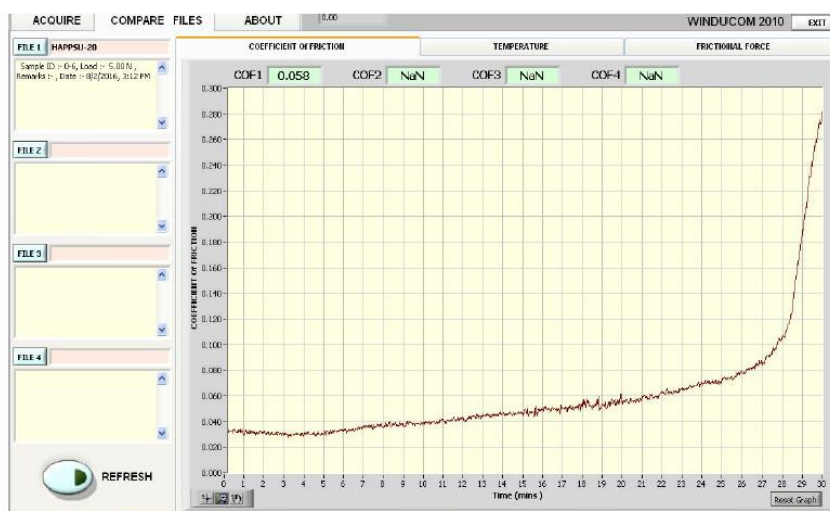


Figure 5.193 COF of 20 vol. % HAp/PSU composite loaded at 5N and 40 Hz frequency



## 5.2.4.1 Prediction of fretting wear behaviour of composites

### 5.2.4.1.1 Adaptive neuro fuzzy inference system (ANFIS) methodology used for HAp/PC composite

(According to Isla et al. [176] to Sahu et al. [180]) The FIS editor for input parameters of both HAp/PC and HAp/PSU composites, and membership function editor for output parameter of HAp/PC composite are shown in Figure 5.194 to Figure 5.198.

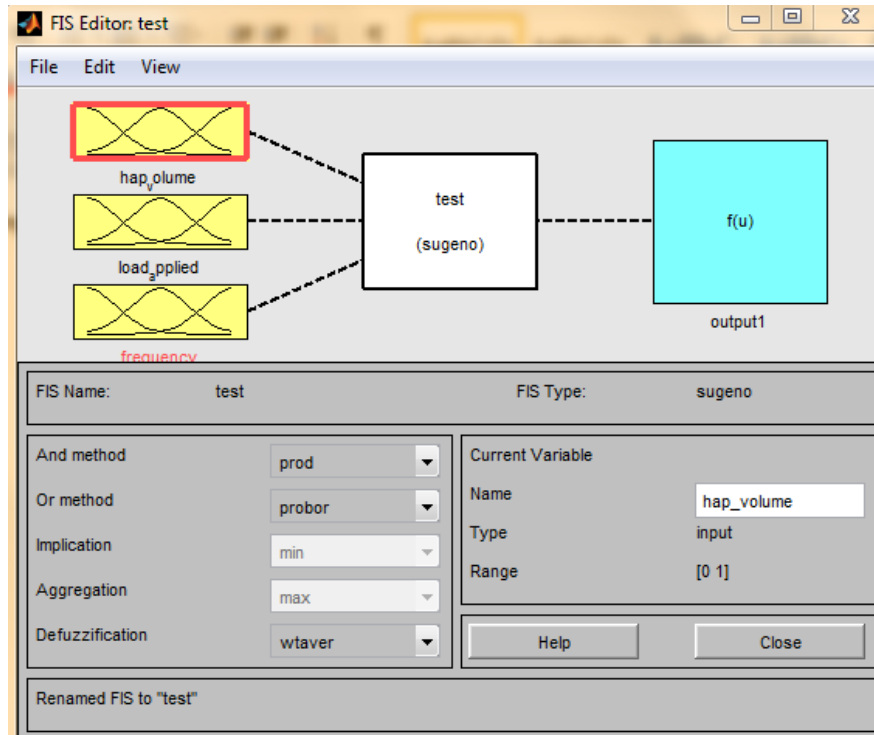


Figure 5.194 FIS editor

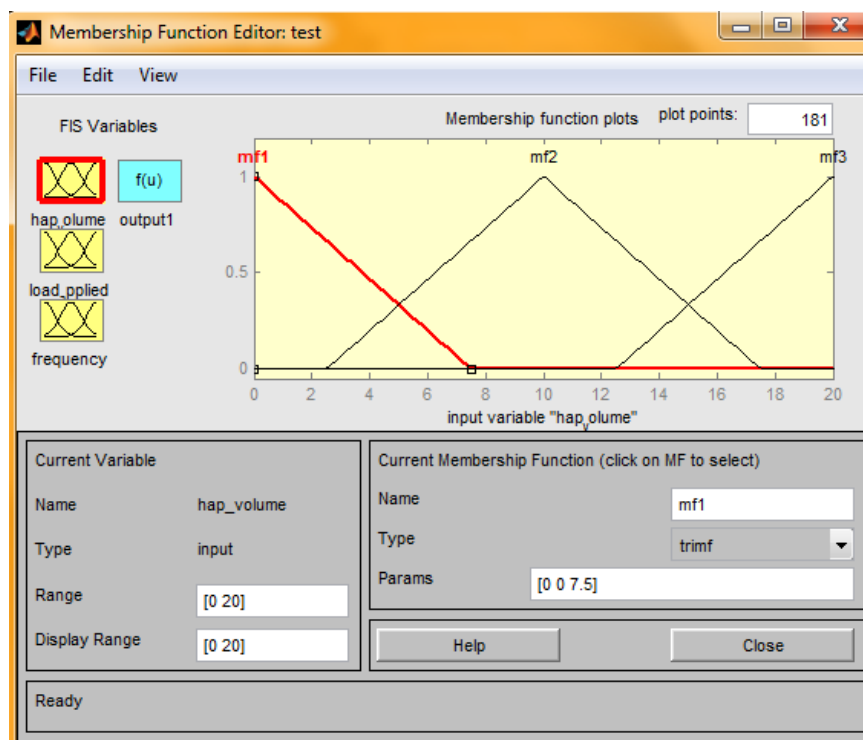


Figure 5.195 Membership function editor of Input 1

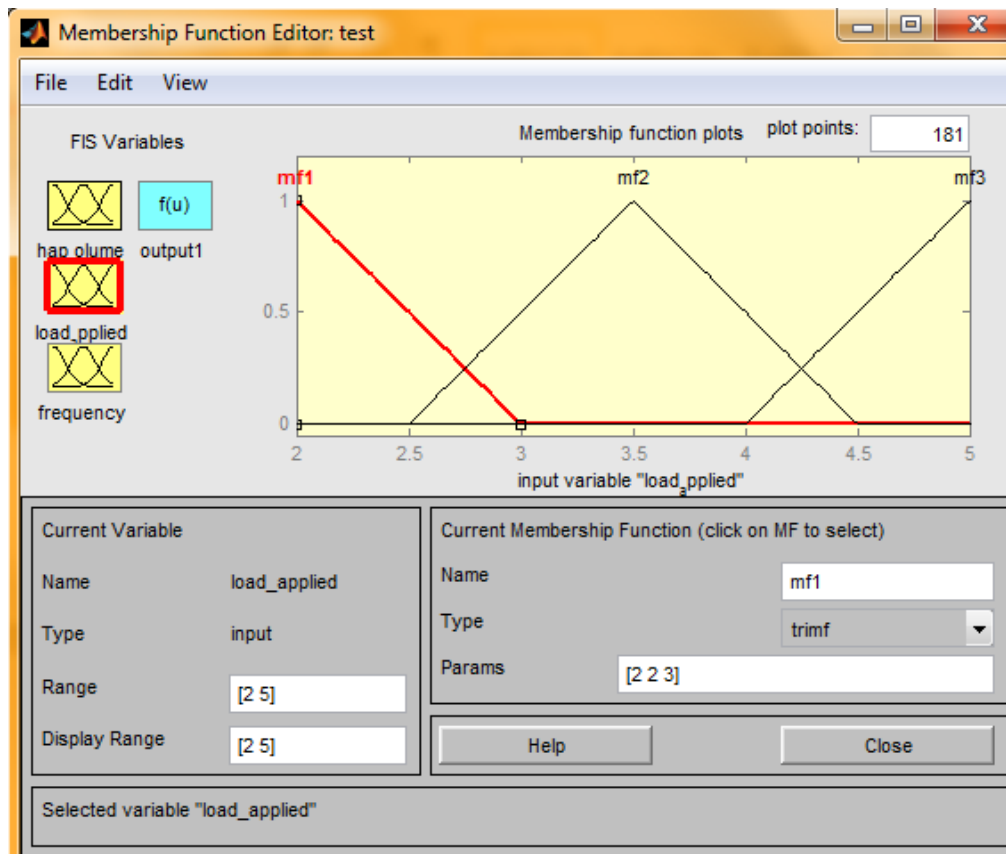


Figure 5.196 Membership function editor of Input 2

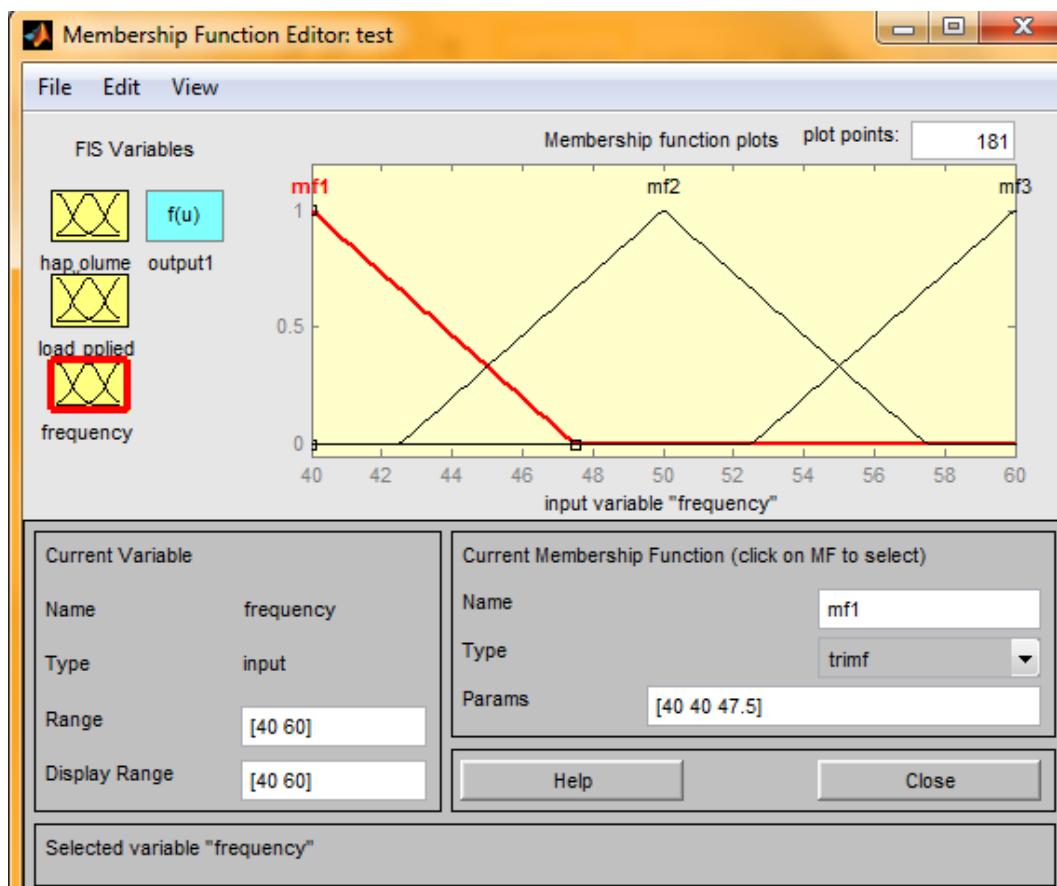


Figure 5.197 Membership function editor of Input 3

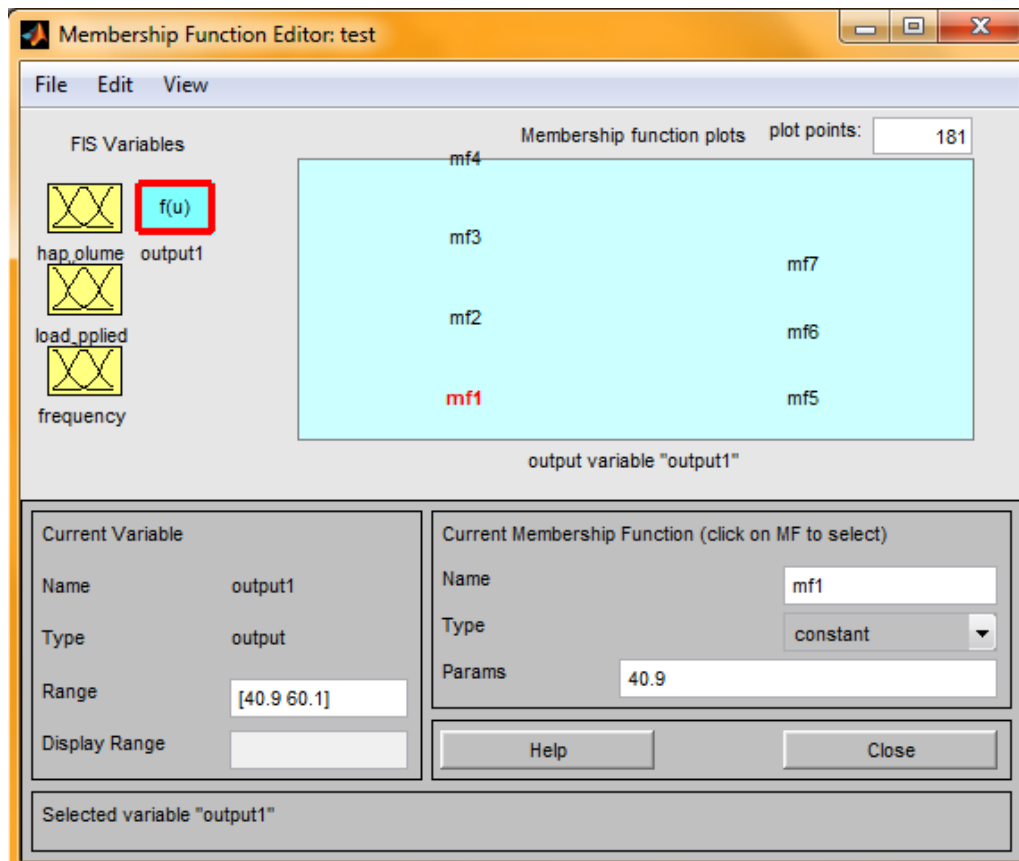


Figure 5.198 Membership function editor for output of HAp/PC composite

The ANFIS model structure of HAp/PC and HAp/PSU composites regarding fretting wear, while ANFIS editor for both training and testing data, rule editor and rule viewer of HAp/PC composite are shown in Figure 5.199 to Figure 5.203 respectively.

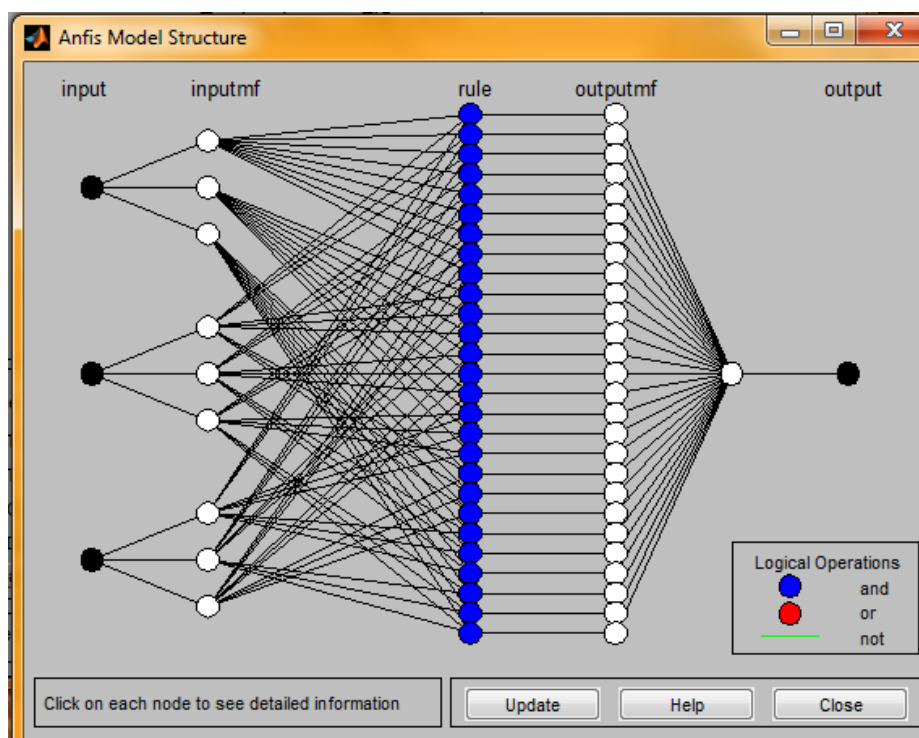


Figure 5.199 ANFIS model structure

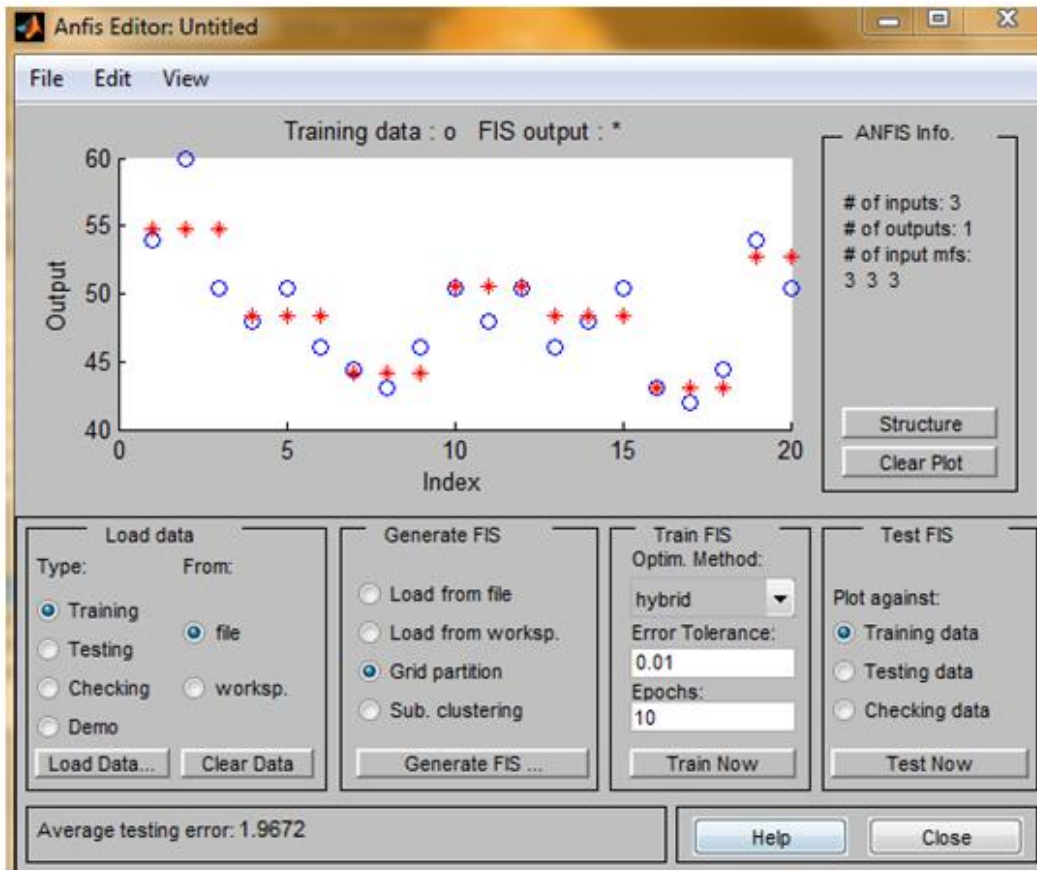


Figure 5.200 Distribution of predicted and actual data (Training)

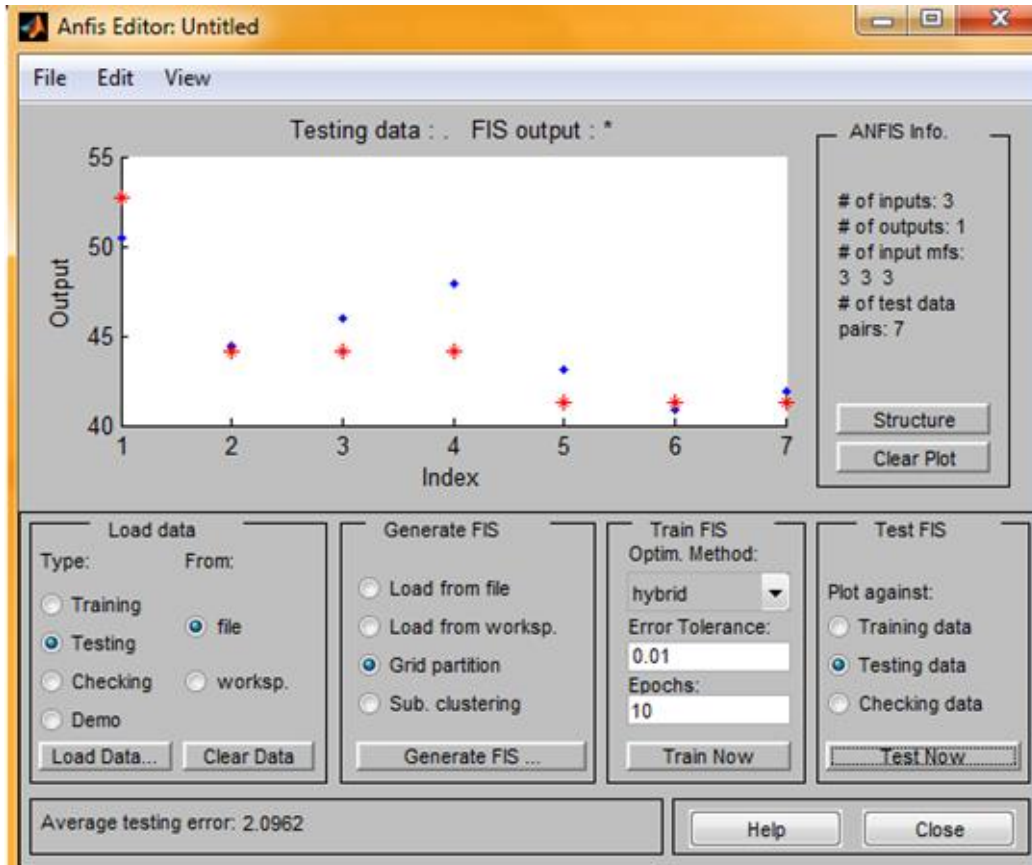


Figure 5.201 Distribution of predicted and actual data (Testing)

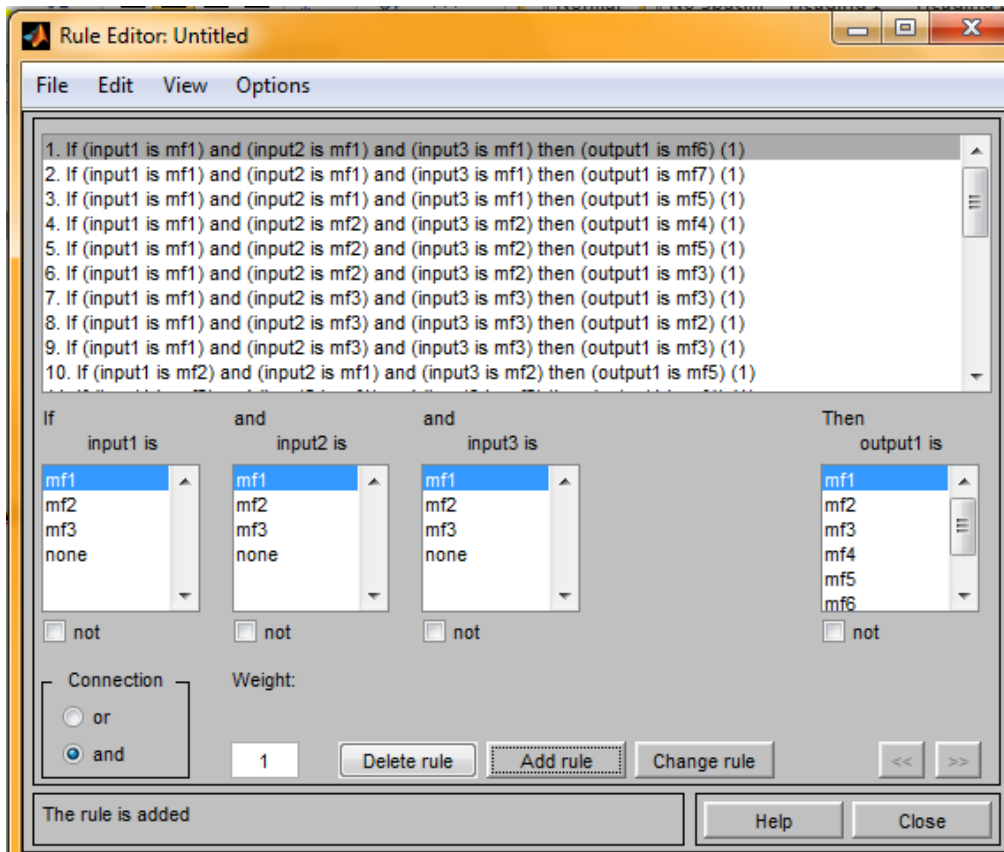


Figure 5.202 Rule editor

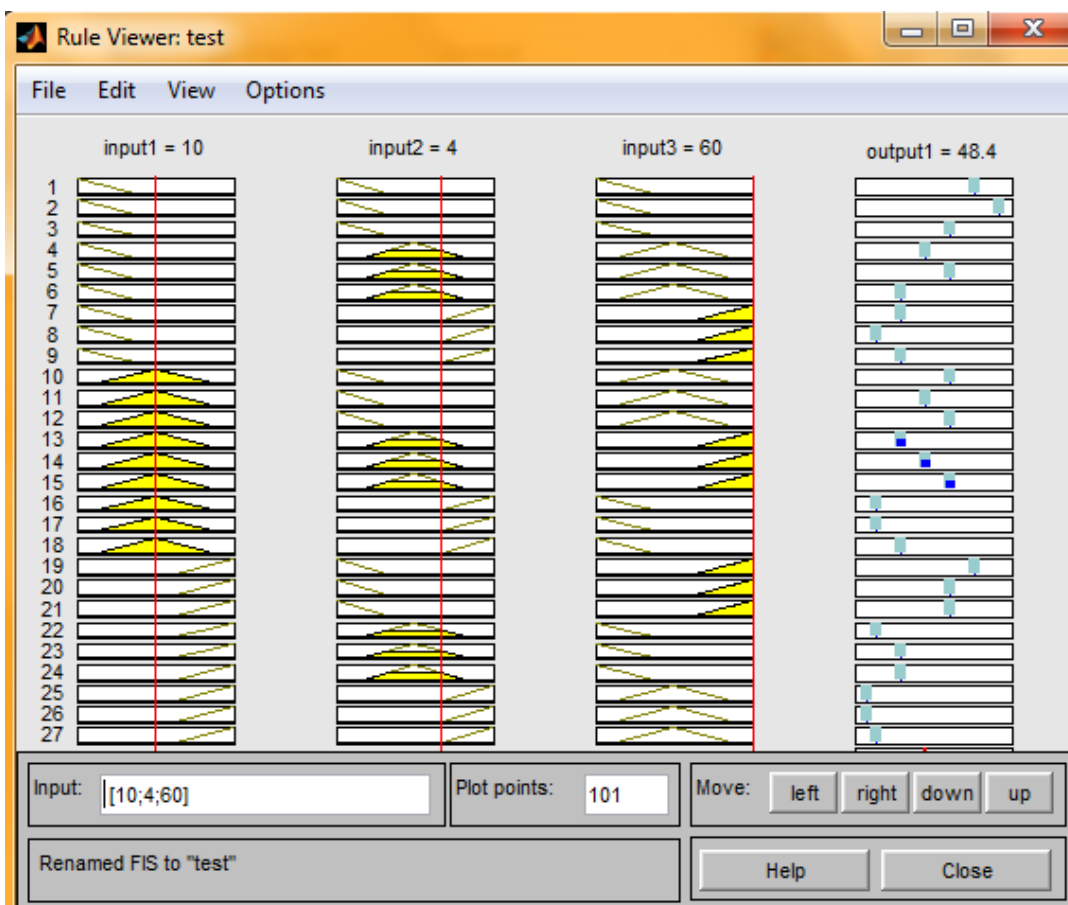


Figure 5.203 Rule viewer

The input and output experimental value with ANFIS predicted value of HAp/PC composite for training purpose is shown in Table 5.71.

Table 5.71 Input and output data with ANFIS predicted value of HAp/PC composite

No.	Factor A HAp Volume (%)	Factor B Load (N)	Factor C Frequency (Hz)	Wear Loss (gm)	S/N ratio of Exp. value	ANFIS output predicted value
1	0	2	40	0.002	53.979	54.8
2	0	2	40	0.001	60.000	54.8
3	0	2	40	0.003	50.457	54.8
4	0	4	50	0.004	47.958	48.4
5	0	4	50	0.003	50.457	48.4
6	0	4	50	0.005	46.020	48.4
7	0	5	60	0.006	44.436	44.1333
8	0	5	60	0.007	43.098	44.1333
9	0	5	60	0.005	46.020	44.1333
10	10	2	50	0.003	50.457	50.5333
11	10	2	50	0.004	47.958	50.5333
12	10	2	50	0.003	50.457	50.5333
13	10	4	60	0.005	46.020	48.4
14	10	4	60	0.004	47.958	48.4
15	10	4	60	0.003	50.457	48.4
16	10	5	40	0.007	43.098	43.0667
17	10	5	40	0.008	41.938	43.0667
18	10	5	40	0.006	44.436	43.0667
19	20	2	60	0.002	53.979	52.6667
20	20	2	60	0.003	50.457	52.6667

The input and output data with ANFIS predicted value of HAp/PC composite for testing purpose is shown in Table 5.72.

Table 5.72 Input and output data with ANFIS predicted value of HAp/PC composite

No.	Factor A HAp Volume (%)	Factor B Load (N)	Factor C Frequency (Hz)	Wear Loss (gm)	S/N ratio of Exp. value	ANFIS output predicted value
1	20	2	60	0.003	50.457	52.6667
2	20	4	40	0.006	44.436	44.1333
3	20	4	40	0.005	46.020	44.1333
4	20	4	40	0.004	47.958	44.1333
5	20	5	50	0.007	43.098	41.2667
6	20	5	50	0.009	40.915	41.2667
7	20	5	50	0.008	41.938	41.2667

By calculating we get the mean relative percentage error for training and testing of HAp/PC composite is 3.23% and 3.41% respectively.

### 5.2.4.1.2 Adaptive neuro fuzzy inference system (ANFIS) methodology used for HAp/PSU composite

The membership function editor for output parameter of HAp/PSU composite is shown in Figure 5.204.

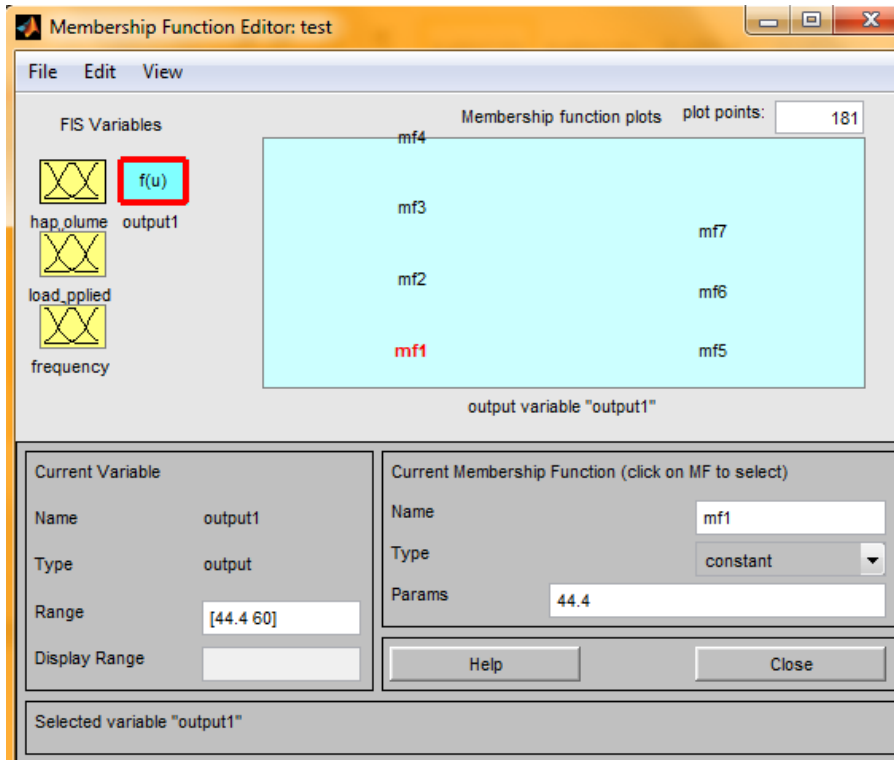


Figure 5.204 Membership function editor for output of HAp/PSU composite

The ANFIS editor for both training and testing data, rule editor and rule viewer of HAp/PSU composite are shown in Figure 5.205 to Figure 5.208 respectively.

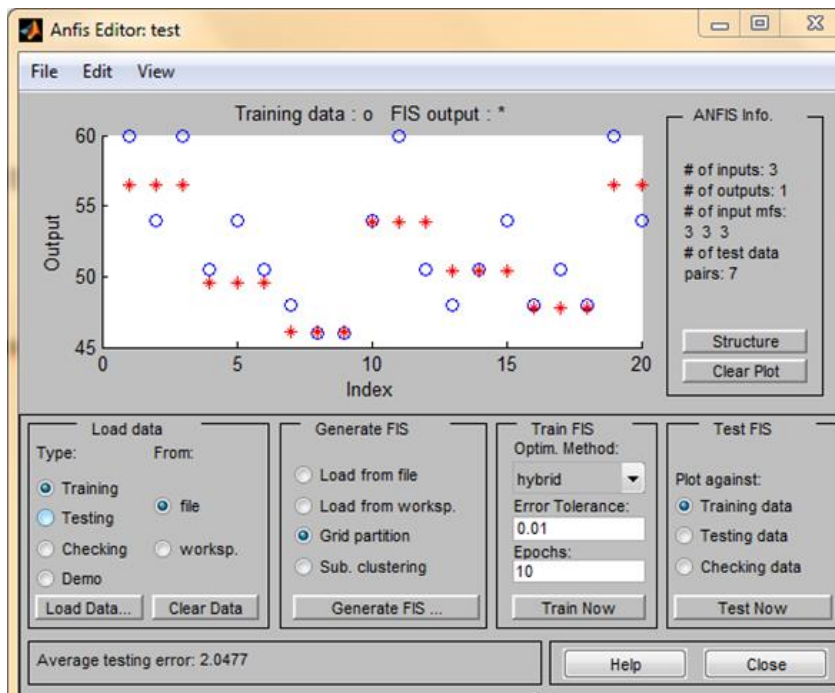


Figure 5.205 Distribution of predicted and actual data (Training)



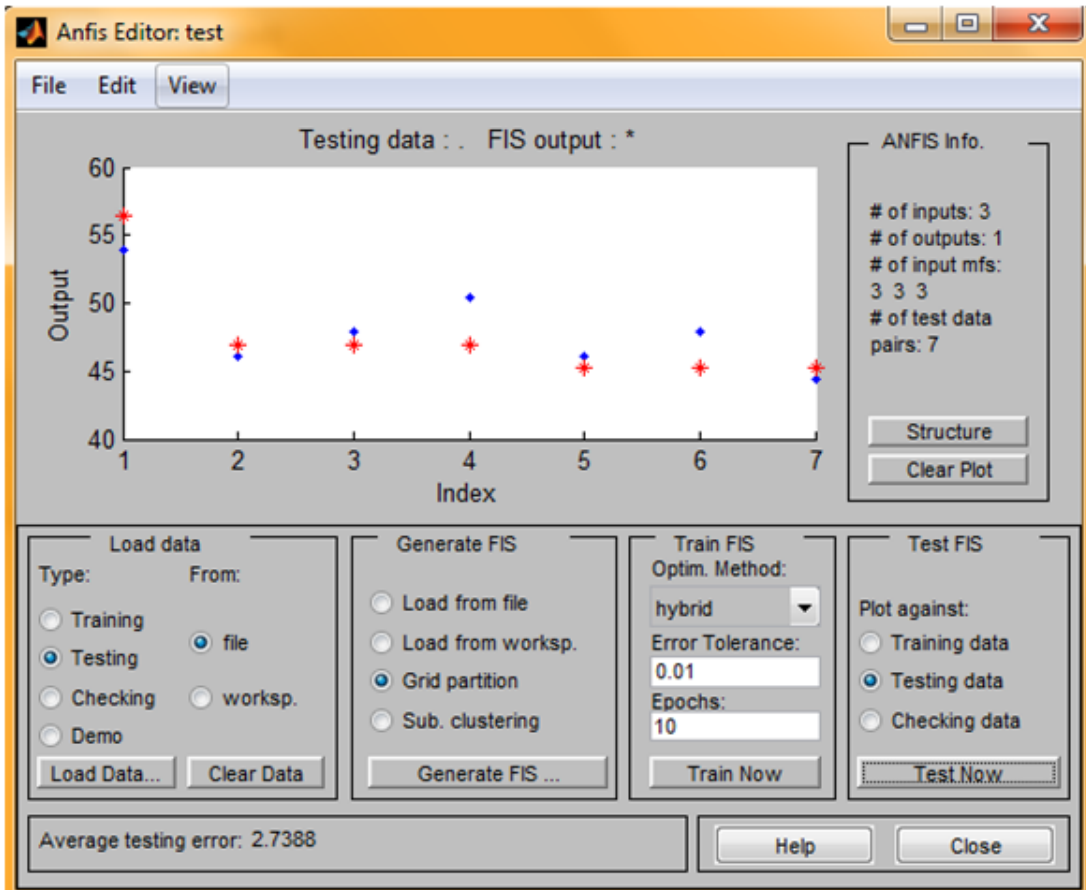


Figure 5.206 Distribution of predicted and actual data (Testing)

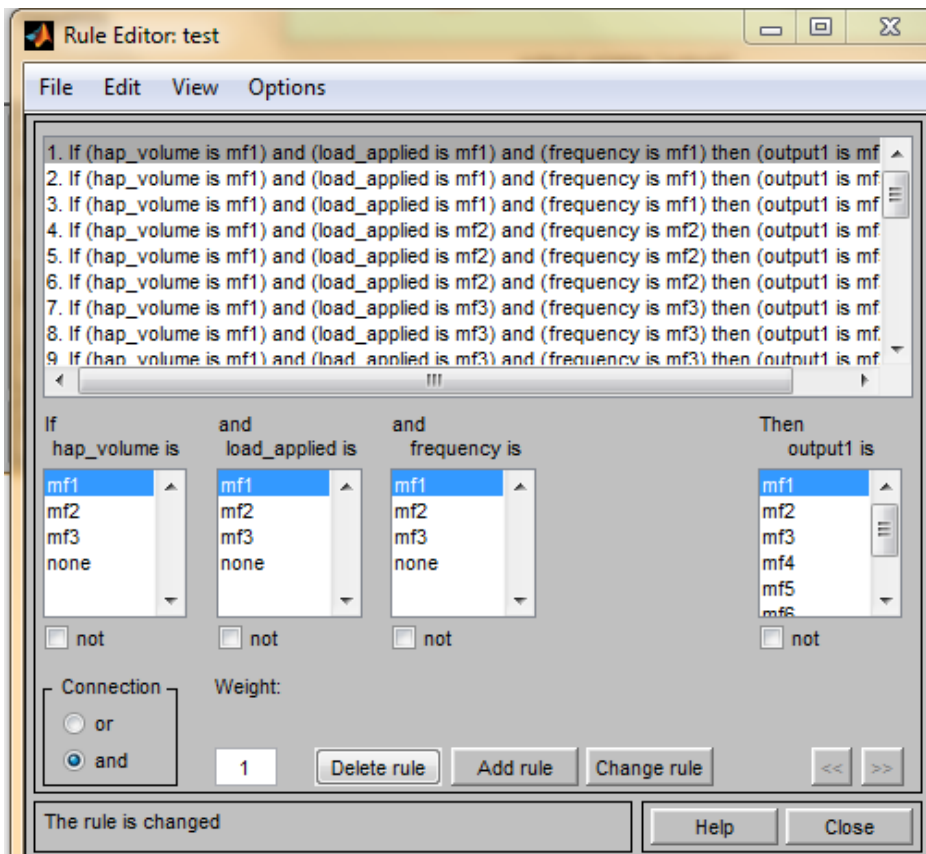


Figure 5.207 Rule editor



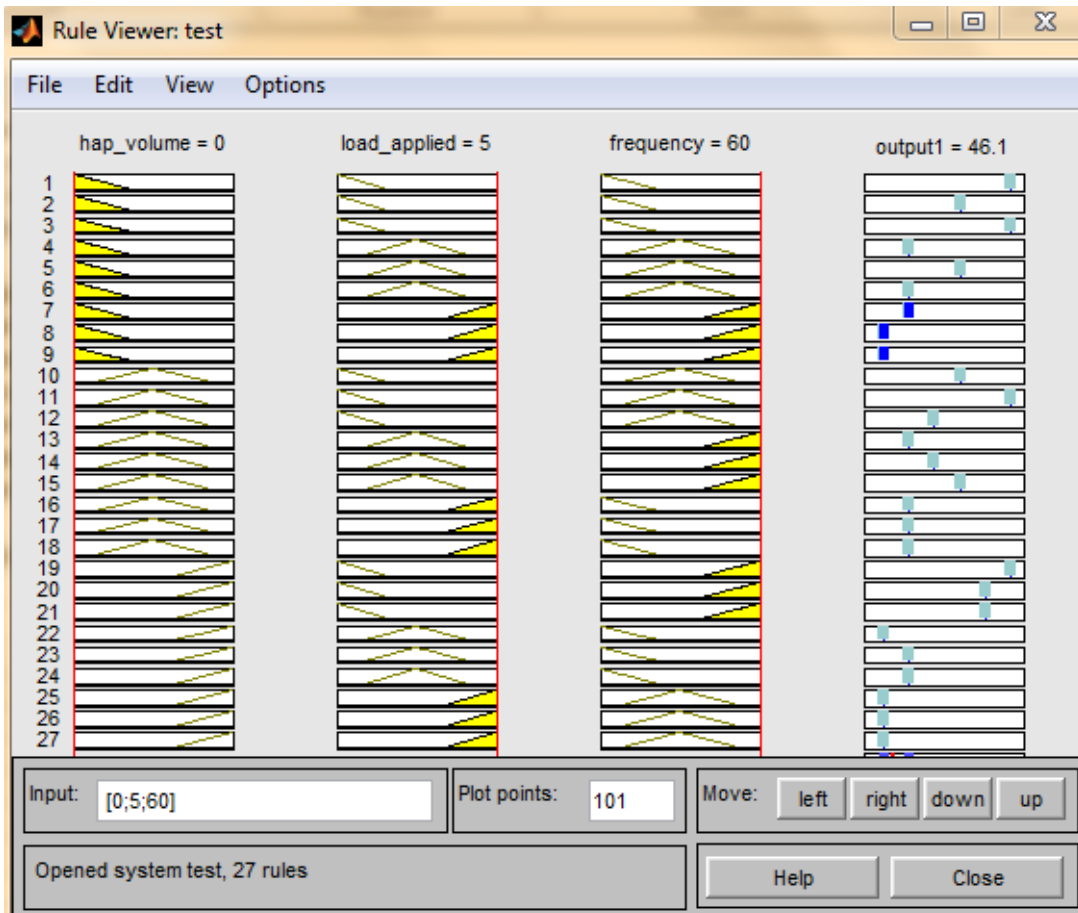


Figure 5.208 Rule viewer

The input and output experimental value with ANFIS predicted value of HAP/PSU composite for training purpose is shown in Table 5.73.

Table 5.73 Input and output data with ANFIS predicted value of Hap/PSU composite

No.	Factor A HAp Volume (%)	Factor B Load (N)	Factor C Frequency (Hz)	Wear Loss (gm)	S/N ratio of Exp. value	ANFIS output predicted value
1	0	2	40	0.001	60.000	56.4667
2	0	2	40	0.002	53.979	56.4667
3	0	2	40	0.001	60.000	56.4667
4	0	4	50	0.003	50.457	49.5333
5	0	4	50	0.002	53.979	49.5333
6	0	4	50	0.003	50.457	49.5333
7	0	5	60	0.004	47.958	46.0667
8	0	5	60	0.005	46.020	46.0667
9	0	5	60	0.005	46.020	46.0667
10	10	2	50	0.002	53.979	53.8667
11	10	2	50	0.001	60.000	53.8667
12	10	2	50	0.003	50.457	53.8667
13	10	4	60	0.004	47.958	50.4
14	10	4	60	0.003	50.457	50.4
15	10	4	60	0.002	53.979	50.4
16	10	5	40	0.004	47.958	47.8
17	10	5	40	0.003	50.457	47.8
18	10	5	40	0.004	47.958	47.8
19	20	2	60	0.001	60.000	56.4667
20	20	2	60	0.002	53.979	56.4667

The input and output data with ANFIS predicted value of HAp/PSU composite for testing purpose is shown in Table 5.74.

Table 5.74 Input and output data with ANFIS predicted value of HAp/PSU composite

No.	Factor A HAp Volume (%)	Factor B Load (N)	Factor C Frequency (Hz)	Wear Loss (gm)	S/N ratio of Exp. value	ANFIS output predicted value
1	20	2	60	0.002	53.979	56.4667
2	20	4	40	0.005	46.020	46.9333
3	20	4	40	0.004	47.958	46.9333
4	20	4	40	0.003	50.457	46.9333
5	20	5	50	0.005	46.020	45.2
6	20	5	50	0.004	47.958	45.2
7	20	5	50	0.006	44.436	45.2

By calculating we get the mean relative percentage error for training and testing of HAp/PSU composite is 3.57% and 3.89% respectively.

#### 5.2.4.2 Worn surface morphology

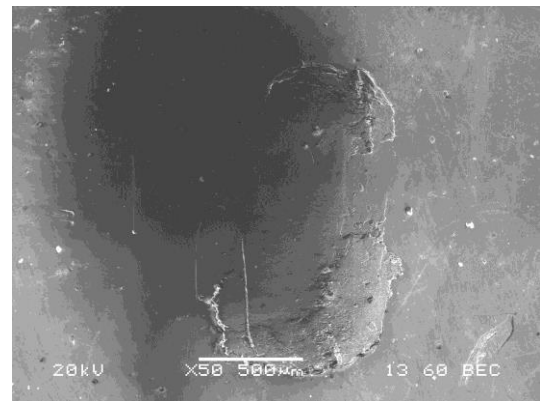
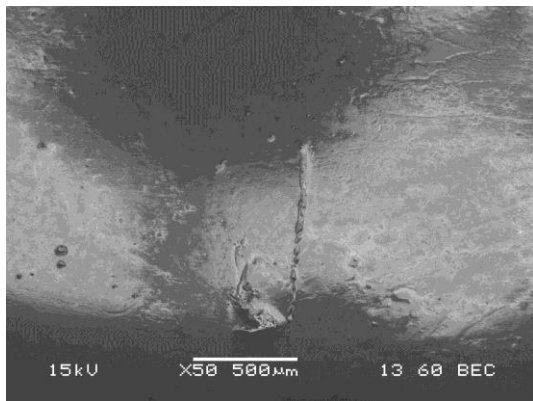


Figure 5.209 Wear of 0 vol. % HAp/PC (x50) Figure 5.210 Wear of 10 vol. % HAp/PC (x50)

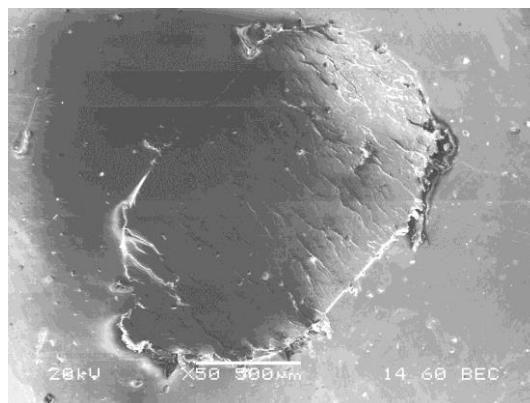


Figure 5.211 Wear of 20 vol. % HAp/PC (x50)

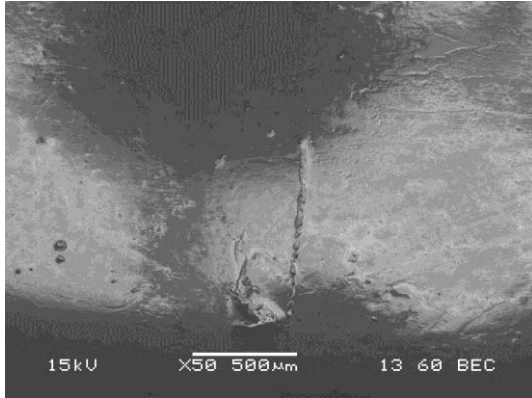


Figure 5.212 Wear of 0 vol. % HAp/PSU(x50)

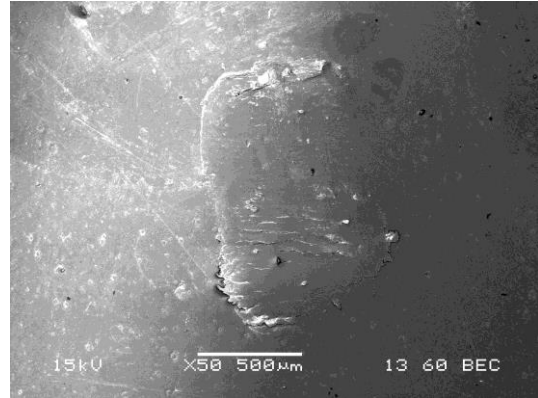


Figure 5.213 Wear of 10 vol. % HAp/PSU (x50)

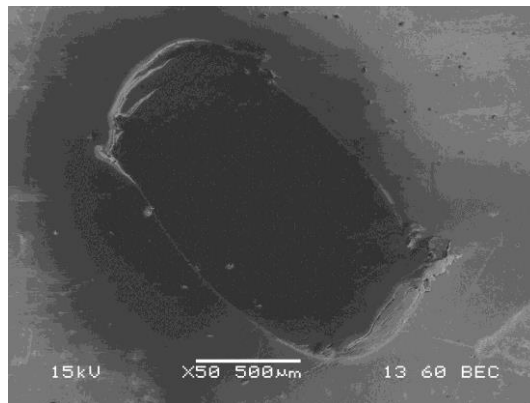


Figure 5.214 Wear of 20 vol. % HAp/PSU (x50)

SEM images of worn surfaces of both HAp/PC and HAp/PSU composite samples is shown from Figure 5.209 to Figure 5.214. According to Figure 5.209 to Figure 5.214, it is clearly shown that as HAp volume increases from 0 vol. % to 20 vol. %, scratch or wear also increases due to HAp particles increases in the polymer matrix. When HAp volume is 0 vol. %, no scratch is found in the polymer matrix due to the absence of HAp particles. When HAp volume is 10 vol. %, small scratches or wear occurs in the polymer matrix due to HAp particles is less but when HAp volume increases from 10 vol. % to 20 vol. %, more scratches are occurs in the polymer matrix.

### 5.3 Conclusion

This chapter describes the introduction and classifications of wear i.e. abrasive wear, adhesive wear, erosive wear, sliding wear, fretting wear, corrosive wear and surface fatigue wear. However, in this study we focussed mainly on abrasive wear, erosive wear, sliding wear, and fretting wear along with their experimental procedure in different machines are discussed briefly. An ANFIS (Adaptive neuro-fuzzy inference system) model is developed for prediction of wear behaviour of composites. Some SEM images of worn surfaces are also shown and discussed in this chapter.

The two-body abrasion wear behavior of the composite was performed using pin-on-disc friction and wear test rig. The experiment was conducted using three different water proof silicon carbide (SiC) abrasive papers of 400, 600 and 1000 grit size. Taguchi's  $L_{27}$  design was used to evaluate the tribological property with four control variables such as HAp volume, load applied, sliding speed and track radius each at three levels. The highest abrasive wear loss was noticed at the specimens worn on 400 grit size SiC paper as compared to both 600 grit size and 1000 grit size SiC paper. This is due to the larger size of the abrasive grains in 400 grit size SiC paper causing greater damage to the specimen surface. The experimental data of abrasion wear test of the composite showed that the wear behavior of the composite strongly depends on the grit size of the SiC abrasive papers. It is shown that as HAp volume percentage increases in both HAp/PC and HAp/PSU composites, abrasive wear increases in the surface of the samples.

Erosion wear of ceramic composites was performed on Air jet erosion test rig. In this study, dry silica sand (spherical) of different particle size of 300 $\mu$ m, 400 $\mu$ m and 500 $\mu$ m are used as erodent. Taguchi's  $L_{27}$  design was used to evaluate the tribological properties with three control variables such as pressure, HAp volume, and impingement angle each at three levels. The highest erosive wear loss was noticed at the specimens worn on 500 $\mu$ m erodent particle size as compared to both 300 $\mu$ m and 400 $\mu$ m erodent particle size. This is due to the larger size of the abrasive grains in 500 $\mu$ m causing greater damage to the specimen surface. The experimental data of erosion wear test showed that the wear behavior of the composite strongly depends on the erodent size of the silica sand. It is shown that erosive wear increases slightly as increases in the HAp volume percentage in both HAp/PC and HAp/PSU composites.

The sliding wear test of ceramic composites was performed on ball on plate wear tester. Taguchi's  $L_{27}$  design was used to evaluate the tribological properties with three control variables such as HAp volume, load applied, and sliding speed each at three levels. It is shown that sliding wear increases as increases in the HAp volume percentage in both HAp/PC and HAp/PSU composites.

The fretting wear test of ceramic composites was performed on high frequency reciprocating rig (HFRR) testing machine. Taguchi's  $L_{27}$  design was used to evaluate the tribological properties with three control variables such as HAp volume, load applied, and frequency each at three levels. It is depicted that as HAp volume percentage increases from 0 vol. % to 20 vol. %, there is an increase in fretting wear which occurs in the surface of the samples in both HAp/PC and HAp/PSU composites.

## Chapter 6

# A study on Machining Analysis of Ceramic Composites

### 6.1 Introduction

(According to Biswas et al. [181] to Dorao et al. [185]) Selection of machining parameter combinations for obtaining optimum circularity at both entry and exit, and optimum torque and thrust force is a challenging task owing to the presence of a large number of process variables. There is no perfect combination of parameters that can simultaneously result in higher circularity at both entry and exit with lower torque and thrust force. The aim is to develop a strategy for predicting machining parameter settings for the generation of the maximum circularity at both entry and exit with minimum torque and thrust force.

### 6.2 Machining parameters and their levels

For obtaining optimum circularity at both entry and exit with optimum torque and thrust force, some machining parameters are considered with their levels are shown in Table 6.1. Four parameters were chosen as inputs i.e., HAp vol. %, drilling speed, feed rate, and drill bit diameter. Experiments were carried out using Taguchi's  $L_{27}$  design combinations of these factors and their different levels.

Table 6.1 Control parameters and their levels

<b>Drilling parameters</b>	<b>Level 1</b>	<b>Level 2</b>	<b>Level 3</b>
HAp Volume (%)	0	10	20
Drilling Speed (rpm)	500	1000	1500
Feed Rate (mm/min)	50	60	70
Drill Bit Diameter (mm)	4	6	8

### 6.3 Specifications of CNC milling machine

The overall details of CNC milling machine specifications are shown in Table 6.2 to Table 6.9.

Table 6.2 Machine specifications

Specification	Description
X Axis travel (Longitudinal Travel)	300 mm
Y Axis travel (Cross Travel)	250 mm
Z Axis travel (Vertical Travel)	250 mm
Clamping Surface	500 x 350 mm
Repeatability	± 0.005 mm
Positional Accuracy	0.010 mm
Coolant Motor	RKM 02505 (Rajamane)
Motor Power	0.37 kW
Tank Capacity	110 ltr (Filter & Tray)

Table 6.3 X-Axis drive data

Specification	Description
Table Size	500 x 350 mm
Weight of the table	35 kg.
Thrust force on Table	200 kg.
Rapid feed	10 m/min
Stroke	300 mm
Ball Screw	R20-5B2-FDW (Hiwin)
Bearings	BSB 017047 DUMP3 (RHP)
Servo Motor	FANUC $\beta$ 4/4000i s
L M Guide	HGH 20 HA (Hiwin)
Coupling	SFC-SA-050-14H7-15H7 (Mikipulley)

Table 6.4 Y-Axis drive data

Specification	Description
Saddle Size	468 x 350 mm
Weight of the Saddle	50 kg.
Thrust force on Saddle	300 kg.
Rapid feed	10 m/min
Stroke	250 mm
Ball Screw	R20-5B2-FDW (Hiwin)
Bearings	BSB 025062 DUMP3 (RHP)
Servo Motor	FANUC $\beta$ 4/4000i s
L M Guide	HGH 20 HA (Hiwin)
Coupling	SFC-SA-050-14H7-15H7 (Mikipulley)

Table 6.5 Z-Axis drive data

Specification	Description
Column Size	400 x 363 x 850 mm
Rapid feed	10 m/min
Stroke	250 mm
Ball Screw	R25-5B2-FDW (Hiwin)
Bearings	BSB 020047 (RHP)
Servo Motor	FANUC $\beta$ 4/4000i s
L M Guide	HGH 25 HA (Hiwin)
Coupling	SFC-SA-050-14H7-15H7 (Mikipulley)

Table 6.6 Electrical Specification

Specification	Description
Power ratings	415 V, 3 $\phi$ , 15 kVA
Axes motor	Fanuc Servo Motor $\beta$ 4i series
Spindle motor	Fanuc Spindle Motor $\beta$ 3i series

Table 6.7 Specification of Spindle Motor

Specification	Description
Model	FANUC $\beta$ 3/10000i
Cont. Rated Output	3.7 kW
Maximum Speed	10000 rpm
ATC make	MACO
Tool Type	BT 30
3 Axis Cont. Path Control System	Fanuc Oi Mate MC
Automatic centralized lubrication for slides and ball screws	DMCLS-2800 DX (Dropco)

Table 6.8 Specification of X, Y & Z Axis Drive

Specification	Description
Motor model	FANUC $\beta$ 4/4000i s
Rated output	0.75 kW
Stalling Torque	3.5 Nm
Maximum Speed	4000 rpm

Table 6.9 Drill bit Specification

Specification	Description
VDS201A04300 WU25PD	TiN coated Tungsten carbide drill bit dia of 4 mm
VDS201A06700 WU25PD	TiN coated Tungsten carbide drill bit dia of 6 mm
VDS201A08433 WU25PD	TiN coated Tungsten carbide drill bit dia of 8 mm

## 6.4 Experimental details

The experiments were performed on a CNC milling machine (Figure 6.1). The drilling operation (Figure 6.2) is performed on both HAp/PC and HAp/PSU composite specimens having mean thickness of 3.7 mm.



Figure 6.1 CNC Maxmill Machine



Figure 6.2 Drilling of composites

In this experiment, analysis of the effect of different parameter settings on circularity at both entry and exit, torque and applied thrust force on both HAp/PC and HAp/PSU

composites are carried out. The responses considered were circularity at entry, circularity at exit, torque and thrust force. The thickness of the job sample is measured at different sections using a digital vernier caliper having least count of 0.01mm. Then, drilling operations were carried out on the work piece with the selected parameter settings, keeping the job thickness and type of gas to exert pressure fixed. The diameters of the drilled holes were in millimeter range and the holes were drilled without any relative motion between the job and the work piece. After completion of the experiment, microscopic views of the drilled holes at both top (entry) and bottom (exit) were taken with the help of an optical measuring microscope. (According to Gopalsamy et al. [186] to Krishnaraj et al. [188]) The circularity at both entry and exit, and the diameter of the drilled hole at entry and exit, were measured by analyzing the microscopic views of holes with image analysis software. The circularity at both entry and exit is measured by using the ratio of minimum diameter ( $D_{min}$ ) to maximum diameter ( $D_{max}$ ) of the hole.

## 6.5 Results and discussion

### 6.5.1 Experimental data collection for HAp/PC composite

The experimental data calculated for both circularity at entry and exit, torque and thrust force of HAp/PC composite are shown in Table 6.10.

Table 6.10 Collection of data for both circularity at entry and exit, torque and thrust force of HAp/PC composite

Experimental Run	HAp Volume (%) (A)	Drilling Speed (rpm) (B)	Feed Rate (mm/min) (C)	Drill Bit Diameter (mm) (D)	Torque (KN-mm)	Thrust force (KN)	Circularity at entry (mm)	Circularity at exit (mm)
1	0	500	50	4	0.14	0.026	0.899	0.924
2	0	500	50	4	0.16	0.027	0.905	0.895
3	0	500	50	4	0.11	0.028	0.887	0.897
4	0	1000	60	6	0.23	0.042	0.999	0.956
5	0	1000	60	6	0.24	0.050	0.912	0.930
6	0	1000	60	6	0.29	0.052	0.985	0.988
7	0	1500	70	8	0.11	0.068	0.965	0.989
8	0	1500	70	8	0.10	0.078	0.999	0.988
9	0	1500	70	8	0.11	0.080	0.899	0.882
10	10	500	60	8	0.23	0.041	0.854	0.884
11	10	500	60	8	0.28	0.045	0.993	0.982
12	10	500	60	8	0.23	0.051	0.901	0.999
13	10	1000	70	4	0.14	0.023	0.876	0.909
14	10	1000	70	4	0.09	0.020	0.973	0.980
15	10	1000	70	4	0.08	0.025	0.963	0.981
16	10	1500	50	6	0.21	0.042	0.925	0.929
17	10	1500	50	6	0.18	0.041	0.987	0.969
18	10	1500	50	6	0.13	0.044	0.911	0.921
19	20	500	70	6	0.19	0.055	0.972	0.963
20	20	500	70	6	0.28	0.058	0.955	0.973
21	20	500	70	6	0.19	0.060	0.921	0.950
22	20	1000	50	8	0.19	0.079	0.909	0.904
23	20	1000	50	8	0.18	0.081	0.940	0.989
24	20	1000	50	8	0.16	0.086	0.956	0.955
25	20	1500	60	4	0.29	0.017	0.975	0.918
26	20	1500	60	4	0.20	0.023	0.901	0.934
27	20	1500	60	4	0.22	0.024	0.941	0.896



### 6.5.1.1 Prediction of optimal responses

The analysis of variance (ANOVA) Tables and main effects plots for both circularity at entry and exit, torque and thrust force of HAP/PC composite are shown in Tables 6.11, 6.12, 6.13 and 6.14, and Figures 6.3, 6.4, 6.5 and 6.6 respectively.

Table 6.11 ANOVA Table for Torque

Source	DF	Seq SS	Adj SS	Adj MS	F	P
A	2	0.010496	0.010496	0.005248	4.56	0.025
B	2	0.004230	0.004230	0.002115	1.84	0.188
C	2	0.053252	0.053252	0.026626	23.12	0.000
D	2	0.015119	0.015119	0.007559	6.56	0.007
Error	18	0.020733	0.020733	0.001152		
Total	26	0.103830				

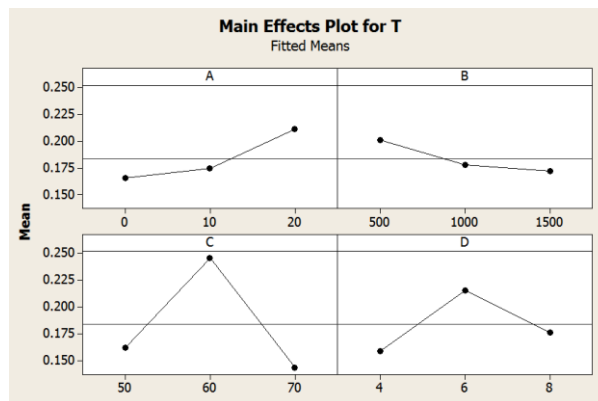


Figure 6.3 Main effects plot for means of Torque

Table 6.12 ANOVA Table for Thrust force

Source	DF	Seq SS	Adj SS	Adj MS	F	P
A	2	0.0014069	0.0014069	0.0007034	45.88	0.000
B	2	0.0002536	0.0002536	0.0001268	8.27	0.003
C	2	0.0009976	0.0009976	0.0004988	32.53	0.000
D	2	0.0087927	0.0087927	0.0043963	286.72	0.000
Error	18	0.0002760	0.0002760	0.0000153		
Total	26	0.0117267				

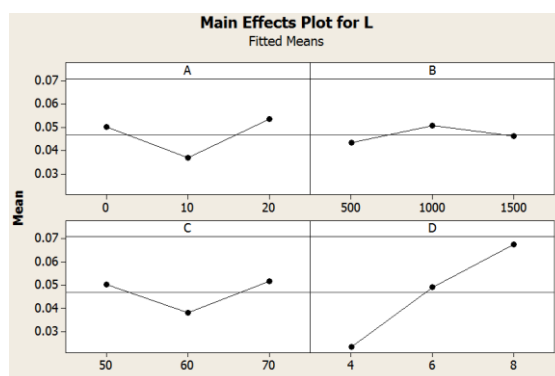


Figure 6.4 Main effects plot for means of Thrust force

Table 6.13 ANOVA Table for circularity at entry

Source	DF	Seq SS	Adj SS	Adj MS	F	P
A	2	0.000461	0.000461	0.000231	0.12	0.885
B	2	0.003623	0.003623	0.001812	0.96	0.401
C	2	0.002431	0.002431	0.001215	0.65	0.536
D	2	0.003445	0.003445	0.001723	0.91	0.418
Error	18	0.033901	0.033901	0.001883		
Total	26	0.043861				

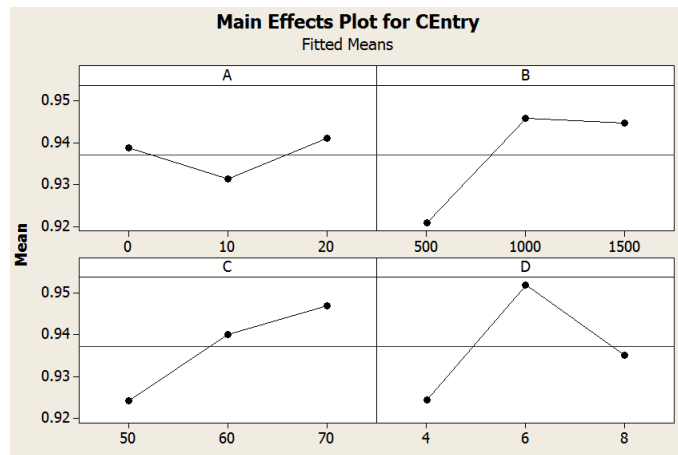


Figure 6.5 Main effects plot for means of circularity at entry

Table 6.14 ANOVA Table for circularity at exit

Source	DF	Seq SS	Adj SS	Adj MS	F	P
A	2	0.000641	0.000641	0.000320	0.21	0.809
B	2	0.001662	0.001662	0.000831	0.56	0.583
C	2	0.003001	0.003001	0.001500	1.01	0.386
D	2	0.004323	0.004323	0.002161	1.45	0.261
Error	18	0.026867	0.026867	0.001493		
Total	26	0.036493				

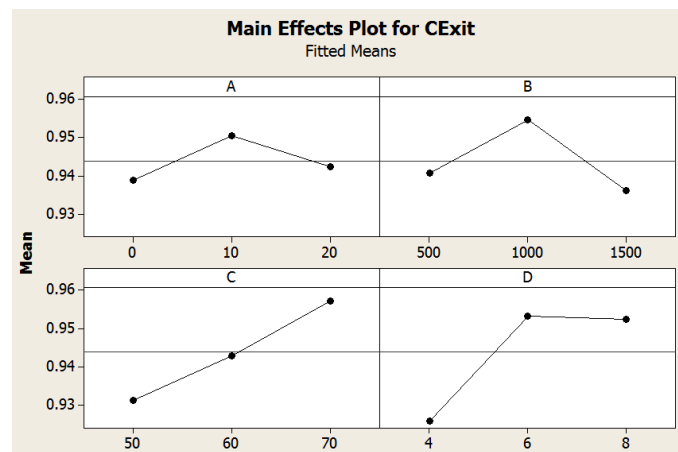


Figure 6.6 Main effects plot for means of circularity at exit

### 6.5.1.1.1 Optimization of multiple responses

(According to Moshat et al. [189]) To optimize the multiple responses into a single response to get the optimum parametric combination, various methods are used. To get the best optimum parametric condition in less time, we used Weighted Principal Component Method. This method takes few times and gives the optimum combination value simultaneously. The process parameters need to be determined in such a way that they collectively optimize more than one response simultaneously. To address this issue, effect of important process parameters viz., HAp vol. %, drilling, feed rate, and drill bit diameter have been studied. The responses considered in this study are torque, thrust force, circularity at entry and circularity at exit. The multiple responses are converted into a single response using principal component analysis (PCA) so that influence of correlation among the responses can be eliminated. Resulting single response is nothing but the weighted sum of four principal components that explain hundred percent of variation. The experiments have been conducted in accordance with Taguchi's L27 design to reduce the experimental runs.

Let  $Y_i$  be the normalized value of the  $i^{\text{th}}$  response, for  $i = 1, 2, \dots, p$ . To compute PCA,  $k$  ( $k \leq p$ ) components will be obtained to explain variance in the  $p$  responses. Principal components are independent (uncorrelated) of each other. Simultaneously, the explained variance of each principal component for the total variance of the responses is also obtained. The formed  $j$  principal component is a linear combination  $Z_j = \sum_{i=1}^p a_{ji} Y_i$  for  $j = 1,$

$2, \dots, k$  subjected to  $\sum_{i=1}^p a_{ji}^2 = 1$ ; also, the coefficient  $a_{ji}$  is called eigenvector.

In weighted principal component method, all principal components will be used; thus the explained variance can be completely explained in all responses. Second, because different principal components have their own variance to account for the total variance, the variance of each principal component is regarded as the weight. Because these principal components are independent to each other (which means that these principal components are in an additive model), the multi-response performance index (MPI) is  $MPI = \sum_{j=1}^k W_j Z_j$ , where  $W_j$  is the weight of  $j^{\text{th}}$  principal components. The larger the MPI is the higher the quality. Finally, with the application of ANOVA (Analysis of Variance), significant factors in this quality index and their contribution percentage for total variation in MPI can be obtained. First, four responses are normalized to avoid the scaling effect. Four principal components are obtained using PCA. It is evident from Table 6.15 that principal component 1 (PC1) explains 0.490 of variance, (PC2) explains

0.241 of variance, (PC3) explains 0.201 of variance and (PC4) explains 0.068 of total variance.

Table 6.15 Eigen value, proportion, cumulative and eigen vector for all components

Principal Component	Eigen value	Explained variation	Cumulative variation	Eigen vector (Torque, Thrust force, Circularity at entry, Circularity at exit)
PC1	1.9593	0.490	0.490	[0.261, 0.384, 0.621, 0.632]
PC2	0.9623	0.241	0.730	[0.876, -0.459, 0.054, -0.136]
PC3	0.8048	0.201	0.932	[-0.395, -0.792, 0.375, 0.276]
PC4	0.2735	0.068	1.000	[0.089, -0.121, -0.686, 0.711]

The calculations for principal components are done according to the following relation:

$$PC1 = (0.261 \times \text{Torque}) + (0.384 \times \text{Thrust force}) + (0.621 \times \text{Circ. at entry}) + (0.632 \times \text{Circ. at exit})$$

$$PC2 = (0.876 \times \text{Torque}) + (-0.459 \times \text{Thrust force}) + (0.054 \times \text{Circ. at entry}) + (-0.136 \times \text{Circ. at exit})$$

$$PC3 = (-0.395 \times \text{Torque}) + (-0.792 \times \text{Thrust force}) + (0.375 \times \text{Circ. at entry}) + (0.276 \times \text{Circ. at exit})$$

$$PC4 = (0.089 \times \text{Torque}) + (-0.121 \times \text{Thrust force}) + (-0.686 \times \text{Circ. at entry}) + (0.711 \times \text{Circ. at exit})$$

The relation for weighted principal component, MPI, is given by

$$MPI = (0.490 \times PC1) + (0.241 \times PC2) + (0.201 \times PC3) + (0.068 \times PC4)$$

Following Table 6.16 shows the principal components and MPI values with normalized values of responses. ANOVA Table for MPI is shown in Table 6.17. Also, main effects plot for MPI is shown in Figure 6.7.

Table 6.16 Normalized values of responses, principal components and MPI values

Expt.	Normalized Value				Principal Components				MPI
	Torque	Thrust force	Circularity at entry	Circularity at exit	PC1	PC2	PC3	PC4	
1	0.482759	0.302326	0.8999	0.924925	1.385484	0.206934	0.16261	0.046674	0.764617
2	0.551724	0.313953	0.905906	0.895896	1.393332	0.266283	0.1204	0.026646	0.772919
3	0.37931	0.325581	0.887888	0.897898	1.342873	0.108666	0.17309	0.023678	0.720597
4	0.793103	0.488372	1	0.956957	1.620332	0.394449	-0.06095	0.00589	0.877174
5	0.827586	0.581395	0.912913	0.930931	1.594523	0.380796	-0.18808	0.03894	0.837932
6	1	0.604651	0.985986	0.988989	1.730524	0.517206	-0.23118	0.042622	0.929035
7	0.37931	0.790698	0.965966	0.98999	1.628167	-0.11313	-0.14059	-0.02069	0.740872
8	0.344828	0.906977	1	0.988989	1.68432	-0.19474	-0.20657	-0.06188	0.732656
9	0.37931	0.930233	0.8999	0.882883	1.573029	-0.16618	-0.30543	-0.0684	0.664692
10	0.793103	0.476744	0.854855	0.884885	1.480182	0.401751	-0.12606	0.055623	0.800555
11	0.965517	0.523256	0.993994	0.982983	1.691446	0.525608	-0.15175	0.039638	0.927674
12	0.793103	0.593023	0.901902	1	1.626802	0.335263	-0.16874	0.091126	0.850211
13	0.482759	0.267442	0.876877	0.90991	1.348302	0.223745	0.17746	0.056013	0.754069
14	0.310345	0.232558	0.973974	0.980981	1.385484	0.084299	0.329219	0.028813	0.767336
15	0.275862	0.290698	0.963964	0.981982	1.393332	0.026729	0.293315	0.026287	0.749918
16	0.724138	0.488372	0.925926	0.92993	1.342873	0.333712	-0.06894	0.03135	0.726707
17	0.62069	0.476744	0.987988	0.96997	1.620332	0.246334	0.015453	0.009444	0.857077
18	0.448276	0.511628	0.911912	0.921922	1.594523	0.081714	0.014139	0.007904	0.804389
19	0.655172	0.639535	0.972973	0.963964	1.730524	0.201826	-0.13439	-0.00115	0.869506
20	0.965517	0.674419	0.955956	0.973974	1.628167	0.455396	-0.28822	0.041036	0.85241
21	0.655172	0.697674	0.921922	0.950951	1.68432	0.174153	-0.20317	0.017579	0.827646
22	0.655172	0.918605	0.90991	0.904905	1.573029	0.078359	-0.39536	-0.03365	0.707913
23	0.62069	0.94186	0.940941	0.98999	1.480182	0.027583	-0.36504	-0.00033	0.658541
24	0.551724	1	0.956957	0.955956	1.385484	-0.05402	-0.38723	-0.04868	0.584725
25	1	0.197674	0.975976	0.918919	1.393332	0.712997	0.068055	0.048913	0.87157
26	0.689655	0.267442	0.901902	0.934935	1.342873	0.402933	0.112028	0.075053	0.782736
27	0.758621	0.27907	0.941942	0.896897	1.620332	0.465346	0.080093	0.025271	0.923928

### 6.5.1.1.2 Analysis of multi-objective responses

Effect of various process parameters on multi-objective response called MPI is analyzed as per Taguchi's parameter design using MINITAB 16.

Table 6.17 ANOVA Table for MPI

Source	DF	Seq SS	Adj SS	Adj MS	F	P
A	2	0.002435	0.002435	0.001217	0.49	0.622
B	2	0.015028	0.015028	0.007514	3.01	0.075
C	2	0.084713	0.084713	0.042356	16.95	0.000
D	2	0.046436	0.046436	0.023218	9.29	0.002
Error	18	0.044993	0.044993	0.002500		
Total	26	0.193605				

Here, we got the  $S = 0.0499963$ ,  $R-Sq = 76.76\%$ , and  $R-Sq(adj) = 66.43\%$

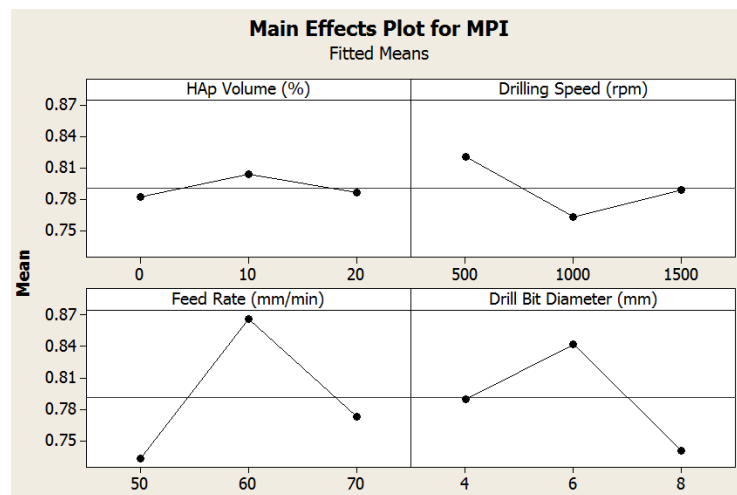


Figure 6.7 Main effects plot for MPI

Hence, main effects plot for means of MPI (Figure 6.7) shows the optimal parametric combination is  $A_2B_1C_2D_2$ , which shows the higher-the-better (HTB) value. It means that when feed rate of 60 mm/min, drilling speed of 500 rpm and 6 mm drill diameter is machined or drilled in 10 vol. % of HAp/PC composite plate sample, then we get minimum torque and thrust force with maximum circularity at both entry and exit.

## 6.5.2 Experimental data collection for HAp/PSU composite

The experimental data calculated for both circularity at entry and exit, torque and thrust force of HAp/PSU composite are shown in Table 6.18.

Table 6.18 Collection of data for both circularity at entry and exit, torque and thrust force of HAp/PSU composite

Experimental Run	HAp Volume (%)	Drilling Speed (rpm)	Feed Rate (mm/min)	Drill Bit Diameter (mm)	Torque (KN-mm)	Thrust force (KN)	Circularity at entry (mm)	Circularity at exit (mm)
1	0	500	50	4	0.12	0.028	0.921	0.900
2	0	500	50	4	0.10	0.023	0.933	0.893
3	0	500	50	4	0.08	0.027	0.957	0.959
4	0	1000	60	6	0.21	0.046	0.883	0.914
5	0	1000	60	6	0.21	0.049	0.917	0.904
6	0	1000	60	6	0.29	0.053	0.879	0.873
7	0	1500	70	8	0.28	0.048	0.912	0.896
8	0	1500	70	8	0.16	0.062	0.922	0.907
9	0	1500	70	8	0.23	0.073	0.931	0.913
10	10	500	60	8	0.36	0.081	0.903	0.914
11	10	500	60	8	0.33	0.083	0.912	0.910
12	10	500	60	8	0.32	0.089	0.905	0.901
13	10	1000	70	4	0.06	0.023	0.902	0.880
14	10	1000	70	4	0.09	0.026	0.900	0.918
15	10	1000	70	4	0.08	0.024	0.892	0.888
16	10	1500	50	6	0.43	0.041	0.926	0.906
17	10	1500	50	6	0.40	0.043	0.927	0.904
18	10	1500	50	6	0.46	0.047	0.886	0.892
19	20	500	70	6	0.25	0.058	0.908	0.843
20	20	500	70	6	0.24	0.057	0.910	0.853
21	20	500	70	6	0.20	0.050	0.918	0.842
22	20	1000	50	8	0.05	0.080	0.915	0.887
23	20	1000	50	8	0.08	0.082	0.917	0.887
24	20	1000	50	8	0.08	0.088	0.925	0.876
25	20	1500	60	4	0.20	0.021	0.909	0.890
26	20	1500	60	4	0.15	0.023	0.921	0.891
27	20	1500	60	4	0.10	0.024	0.924	0.873

### 6.5.2.1 Prediction of optimal responses

The analysis of variance (ANOVA) Tables and main effects plots for both circularity at entry and exit, torque and thrust force of HAp/PSU composite are shown in Tables 6.19, 6.20, 6.21, and 6.22 and Figures 6.8, 6.9, 6.10, and 6.11 respectively.

Table 6.19 ANOVA Table for Torque

Source	DF	Seq SS	Adj SS	Adj MS	F	P
A	2	0.082363	0.082363	0.041181	32.99	0.000
B	2	0.091785	0.091785	0.045893	36.77	0.000
C	2	0.019163	0.019163	0.009581	7.68	0.004
D	2	0.162674	0.162674	0.081337	65.17	0.000
Error	18	0.022467	0.022467	0.001248		
Total	26	0.378452				

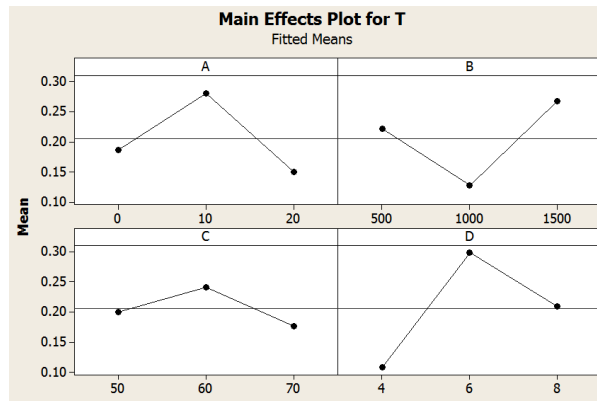


Figure 6.8 Main effects plot for means of Torque

Table 6.20 ANOVA Table for Thrust force

Source	DF	Seq SS	Adj SS	Adj MS	F	P
A	2	0.0003132	0.0003132	0.0001566	5.78	0.012
B	2	0.0007979	0.0007979	0.0003989	14.71	0.000
C	2	0.0001425	0.0001425	0.0000713	2.63	0.100
D	2	0.0121214	0.0121214	0.0060607	223.55	0.000
Error	18	0.0004880	0.0004880	0.0000271		
Total	26	0.0138360				

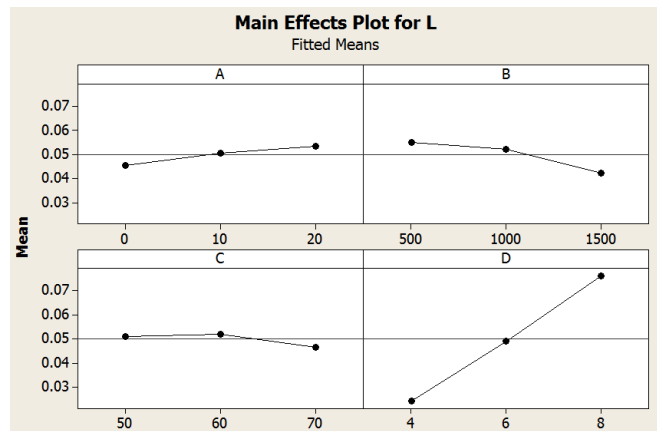


Figure 6.9 Main effects plot for means of Thrust force

Table 6.21 ANOVA Table for circularity at entry

Source	DF	Seq SS	Adj SS	Adj MS	F	P
A	2	0.0007150	0.0007150	0.0003575	2.04	0.159
B	2	0.0013050	0.0013050	0.0006525	3.72	0.044
C	2	0.0014083	0.0014083	0.0007041	4.01	0.036
D	2	0.0007059	0.0007059	0.0003529	2.01	0.163
Error	18	0.0031573	0.0031573	0.0001754		
Total	26	0.0072914				



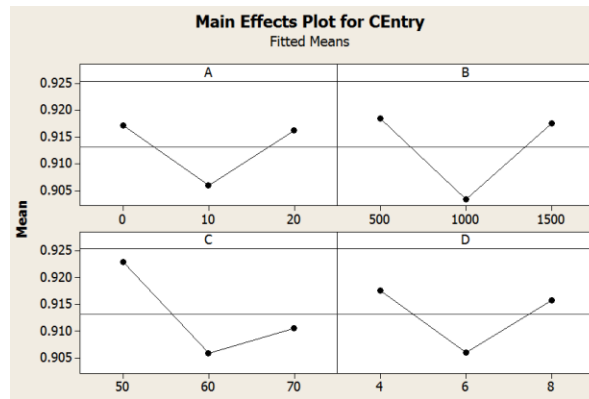


Figure 6.10 Main effects plot for means of circularity at entry

Table 6.22 ANOVA Table for circularity at exit

Source	DF	Seq SS	Adj SS	Adj MS	F	P
A	2	0.0065202	0.0065202	0.0032601	11.60	0.001
B	2	0.0002007	0.0002007	0.0001003	0.36	0.705
C	2	0.0016649	0.0016649	0.0008324	2.96	0.077
D	2	0.0019082	0.0019082	0.0009541	3.40	0.056
Error	18	0.0050567	0.0050567	0.0002809		
Total	26	0.0153507				

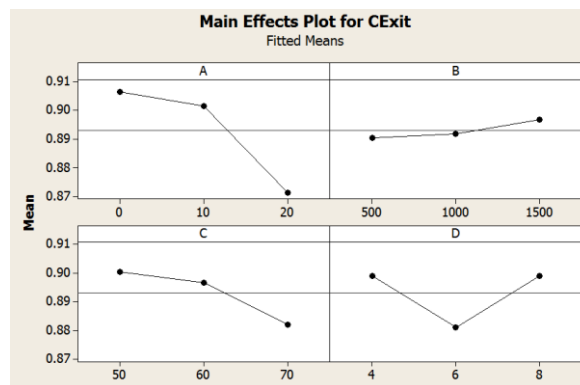


Figure 6.11 Main effects plot for means of circularity at exit

### 6.5.2.1.1 Optimization of multiple responses

It is evident from Table 6.23 that principal component 1 (PC1) explains 0.393 of variance, (PC2) explains 0.309 of variance, (PC3) explains 0.184 of variance and (PC4) explains 0.114 of total variance.

Table 6.23 Eigen value, proportion, cumulative and eigen vector for all components

Principal Component	Eigen value	Explained variation	Cumulative variation	Eigen vector (Torque, Thrust force, Circularity at entry, Circularity at exit)
PC1	1.5725	0.393	0.393	[0.434, 0.424, 0.506, 0.613]
PC2	1.2349	0.309	0.702	[-0.577, -0.522, 0.538, 0.325]
PC3	0.7369	0.184	0.886	[0.518, -0.682, -0.341, 0.388]
PC4	0.4556	0.114	1.000	[-0.460, 0.287, -0.581, 0.607]

The calculations for principal components are done according to the following relation:

$$PC1 = (0.434 \times \text{Torque}) + (0.424 \times \text{Thrust force}) + (0.506 \times \text{Circ. at entry}) + (0.613 \times \text{Circ. at exit})$$

$$PC2 = (-0.577 \times \text{Torque}) + (-0.522 \times \text{Thrust force}) + (0.538 \times \text{Circ. at entry}) + (0.325 \times \text{Circ. at exit})$$

$$PC3 = (0.518 \times \text{Torque}) + (-0.682 \times \text{Thrust force}) + (-0.341 \times \text{Circ. at entry}) + (0.388 \times \text{Circ. at exit})$$

$$PC4 = (-0.460 \times \text{Torque}) + (0.287 \times \text{Thrust force}) + (-0.581 \times \text{Circ. at entry}) + (0.607 \times \text{Circ. at exit})$$

The relation for weighted principal component, MPI, is given by

$$MPI = (0.393 \times PC1) + (0.309 \times PC2) + (0.184 \times PC3) + (0.114 \times PC4)$$

Following Table 6.24 shows the principal components and MPI values with normalized values of responses. ANOVA Table for MPI is shown in Table 6.25. Also, main effects plot for MPI is shown in Figure 6.12.

Table 6.24 Normalized values of responses, principal components and MPI values

Expt.	Normalized Value				Principal Components				MPI
	Torque	Thrust force	Circularity at entry	Circularity at exit	PC1	PC2	PC3	PC4	
1	0.26087	0.314607	0.962382	0.938478	1.308863	0.50802	-0.04347	-0.0192	0.661174
2	0.217391	0.258427	0.974922	0.931178	1.268043	0.566807	-0.03479	-0.02704	0.664
3	0.173913	0.303371	1	1	1.323108	0.604293	-0.06981	0.033067	0.697633
4	0.456522	0.516854	0.922675	0.953076	1.468386	0.272938	-0.06085	-0.01922	0.648026
5	0.456522	0.550562	0.958203	0.942649	1.494263	0.271068	-0.1	-0.03652	0.648442
6	0.630435	0.595506	0.918495	0.910323	1.54889	0.11539	-0.03957	-0.10017	0.625669
7	0.608696	0.539326	0.952978	0.934307	1.547785	0.183606	-0.01497	-0.11177	0.649517
8	0.347826	0.696629	0.963427	0.945777	1.513583	0.261365	-0.25649	0.054268	0.634592
9	0.5	0.820225	0.972832	0.952033	1.640625	0.116137	-0.26274	0.018073	0.634368
10	0.782609	0.910112	0.943574	0.953076	1.787224	-0.10925	-0.16727	-0.0685	0.630034
11	0.717391	0.932584	0.952978	0.948905	1.770649	-0.07965	-0.2212	-0.04004	0.625988
12	0.695652	1	0.945664	0.93952	1.780345	-0.10928	-0.27959	-0.01214	0.61308
13	0.130435	0.258427	0.942529	0.917623	1.205604	0.595148	-0.07405	0.023556	0.646763
14	0.195652	0.292135	0.940439	0.957247	1.271433	0.551676	-0.04717	0.028497	0.66471
15	0.173913	0.269663	0.932079	0.925965	1.229064	0.561285	-0.05239	0.017916	0.648862
16	0.934783	0.460674	0.967607	0.944734	1.669753	0.047769	0.206641	-0.28651	0.676333
17	0.869565	0.483146	0.968652	0.942649	1.650227	0.073554	0.156367	-0.25194	0.671318
18	1	0.52809	0.92581	0.930136	1.696543	-0.05228	0.203034	-0.28174	0.655827
19	0.543478	0.651685	0.948798	0.879041	1.531128	0.142375	-0.1454	-0.08064	0.609781
20	0.521739	0.640449	0.950888	0.889468	1.524378	0.165297	-0.14566	-0.06875	0.615518
21	0.434783	0.561798	0.959248	0.877998	1.45049	0.257296	-0.14437	-0.06314	0.615785
22	0.108696	0.898876	0.956113	0.924922	1.479068	0.283058	-0.52389	0.213903	0.596728
23	0.173913	0.921348	0.958203	0.924922	1.517958	0.234821	-0.50615	0.189139	0.597547
24	0.173913	0.988764	0.966562	0.913452	1.543741	0.2004	-0.55943	0.196668	0.588099
25	0.434783	0.235955	0.949843	0.92805	1.338256	0.438593	0.100483	-0.12081	0.666176
26	0.326087	0.258427	0.962382	0.929093	1.307594	0.496666	0.024982	-0.07102	0.663855
27	0.217391	0.269663	0.965517	0.910323	1.255264	0.549104	-0.04734	-0.03101	0.650746

### 6.5.2.1.2 Analysis of multi-objective responses

Effect of various process parameters on multi-objective response called MPI is analyzed as per Taguchi's parameter design using MINITAB 16.

Table 6.25 ANOVA Table for MPI

Source	DF	Seq SS	Adj SS	Adj MS	F	P
A	2	0.0044594	0.0044594	0.0022297	19.05	0.000
B	2	0.0033350	0.0033350	0.0016675	14.24	0.000
C	2	0.0004422	0.0004422	0.0002211	1.89	0.180
D	2	0.0086227	0.0086227	0.0043114	36.83	0.000
Error	18	0.0021073	0.0021073	0.0001171		
Total	26	0.0189665				

Here, we got the S = 0.0108199, R-Sq = 88.89%, and R-Sq(adj) = 83.95%

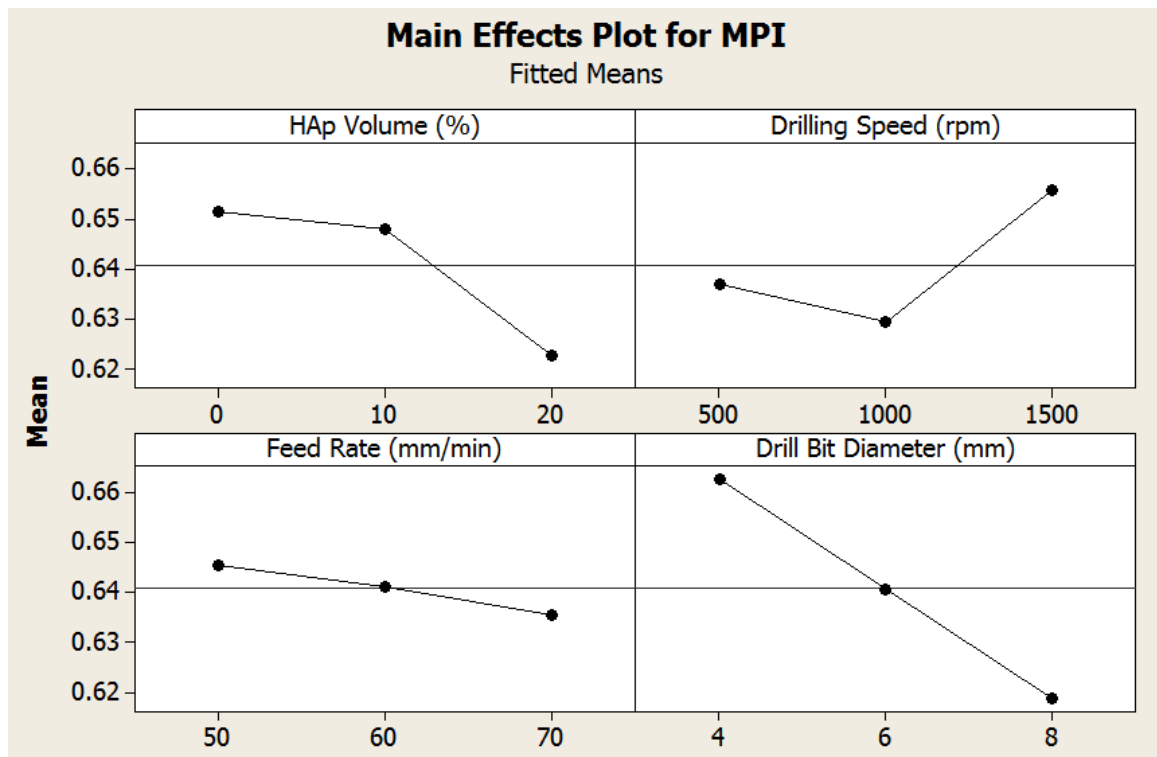


Figure 6.12 Main effects plot for MPI

Hence, main effects plot for means of MPI (Figure 6.12) shows the optimal parametric combination is  $A_1B_3C_1D_1$ , which shows the higher-the-better (HTB) value. (According to Pandey and Panda [190] to Singh et al. [193]) It means that when feed rate of 50 mm/min, drilling speed of 1500 rpm and 4 mm drill diameter is machined or drilled in 0 vol. % of HAp/PSU composite plate sample, and then we get minimum torque and thrust force with maximum circularity at both entry and exit.

### 6.5.3 SEM of drilled holes in composites

Some SEM micrographs of drilled holes in HAp/PC composite and HAp/PSU composite at varying volume percentage of HAp from 0 to 20 vol. % at different machining conditions are shown in Figure 6.13 to Figure 6.15 and Figure 6.16 to Figure 6.18 respectively. It can be observed that circularity decreases as the tool bit diameter increases for both the composites.

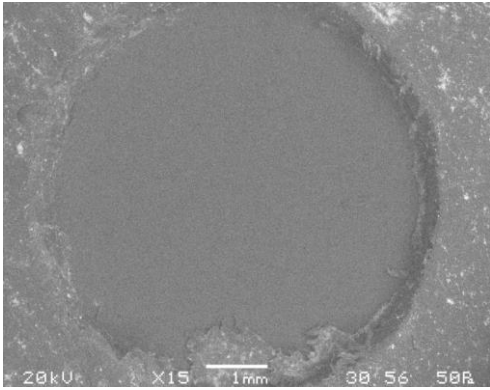


Figure 6.13 SEM of 0 vol. % HAp/PC (15x) at drilling speed of 500 rpm, feed rate of 50 mm/min, and 4 mm drill diameter

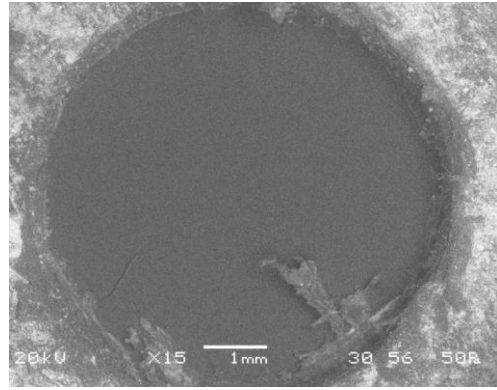


Figure 6.14 SEM of 10 vol. % HAp/PC (15x) at drilling speed of 1000 rpm, feed rate of 60 mm/min, and 6 mm drill bit diameter

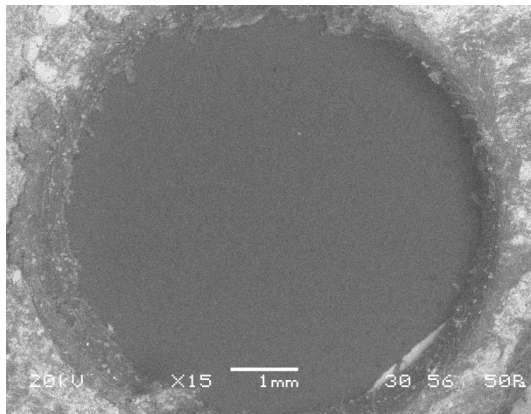


Figure 6.15 SEM of 20 vol. % HAp/PC (15x) at drilling speed of 1500 rpm, feed rate of 70 mm/min, and 8 mm drill bit diameter

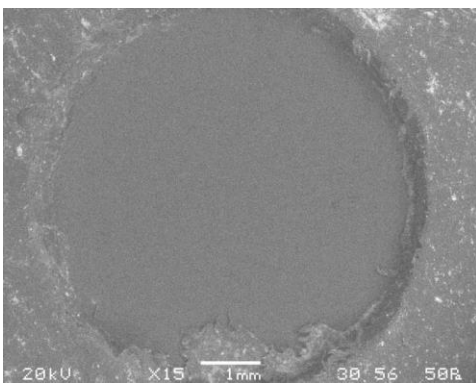


Figure 6.16 SEM of 0 vol. % HAp/PSU (15x) at drilling speed of 500 rpm, feed rate of 50 mm/min, and 4 mm drill bit diameter

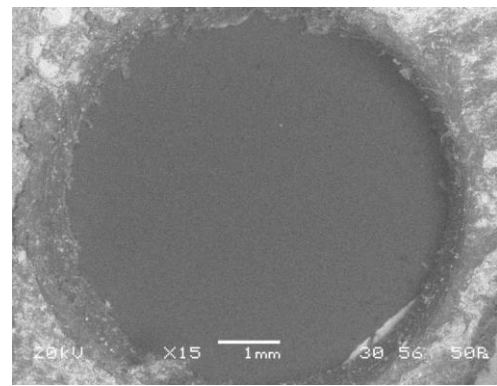


Figure 6.17 SEM of 10 vol. % HAp/PSU (15x) at drilling speed of 1000 rpm, feed rate of 60 mm/min, and 6 mm drill bit diameter

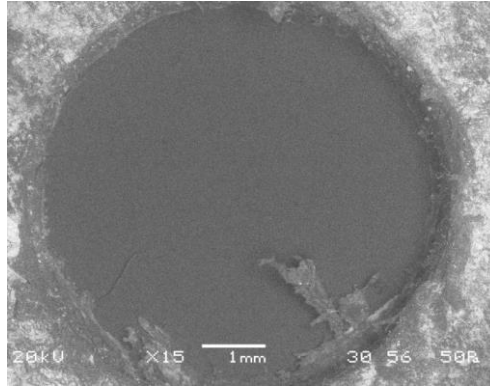


Figure 6.18 SEM of 20 vol. % HAp/PSU (15x) at drilling speed of 1500 rpm, feed rate of 70 mm/min, and 8 mm drill bit diameter

## 6.6 Conclusion

This chapter describes the drilling of ceramic composites. The aim is to develop a strategy for predicting machining parameter settings for the generation of the maximum circularity at both entry and exit with minimum torque and thrust force. For obtaining optimum circularity at both entry and exit with optimum torque and thrust force, some machining parameters with three levels are considered as inputs i.e. HAp vol. %, drilling speed, feed rate, and drill bit diameter. Experiments were carried out using Taguchi's  $L_{27}$  design array of these factors and their different levels. In this experiment, analysis of the effect of different parameters on circularity at both entry and exit, torque and applied thrust force for both HAp/PC and HAp/PSU composites are carried out. The responses considered were circularity at entry, circularity at exit, torque and thrust force. It is observed that minimum torque and thrust force with maximum circularity at both entry and exit can be obtained for 10 vol. % of HAp/PC composite plate sample can be obtained at feed rate of 60 mm/min, drilling speed of 500 rpm and 6 mm drill bit diameter. Similarly, minimum torque and thrust force with maximum circularity at both entry and exit can be obtained for 0 vol. % of HAp/PSU composite plate sample when feed rate of 50 mm/min, drilling speed of 1500 rpm and 4 mm drill bit diameter is maintained.

## Chapter 7

# Executive Summary and Conclusions

- A composite possesses superior properties than the individual constituents. A composite has light weight, high strength to weight ratio and stiffness properties and replaces the conventional materials such as metals and wood. The strength of bone is higher than both of its constituents like collagen and HAp. The softer component in the bone prevents the stiff one from brittle cracking while the stiff component prevents the soft one from yielding. The purpose of making composites is to reinforce the polymer and improve the bone bonding properties of the material. The interfacial bonding between inorganic and organic phase plays an important role in determining the ultimate mechanical properties of the composites. The compatibility of an implant material is strongly determined by the primary chemical structure.
- Bone has relatively high compressive strength of about 170 MPa but poor tensile strength of (104-121) MPa and very low shear strength (51.6) MPa. In other words, it resists pushing forces well but not pulling or torsional forces. Artificial bone can be produced from ceramics such as calcium phosphates (i.e. hydroxyapatite and tricalcium phosphate), Bioglass and calcium sulphate, all of which bioactive to different degrees depending on solubility in the physiological environment.
- Polymers are widely used in biomedical applications due to the range of physical and chemical properties possible with these materials. Polymers can be easily fabricated to various complex shapes and structures and additionally surface properties can be easily tuned. Polymers that are used as implant materials can be either derived from natural sources such as proteins or from synthetic sources. The similarity in the chemistry of ceramics and that of native bone makes ceramics often used as a part of orthopaedic implants or as dental materials. Mostly biocompatible ceramics are used in coherence with the human skeleton, bones, joints and teeth. HAp is one of the ideal materials for bone substitutions due to the nature of its biocompatibility and mechanical strength.
- Dry methods do not use a solvent unlike wet methods. The characteristics of a powder synthesized by a dry method are not strongly influenced by the processing parameters; hence most dry methods do not require precisely controlled conditions making them suitable for mass production of powders.
- HAp powder generated from a typically dry method is usually large in size and irregular in shape. Therefore, wet methods have conventionally been applied to the preparation of HAp particles having a nano-sized structure with a regular

morphology. Wet chemical reactions have advantages in their ability to control the morphology and the mean size of the powder. Based on many experimental data, they are the most promising techniques for the fabrication of nano-HAp powder. Wet processes are usually easy to manage and growth conditions can be directly controlled by adjusting the reaction parameters. Among the various wet processing methods, conventional chemical precipitation is the simplest route for the synthesis of nano-HAp powder. Wet chemical precipitation method is chosen widely to synthesize HAp in comparison to the other techniques because of relatively large amount of HAp can be produced by precipitation technique in absence of organic solvents at a reasonable cost. The size, shape and surface area of the HAp particles obtained by this reaction are very sensitive to the orthophosphoric acid addition rate and the reaction temperature. The orthophosphoric acid addition rate is strongly linked to the pH obtained at the end of the synthesis and also to the suspension stabilization.

- The particle size distribution by intensity of dry hydroxyapatite (DHAp) which has taken randomly a single peak of radius size of 481 nm and radius width of 51.8 nm with 100% intensity while the average radius size of DHAp is 1418 nm. The calculated average diameter of dry HAp is 2.836  $\mu\text{m}$  while the particle size distribution by intensity of sintered hydroxyapatite (SHAp) which has taken randomly a single peak of radius size of 581.1 nm and radius width of 78.39 nm with 100% intensity while the average radius size of SHAp is 1124 nm. The calculated average diameter of sintered HAp is 2.248  $\mu\text{m}$ .
- XRD analysis of dry HAp reveals that there is a very broad peak. It means that it is non-crystalline in nature of HAp. In other hand, XRD analysis of sintered HAp results that there is a very narrow peak as compared to dry HAp i.e. it shows crystalline nature of HAp with pure phase.
- A FTIR spectrum of dry HAp was recorded in the transmission mode in the range 4000 to 400  $\text{cm}^{-1}$ . The lower wavelength limit was chosen to encompass the highest known vibration frequency due to a fundamental molecular vibration. Broad peak between 3500 and 3000  $\text{cm}^{-1}$  were noticed on IR spectra indicated that the vibration of absorbed water ( $\text{OH}^-$ ) in the apatite lattice in accordance with the HAp chemical formula  $(\text{Ca}_{10}(\text{PO}_4)_6(\text{OH})_2)$ . There are various vibration modes representing the phosphate functional group. Those vibration modes were found on the FTIR spectra; thus confirming that the dry HAp powders were composed of phosphate group. The peaks of phosphate group were represented between 700 and 900  $\text{cm}^{-1}$  and 1200 and 1400  $\text{cm}^{-1}$  while the peaks of phosphate group were represented between 600 and 800  $\text{cm}^{-1}$  and 1100 and 1400  $\text{cm}^{-1}$  in the spectrum of sintered HAp.



- SEM micrograph of HAp/PC shows that chance of increasing voids increases as HAp content increases from 10 vol. % to 20 vol. %. However, there is a very good distribution of HAp particles into PC polymer matrix which increases bonding characteristics of HAp/PC composite. SEM micrograph of HAp/PSU shows that there is a very less chance of increasing voids as compared to HAp/PC composite as HAp content increases from 10 vol. % to 20 vol. %.
- It is clear that in A0 and B0 the volume fraction of voids is negligible due to absence of ceramic particles. With the addition of ceramic particles, more voids are found in the composite. As the ceramic content increases, the volume fraction of voids is also found to be increasing. This is due to the presence of empty spaces near sharp edges of the ceramic particles. This trend is observed in both the ceramic polymer composites from A1 to A2 and B1 to B2 irrespective of the ceramic particles. Density of a composite depends on the relative proportion of the matrix and reinforcing material and this is one of the most important factor determining the properties of the composites. The voids significantly affect some of the mechanical properties and even the performance of the composites. The knowledge of void content is desirable for estimation of the quality of the composites. It is understandable that an excellent composite should have fewer voids.
- It can be seen that Young's modulus continuously increases from 0 vol. % up to 30 vol. % and then it is decreases in 40 vol. %. in HAp/PC composite. Hence, 30 vol. % gives maximum Young's modulus for HAp/PC composite while 15 vol. % gives maximum Young's modulus in case of HAp/PSU composite. It is revealed that there tensile strength is decreasing as HAp volume percentage increases for both the composites. It can be seen that compressive strength is initially increasing and then it is gradually decreasing as HAp vol. % increasing in HAp/PC composite. For HAp/PSU composite, it shows that compressive strength is initially decreasing and then increasing as HAp vol. % increases. It is clearly shown through experimentation that HAp/PC composite of 40 vol. % gives maximum impact strength while, it can be seen that impact strength initially increases and then it decreases as HAp vol. % increases in case of HAp/PSU composite. It can also be seen that micro-indentation hardness increases as HAp vol. % increases in both composites. It is clearly shown that flexural strength gradually decreases as HAp vol. % increases for HAp/PC composite while flexural strength initially increases and then decreases as HAp vol. % increases in HAp/PSU composite,.
- The two-body abrasion wear behaviour of the composite was performed using pin-on-disc friction and wear test rig. The experiment was conducted using three different water proof silicon carbide (SiC) abrasive papers of 400, 600 and 1000 grit size.

Taguchi's  $L_{27}$  design array was used to evaluate the tribological properties with four control variables such as HAp volume percentage, load applied, sliding speed and track radius, each at three levels. The highest abrasive wear loss was noticed for the specimens worn on 400 grit size SiC paper as compared to both 600 grit size and 1000 grit size SiC paper. This is due to fact that larger size of the abrasive grains in 400 grit size SiC paper causes greater damage to the specimen surface. The experimental data of abrasion wear test of the composite showed that the wear behaviour of the composite strongly depends on the grit size of the SiC abrasive papers. It is shown that abrasive wear increases in the surface of the samples as HAp volume percentage increases in both HAp/PC and HAp/PSU composites,

- Erosion wear of ceramic composites was performed on air jet erosion test rig. In this study, dry silica sand (spherical) of different particle size of 300 $\mu$ m, 400 $\mu$ m and 500 $\mu$ m are used as erodent. Taguchi's  $L_{27}$  design array was used to evaluate the tribological properties with three control variables such as pressure, HAp volume, and impingement angle, each at three levels. The highest erosive wear loss was noticed on the specimens eroded by 500 $\mu$ m erodent particle size as compared to both 300 $\mu$ m and 400 $\mu$ m erodent particle size. This is due to fact that larger size of the abrasive grains causes greater damage to the specimen surface. The experimental data of erosion wear test showed that the wear behavior of the composite strongly depends on the erodent size of the silica sand. It is shown that erosive wear increases slightly as HAp volume percentage increases in both the HAp/PC and HAp/PSU composites.
- The sliding wear test of ceramic composites was performed on ball on plate wear tester. Taguchi's  $L_{27}$  design array was used to evaluate the tribological properties with three control variables such as HAp volume, load applied and sliding speed, each at three levels. It is shown that sliding wear increases as HAp volume percentage increases in both the HAp/PC and HAp/PSU composites.
- The fretting wear test of ceramic composites was performed on high frequency reciprocating rig (HFRR) testing machine. Taguchi's  $L_{27}$  design array was used to evaluate the tribological properties with three control variables such as HAp volume, load applied, and frequency, each at three levels. It is concluded that, fretting wear decreases as HAp volume percentage increases from 0 vol. % to 20 vol. % for both the HAp/PC and HAp/PSU composites.
- The strategy is developed for predicting machining parameter settings for the generation of the maximum circularity at both entry and exit with minimum torque and thrust force. For obtaining maximum circularity at both entry and exit with optimum torque and thrust force, some machining parameters considered at three levels are

HAp vol. %, drilling speed, feed rate, and drill bit diameter. Experiments were carried out using Taguchi's  $L_{27}$  orthogonal array. The responses considered were circularity at entry, circularity at exit, torque and thrust force. It is observed that minimum torque and thrust force with maximum circularity at both entry and exit can be obtained when feed rate of 60 mm/min, drilling speed of 500 rpm and 6 mm drill bit diameter is maintained for 10 vol. % of HAp/PC composite plate sample. Similarly, minimum torque and thrust force with maximum circularity at both entry and exit can be achieved when feed rate of 50 mm/min, drilling speed of 1500 rpm and 4 mm drill bit diameter is used for 0 vol. % of HAp/PSU composite plate sample.

- The mean relative percentage error for training and testing of HAp/PC composite conducted at 400 grit size paper in abrasive mode through ANFIS modelling is 7.38% and 14.26% respectively.
- The mean relative percentage error for training and testing of HAp/PSU composite conducted at 400 grit size paper in abrasive mode through ANFIS modelling is 3.80% and 6.30% respectively.
- The mean relative percentage error for training and testing of HAp/PC composite conducted at 600 grit size paper in abrasive mode through ANFIS modelling is 8.80% and 13.90% respectively.
- The mean relative percentage error for training and testing of HAp/PSU composite conducted at 600 grit size paper in abrasive mode through ANFIS modelling is 4.32% and 4.91% respectively.
- The mean relative percentage error for training and testing of HAp/PC composite conducted at 1000 grit size paper in abrasive mode through ANFIS modelling is 9.77% and 10.90% respectively.
- The mean relative percentage error for training and testing of HAp/PSU composite conducted at 1000 grit size paper in abrasive mode through ANFIS modelling is 4.31% and 7.21% respectively.
- The mean relative percentage error for training and testing of HAp/PC composite conducted at 300 micron size in erosive mode through ANFIS modelling is 4.11% and 9.00% respectively.
- The mean relative percentage error for training and testing of HAp/PSU composite conducted at 300 micron size in erosive mode through ANFIS modelling is 5.06% and 8.49% respectively.
- The mean relative percentage error for training and testing of HAp/PC composite conducted at 400 micron size in erosive mode through ANFIS modelling is 4.89% and 7.42% respectively.

- The mean relative percentage error for training and testing of HAp/PSU composite conducted at 400 micron size in erosive mode through ANFIS modelling is 4.84% and 5.62% respectively.
- The mean relative percentage error for training and testing of HAp/PC composite conducted at 500 micron size in erosive mode through ANFIS modelling is 4.34% and 6.37% respectively.
- The mean relative percentage error for training and testing of HAp/PSU composite conducted at 500 micron size in erosive mode through ANFIS modelling is 5.30% and 5.80% respectively.
- The mean relative percentage error for training and testing of HAp/PC composite in sliding mode through ANFIS modelling is 2.12% and 2.22% respectively.
- The mean relative percentage error for training and testing of HAp/PSU composite in sliding mode through ANFIS modelling is 2.14% and 3.66% respectively.
- The mean relative percentage error for training and testing of HAp/PC composite in fretting mode through ANFIS modelling is 3.23% and 3.41% respectively.
- The mean relative percentage error for training and testing of HAp/PSU composite in fretting mode through ANFIS modelling is 3.57% and 3.89% respectively.

## Scope for Future Research Work

The following issues should be considered for future research and development:-

- Enhance the investigation in control methods in pretreatment, processing and quality assurance.
- Investigate more detailed materials models for description of the mechanical and thermal behavior of the bio-composites.
- Improve simulation of structures, molding and curing, and needed data sets from testing or modify existing simulation codes according to bio-composites properties.
- More complex products by co-extrusion, multi-components injection molding, foaming, back injection molding, flow molding etc.
- Develop hybrid materials e.g. wood/bio-composites or ceramic/bio-composites and integrate surface finishing.
- Use special technical advantages like acoustics, fire and chemical resistance or dimensional stability of bio-composites for design of innovative products.

# References

- [1] Kannan, S., Balamurugan, A., and Rajeswarri, S., "Bio-composites: A review of Literature", *Journal of Trends in Biomaterials & Artificial Organs*, **vol. 14**, no. 2, pp. 30-36, 2001.
- [2] Ramakrishna, S., Huang, Z.-M., Kumar, G. V., Batchelor, A. W., and Mayer, J., "*An introduction to biocomposites*", **vol. 1**: World Scientific, 2004.
- [3] Meredith, J. O., "*Biocomposites for bone tissue engineering: innovation report*", University of Warwick, 2009.
- [4] Amini, A. R., Laurencin, C. T., and Nukavarapu, S. P., "Bone tissue engineering: recent advances and challenges", *Critical Reviews™ in Biomedical Engineering*, **vol. 40**, no. 5, 2012.
- [5] Bauer, S., Barron, V., and Mc Hugh, P. E. (2013), "Bio-models of Bone: A Review", *Journal of Annals of Biomedical Engineering*, **vol.33**, no.10, pp. 1295–1311.
- [6] Sarkar, D., Chu, M. C., and Cho, S. J., "Ceramic–Polymer Nanocomposite: Alternate Choice of Bone (Review)", *Journal of the Korean Ceramic Society*, **vol. 45**, no. 6, pp. 309-319, 2008.
- [7] Dorozhkin, S. V., "Calcium orthophosphate cements for biomedical application", *Journal of Materials Science*, **vol. 43**, no. 9, pp. 3028-3057, 2008.
- [8] Hribar, G., Znidarsic, A., and Maver, U., "Calcium Phosphate as a Biomaterial and its use in Biomedical Applications", Nova Science Publishers, 2012.
- [9] Ramesh, S., Tan, C., Bhaduri, S., and Teng, W., "Rapid densification of nanocrystalline hydroxyapatite for biomedical applications", *Ceramics International*, **vol. 33**, no. 7, pp. 1363-1367, 2007.
- [10] Kalita, S. J., Bhardwaj, A., and Bhatt, H. A., "Nanocrystalline calcium phosphate ceramics in biomedical engineering", *Materials Science and Engineering: C*, **vol. 27**, no. 3, pp. 441-449, 2007.
- [11] Zhou, H., and Lee, J., "Nanoscale hydroxyapatite particles for bone tissue engineering", *Acta biomaterialia*, **vol. 7**, no. 7, pp. 2769-2781, 2011.
- [12] Garnett, J. and Dieppe, P., "The effects of serum and human albumin on calcium hydroxyapatite crystal growth", *Journal of Biochemistry*, **vol. 266**, no. 3, pp. 863-868, 1990.
- [13] Orlovskii, V., Komlev, V., and Barinov, S., "Hydroxyapatite and hydroxyapatite-based ceramics", *Inorganic Materials*, **vol. 38**, no. 10, pp. 973-984, 2002.
- [14] Abdurrahim, T., and Sopyan, I., "Recent progress on the development of porous bioactive calcium phosphate for biomedical applications", *Recent Patents on Biomedical Engineering*, **vol.1**, no. 3, pp. 213-229, 2008.
- [15] Math, S., and Basu, B., "Materials for orthopedic applications", *Advanced Biomaterials: Fundamentals, Processing, and Applications*, **vol. 53**, no. 1, 2010.
- [16] Zhang, L., and Sirivisoot, S., "Nanomaterials for improved orthopedic and bone tissue engineering applications", *Advanced Biomaterials: Fundamentals, Processing, and Applications*, **vol. 205**, no. 1, 2010.
- [17] Chakraborty, J., and Basu, D., "Bioceramics—a new era", *Transactions of the Indian Ceramic Society*, **vol. 64**, no. 4, pp. 171-192, 2005.
- [18] Cavanaugh, G., "*Nano-Materials for Bone Implants*", WORCESTER POLYTECHNIC INSTITUTE.
- [19] Liu, H., and Webster, T. J., "Nanomedicine for implants: a review of studies and necessary experimental tools", *Biomaterials*, **vol. 28**, no. 2, pp. 354-369, 2007.
- [20] Parchi, P., Vittorio, O., Andreani, L., Piolanti, N., Cirillo, G., Iemma, F., and Lisanti, M., "How nanotechnology can really improve the future of orthopedic implants and scaffolds for bone and cartilage defects", *Journal of Nanomedicine & Biotherapeutic Discovery*, 2013.
- [21] Jagur, G. J., "Polymers for tissue engineering, medical devices, and regenerative medicine. Concise general review of recent studies", *Journal of Polymers for Advanced Technologies*, **vol. 17**, no. 6, pp. 395-418, 2006.
- [22] Nayak, A. K., "Hydroxyapatite synthesis methodologies: an overview", *International Journal of ChemTech Research*, **vol. 2**, no. 2, pp. 903-907, 2010.
- [23] Sadat-Shojai, M., Khorasani, M.-T., Dinpanah-Khoshdargi, E., and Jamshidi, A., "Synthesis methods for nanosized hydroxyapatite with diverse structures", *Acta biomaterialia*, **vol. 9**, no. 8, pp. 7591-7621, 2013.
- [24] Afshar, A., Ghorbani, M., Ehsani, N., Saeri, M., and Sorrell, C., "Some important factors in the wet precipitation process of hydroxyapatite", *Materials & Design*, **vol. 24**, no. 3, pp. 197-202, 2003.

- [25] Anee, T., Ashok, M., Palanichamy, M., and Kalkura, S. N., "A novel technique to synthesize hydroxyapatite at low temperature", *Materials Chemistry and Physics*, **vol. 80**, no. 3, pp. 725-730, 2003.
- [26] Donadel, K., Laranjeira, M. C. M., Goncalves, V. L., Favere, V.T., Machado, K. D., Lima, J. C. de, and Prates, L. H. M., "Structural, vibrational, and mechanical studies of Hydroxyapatite produced by wet-chemical methods", *Journal of Chemical Physics*, **vol. 1**, no. 2, pp. 1-10, 2008.
- [27] Eslami, H., Tahri, M., and Bakhshi, F., "Synthesis and characterization of nanocrystalline hydroxyapatite obtained by the wet chemical technique", *Materials Science Poland*, **vol. 28**, no. 1, pp. 5-13, 2010.
- [28] Kweh, S., Khor, K., and Cheang, P., "The production and characterization of hydroxyapatite (HA) powders", *Journal of Materials Processing Technology*, **vol. 89**, pp. 373-377, 1999.
- [29] Lin, K., Wu, C., and Chang, J., "Advances in synthesis of calcium phosphate crystals with controlled size and shape", *Acta biomaterialia*, **vol. 10**, no. 10, pp. 4071-4102, 2014.
- [30] Monmaturapoj, N., "Nano-size hydroxyapatite powders preparation by wet-chemical precipitation route", *Journal of Metals, Materials and Minerals*, **vol. 18**, no. 1, pp. 15-20, 2008.
- [31] Muralithran, G., and Ramesh, S., "The effects of sintering temperature on the properties of hydroxyapatite", *Ceramics International*, **vol. 26**, no. 2, pp. 221-230, 2000.
- [32] Pramanik, S., and Kar, K. K., "Nanohydroxyapatite synthesized from calcium oxide and its characterization", *The International Journal of Advanced Manufacturing Technology*, **vol. 66**, no. 5-8, pp. 1181-1189, 2013.
- [33] Saeri, M. R., Afshar, A., Ghorbani, M., Ehsani, N., and Sorrell, C. C., "The wet precipitation process of hydroxyapatite", *Materials Letters*, **vol. 57**, no. 24, pp. 4064-4069, 2003.
- [34] Salma, K., Berzina-Cimdina, L., and Borodajenko, N., "Calcium phosphate bioceramics prepared from wet chemically precipitated powders", *Processing and Application of Ceramics*, **vol. 4**, no. 1, pp. 45-51, 2010.
- [35] Santhosh, S., and Prabu, S. B., "Thermal stability of nano hydroxyapatite synthesized from sea shells through wet chemical synthesis", *Materials Letters*, **vol. 97**, no. 1, pp. 121-124, 2013.
- [36] Tas, A. C., "Synthesis of biomimetic Ca-hydroxyapatite powders at 37°C in synthetic body fluids", *Biomaterials*, **vol. 21**, no. 14, pp. 1429-1438, 2000.
- [37] Tas, A. C., "Preparation of porous apatite granules from calcium phosphate cement", *Journal of Materials Sciences: Materials in Medicine*, **vol. 19**, no. 12, pp. 2231-2239, 2008.
- [38] Pang, Y., and Bao, X., "Influence of temperature, ripening time and calcination on the morphology and crystallinity of hydroxyapatite nanoparticles", *Journal of the European Ceramic Society*, **vol. 23**, no. 10, pp. 1697-1704, 2003.
- [39] Pramanik, S., Agarwal, A. K., and Rai, K., "Development of high strength hydroxyapatite for hard tissue replacement", *Trends in Biomaterials and Artificial Organs*, **vol. 19**, no. 1, pp. 46-51, 2005.
- [40] Ramesh, S., Tan, C. Y., Tolouei, R., Amiriyan, M., Purbolaksono, J., Sopyan, I., and Teng, W. D., "Sintering behavior of hydroxyapatite prepared from different routes", *Materials & Design*, **vol. 34**, no. 1, pp. 148-154, 2012.
- [41] Ruys, A., Wei, M., Sorrell, C., Dickson, M., Brandwood, A., and Milthorpe, B., "Sintering effects on the strength of hydroxyapatite", *Biomaterials*, **vol. 16**, no. 5, pp. 409-415, 1995.
- [42] Neuendorf, R. E., Saiz, E., Tomsia, A.P., and Ritchie, R.O., "Adhesion between biodegradable polymers and hydroxyapatite", *Journal of Acta Biomaterialia*, **vol. 4**, no. 5, pp. 1288-1296, 2008.
- [43] Tin-Oo, M. M., Gopalakrishnan, V., Samsuddin, A. R., Al Salihi, K. A., and Shamsuria, O., "Antibacterial property of locally produced hydroxyapatite", *Archives of Orofacial Sciences*, **vol. 2**, no. 11, pp. 41-44, 2007.
- [44] Velayudhan, S., Ramesh, P., Sunny, M. C., and Varma, H. K., "Extrusion of hydroxyapatite to clinically significant shapes", *Journal of Materials Letters*, **vol. 46**, no. 2, pp. 142-146, 2000.
- [45] Yeong, K., Wang, J., and Ng, S., "Fabricating densified hydroxyapatite ceramics from a precipitated precursor", *Materials Letters*, **vol. 38**, no. 3, pp. 208-213, 1999.
- [46] Yoruc, A. B. H., and Koca, Y., "Double step stirring: A novel method for precipitation of nano-sized hydroxyapatite powder", *Digest J. Nanomater. Biostructures*, **vol. 4**, no. 1, pp. 73-81, 2009.
- [47] Zhang, Y., and Lu, J., "A simple method to tailor spherical nanocrystal hydroxyapatite at low temperature", *Journal of Nanoparticle Research*, **vol. 9**, no. 4, pp. 589-594, 2007.

- [48] Cao, L.-y., Zhang, C.-b., and Huang, J.-f., "Synthesis of hydroxyapatite nanoparticles in ultrasonic precipitation", *Ceramics International*, **vol. 31**, no. 8, pp. 1041-1044, 2005.
- [49] Ferraz, M., Monteiro, F., and Manuel, C., "Hydroxyapatite nanoparticles: a review of preparation methodologies", *Journal of Applied Biomaterials and Biomechanics*, **vol. 2**, no. 2, pp. 74-80, 2004.
- [50] Kivrak, N., and Taş, A. C., "Synthesis of Calcium Hydroxyapatite-Tricalcium Phosphate (HA-TCP) Composite Bioceramic Powders and Their Sintering Behavior", *Journal of the American Ceramic Society*, **vol. 81**, no. 9, pp. 2245-2252, 1998.
- [51] Kumar, R., Prakash, K., Cheang, P., and Khor, K., "Temperature driven morphological changes of chemically precipitated hydroxyapatite nanoparticles", *Langmuir*, **vol. 20**, no. 13, pp. 5196-5200, 2004.
- [52] Liu, Y., Hou, D., and Wang, G. A., "Simple wet chemical synthesis and characterization of hydroxyapatite nanorods", *Materials Chemistry and Physics*, **vol. 86**, no. 1, pp. 69-73, 2004.
- [53] Lopez-Macipe, A., Rodriguez-Clemente, R., Hidalgo-Lopez, A., Arita, I., Garcia-Garduno, M., Rivera, E., and Castano, V., "Wet chemical synthesis of hydroxyapatite particles from nonstoichiometric solutions", *Journal of Materials Synthesis and Processing*, **vol. 6**, no. 1, pp. 21-26, 1998.
- [54] Mahabole, M., Aiyer, R., Ramakrishna, C., Sreedhar, B., and Khairnar, R., "Synthesis, characterization and gas sensing property of hydroxyapatite ceramic", *Bulletin of Materials Science*, **vol. 28**, no. 6, pp. 535-545, 2005.
- [55] Mobasherpour, I., Heshajin, M. S., Kazemzadeh, A., and Zakeri, M., "Synthesis of nanocrystalline hydroxyapatite by using precipitation method", *Journal of Alloys and Compounds*, **vol. 430**, no. 1, pp. 330-333, 2007.
- [56] Mostafa, N. Y., "Characterization, thermal stability and sintering of hydroxyapatite powders prepared by different routes", *Materials Chemistry and Physics*, **vol. 94**, no. 2, pp. 333-341, 2005.
- [57] Murugan, R., and Ramakrishna, S., "Aqueous mediated synthesis of bioresorbable nanocrystalline hydroxyapatite", *Journal of Crystal Growth*, **vol. 274**, no. 1, pp. 209-213, 2005.
- [58] Raynaud, S., Champion, E., Bernache-Assollant, D., and Thomas, P., "Calcium phosphate apatites with variable Ca/P atomic ratio I. Synthesis, characterisation and thermal stability of powders", *Biomaterials*, **vol. 23**, no. 4, pp. 1065-1072, 2002.
- [59] Santos, M. H., Oliveira, M. d., Souza, L. P. d. F., Mansur, H. S., and Vasconcelos, W. L., "Synthesis control and characterization of hydroxyapatite prepared by wet precipitation process", *Materials Research*, **vol. 7**, no. 4, pp. 625-630, 2004.
- [60] Wang, P., Li, C., Gong, H., Jiang, X., Wang, H., and Li, K., "Effects of synthesis conditions on the morphology of hydroxyapatite nanoparticles produced by wet chemical process", *Powder Technology*, **vol. 203**, no. 2, pp. 315-321, 2010.
- [61] Bakar, M. A., Cheng, M., Tang, S., Yu, S., Liao, K., Tan, C., and Cheang, P., "Tensile properties, tension-tension fatigue and biological response of polyetheretherketone-hydroxyapatite composites for load-bearing orthopedic implants", *Biomaterials*, **vol. 24**, no. 13, pp. 2245-2250, 2003.
- [62] Fang, L., Gao, P., and Leng, Y., "High strength and bioactive hydroxyapatite nano-particles reinforced ultrahigh molecular weight polyethylene", *Composites Part B: Engineering*, **vol. 38**, no. 3, pp. 345-351, 2007.
- [63] Hutmacher, D. W., Sittinger, M. and Risbud, M. V., "Scaffold-based tissue engineering: rational for computer-aided design and solid free-form fabrication systems", *Journal of Trends in biotechnology*, **vol. 22**, no. 7, pp. 354-362, 2004.
- [64] Joseph, R., McGregor, W., Martyn, M. T., Tanner, K., and Coates, P. D., "Effect of hydroxyapatite morphology/surface area on the rheology and processability of hydroxyapatite filled polyethylene composites", *Biomaterials*, **vol. 23**, no. 21, pp. 4295-4302, 2002.
- [65] Juang, H. Y., and Hon, M. H., "Fabrication and mechanical properties of hydroxyapatite-alumina composites", *Materials Science and Engineering: C*, **vol. 2**, no. 1, pp. 77-81, 1994.
- [66] Li, Y., Jianguo, L., ZHANG, L., Yi, Z., Huanan, W., Jidong, L., and Yubao, L., "Development of nano-hydroxyapatite/polycarbonate composite for bone repair", *Journal of biomaterials applications*, 2009.
- [67] Liao, C. Z., Li, K., Wong, H. M., Tong, W. Y., Yeung, K. W. K., and Tjong, S. C., "Novel polypropylene biocomposites reinforced with carbon nanotubes and hydroxyapatite nanorods for bone replacements", *Materials Science and Engineering: C*, **vol. 33**, no. 3, pp. 1380-1388, 2013.



- [68] Liu, X. and Ma, P. X., "Polymeric scaffolds for bone tissue engineering", *Journal of Annals of Biomedical Engineering*, **vol. 32**, no. 3, pp. 477-486, 2004.
- [69] Liu, Y., and Wang, M., "Developing a composite material for bone tissue repair", *Current Applied Physics*, **vol. 7**, no. 5, pp. 547-554, 2007.
- [70] Liu, Y., and Wang, M., "Fabrication and characteristics of hydroxyapatite reinforced polypropylene as a bone analogue biomaterial", *Journal of applied polymer science*, **vol. 106**, no. 4, pp. 2780-2790, 2007.
- [71] Nath, S., Bodhak, S. and Basu, B., "HDPE-Al<sub>2</sub>O<sub>3</sub>-HAp composites for biomedical applications: processing and characterizations", *Journal of Biomedical Materials Research Part B: Applied Biomaterials*, **vol. 88**, no. 2, pp. 1-18, 2008.
- [72] Ramakrishna, S., Mayer, J., Wintermantel, E., and Leong, K. W., "Biomedical applications of polymer-composite materials: a review", *Journal of Composites Science and Technology*, **vol. 61**, no. 9, pp. 1189-1224, 2001.
- [73] Robinson, P., Wilson, C., and Mecholsky, J., "Processing and mechanical properties of hydroxyapatite-polysulfone laminated composites", *Journal of the European Ceramic Society*, **vol. 34**, no. 5, pp. 1387-1396, 2014.
- [74] Sendemir, A. and Altintas, S., "Production of HAp reinforced polymer composites for biomedical applications", *Proceedings of the 2nd International conference Biomedical Engineering Days*, no. 5, pp. 114-117, 1997.
- [75] Sim, C., Cheang, P., Liang, M., and Khor, K., "Injection moulding of hydroxyapatite composites", *Journal of Materials Processing Technology*, **vol. 69**, no. 1, pp. 75-78, 1997.
- [76] Sousa, R. A., Reis, R. L., Cunha, A. M. and Bevis, M. J., "Coupling of HDPE/hydroxyapatite composites by silane-based methodologies", *Journal of Materials Sciences: Materials in Medicine*, **vol. 14**, no. 8, pp. 475-487, 2003.
- [77] Szaraniec, B., Rosół, P., and Chłopek, J., "Carbon composite material and polysulfone modified by nano-hydroxyapatite", *e-Polymers*, **vol. 5**, no. 1, pp. 314-320, 2005.
- [78] Wahl, D., and Czernuszka, J., "Collagen-hydroxyapatite composites for hard tissue repair", *Eur Cell Mater*, **vol. 11**, no. 1, pp. 43-56, 2006.
- [79] Wang, M., Yue, C., and Chua, B., "Production and evaluation of hydroxyapatite reinforced polysulfone for tissue replacement", *Journal of Materials Science: Materials in Medicine*, **vol. 12**, no. 9, pp. 821-826, 2001.
- [80] Wang, X., Li, Y., Wei, J., and De Groot, K., "Development of biomimetic nano-hydroxyapatite/poly (hexamethylene adipamide) composites", *Biomaterials*, **vol. 23**, no. 24, pp. 4787-4791, 2002.
- [81] Weigel, T., Schinkel, G., and Lendlein, A., "Design and preparation of polymeric scaffolds for tissue engineering", *Journal of Expert Review of Medical Devices*, **vol. 3**, no. 6, pp. 835-851, 2006.
- [82] Chu, P. K., and Liu, X., "*Biomaterials fabrication and processing handbook*: CRC press", 2008.
- [83] Goswami, J., Bhatnagar, N., Mohanty, S., and Ghosh, A., "Processing and characterization of poly (lactic acid) based bioactive composites for biomedical scaffold application", *Express Polymer Letters*, **vol. 7**, no. 9, 2013.
- [84] Mehar, A. K., Mahapatra, S. S., and Patel, S. K., "Fabrication, Processing and Assessment of Mechanical behaviour of Hydroxyapatite (HAp) reinforced Polycarbonate (PC) Composite for Bio-medical Applications", *Trends in Industrial and Mechanical Engineering*, **vol. 3**, no. 1, pp. 84-90, 2016.
- [85] Wang, M., "*Bioactive ceramic-polymer composites for bone replacement*", Paper presented at the Proceedings of the 13th International Conference on Composite Materials (ICCM-13), Beijing, China, 2001.
- [86] Wang, M., "Developing bioactive composite materials for tissue replacement", *Biomaterials*, **vol. 24**, no. 13, pp. 2133-2151, 2003.
- [87] Wang, M., "Bioactive ceramic-polymer composites for tissue replacement", *Biomaterials Engineering and processing, School of Mechanical and Production Engineering, Nanyang Tech. University Singapore*, 2004.
- [88] Xiao, X., Huang, Q., Liu, R., She, H., and Lin, Z., "Nano-hydroxyapatite/polymer composite porous scaffold materials", *Acta Materiae Compositae Sinica*, **vol. 6**, no. 9, 2008.
- [89] Viswanath, B., Ravishankar, N., Nayar, S., and Sinha, A., "Synthesis, Sintering and Micro structural characterization of nano crystalline Hydroxyapatite composites", *Material Research Society Symposium proceedings*, **vol. 845**, No. 11-12, pp. 1-6, 2005.

- [90] Murugan, R., and Ramakrishna, S., "Bioresorbable composite bone paste using polysaccharide based nano hydroxyapatite", *Biomaterials*, **vol. 25**, no. 1, pp. 3829-3835, 2004.
- [91] Murugan, R., and Ramakrishna, S., "Crystallographic study of hydroxyapatite bioceramics derived from various sources", *Crystal growth & design*, **vol. 5**, no. 1, pp. 111-112, 2005.
- [92] Bakshi, S. R., Tercero, J. E., and Agarwal, A., "Synthesis and characterization of multiwalled carbon nano tube reinforced ultrahigh molecular weight polyethylene composite by electrostatic spraying technique", *Journal of Composites Part A: Applied Science and Manufacturing*, **vol. 38**, No. 12, pp. 2493-2499, 2007.
- [93] Beherei, H. H., El-Bassyouni, G. T., and Mohamed, K. R., "Modulation, characterization and bioactivity of new biocomposites based on apatite", *Ceramics International*, **vol. 34**, no. 8, pp. 2091-2097, 2008.
- [94] Chen, L., and Wang, M., "Production and evaluation of biodegradable composites based on PHB-PHV copolymer", *Biomaterials*, **vol. 23**, no. 1, pp. 2631-2639, 2002.
- [95] Coombes, A. G. A. and Meikle, M. C., "Resorbable synthetic polymers as replacements for bone graft", *Journal of clinical materials*, **vol. 17**, no. 1, pp. 35-67, 1994).
- [96] Degirmenbasi, N., Kalyon, D. M., and Birinci, E., "Biocomposites of nanohydroxyapatite with collagen and poly (vinyl alcohol)", *Colloids and Surfaces B: Biointerfaces*, **vol. 48**, no. 1, pp. 42-49, 2006.
- [97] Meenan, B. J., Mc Clorey, C., and Akay, M., "Thermal analysis studies of HAp-PEEK biocomposite mixtures", *Journal of Materials Sciences: Materials in Medicine*, **vol. 11**, no. 8, pp. 481-489, 2000.
- [98] Ni, J., and Wang, M., "In vitro evaluation of hydroxyapatite reinforced polyhydroxybutyrate composite", *Materials Science and Engineering: C*, **vol. 20**, no. 1, pp. 101-109, 2002.
- [99] Pompe, W., Worch, H., Eppele, M., Friess, W., Gelinsky, M., Greil, P., Hempel, U., Scharnweber, D., and Schulte, K., "Functionally graded materials for biomedical applications", *Journal of Materials Science and Engineering: Part A*, **vol. 362**, no. 1-2, pp. 40-60, 2003.
- [100] Rai, D. V. and Singh, R., "Thermodynamic study of bone bio-composites", *Journal of Trends in Biomaterials Artificial Organs*, **vol. 19**, no. 1, pp. 33-38, 2005.
- [101] Ramay, H. R., and Zhang, M., "Preparation of porous hydroxyapatite scaffolds by combination of the gel-casting and polymer sponge methods", *Biomaterials*, **vol. 24**, no. 19, pp. 3293-3302, 2003.
- [102] Sounderya, N. and Zhang, Y., "Use of Core/Shell Structured Nano particles for Biomedical Applications", *Journal of Recent Patents on Biomedical Engineering*, **vol. 1**, no. 1, pp. 34-42, 2008.
- [103] Sousa, R. A., Reis, R. L., Cunha, A. M., and Bevis, M. J., "Processing and properties of bone-analogue biodegradable and bio-inert polymeric composites", *Journal of Composites Science and Technology*, **vol. 63**, no. 3-4, pp. 389-402, 2003.
- [104] Zhang, Z., and Friedrich, K., "Artificial neural networks applied to polymer composites: a review", *Journal of Composites Science and Technology*, **vol. 63**, no. 3, pp. 2029-2044, 2003.
- [105] Ignjatovic, N., and Uskokovic, D., "Synthesis and application of hydroxyapatite/poly lactide composite biomaterial", *Applied Surface Science*, **vol. 238**, no. 1, pp. 314-319, 2004.
- [106] Kim, B. S., Yang, S. S., and Lee, J., "A polycaprolactone/cuttlefish bone-derived hydroxyapatite composite porous scaffold for bone tissue engineering", *Journal of Biomedical Materials Research Part B: Applied Biomaterials*, **vol. 102**, no. 5, pp. 943-951, 2014.
- [107] Piticescu, R. M., Popescu, M. L., Łojkowski, W., Opalińska, A., and Strachowski, T., "New hydroxyapatite based nanomaterials for potential use in medical fields".
- [108] Sailaja, G., Velayudhan, S., Sunny, M., Sreenivasan, K., Varma, H., and Ramesh, P., "Hydroxyapatite filled chitosan-polyacrylic acid polyelectrolyte complexes", *Journal of materials science*, **vol. 38**, no. 17, pp. 3653-3662, 2003.
- [109] Tripathi, G., Choudhury, P., and Basu, B., "Development of polymer based biocomposites: a review", *Materials Technology*, **vol. 25**, no. 3-4, pp. 158-176, 2010.
- [110] Verma, D., "Design of polymer-biopolymer-hydroxyapatite biomaterials for bone tissue engineering: Through molecular control of interfaces: ProQuest", 2008.
- [111] Zhang, R., and Ma, P. X., "Poly (α-hydroxyl acids)/hydroxyapatite porous composites for bone-tissue engineering. I. Preparation and morphology", *Journal of biomedical materials research*, **vol. 44**, no. 4, pp. 446-455, 1999.
- [112] Bonfield, W., "Design of bioactive ceramic-polymer composites", *Advanced series in ceramics*, **vol. 1**, no. 1, pp. 299-304, 1993.

- [113]Hiep, N. T., Lee, B.-T., and Van Toi, V., "Fabrication of PCL/PLGA-BCP porous scaffold for bone tissue engineering applications.
- [114]Li, Y., Jianguo, L., ZHANG, L., Yi, Z., Huanan, W., Jidong, L., and Yubao, L., "Development of nano-hydroxyapatite/polycarbonate composite for bone repair", *Journal of biomaterials applications*, 2009.
- [115]Pilia, M., Guda, T., and Appleford, M., "Development of composite scaffolds for load-bearing segmental bone defects", *BioMed research international*, 2013.
- [116]Tayton, E., Purcell, M., Smith, J. O., Lanham, S., Howdle, S. M., Shakesheff, K. M., and Dunlop, D. G., "The scale-up of a tissue engineered porous hydroxyapatite polymer composite scaffold for use in bone repair: An ovine femoral condyle defect study", *Journal of Biomedical Materials Research Part A*, vol. **103**, no. 4, pp. 1346-1356, 2015.
- [117]Ahmad, M., Wahit, M. U., Abdul Kadir, M. R., and Mohd Dahlan, K. Z., "Mechanical, rheological, and bioactivity properties of ultrahigh-molecular-weight polyethylene bioactive composites containing polyethylene glycol and hydroxyapatite", *The Scientific World Journal*, 2012.
- [118]Asuke, F., Aigbodion, V., Abdulwahab, M., Fayomi, O., Popoola, A., Nwoyi, C., and Garba, B., "Effects of bone particle on the properties and microstructure of polypropylene/bone ash particulate composites", *Results in Physics*, vol. **2**, no. 1, pp. 135-141, 2012.
- [119]Bakar, M. A., Cheang, P., and Khor, K., "Mechanical properties of injection molded hydroxyapatite-polyetheretherketone biocomposites", *Composites Science and Technology*, vol. **63**, no. 3, pp. 421-425, 2003.
- [120]Converse, G. L., Conrad, T. L., and Roeder, R. K., "Mechanical properties of hydroxyapatite whisker reinforced polyetherketoneketone composite scaffolds", *Journal of the mechanical behavior of biomedical materials*, vol. **2**, no. 6, pp. 627-635, 2009.
- [121]Hossan, M., Gafur, M., Karim, M., and Rana, A., "Mechanical properties of Gelatin–Hydroxyapatite composite for bone tissue engineering", *Bangladesh Journal of Scientific and Industrial Research*, vol. **50**, no. 1, pp. 15-20, 2015.
- [122]Hsiao-Che, J. S.-S. W., Hung, L. J.-P., and Chen, J.-H., "Effects of bone mineral fraction and volume fraction on the mechanical properties of cortical bone", *Journal of Medical and Biological Engineering*, vol. **26**, no. 1, pp. 1-7, 2006.
- [123]Huang, Q.-w., Wang, L.-p., and Wang, J.-y., "Mechanical properties of artificial materials for bone repair", *Journal of Shanghai Jiaotong University (Science)*, vol. **19**, no. 1, pp. 675-680, 2014.
- [124]Jaggi, H. S., Kumar, Y., Satapathy, B. K., Ray, A. R., and Patnaik, A., "Analytical interpretations of structural and mechanical response of high density polyethylene/hydroxyapatite bio-composites", *Materials & Design*, vol. **36**, no. 1, pp. 757-766, 2012.
- [125]Kang, X., Zhang, W., and Yang, C., "Mechanical properties study of micro- and nano-hydroxyapatite reinforced ultrahigh molecular weight polyethylene composites", *Journal of applied polymer science*, vol. **133**, no. 3, 2016.
- [126]Nainar, S. M., Begum, S., Ansari, M., and Anuar, H., "Tensile Properties and Morphological Studies on HA/PLA Biocomposites for Tissue Engineering Scaffolds", *International Journal of Engineering Research*, vol. **3**, no. 3, pp. 186-189, 2014.
- [127]Nazhat, S. N., Joseph, R., Wang, M., Smith, R., Tanner, K. E., and Bonfield, W., "Dynamic mechanical characterization of HAp reinforced polyethylene: effect of particle size", *Journal of Materials Sciences: Materials in Medicine*, vol. **11**, no. 10, pp. 621-628., 2000.
- [128]Roeder, R. K., Sproul, M. M., and Turner, C. H., "Hydroxyapatite whiskers provide improved mechanical properties in reinforced polymer composites", *Journal of Biomedical Materials Research: Part A*, vol. **67**, no. 3, pp. 801-812, 2003.
- [129]SM, Z., S A, S., T Ebrahimi, S., and S A, S., "A study on mechanical properties of PMMA/hydroxyapatite nanocomposite", *Engineering*, 2011.
- [130]Zhang, Y., and Tanner, K. E., "Impact behavior of hydroxyapatite reinforced polyethylene composites", *Journal of Materials Sciences: Materials in Medicine*, vol. **14**, no. 1, pp. 63-68, 2003.
- [131]Zhou, C., Ye, X., Fan, Y., Qing, F., Chen, H., and Zhang, X., "Synthesis and characterization of CaP/Col composite scaffolds for load-bearing bone tissue engineering", *Composites Part B: Engineering*, vol. **62**, no. 1, pp. 242-248, 2014.
- [132]Bajpai, A., and Bundela, H., "Development of poly (acrylamide)-hydroxyapatite composites as bone substitutes: Study of mechanical and blood compatible behavior", *Polymer composites*, vol. **30**, no. 10, pp. 1532-1543, 2009.

- [133]Deng, X., Hao, J., and Wang, C., "Preparation and mechanical properties of nanocomposites of poly (D, L-lactide) with Ca-deficient hydroxyapatite nanocrystals", *Biomaterials*, **vol. 22**, no. 21, pp. 2867-2873, 2001.
- [134]DineshKumar, S., and Purushothaman, S., "Synthesis and Characterization of Polymer Nanocomposites for Biomedical Applications-Current Perspectives and Challenges", *International Journal of Research in Engineering and Science (IJRES)*, **vol. 4**, no. 10, pp. 1-6, 2016.
- [135]Estevez, M., Escamilla, A., Vargas, S., Hernandez-Martinez, A., and Rodriguez, R., "Synthesis and characterization of porous hybrid biomaterials with improved mechanical properties", *Journal of Composite Materials*, 0021998311426623, 2011.
- [136]Greish, Y., and Brown, P., "Characterization of bioactive glass-reinforced HAP-polymer composites", *Journal of biomedical materials research*, **vol. 52**, no. 4, pp. 687-694, 2000.
- [137]Greish, Y., and Brown, P., "Characterization of wollastonite-reinforced HAP-Ca polycarboxylate composites", *Journal of biomedical materials research*, **vol. 55**, no. 4, pp. 618-628, 2001.
- [138]Jiang, H. J., Wang, Y. L., Jia, S. R., Huang, Y., He, F., and Wan, Y. Z., "Preparation and characterization of hydroxyapatite/bacterial cellulose nanocomposite scaffolds for bone tissue engineering", Paper presented at the Key Engineering Materials, 2007.
- [139]Mehtar, A. K., Mahapatra, S. S., and Patel, S. K., "Assessment of Mechanical Properties and Wear Behaviour of Ceramic Composites", *International Journal of Engineering Technology, Management and Applied Sciences (IJETMAS)*, **vol. 3**, special issue, pp. 594-604, 2015.
- [140]Nathanael, A. J., Mangalaraj, D., Chen, P. C., and Nataraj, D., "Improved Mechanical Property of Hydrothermally Synthesized Hydroxyapatite Nanorods Reinforced with Polyethylene", *International Journal of Modern Physics B*, **vol. 24**, no. 1, pp. 215-223, 2010.
- [141]Nathanael, A. J., Mangalaraj, D., Chen, P. C., and Ponpandian, N., "Enhanced mechanical strength of hydroxyapatite nanorods reinforced with polyethylene", *Journal of Nanoparticle Research*, **vol. 13**, no. 5, pp. 1841-1853, 2011.
- [142]Nieh, T., Choi, B., and Jankowski, A., "Synthesis and characterization of porous hydroxyapatite and hydroxyapatite coatings", Paper presented at the Report submitted to Minerals, Metals and Materials Society annual meeting and exhibition, LA, USA, 2001.
- [143]Pazourková, L., Martynková, G., and Plachá, D., "Preparation and Mechanical Properties of Polymeric Nanocomposites with Hydroxyapatite and Hydroxyapatite", *Clay Mineral Fillers-Review, J Nanotechnol Nanomed Nanobiotechnol*, **vol. 2**, no. 7, 2015.
- [144]Pramanik, N., Bhargava, P., Alam, S., and Pramanik, P., "Processing and properties of nano- and macro-hydroxyapatite/poly (ethylene-co-acrylic acid) composites", *Polymer composites*, **vol. 27**, no. 6, pp. 633-641, 2006.
- [145]Ribeiro, C., Barrias, C., and Barbosa, M., "Preparation and characterisation of calcium-phosphate porous microspheres with a uniform size for biomedical applications", *Journal of Materials Science: Materials in Medicine*, **vol. 17**, no. 5, pp. 455-463, 2006.
- [146]Uskokovic, V., Ignjatovic, N., and Petranovic, N., "Synthesis and Characterization of Hydroxyapatite-Collageu Biocomposite Materials", Paper presented at the Materials Science Forum, 2003.
- [147]Wan, Y., Wu, C., Xiong, G., Zuo, G., Jin, J., Ren, K., and Luo, H., "Mechanical properties and cytotoxicity of nanoplate-like hydroxyapatite/poly(lactide) nanocomposites prepared by intercalation technique", *Journal of the mechanical behavior of biomedical materials*, **vol. 47**, no. 1, pp. 29-37, 2015.
- [148]Wei, G., and Ma, P. X., "Structure and Properties of Poly ( $\alpha$ -hydroxyl acids)/Nano Hydroxyapatite Composite Scaffolds", Paper presented at the MRS Proceedings, 2002.
- [149]Xu, H. H., and Quinn, J. B., "Whisker-reinforced bioactive composites containing calcium phosphate cement fillers: Effects of filler ratio and surface treatments on mechanical properties", *Journal of biomedical materials research*, **vol. 57**, no. 2, pp. 165-174, 2001.
- [150]Zhou, C., Ye, X., Fan, Y., Qing, F., Chen, H., and Zhang, X., "Synthesis and characterization of CaP/Col composite scaffolds for load-bearing bone tissue engineering", *Composites Part B: Engineering*, **vol. 62**, no. 1, pp. 242-248, 2014.
- [151]Huang, A. H., Farrell, M. J., Kim, M., and Mauck, R. L., "Long-Term dynamic loading improves the mechanical properties of chondrogenic mesenchymal stem cell-Laden Hydrogels", *Journal of European Cells and Materials*, **vol. 19**, no. 215, pp. 72-85, 2010.
- [152]Kadi, H. El, "Modeling the mechanical behavior of fiber-reinforced polymeric composite materials using artificial neural networks: A review", *Journal of Composite Structures*, **vol. 73**, no. 1, pp. 1-23, 2006.

- [153]Katti, K. S., Turlapati, P., Verma, D., Bhowmik, R., Gujjula, P. K., and Katti, D. R., "Static and Dynamic Mechanical behavior of HAp-Polyacrylic acid composites under simulated body fluid", *American Journal of Biochemistry and Biotechnology*, **vol. 2**, no. 2, pp. 73-79, 2006.
- [154]Li, X., Ma, X.-Y., Feng, Y.-F., Wang, L., and Wang, C., "A novel composite scaffold consisted of porous titanium and chitosan sponge for load-bearing applications: Fabrication, characterization and cellular activity", *Composites Science and Technology*, **vol. 117**, no. 1, pp. 78-84, 2015.
- [155]Antonov, E., Popova, A., Selezneva, I., Trofimov, V., Fedotov, A. Y., and Fomin, A., "Mechanical characteristics of composites of polylactide and nanosized calcium phosphates formed in supercritical carbon dioxide", *Russian Journal of Physical Chemistry B*, **vol. 5**, no. 8, pp. 1189-1194, 2011.
- [156]Balamurugan, A., Kannan, S., Selvaraj, V., and Rajeswari, S., "Development and spectral characterization of poly (methyl methacrylate)/hydroxyapatite composite for biomedical applications", *Trends Biomater. Artif. Organs*, **vol. 18**, no. 1, pp. 41-45, 2004.
- [157]Ahn, E. S., Gleason, N. J., and Ying, J. Y., "The Effect of Zirconia Reinforcing Agents on the Microstructure and Mechanical Properties of Hydroxyapatite-Based Nanocomposites", *Journal of the American Ceramic Society*, **vol. 88**, no. 12, pp. 3374-3379, 2005.
- [158]Wei, G., and Ma, P. X., "Structure and properties of nano-hydroxyapatite/polymer composite scaffolds for bone tissue engineering", *Biomaterials*, **vol. 25**, no. 19, pp. 4749-4757, 2004.
- [159]Zhang, J., Iwasa, M., Kotobuki, N., Tanaka, T., Hirose, M., Ohgushi, H., and Jiang, D., "Fabrication of hydroxyapatite-zirconia composites for orthopedic applications", *Journal of the American Ceramic Society*, **vol. 89**, no. 11, pp. 3348-3355, 2006.
- [160]Bodhak, S., Nath, S., and Basu, B., "Friction and wear properties of novel HDPE-HAp-Al<sub>2</sub>O<sub>3</sub> bio-composites against Alumina counterface", *Journal of Biomaterials Applications*, **vol. 23**, no. 5, pp. 407-433, 2008.
- [161]Chauhan, S., and Thakur, S., "Effects of particle size, particle loading and sliding distance on the friction and wear properties of cenosphere particulate filled vinylester composites", *Materials & Design*, **vol. 51**, no. 1, pp. 398-408, 2013.
- [162]Chowdhury, S. R., Kulkarni, A., Basak, A., and Roy, S., "Wear characteristic and biocompatibility of some hydroxyapatite-collagen composite acetabular cups", *Wear*, **vol. 262**, no. 11, pp. 1387-1398, 2007.
- [163]Hu, J., Li, D., and Llewellyn, R., "Computational investigation of microstructural effects on abrasive wear of composite materials", *Wear*, **vol. 259**, no. 1, pp. 6-17, 2005.
- [164]Mohan, N., Natarajan, S., Kumaresh Babu, S. and Siddaramaiah, "Investigation on two-body abrasive wear behavior of silicon carbide filled glass fabric-epoxy composites", *Journal of Minerals and Materials Characterization and Engineering*, **vol. 9**, no. 3, pp. 231-246, 2010.
- [165]Silva, F. J., Casais, R., Martinho, R., and Baptista, A., "Role of abrasive material on micro-abrasion wear tests", *Wear*, **vol. 271**, no. 9, pp. 2632-2639, 2011.
- [166]Younesi, M., Bahrololoom, M., and Ahmadzadeh, M., "Prediction of wear behaviors of nickel free stainless steel-hydroxyapatite bio-composites using artificial neural network", *Computational Materials Science*, **vol. 47**, no. 3, pp. 645-654, 2010.
- [167]Basu, B., and Kalin, M., *Tribology of ceramics and composites: materials science perspective*: John Wiley & Sons, 2011.
- [168]Galetz, M., Blaß, T., Ruckdäschel, H., Sandler, J., Altstädt, V., and Glatzel, U., "Carbon nanofibre-reinforced ultrahigh molecular weight polyethylene for tribological applications", *Journal of applied polymer science*, **vol. 104**, no. 6, pp. 4173-4181, 2007.
- [169]Perumal, G., Geetha, M., Asokamani, R., and Alagumurthi, N., "Wear studies on plasma sprayed Al<sub>2</sub>O<sub>3</sub>-40wt% 8YSZ composite ceramic coating on Ti-6Al-4V alloy used for biomedical applications", *Wear*, **vol. 311**, no. 1, pp. 101-113, 2014.
- [170]Xiong, L., Xiong, D., Yang, Y., and Jin, J., "Friction, wear, and tensile properties of vacuum hot pressing crosslinked UHMWPE/nano-HAP composites", *Journal of Biomedical Materials Research Part B: Applied Biomaterials*, **vol. 98**, no. 1, pp. 127-138, 2011.
- [171]Harsha, A., and Tewari, U., "Tribo performance of polyaryletherketone composites", *Polymer Testing*, **vol. 21**, no. 6, pp. 697-709, 2002.
- [172]Karanjai, M., Kumar, B. M., Sundaresan, R., Basu, B., Mohan, T. R., and Kashyap, B., "Fretting wear study on Ti-Ca-P biocomposite in dry and simulated body fluid", *Materials Science and Engineering: A*, **vol. 475**, no. 1, pp. 299-307, 2008.
- [173]Liu, Y., Li, X., Zou, B., Chen, J., Cai, Z., Qu, S., and Qian, L., "Fretting behaviors of hot-pressed electrospun hydroxyapatite/poly (dl-lactide) fibrous composites as potential orthopedic implants", *Tribology International*, **vol. 53**, no. 1, pp. 124-133, 2012.

- [174]Tan, Z., Guo, Q., Zhao, Z., Liu, H., and Wang, L., "Characteristics of fretting wear resistance for unfilled engineering thermoplastics", *Wear*, **vol. 271**, no. 9, pp. 2269-2273, 2011.
- [175]Yoon, Y., Etsion, I., and Talke, F., "The evolution of fretting wear in a micro-spherical contact", *Wear*, **vol. 270**, no. 9, pp. 567-575, 2011.
- [176]Isla, A. d. I., Pacheco, S., Estevez, M., Vargas, S., Castaño, V., and Rodriguez, R., "Synthesis and characterization of a wear-resistant hybrid polymer-ceramic coating for dental applications", *International Journal of Polymeric Materials*, **vol. 53**, no. 10, pp. 859-869, 2004.
- [177]QI, L. H.-J. F. J., LI, L.-H. F. Y.-W., and Peng-Yun, X.-T. W., "Effect of Porosity Percentage on the Friction and Wear Performance of Carbon Fiber Reinforced Paper-based Friction Materials", *Journal of Inorganic Materials*, **vol. 6**, no. 1, 2007.
- [178]Ribeiro, R., "A tribological and biomimetic study of potential bone joint repair materials", Texas A&M University, 2006.
- [179]Singh, A., Abhishek, K., Datta, S., and Mahapatra, S. S., "ANFIS based modeling for prediction of surface roughness during machining of glass fiber reinforced epoxy composites", *International Journal of Materials, Manufacturing and Design*, **vol. 1**, no. 1, pp. 1-15, 2012.
- [180]Sahu, M., Singh, P., Mahapatra, S. S., and Khatua, K. K., "Prediction of entrance length for low Reynold's number flow in pipe using neuro-fuzzy inference system", *Expert Systems with Applications*, **vol. 39**, no. 1, pp. 4545-4557.
- [181]Biswas, R., Kuar, A. S., Biswas, S. K., and Mitra, S., "Artificial neural network modeling of Nd:YAG laser micro-drilling on titanium nitride-alumina composite", *Proceedings of the Institution of Mechanical Engineers, Part B: Journal of Engineering Manufacture*, **vol. 224**, no. 8, pp. 473-482, 2010.
- [182]Biswas, R., Kuar, A. S., Sarkar, S., and Mitra, S., "A parametric study of pulsed Nd:YAG laser micro-drilling of gamma-titanium aluminide", *Journal of Optics & Laser Technology*, **vol. 42**, no. 1, pp. 23-31, 2010.
- [183]Chandramohan, D., and Marimuthu, K., "Drilling of natural fiber particle reinforced polymer composite material", *International Journal of Advanced Engineering Research and Studies*, **vol. 1**, no. 1, pp. 134-145, 2011.
- [184]Chandramohan, D., and Marimuthu, K., "Thrust force and torque in drilling the natural fiber reinforced polymer composite materials and evaluation of delamination factor for bone graft substitutes-a work of fiction approach", *International Journal of Engineering Science and Technology*, **vol. 1**, no. 2, pp. 6437-6451, 2010.
- [185]Durão, L. M. P., Magalhães, A. G., Marques, A. T., and Tavares, J. M. R. S., "Effect of drilling parameters on composite plates damage", *International conference HSIMP-High Speed Industrial Manufacturing Processes*, no. 11, pp. 1-8, 2007.
- [186]Gopalsamy, B. M., Mondal, B. and Ghosh, S., "Taguchi method and ANOVA: An approach for process parameters optimization of hard machining while machining hardened steel", *Journal of Scientific & Industrial Research*, **vol. 68**, no. 8, pp. 686-695, 2009.
- [187]Kilickap, E., "Determination of optimum parameters on delamination in drilling of GFRP composites by Taguchi method", *Indian Journal of Engineering & Materials Sciences*, **vol. 17**, no. 4, pp. 265-274, 2010.
- [188]Krishnaraj, V., Prabukarthi, A., Ramanathan, A., Elanghovan, N., Kumar, M. S., Zitoun, R., and Davim, J., "Optimization of machining parameters at high speed drilling of carbon fiber reinforced plastic (CFRP) laminates", *Composites Part B: Engineering*, **vol. 43**, no. 4, pp. 1791-1799, 2012.
- [189]Moshat, S., Datta, S., Bandyopadhyay, A., and Pal, P., "Optimization of CNC end milling process parameters using PCA-based Taguchi method", *International Journal of Engineering, Science and Technology*, **vol. 2**, no. 1, pp. 95-102, 2010.
- [190]Pandey, R. K., and Panda, S., "Multi-performance optimization of bone drilling using Taguchi method based on membership function", *Measurement*, **vol. 59**, no. 1, pp. 9-13, 2015.
- [191]Pandey, R. K., and Panda, S. S., "Evaluation of delamination in drilling of bone", *Medical engineering & physics*, **vol. 37**, no. 7, pp. 657-664, 2015.
- [192]Rajmohan, T., Palanikumar, K., and Davim, J. P., "Analysis of surface integrity in drilling metal matrix and hybrid metal matrix composites", *Journal of Materials Science & Technology*, **vol. 28**, no. 8, pp. 761-768, 2012.
- [193]Singh, G., Jain, V., Gupta, D., and Ghai, A., "Optimization of process parameters for drilled hole quality characteristics during cortical bone drilling using Taguchi method", *Journal of the mechanical behavior of biomedical materials*, **vol. 62**, no. 1, pp. 355-365, 2016.

# Dissemination

## International Journals

1. **Mehar A. K.**, Mahapatra S. S. and Patel S. K. (2015). Assessment of Mechanical Properties and Wear Behavior of Ceramic Composites, **International Journal of Engineering Technology, Management and Applied Sciences (IJETMAS)**, Special Issue, ISSN 2349-4476, ISBN 978-93-325-4896-1, Pearson Publisher, INDIA (DIIF Impact Factor Value: 2.24).
2. **Mehar A. K.**, Mahapatra S. S. and Patel S. K. (2016). Fabrication, Processing and Assessment of Mechanical Behavior of Hydroxyapatite (HAp) reinforced Polycarbonate Composite for Bio-Medical Applications, **Indian Journal of Engineering, An International Journal, Discovery Publication**, ISSN 2319-7757, EISSN 2319-7765, 13(33), pp. 386-393, INDIA.
3. **Mehar A. K.**, Mahapatra S. S. and Patel S. K. (2016). Assessment of Mechanical Behavior of Hydroxyapatite (HAp) reinforced Polysulfone Composite, **Journal of Applied and Engineering Sciences, Published by Anna University, Chennai, INDIA**.

## Edited Book Chapter

1. **Mehar A. K.**, Mahapatra S. S. and Patel S. K., "Fabrication, Processing and Assessment of Mechanical Behavior of Hydroxyapatite (HAp) reinforced Polycarbonate Composite for Bio-Medical Applications", **Trends in Industrial and Mechanical Engineering, Published by Excellent Publisher, New Delhi, INDIA**, Vol. 3(1), pp. 84-90, ISBN 978-93-84935-68-9.

## Conferences

1. **Mehar A. K.**, Mahapatra S. S. and Patel S. K., "Effect of Machining Parameters in Drilling of Composites", **Proceedings of the 2<sup>nd</sup> International Conference on Industrial Engineering (ICIE), November 20-22, 2013, SVNIT, Surat (Gujarat), INDIA**, Vol. 2(1), pp. 893-897.
2. **Mehar A. K.**, Chatterjee S., Mohanty C. P., and Mahapatra S. S., "Evaluation of Two-body abrasive wear using FIS and ANN", **International Conference on Advanced**

- Materials and Manufacturing (ICAMM-2013, 11-12 April)**, CAPE Institute of Technology, Tirunelveli, Tamilnadu, INDIA.
3. **Mehar A. K.**, Mahapatra S. S. and Patel S. K., “Assessment of Mechanical Properties and Wear Behavior of Ceramic Composites”, **Proceedings in Pearson Publication & Associated Journals of the International Conference on Emerging Trends of Engineering, Science, Management and its Applications (ICETESMA-15), March 01, 2015**, JNU (New Delhi), INDIA, Vol. 1(1), pp. 271-280.
  4. **Mehar A. K.**, Mahapatra S. S. and Patel S. K., “Fabrication, Processing and Assessment of Mechanical Behavior of Hydroxyapatite (HAp) reinforced Polycarbonate Composite for Bio-Medical Applications”, **International Conference on Trends in Industrial and Mechanical Engineering (IC TIME 2016), February 4-6, 2016, MANIT (Bhopal), INDIA.**
  5. **Mehar A. K.**, Mahapatra S. S. and Patel S. K., “Assessment of Mechanical Behavior of Hydroxyapatite (HAp) reinforced Polysulfone Composite”, **Proceedings of the First International Conference on Materials, Design and Manufacturing Process (ICMDM 2016), February 17-19, 2016, College of Engineering, Guindy, Anna University, Chennai (Tamilnadu) INDIA**, Vol. 1(1), pp. 1-6.
  6. **Mehar A. K.**, Mahapatra S. S. and Patel S. K., “Ceramic/Polymer bio-composite as bone substitute materials for bio-medical applications”, **National Conference on Processing and Characterization of Materials (NCPCM), December 6-7, 2013**, National Institute of Technology, Rourkela (Odisha), INDIA.
  7. **Mehar A. K.**, Mahapatra S. S. and Patel S. K., “Hydroxyapatite-reinforced Polymer biocomposite as bone biomaterials”, **Proceedings of the National Conference on Condensed Matter Physics (CMDAYS), August 29-31, 2013**, National Institute of Technology, Rourkela (Odisha), INDIA.



# Index

- Abrasive wear, 51
- Actual density, 42
- Adaptive neuro fuzzy inference system, 86
- Adhesive wear, 52
- Allograft, 7
  
- Batch mixer, 32
- Biocompatibility, 9
- Biocomposite, 1
- Biomaterials, 7
- Bone, 2
- Bone production, 6
- Bone remodelling, 6
  
- Cancellous bone, 5
- Ceramics, 8
- Circularity, 190
- Compact bone, 5
- Composite, 1
  
- Dry hydroxyapatite, 34
- Dry methods, 40
  
- Erosive wear, 52
  
- FTIR spectrometer, 37
- Fretting wear, 52
  
- Hydroxyapatite, 9
  
- Inflammation, 6
  
- Metals, 7
- Micro-compounder, 32
- Micro-injection molding, 33
  
- Osteoblasts, 6
- Osteoclasts, 6
- Osteoconduction, 10
- Osteocytes, 6
- Osteogenesis, 11
- Osteoinduction, 11
  
- Particle size analyser, 34
- Polycarbonate, 27
- Polymers, 8
- Polysulfone, 12
- Principal component analysis, 193
  
- Sliding wear, 52
- Specific wear rate, 57
- Surface fatigue wear, 52
  
- Theoretical density, 42
- Tribo-chemical or corrosion wear, 52
- Two-body abrasive wear, 51
  
- Volume loss, 57
  
- Wear, 51
- Wear rate, 57
- Wet methods, 28
  
- X-ray diffractometer, 35

# Curriculum Vitae



Mr. **Amit Kumar Mehar** is an Associate Professor in the Department of Mechanical Engineering, Raghu Engineering College (REC) (Autonomous), Vishakhapatnam, Andhra Pradesh, INDIA. He has 3 years of industrial, 2 years of teaching, and 6 years of research experience in his field. He had 3 international journals, 10 national and international conferences, and 1 edited book chapter. He has 6 professional memberships. He was born on 24<sup>th</sup> January 1984 in Raipur, Chhattisgarh (INDIA). He did B.E. in Mechanical Engineering from K.I.T., Raigarh (Chhattisgarh) INDIA in 2006. He did M. Tech. (Research) in Mechanical Engineering from N.I.T., Rourkela (Odisha) INDIA in 2011. This thesis is being submitted for the fulfilment the Ph.D. degree. His area of research is related to biomaterials, composite materials, tribology, machining, optimization techniques, soft computing etc. The contact address is:

## **Official Address:-**

Amit Kumar Mehar  
(Associate Professor), Department of Mechanical Engineering,  
Raghu Engineering College (REC), (Autonomous)  
Dakamarri village, Bheemunipatnam Mandal,  
Vishakhapatnam, Andhra Pradesh-531162 INDIA.  
Email: [amitkumarmehar@gmail.com](mailto:amitkumarmehar@gmail.com)  
[amitkumar.mech@raghuenggcollege.in](mailto:amitkumar.mech@raghuenggcollege.in)

## **Residence:-**

Qtr. No. 58/2400,  
Kelo vihar colony, In front of pump house,  
Raigarh (Chhattisgarh)-496001 INDIA